

**PROCEEDINGS OF THE  
NINTH ANNUAL  
PACIFIC CLIMATE (PACLIM) WORKSHOP**

Asilomar, California – April 21-24, 1992

Edited by  
Kelly T. Redmond and Vera L. Tharp

Technical Report 34  
of the  
Interagency Ecological Studies Program  
for the  
Sacramento-San Joaquin Estuary

March 1993

**Copies of this report may be obtained without charge from:**

**California Department of Water Resources  
P.O. Box 942836  
Sacramento, CA 94236-0001**

## Sponsors

---

The Ninth Annual Pacific Climate Workshop was sponsored by the

U.S. GEOLOGICAL SURVEY  
Water Resources Division

U.S. GEOLOGICAL SURVEY  
Geologic Division

NATIONAL OCEANIC AND ATMOSPHERIC ADMINISTRATION  
National Geophysical Data Center

U.S. ENVIRONMENTAL PROTECTION AGENCY  
EMAP Program

NATIONAL PARK SERVICE  
Global Change Program

CALIFORNIA DEPARTMENT OF WATER RESOURCES  
Environmental Services Office

NATIONAL OCEANIC AND ATMOSPHERIC ADMINISTRATION  
Western Regional Climate Center

AMERICAN GEOPHYSICAL UNION

SOUTHERN CALIFORNIA EDISON CORPORATION

Publication of this proceedings has been sponsored by the

INTERAGENCY ECOLOGICAL STUDIES PROGRAM

for the

SACRAMENTO-SAN JOAQUIN ESTUARY

A Cooperative Program of:

California Department of Water Resources  
State Water Resources Control Board  
U.S. Bureau of Reclamation  
U.S. Geological Survey

California Department of Fish and Game  
U.S. Fish and Wildlife Service  
U.S. Army Corps of Engineers  
U.S. Environmental Protection Agency

These proceedings were published by the Interagency Ecological Studies Program for the Sacramento-San Joaquin Estuary (Interagency Program) in a cooperative effort with the

Western Regional Climate Center, Desert Research Institute, Reno, Nevada.

Information generated by the PACLIM workshop provides the Interagency Program with a climatological perspective that cannot be obtained from its own studies.

Views and conclusions contained in this publication do not necessarily reflect the opinions of the Interagency Program or its member agencies.



# Contents

---

Sponsors . . . . .	iii
Authors . . . . .	vii
Acknowledgments . . . . .	ix
Statement of Purpose . . . . .	xi
Introduction . . . . . <i>Kelly T. Redmond</i>	1
Climate Studies in the Long-Term Ecological Program . . . . . <i>David Greenland</i>	5
Meteorological and Hydrologic Studies in the Alaskan Arctic in Support of Long-Term Ecological Research . . . . . <i>Douglas L. Kane</i>	13
Sea Surface Temperature and the Subsequent Freshwater Survival Rate of Some Salmon Stocks: A Surprising Link Between the Climate of Land and Sea . . . . . <i>David J. Blackbourn</i>	23
Climate Change and Salmonid Production in the North Pacific Ocean . . . . . <i>Robert C. Francis</i>	33
Year-to-Year Changes of Vertical Temperature Distribution in the California Current Region: 1954 to 1986 . . . . . <i>Jerrold G. Norton and Douglas R. McLain</i>	45
An Objective Classification of Climatic Regions in the Pacific and Indian Oceans . . . . . <i>Henry F. Diaz and Timothy J. Brown</i>	55
ENSO and Precipitation Variability Over Mexico During the Last 90 Years . . . . . <i>George N. Kiladis and Henry F. Diaz</i>	63
Changes in Frost Frequency and Desert Vegetation Assemblages in Grand Canyon, Arizona . . . . . <i>Robert H. Webb and Janice E. Bowers</i>	71
Relationships Between ENSO Events and San Francisco Rainfall, 1949-1991 . . . . . <i>Jan Null</i>	83
Streamflow and La Niña Event Relationships in the ENSO-Streamflow Core Areas . . . . . <i>Ercan Kahya and John A. Dracup</i>	89

A Mechanism for the Link Between Solar-Irradiance Variations and Regional Precipitation . . . . .	97
<i>Charles A. Perry</i>	
A Preliminary Description of Climatology in the Western United States . . . . .	103
<i>John O. Roads, Shyh-Chin Chen, Kyozo Ueyoshi, James Bossert, and Judith Winterkamp</i>	
Climatic Impacts of the 1991-92 Western Winter . . . . .	123
<i>Kelly T. Redmond</i>	
Drought Frequency Analysis for California from Observed, Synthetic, and Proxy Data . . . . .	133
<i>Frederick Wade Freeman and John A. Dracup</i>	
A Multi-Basin Seasonal Streamflow Model for the Sierra Nevada . . . . .	141
<i>Daniel R. Cayan and Laurence G. Riddle</i>	
Patterns of Orographic Uplift in the Sierra Nevada and Their Relationship to Upper-Level Atmospheric Circulation . . . . .	153
<i>Edward Aguado, Dan Cayan, Brian Reece, and Larry Riddle</i>	
A Stochastic Model of Temporal Variations in Monthly Temperature, Precipitation, Snowfall, and Resulting Snowpack. . . . .	165
<i>Richard L. Orndorff, Richard G. Craig, and John F. Stamm</i>	

## **Appendixes**

---

A	Agenda, Ninth Annual Pacific Climate (PACLIM) Workshop, April 21-24, 1992 . . . . .	173
B	Posters, Ninth Annual Pacific Climate (PACLIM) Workshop, April 21-24, 1992 . . . . .	181
C	Attendees, Ninth Annual Pacific Climate (PACLIM) Workshop, April 21-24, 1992 . . . . .	185

## Authors

---

Edward Aguado  
Department of Geography  
San Diego State University  
San Diego, California 92182-0381

David J. Blackbourn  
Canada Department of Fisheries and Oceans  
Pacific Biological Station  
Nanaimo, BC, Canada  
V9R 5K6

Timothy J. Brown  
CIRES  
University of Colorado  
Boulder, CO 80309

James Bossert  
Los Alamos National Laboratory  
Los Alamos, NM 87545

Janice E. Bowers  
U.S. Geological Survey  
1675 West Anklam Road  
Tucson, AZ 85745

Daniel R. Cayan  
Scripps Institution of Oceanography  
Climate Research Division  
A-0224, University of California, San Diego  
La Jolla, CA 92093-0224

Shyh-Chin Chen  
Climate Research Division  
Scripps Institution of Oceanography, 0224  
University of California, San Diego  
La Jolla, CA 92093

Richard G. Craig  
Department of Geology  
Kent State University  
Kent, OH 44242-0001

Henry F. Diaz  
NOAA/ERL  
325 Broadway  
Boulder, CO 80303

John A. Dracup  
Civil Engineering Department  
University of California, Los Angeles  
3066B Engineering I  
Los Angeles, CA 90024

Robert C. Francis  
Fisheries Research Institute, WH-10  
School of Fisheries  
University of Washington  
Seattle, WA 98195

Frederick Wade Freeman  
Civil Engineering Department  
University of California, Los Angeles  
4532 Boelter Hall  
Los Angeles, CA 90024

David Greenland  
Department of Geography  
University of Oregon  
Eugene, OR 97430-1251

Ercan Kahya  
Civil Engineering Department  
University of California, Los Angeles  
3066 Engineering I  
Los Angeles, CA 90024

Douglas L. Kane  
Water Research Center  
University of Alaska  
Fairbanks, Alaska 99775-1760

George N. Kiladis  
Cooperative Institute for Research in  
Environmental Sciences  
Box 449  
University of Colorado  
Boulder, CO 80309

Douglas R. McLain  
National Ocean Service  
Ocean Applications Branch  
2560 Garden Road, Suite 101  
Monterey, CA 93940

Jerrold G. Norton  
Southwest Fisheries Science Center-PFEG  
National Marine Fisheries Service  
P.O. Box 831  
Monterey, CA 93942

Jan Null  
National Weather Service Forecast Office  
660 Price Avenue  
Redwood City, CA 94063

Richard L. Orndorff  
Department of Geology  
Kent State University  
Kent, OH 44242-0001

Charles A. Perry  
U.S. Geological Survey  
4821 Quail Crest Place  
Lawrence, KS 66049

Kelly T. Redmond  
Western Regional Climate Center  
PO Box 60220  
Reno, NV 89506

Brian Reece  
Department of Geography  
San Diego State University  
San Diego, CA 92182-0381

Laurence G. Riddle  
Scripps Institution of Oceanography  
Climate Research Division  
0224, University of California, San Diego  
La Jolla, CA 92093-0224

John O. Roads  
Climate Research Division  
Scripps Institution of Oceanography, 0224  
University of California, San Diego  
La Jolla, CA 92093

John F. Stamm  
Department of Civil Engineering and  
Operations Research  
Princeton University  
Princeton, NJ 08544

Kyozo Ueyoshi  
Climate Research Division  
Scripps Institution of Oceanography, 0224  
University of California, San Diego  
La Jolla, CA 92093

Robert H. Webb  
U.S. Geological Survey  
1675 West Anklam Road  
Tucson, AZ 85745

Judith Winterkamp  
Los Alamos National Laboratory  
Los Alamos, NM 87545

## **Acknowledgments**

---

Once again I would like to thank Vera Tharp for her ability to transform the caterpillar of a collection of papers into the butterfly of a finished volume. This never-easy task is performed with a cheerful and purposeful attitude. Also, a thank-you to the authors, whose adherence to the guidelines furnished to them made this process flow appreciably better than it might otherwise have.

Thank you, Vera, from all of us!

Kelly Redmond  
Co-editor



## **STATEMENT OF PURPOSE**

### **Pacific Climate (PACLIM) Workshops**

---

In 1984, a workshop was held on "Climatic Variability of the Eastern North Pacific and Western North America". From it has emerged an annual series of workshops held at the Asilomar Conference Center, Monterey Peninsula, California. These annual meetings, which involve 80-100 participants, have come to be known as PACLIM (Pacific Climate) Workshops, reflecting broad interests in the climatologies associated with the Pacific Ocean. Participants have included atmospheric scientists, hydrologists, glaciologists, oceanographers, limnologists, and both marine and terrestrial biologists. A major collective goal of PACLIM is to connect their various interests with a common target.

PACLIM arose from broad concern about the impact of possible climate change over the next century. From observed changes in the historical record, it is certain that climate change will have tremendous societal impacts through coincident effects on global ecology, hydrology, geology, and oceanography. It is increasingly clear that our ability to predict climate change is best derived from an understanding of global processes. Human impacts are primarily terrestrial in nature, but the major forcing processes are atmospheric and oceanic in origin and transferred through geologic and biologic conditions. Our understanding of the global climate system and its relationship to ecosystems will arise from a regional study of its components in the Pacific Ocean and the western Americas, where ocean/atmosphere coupling is strongly expressed. With such diverse meteorologic phenomena as the El Niño-Southern Oscillation and shifts in the Aleutian Low and North Pacific High, the Eastern Pacific is a region that has tremendous global influences, and strong effects on North America in particular. This region is rich in climatic records, both instrumental and proxy. Recent research efforts are beginning to focus on better paleoclimatic reconstructions that will put present day climatic variability in context and should allow better anticipation of future changes.

The PACLIM workshops have addressed the problem of defining regional coupling of multifold elements, as organized by phenomena that are global in extent. Because climate expresses itself through the natural system, our activity has been, from the beginning, multidisciplinary in scope and is evolving into a truly interdisciplinary cooperative effort. The specialized knowledge from different disciplines has brought together these characteristic climatic records and process measurements to provide a synthesis of understanding of the complete system.

Our interdisciplinary group uses diverse time series, measured both directly and through proxy indicators, to study past climatic conditions and current processes in this region. Characterizing and linking the geosphere, biosphere, and hydrosphere in this region will provide a scientific analogue and, hence, a basis for understanding similar linkages in other regions, as well as for anticipating the response to future climate variations. Our emphasis in PACLIM is to study the interrelationships among diverse data. The resultant information obtained will be complementary and lead to better synthesis of biological and geophysical variability in the region. By necessity, in order to understand these interactive phenomena, we will incorporate studies that consider a broad range of topics and multiple time scales, from months to millennia.

The benefit of the effort to understand the regulation of ecosystems and their variability is clear. It is critical now, from both a management and scientific point of view, that we develop a more complete understanding of how climatic change affects the structure and function of these systems. The PACLIM venue covers an extraordinary range of ecosystem types and richness. There is empirical evidence that large-scale climatic fluctuations force large-scale ecosystem response in the California current and in a very different system, the North Pacific central gyre. The implications of these observations are highly significant and indicate the need for aggressive pursuit of multidisciplinary studies.

Water supplies in the western Americas exhibit fluctuations over a continuum of scales, with considerable social and economic impact, especially in the Southwest, where demand exceeds supply. The spatial extent and variability of the hydrologic system, such as precipitation deficits and drought, are strongly coupled to climate. For instance, in the western United States where rainfall is primarily a cool-season phenomenon, year-to-year changes in the activity and tracking of North Pacific winter storms have substantial influence on the hydrological balance. In turn, this atmospheric variability is at least weakly coupled to anomalous thermal conditions in the upper ocean. Thus, a primary objective of PACLIM is to better understand the linkage between large-scale atmospheric and hydrologic variabilities, with their complex effects on chemical and biological systems.

Proceedings of the first PACLIM workshops were published as  
AGU Geophysical Monograph 55 (Peterson, ed., 1989).  
Beginning with the Sixth Annual Workshop in 1989, the proceedings have been published by the  
California Department of Water Resources as Technical Reports of the  
Interagency Ecological Studies Program for the Sacramento-San Joaquin Estuary.

Kelly T. Redmond

The 1992 PACLIM meeting featured the Long-Term Ecological Research (LTER) program, sponsored by the National Science Foundation. Ranging from hot to cold and wet to dry climatic regimes, these 18 sites are attempting to understand the web of relationships in different locations as communities evolve over time scales of years to decades to centuries. During this time they are subject to external forcings, including those that vary smoothly and somewhat predictably, like the seasons, upon which are superimposed random "shocks" of various magnitudes.

David Greenland stresses that climate must be recognized as a significant influence on temporal behavior of integrated natural biological and physical systems. He discusses the importance of environmental monitoring and the need for minimum and consistent standards for observational programs.

Following this, Douglas Kane highlights the difficulties and frustrations of understanding the interaction between climate and northern tundra ecosystems. These include the logistical problems and even dangers that accompany measurement efforts in the high Arctic, and the lack of sufficient pre-existing, lengthy climate records from nearby representative sites. This seems particularly important when one considers that global climate models suggest the Arctic may be particularly sensitive to changes in climate.

Shifting attention southward, David Blackbourn assembles evidence from several locations that the survival rate of salmon eggs and young fish is quite well linked with conditions experienced by their parents well before they even entered fresh water on their last spawning run. These conditions include sea surface temperature, which is in turn linked with climate. Thus, survival of offspring depends on conditions encountered during a significant fraction of the total life expectancy of a salmon. This unexpectedly strong relationship, which is fascinating in its own right, may have significant management implications as well.

Robert Francis shows a general out-of-phase relationship between salmon catches off the West Coast and those in the Gulf of Alaska. These variations in catches correspond to the presence of large-scale climate fluctuations in the equatorial and northern Pacific and, in particular, two major "regimes". The relative importance of biological factors (for example, competitive interaction) versus more purely physical factors (oceanic or atmospheric conditions) has been the subject of much discussion among those attempting to explain catch behavior. This paper adds weight to the latter.

Jerrold Norton and Doug McLain examine ocean temperatures along the immediate West Coast from Southern California to Vancouver Island, at depths ranging from the surface to 300 meters. They find September-February temperatures in the upper layers are more highly correlated with pressure several months earlier during the previous summer at Darwin, Australia, with the highest correlation becoming synchronous in time at the 300-meter depth. This is consistent with relationships between SOI and western US climate. Using a point in the northeastern Pacific as "local forcing", they find that pressure variations there are essentially synchronous with ocean temperature variations at all depths.

In another study of the Pacific, Henry Diaz and Timothy Brown use the shape of the seasonal cycle of sea surface temperature in the Comprehensive Ocean-Atmosphere Data Set to classify homogeneous regions in the Indian and Pacific Oceans. They then examine the temporal behavior, in terms of long-term trends and in the frequency domain, of selected regions. This work is potentially useful in studies such as the salmon variations mentioned just above.

Several papers then follow that deal with the southwestern United States. George Kiladis and Henry Diaz look at Mexican precipitation since 1900, again by first grouping the point data into homogeneous regions. They show that ENSO has opposing effects on precipitation in northern and southern Mexico. The effects are quite mild, almost negligible, in the south and more dramatic and considerably more important in the north.

Robert Webb and Janice Bowers use the technique of photographic replication to assess changes in vegetation in the Grand Canyon. Drawing upon a blend of quantitative and qualitative information, they show how this method, in conjunction with other supplementary data, can be used to derive inferences about climate behavior in the time since the Canyon was first visited by early expeditions. Severe frosts appear to have occurred less frequently in recent years. This paper was presented as a well-attended special slide show during the PACLIM meeting.

Jan Null shows that the stronger and most common ENSO events are associated with wetter conditions at San Francisco during January through March. There are also significantly more rainfall occurrences, both light and heavy, during such events.

Focusing on the opposite condition, La Niña, Ercan Kahya and John Dracup look at precipitation in four "core" areas previously identified as showing a response to El Niño. They use 41 years of observation from a thousand US stream gages. The regions are in the central Missouri River basin, the Gulf Coast, the mid-Atlantic and the Pacific Northwest. In each region, a precipitation anomaly opposite to that associated with EL Niño was found for La Niña years. The results also show potential application for long-range predictions of streamflow.

Charles Perry hypothesizes that variations in solar irradiance are linked with observed precipitation. The presumed link involves a transit time of several years around the gyre in the northern Pacific Ocean. He sees evidence of this in a maximal correlation between annual empirically modeled solar radiation and annual precipitation at a time lag of four years in the Pacific Northwest.

John Roads *et al* use the Colorado State University RAMS model to generate one-month model climatologies for January and July 1988 and compare the results to analyses from the National Meteorological Center models (which have one-fifth the horizontal resolution) and to observational datasets. Although this model version does not improve agreement with values from the coarse NMC grid or with observations at selected points, it is not much worse either, and at least offers the prospect of finer resolution of fields of elements such as precipitation, which are not archived in the global analyses.

The unusual winter of 1991-1992 is discussed by Kelly Redmond. Drought and warmth dominated in the continental western United States, but with dramatic exceptions. Observed patterns of temperature and precipitation agree very well with those typically associated with a negative Southern Oscillation Index (El Niño). The Sierra drought has remained long enough to have developed its own short climatology, akin to those often proposed as climate change scenarios.

Frederick Freeman and John Dracup examine ways of determining return statistics for California drought. Using various methods, a range of 63-346 years between recurrences is found for the current duration and intensity of drought. This is an important problem in applied climatology and hydrology, since the implications of different estimates are quite different in terms of planning horizons and engineering criteria for components of the vital water supply system. Critical societal decisions are affected by such technical considerations.

Staying in the Sierra, Daniel Cayan and Laurence Riddle develop a statistical model that works well over a significant range of elevations to predict streamflow in various seasons. The primary information needed includes temperature, precipitation and snow water content. As the winter progresses, the influence of conditions in various previous seasons on streamflow for the present season becomes apparent, and in an intuitively reasonable manner. One motivation for the model was the ability to perform simple "what if" climate change scenario studies.

Edward Aguado *et al* examine the upper air patterns associated with high or low ratios of mountain (Sierra) to valley (Central Valley) precipitation. This ratio serves as a measure of the effectiveness of orographic uplift in enhancing precipitation. Those years with flow oriented more perpendicular to the mountain chain axis have a higher mountain-to-valley ratio than those years with flow oriented more obliquely. They also find good spatial coherence of these ratios within the mountain stations.

To conclude this set of papers, in a model study, Richard Orndorff *et al* use an extension of a previously developed “local climate model” to investigate the temporal variance of precipitation, snowfall, and temperature at locations in the southwestern United States. Their statistically based model has a grid resolution of 1 kilometer and is run in a Monte Carlo fashion.

# Climate Studies in the Long-Term Ecological Program

David Greenland

**ABSTRACT:** Since the inception of the LTER Program in 1980, climate has been studied at individual LTER sites and an LTER Climate Committee has been responsible for inter-site activities. At individual sites, climate studies support ecological research, emphasize intra-site heterogeneity, and often relate to other national monitoring and research programs. In inter-site work, the Climate Committee has produced protocols for meteorological observations, described and compared climates of the first 11 sites, and raised important issues regarding climate variability and ecosystem response.

The Long-Term Ecological Research (LTER) Program, sponsored by the National Science Foundation, contains 18 sites in a variety of ecosystems. Climate is studied within and between individual sites. This brief review gives some examples of the range of work performed at individual sites and then describes some inter-site activities.

## Climate Studies at Individual Sites

Climate is studied at each of the 18 sites. Although highly variable, the studies have two common goals.

- They seek to support the research — especially long-term research — of ecologists at the site.
- They are usually oriented to one of the five core research areas of the LTER program, particularly the areas of primary productivity, organic and inorganic fluxes, and disturbance.

Availability of a long-term climatic record at most LTER sites makes it possible to identify directional changes and to place a perspective on the importance of individual climatic events. Analysis of the Niwot Ridge climate record, for example, suggests a move to cooler, wetter conditions (Greenland 1989). This move correlates with shifts in plant community composition, reduced soil pH, and modified controls on nitrogen limitation to vegetation. The analysis also suggests some cyclicity in annual precipitation values and identifies years of high or low precipitation, which might be categorized as disturbance to the ecosystem. Similarly, Molles and Dahm (1990), working at the Sevilleta LTER site in New Mexico, have noted important effects of El Niño and La Niña phenomena on stream ecology. At some LTER sites massive climatic disturbance has been documented, as in the case of the huge impact of Hurricane Hugo on the North Inlet Marsh site in South Carolina and the tropical rain forest site at Luquillo Experimental Forest in Puerto Rico.

Within-site climate studies often point up small-scale variability. Alpine tundra, which may appear quite homogeneous, has been shown to have a variety of micro climates when values of the surface heat energy exchanges at different vegetation surfaces are measured (Greenland 1991). Although most sites are generally representative of a particular biome, some sites are on the border of more than one. The Sevilleta site, for example, includes Great Plains grassland, Great Basin shrub-steppe, Chihuahuan Desert, interior chaparral, and montane coniferous forest biomes.

Usually each LTER site is also networked into one or more regional or national climate-related program. Many sites, for example, belong to the National Atmospheric Deposition Network. The Konza tall grass prairie in Kansas was also the site of the first ISLSCP field experiment (FIFE) of the International Satellite Land Surface Climatology Program. The Niwot site is also a long-term monitoring station for carbon dioxide and other gasses in the NOAA Climate Modeling and Diagnostics Laboratory monitoring program.

## **Inter-Site Activities**

---

The LTER Climate Committee initiates inter-site activities. The committee has established standards for meteorological measurements at LTER sites (Swift and Ragsdale 1985; Greenland 1986a, 1986b) and has described and compared climates of the first 11 LTER sites (Greenland 1987). The committee has also examined the topic of climate variability and ecosystem response (Greenland and Swift 1990, 1991).

In establishing standards for LTER site meteorological measurements, Swift and Ragsdale (1985) developed the approach of a hierarchy of measurement sophistication. At the entry level, sites are required to record only daily maximum and minimum air temperatures and precipitation values. At the three higher levels, sites gain increasing complexity and inclusivity in the variables observed and their manner of observation. At least one location within most LTER sites now use electronic data sensing and logging systems. The hierarchical approach proved popular since it allowed greater budgetary flexibility at individual sites.

The network is by no means optimal for giving geographic coverage of the United States. Consequently, approaches other than geographic have to be employed in comparing climates of the individual sites. The committee has presented diagrams of "climate space" into which the LTER sites are placed (Greenland 1987). Such diagrams are two dimensional and have axes indicating simple variables, such as annual mean temperature and precipitation, or derived parameters, such as Thornthwaite's modified moisture index and potential evapotranspiration. These diagrams and accompanying tables of the sites ranked by various climatic parameter values are useful in designing ecological experiments when abiotic gradients across the LTER Network need to be selected.

The Climate Committee also renders services to the LTER community such as providing climate information for publications (eg, Van Cleve and Martin 1991) and an electronic newsletter/bulletin board, CED (Climate/Ecosystem Dynamics), produced by Dr. Bruce Hayden at the Virginia Coast Reserve LTER site.

Some of the most useful ideas from the LTER Climate Committee arose from the workshop "Climate Variability and Ecosystem Response". Most of the following material is drawn from workshop results (Greenland and Swift 1990, 1991). As a committee we identified four issues to be considered in future investigations:

- Need to clarify terms and definitions used in discussing climate variability.
- Importance of recognizing the various time and space scales of climate variability and ecosystem response.
- Need to expand data beyond dependence on traditional summaries of temperature and precipitation.
- Value of insights from examining similarities and dissimilarities among climate episodes and ecosystem responses across LTER sites.

Some of these issues are briefly addressed below.

Scale is an important consideration because it determines what kinds of questions can be asked about the operation of an ecosystem. Researchers must relate scales on which climate systems operate to scales on which the biotic parts of the ecosystems operate. The definition of climate, as perceived by an individual component of the ecosystem, is directly related to scale. A soil micro-organism might regard an individual rainstorm as a significant climatic event, whereas a tree at the Andrews site in Oregon would be acclimated to a climate range far exceeding that found in any 30-year climatic normal. Each ecosystem responder defines its own climate scale. LTER sites should be equipped with the tools to put events such as droughts and storms into perspective. An example of such tools is the Z-T methodology applied at the Coweeta site (Swift *et al* 1990).

Current climatic data impose several time- and space-scale limitations. The time limitation is that the length of the reliable observed climatic record in most parts of the United States is on the order of only a hundred years or less. A scale limitation is that most modeling studies based on current General Circulation Models (GCMs) employed to investigate effects of increase in greenhouse gasses are on a scale so large that a state the size of Colorado might contain only one grid point.

Thus, we concluded that to understand climate variability and ecosystem response demands, we must pay particular attention to space and time scales. We must beware of arbitrarily imposed, human-derived scales and concentrate on those scales that emerge from the functioning of the

ecosystem and climate systems. Research should specifically identify those functions and processes of the ecosystem that cannot keep up with potential rates of abiotic change, such as postulated global warming rates.

We recognized a continuing need for consistency in obtaining and handling data across the LTER network. Of great value would be new indices that are not directly dependent on monthly and annual mean temperature and precipitation values. Dr. Anthony Federer of the Hubbard Brook Experimental Forest, New Hampshire, LTER site believes a water stress variable would be important in this context. Such a variable might be accumulated deviation of daily precipitation (or temperature) or more complicated ones involving soil water budget factors. One such indirect index, the date of lake freezing, was demonstrated for the Northern Lakes LTER site (Robertson 1990). However, this is specific for the LTER site and ecosystem it represents and cannot apply at all to some other sites.

An index that seemed to have wide application for inter-site comparisons emanated from air mass climatology. Wendland and Bryson (1981) used streamline analysis to map airstream regions. The regions are defined by the boundaries between airstreams from different global source areas. Almost every LTER site has periods during the year when there is a shift between being in the region of one airstream and being under the influence of air from another. The number of months duration in different airstream regions provides an index for comparing LTER sites. Wendland has examined air mass frequency data for all LTER sites. The duration of each air mass from various source regions is a representation of the climate for a particular period. In another time period, the air mass frequencies might change, especially at sites near the confluences of airstreams. Thus, this data form may provide evidence of shifts from one climatic episode to another. There is a certain amount of subjectivity in some forms of air mass analysis, and the subject is still being refined (Schwarz 1985, 1988). Nevertheless, the approach has considerable potential for identifying climate variability for some biomes. We recommended that sites, singly and as a network, investigate new and nonstandard climatic indices to supplement information obtained from standard climatic observations and summaries.

A benefit of having LTER sites in different biomes is the possibility of broad-scale comparisons, not often available to ecologists, which should give valuable insight into ecosystem function and processes. This was demonstrated during the workshop when similarities and dissimilarities between sites were examined.

Many sites have not yet identified clear or obvious ecosystem responses to slow climate trends or even to events of mid-scale severity. But most sites have experienced major responses to a severe weather event. The Hubbard Brook ecosystem, for example, was not markedly disturbed by the droughts of the 1960s but still shows the effect of a single hurricane

in 1938. Tree blowdown has been a repeated catastrophic wind-related event at several LTER sites, and hurricane damage has significantly altered both the North Inlet and Luquillo ecosystems (Biotropica 1991). Many ecological responses are due to secondary effects of atmospheric events, such as flooding or landslides. For example, the redistribution of sediment by an intense rainstorm on the otherwise dry Jornada site has marked consequences on the biota either by burying them or by providing new micro habitats.

Several sites reported possible time coincidence for discontinuities in the values of climate variables. The years of changing climatic episodes suggested by shifts in freezing dates of Lake Mendota, Wisconsin, near the Northern Lakes LTER site, in 1880, 1940, and possibly 1980 were also noted as times of change at some other sites. LTER sites may benefit from examining their own records for common break points in datasets. Data at most sites, as well demonstrated by the Central Plains Experimental Range (Kittel 1990), follow hemispheric or at least regional trends in temperature and precipitation. This augurs well for the extrapolation of results from the LTER network to larger areas. Yet unique or isolated sites, such as Niwot Ridge, will not necessarily display the same spatial and temporal trends as adjacent dissimilar areas.

Several fertile areas for further research can capitalize on the similarities and dissimilarities of climate variability and ecosystem response across LTER sites. These include investigation of:

- The importance of catastrophic events in relation to slower trends and cycles.
- The time coincidence of certain major climatic discontinuities that appear to exist at several sites and the effects on ecosystems as they shift from one episode to another.
- The relationship of climate to phenological studies across the LTER network.

## **Conclusion**

---

The LTER program provides a useful base for climate studies, both within individual sites and across the LTER network. By looking at climate problems from an ecological viewpoint, insights may be gained and many questions may emerge. The highly disparate nature of LTER sites allows us to search for indices, like air mass frequency, that go beyond information restrained to local observations of temperature and precipitation. Climate studies in the LTER network are leading to a broader search for new concepts and techniques in ecosystem science as a whole.

## Acknowledgment

---

The Long-Term Ecological Research Program is sponsored by the National Science Foundation (Long-Term Projects in Environmental Biology) through grants to individual sites and to an LTER Coordinating Committee.

## References

---

- Biotropica*. 1991. Special Issue: Ecosystem, Plant, and Animal Responses to Hurricanes in the Caribbean. 23(4) Part A. Available from the Association for Tropical Biology, Inc.; Department of Ecology, Evolution and Organismal Biology; Tulane University; New Orleans 70118.
- Greenland, D. (ed). 1986a. *Standardized Meteorological Measurements for Long Term Ecological Research Sites*. Mimeograph. Available from LTER Central Office, University of Washington.
- \_\_\_\_\_. 1986b. Standardized Meteorological Measurements for Long-Term Ecological Research Sites. *Bulletin of the Ecological Society of America*. 67:275-277.
- \_\_\_\_\_. (ed). 1987. *The Climates of the Long-Term Ecological Research Sites*. Occasional Paper 44. Institute of Arctic and Alpine Research. University of Colorado.
- \_\_\_\_\_. 1989. The Climate of Niwot Ridge, Front Range, Colorado, USA. *Arctic and Alpine Research* 21:380-391.
- \_\_\_\_\_. 1991. Spatial surface energy budgets over alpine tundra in summer, Niwot Ridge, Colorado Front Range. *Mountain Research and Development*. 11:339-351.
- Greenland, DE, and LW Swift, Jr. (eds). 1990. *Climate Variability and Ecosystem Response*. US Forest Service, Southeastern Region. General Technical Report SE-65.
- \_\_\_\_\_. 1991. Climate Variability and Ecosystem Response: Opportunities for the LTER Network. *Bulletin of the Ecological Society of America* 72:118-126.
- Kittel, TGF. 1990. Climatic variability in the shortgrass steppe. pp 67-75 in *Climate Variability and Ecosystem Response*. DE Greenland and LW Swift (eds). US Forest Service, Southeastern Region. General Technical Report SE-65.
- Molles, MC Jr, and CN Dahm. 1990. A perspective on El Niño and La Niña: Global implications for stream ecology. *Journal of the North American Benthological Society* 9:68-76.
- Robertson, DM. 1990. Lakes as indicators of and responders to climate change. pp 38-46 in *Climate Variability and Ecosystem Response*. DE Greenland and LW Swift (eds). US Forest Service, Southeastern Region. General Technical Report SE-65.
- Schwartz, MD. 1988. Integrating the objective and subjective approaches to air mass classification. Abstract in program of Association of American Geographers Annual Meeting, Phoenix, April 1988. p. 169.
- Schwartz, MD, J Harman, and G Marotz. 1985. Air Mass Characteristics over the North Central United States. *Geographical Perspectives* 56:13-26.
- Swift, LW, and HL Ragsdale. 1985. Meteorological Data Stations at Long-Term Ecological Sites. *Proceedings of Forest Environmental Measurements Conference*, October 23-28, 1983, Oak Ridge TN. Reidel, Holland.
- Swift, LW, JB Waide and DL White. 1990. Application of the Z-T Extreme Event Analysis Using Coweeta Streamflow and Precipitation Data. pp 13-18 in *Climate Variability and Ecosystem Response*. DE Greenland and LW Swift (eds). US Forest Service, Southeastern Region. General Technical Report SE-65.

Van Cleve, K, and S Martin. 1991. Long-Term Ecological Research in the United States, A Network of Research Sites. 6th Ed, Revised. LTER Publication 11. Long-Term Ecological Research Network Office, Seattle.

Wendland, WM, and RA Bryson. 1981. Northern Hemisphere airstream regions. *Monthly Weather Review* 109:255-270.



# Meteorological and Hydrologic Studies in the Alaskan Arctic in Support of Long-Term Ecological Research

Douglas L. Kane

**ABSTRACT:** Long-term hydrologic studies in the Arctic simply do not exist. Although the Arctic has been identified as an area that is extremely sensitive to climate change, continuous scientific research has been limited to the past seven years. Earlier research was spotty, of short duration, and directed at only one or two hydrologic elements. Immediate future research needs to encompass all the major hydrologic elements, including winter processes, and needs to address the problem of scaling from small to larger areas in hydrologic models. Also, an international program of cooperation between northern countries is needed to build a greater scientific base for monitoring and identifying potential changes wrought by the climate.

Although the Arctic has been identified as an area that will undergo the greatest climatic warming due to increases in atmospheric greenhouse gases (Schlesinger and Mitchell 1987; Ramanathan 1988), virtually no long-term databases exist for identifying or quantifying this change. Historically, collection of hydrologic and meteorologic datasets has been in response to resource development and, to a lesser extent, defense needs. Scientific goals have never been the driving force behind collecting such data. Just as scientific interest in the Arctic was peaking, the federal government began to reduce its data collection efforts nationwide; therefore the density of Arctic hydrologic and meteorologic stations is only a small fraction of those in the contiguous 48 states.

Hydrologic processes of this region are similar to those of other regions of the world. However, the magnitude of each of these processes varies substantially from region to region. In the Arctic, precipitation in the form of snow plays a dominant role in the hydrologic cycle. The accumulation of snow over 6 months or more, with generally no midwinter melting, guarantees the snowmelt period will be dynamic. In a relatively short time (7 to 10 days), the surface albedo changes by a factor of four, from 0.8 for snowcover, to 0.2 for the snow-free tundra (Kane *et al* 1991a).

Phase change is an integral part of the hydrologic cycle: evaporation, transpiration, sublimation, ablation, soil freezing and thawing, and formation and decay of river and lake ice. In fact, it is impossible to study the hydrologic processes without examining both the mass and energy fluxes (Figure 1).

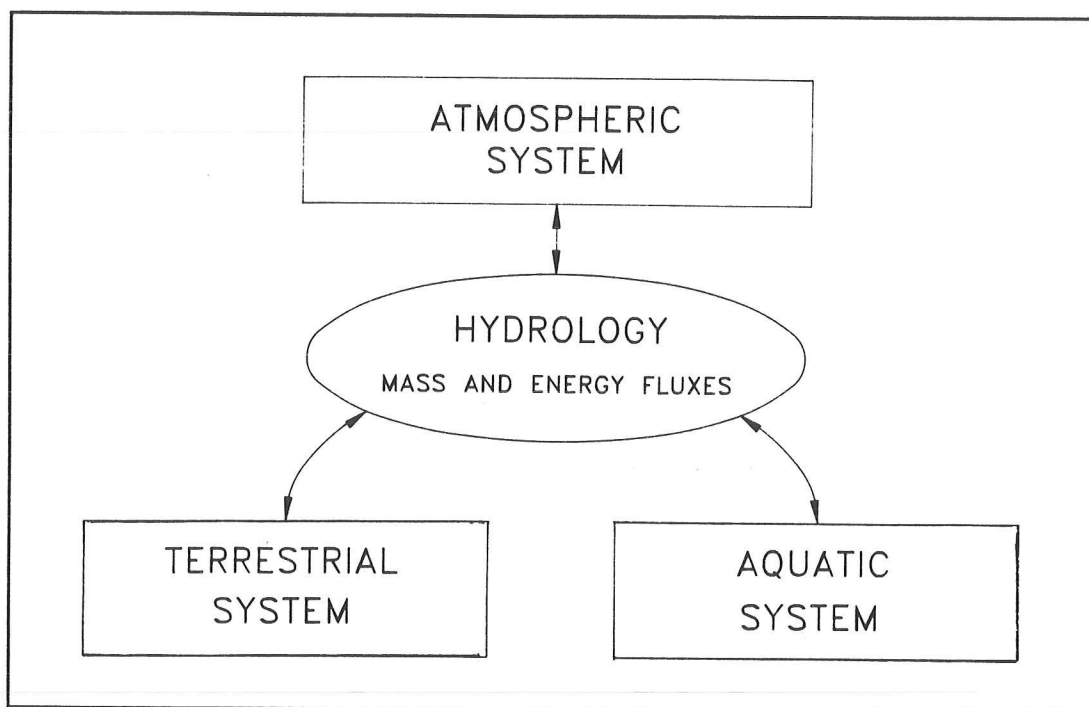


Figure 1. Hydrology, the physical interface between the atmosphere and terrestrial and aquatic systems.

The Alaskan Arctic, north of the Brooks Range, is an area in excess of 200,000 km<sup>2</sup>. To put this in perspective, the area is larger than each of the 36 smallest states and about equivalent in size to Nebraska or Minnesota. The area is completely underlain by permafrost with maximum thicknesses reaching 600 meters. Each summer the ground thaws from the surface downward, forming the active layer. The depth of thaw is closely tied to ice content and drainage, with the latter being impacted primarily by topography. Typical depths of thaw of the active layer are 50 cm, but depths in excess of 100 cm occur in well-drained, steep-sloping sites.

The active layer is critical in the hydrologic cycle. Its capability to store water is severely reduced because of its shallow depth. The fact that precipitation intensities and magnitude are low ensures that flood peaks are not as severe as one would expect. However, flooding from snowmelt is a common phenomenon each year (Kane *et al* 1991a; Hinzman and Kane 1991). Precipitation that accumulates for 7 to 9 months melts just a few weeks before the summer solstice. The ablation period is relatively short (7 to 10 days), and water content of the snowpack is 40 to 50 percent of the annual precipitation. Plants that exist in the arctic get all their nutrients and water from this shallow subsurface system.

In the remainder of the paper, I discuss those hydrologic processes that are presently important in the Arctic and how they would be impacted by climate change. The purpose is to help identify and direct future hydrologic research.

## Arctic Hydrology

Components of the hydrologic cycle in the Arctic are similar to those in other regions of the world, but phase change from snow and ice to water, or vice versa, plays a dominant role. In this paper, the Arctic in United States is confined to that area north of the Brooks Range to the coast (Figure 2). Precipitation is dominantly snow from mid-September through

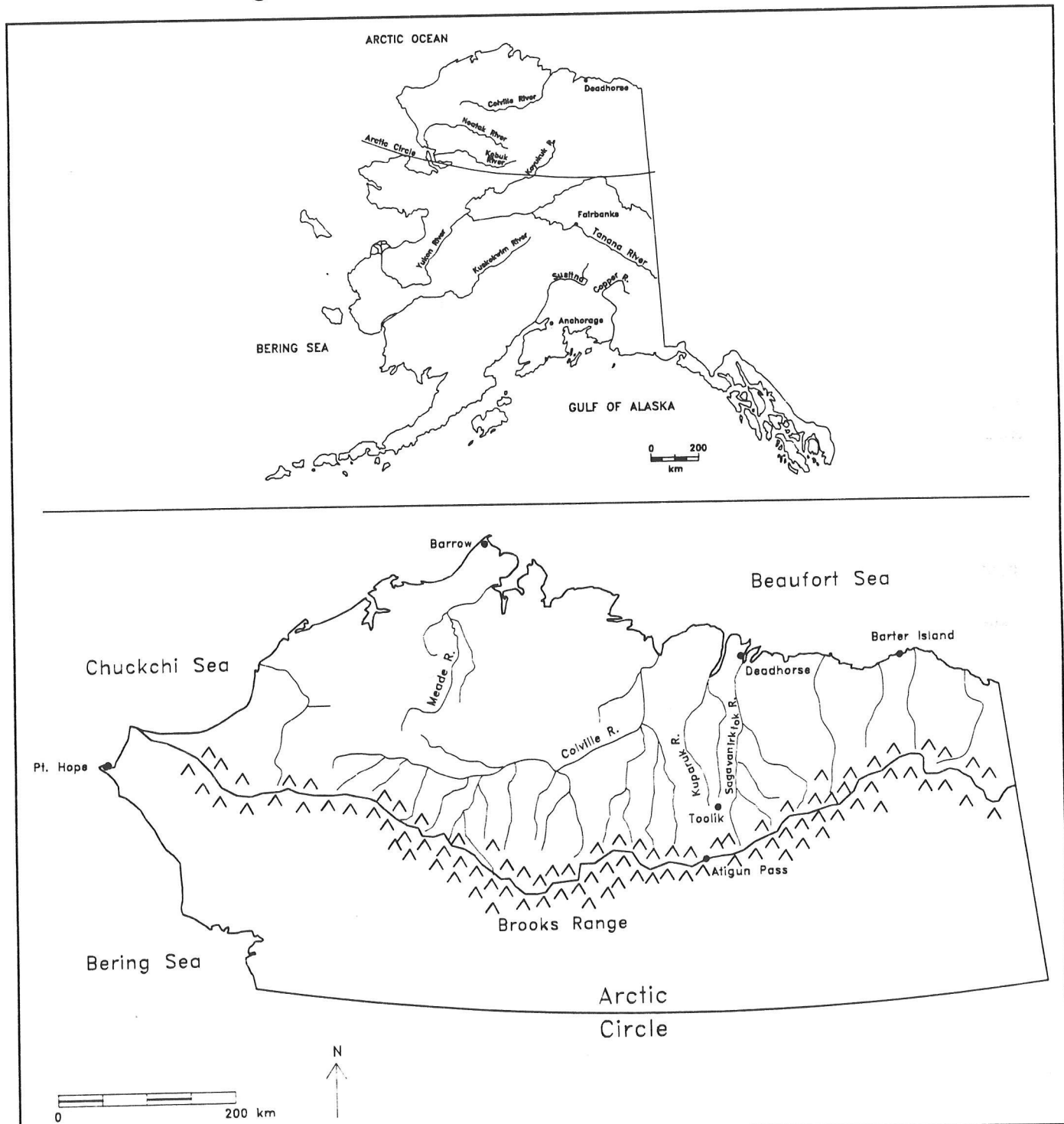


Figure 2. The state of Alaska with an enlarged view of the area north of the Brooks Range that is essentially underlain by continuous permafrost.

April. Melting of the snowpack during this period is rare, but snowfall during the summer is common; with the snow melting within a few days. The major limitation of precipitation data is the lack of quality snowfall data and the complete lack of appreciation for the importance of redistribution of snow by the wind during winter.

Measurement of snowfall precipitation during the winter is a difficult task in windy environments. Continued use by the National Weather Service of precipitation gages without wind shields is discouraging in that the data are almost useless. Detailed surveys of snow on the ground at the end of winter have shown the gages simply do not work in this windy environment (Benson 1982; Woo *et al* 1982). The Soil Conservation Service has tested the Wyoming snow gage in the Arctic, and the catch efficiency is substantially improved over the National Weather Service gages (Clagett 1988).

Considerable redistribution of the snowpack by the wind occurs in this treeless area; therefore, estimates of snow on the ground can only be assessed by making numerous measurements. In addition, to the lee-side of ridges snow collects in and around depressions. These depressions correspond to drainages, and this may result in greater runoff than if the snowpack were uniformly distributed.

In the valley bottom, where the wind increases the snowpack and also the density of the snowpack, runoff is retarded from leaving the basin in headwater streams. This delay has been as great as 2 days when the snowpack in the valley bottom becomes saturated with snowmelt from the slopes. In years when the snowpack is greatest, snow damming seems to be prevalent.

Although winter months exceed summer months, accumulated annual rainfall on the average is much greater than the accumulated annual snowfall (Table 1). Based on 7 years of precipitation data collected with a Wyoming precipitation gage, an average of 35 percent of the annual precipitation could be attributed to snowfall at Imnavait Watershed (Hinzman and Kane, 1992).

Month	Precipitation (cm)	Month	Precipitation (cm)
October	2.10	April	1.53
November	0.87	May	0.98
December	1.34	June	5.41
January	1.30	July	8.68
February	1.42	August	5.37
March	0.65	September	3.12

Even though snowfall is about one-third of the total annual precipitation, runoff generated from melting snow is a much higher percentage than for rainfall (Figure 3). This can be attributed to the fact that the active layer is completely frozen and therefore provides limited storage, snowmelt is relatively rapid as solstice approaches, and transpiration is nonexistent at this time of year. Base flows are very low in arctic rivers and streams during winter. Figure 4 illustrates that each spring a large percentage of the annual runoff occurs during ablation and that a flood is guaranteed. In Figure 3, the initial value of precipitation represents the snow on the ground on the first day of ablation. In Figure 4, runoff prior to ablation is

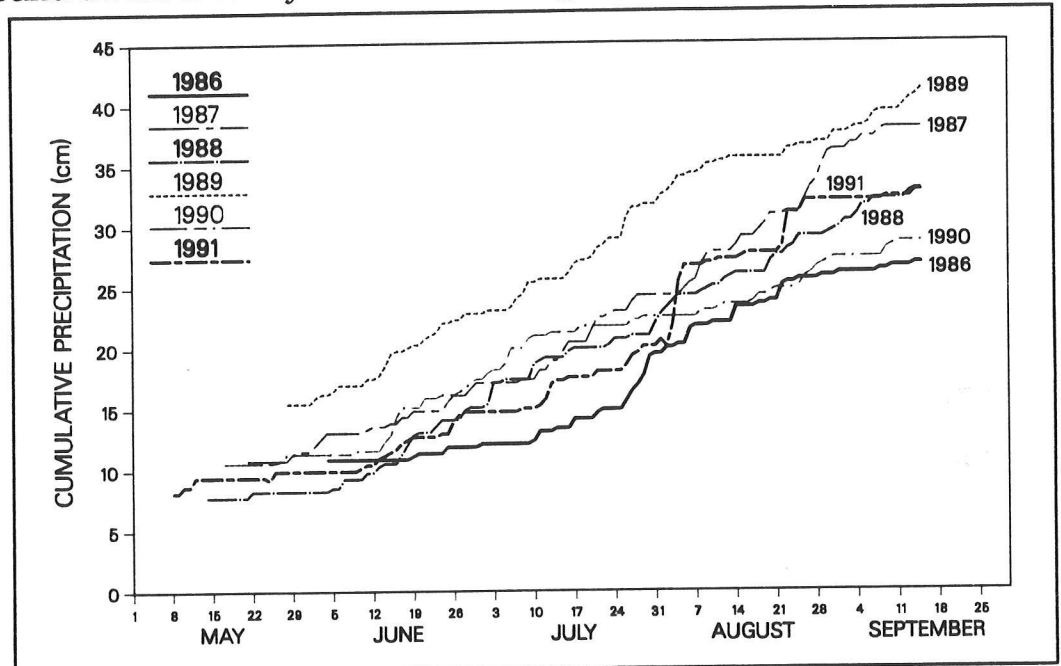


Figure 3. Cumulative curves of precipitation for a small arctic watershed, Innavait Creek.

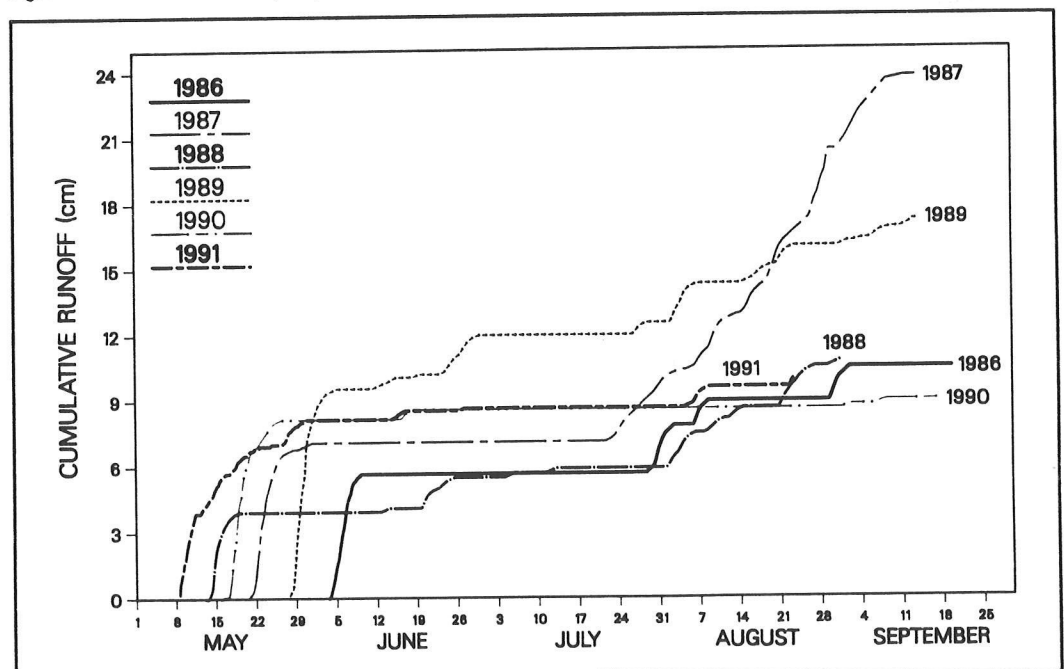


Figure 4. Cumulative curves of runoff for a small arctic watershed, Innavait Creek.

nil, and for many of the summers this is also true after snowmelt. However, 1987 and 1989 have substantial runoff.

Headwater streams that flow all summer (in other regions these would be called first order streams) tend to completely freeze during winter. An interesting feature of permafrost terrain is hillslope drainages referred to as "water tracks" — subtle drainages that are very efficient at carrying water off the slopes as surface flow. Flow occurs in these drainages every year during snowmelt and significant summer rainfall events, often lasting several days. These water tracks take the shortest route down the slope, but when they reach the valley bottom they disperse and seldom connect directly to the stream. Larger water tracks are visible when viewed under the right conditions, but many more are only apparent when they are transferring surface water.

Water also moves downslope through the active layer as subsurface flow. This water is obviously important in many biologic processes, but the quantity of flow during the summer is meager compared to surface runoff. The only exception to this is water movement downslope through the surficial organic soils during snowmelt and major runoff events. When there is flow in the water tracks, this generally implies the active layer is saturated. Usually the active layer is composed of organic soils overlying mineral soils; the mineral soils have relatively low hydraulic conductivities, while organic soils have high saturated hydraulic conductivities.

A large proportion of incoming energy is utilized for evaporation during snowmelt (Kane *et al* in press) and evapotranspiration during summer (Kane *et al* 1990). During the snowmelt period, the major mechanism for water loss from the basins is runoff; during summer, evapotranspiration dominates. In summer, daily evapotranspiration averages about 1.8 mm, being greater in early summer and dropping off in late summer.

The only watershed in the Alaskan Arctic where a complete water balance can be determined with available data is Innvait Creek, near Toolik Lake (latitude 68°37'N, longitude 149°17'W). Data starting in 1985 and extending into 1992 are summarized in Table 2. Computations in this table are from freeze-up in the fall extending to when snow starts to accumulate the next fall. The table nicely illustrates the magnitude of the major hydrologic components. For example, annual precipitation on this modified water year varies from 27 to 41 cm; at the same time, snowfall precipitation ranged from 8 to 19 cm and rainfall precipitation ranged from 16 to 27 cm. The only assumption in these calculations is that storage in the active layer does not change. The rationale for this is that it always rains late in the summer before freeze-up, producing a saturated active layer. Field measurements of soil moisture have confirmed this assumption (Kane and Hinzman 1988), which allows us to equate precipitation to the sum of runoff and evapotranspiration.

Table 2  
 Water Balance for Imnavait Creek Watershed

Year	Snowpack Water (cm)	Summer Precipitation (cm)	Total Precipitation (cm)	Snowmelt Runoff (cm)	Summer Runoff (cm)	Total Runoff (cm)	Evapo-Transpiration (cm)	Pan Evaporation (cm)
1985	10.2	25.1	35.3	6.6	*	*	*	*
1986	10.9	16.3	27.2	5.7	6.2	11.9	15.3	31.0
1987	10.8	27.2	38.0	7.1	17.9	25.0	13.0	32.0
1988	7.8	25.2	33.0	3.9	7.2	11.1	21.9	33.2
1989	15.5	25.7	41.2	9.4	7.8	17.2	24.0	42.0
1990	10.6	16.3	26.9	6.4	2.8	9.2	17.7	39.4
1991	8.2	24.9	33.1	5.6	3.3	8.9	24.2	37.7
1992	19.1	#	#	14.4	#	#	#	#

\* Data unavailable.

# Data collected but not reduced yet.

Runoff in Table 2 is shown to represent a large percentage of the snowpack. During summer this ratio is much lower, as evapotranspiration is the dominant form of water loss from the watershed. Evapotranspiration greatly exceeded summer runoff in 1988, 1990 and 1991.

## Impact of Climate Change on Arctic Hydrology

Schlesinger and Mitchell (1987) and Ramanathan (1988) found that general circulation models (GCMs) predict that, in response to a doubling of carbon dioxide in our atmosphere, the greatest warming will occur in the high latitudes. The impact of climate change is twofold in the Arctic. In addition to influencing hydrologic processes such as ablation, evapotranspiration, and soil moisture levels (Woo 1990), it would also influence the physical structure of the watershed by altering the active layer depth. Differences from year to year would not be great, but the cumulative effect would be significant over a long period. Kane *et al* (1991b) found that a linear increase of 4°C warming over a 50-year period would double the depth of thaw of the active layer from 50 cm to 100 cm. Hinzman and Kane (1992) also found that the depth of thaw over this 50-year period was not very sensitive to the annual distribution of this warming.

Hydrologically, one would expect that climatic warming in the Arctic would result in earlier ablation, greater evapotranspiration and subsequently less runoff, and later freeze-up in the fall. This is what Hinzman and Kane (1992) found for the Imnavait Creek watershed. Other issues complicate the picture.

- Will precipitation quantities and patterns change?
- What will be the response of vegetation to this warming?
- Will there be a change in cloud cover that would alter the surface energy balance?

It is obvious that with a shorter season of ice and snow, reduced albedos will increase the amount of absorbed radiation. Also the quandary about production of either methane or carbon dioxide in arctic environments is closely tied to soil moisture levels.

At this time, we can try to forecast the hydrologic impacts of climate change on hydrologic processes. The unfortunate fact is that we have very little quality hydrologic data in the Arctic with which to compare forecasted results. This is illustrated in the results of Hinzman and Kane (1992), where most of the changes predicted for the Imnavait Creek Basin are on the order of 10 to 15 Percent. This order of change is of the same magnitude as the error of many of the present hydrologic measurements in this area.

## **Conclusions**

---

There is a need to develop a better physical understanding of coupled meteorologic and hydrologic processes in the Arctic. This urgent need derives from the fact that arctic regions of the world are more sensitive to potential climate changes. Primarily because of funding constraints, the current understanding and database is limited for this region. We are only beginning to appreciate the global role the arctic regions play in the energy balance. Future work needs to be done at many scales, and there needs to be a combined modeling and field data collection effort.

## **Acknowledgment**

---

The U.S. Department of Energy, Office of Health and Environmental Research, Ecological Research Division, in part made it possible to produce this article.

## References

---

- Benson, CS. 1982. *Reassessment of winter precipitation on Alaska's Arctic Slope and measurements on the flux of wind blown snow*. Rep. UAG R-288, 26 pp. University of Alaska, Geophysical Institute, Fairbanks.
- Clagett, GP. 1988. The Wyoming windshield — an evaluation after 12 years of use in Alaska. *Proc. of Western Snow Conference*, pp. 113-123.
- Hinzman, LD, and DL Kane. 1991. Snow hydrology of a headwater arctic basin. 2. Conceptual analysis and computer modeling. *Water Resources Research* 27(6):1111-1121.
- \_\_\_\_\_. 1992. Potential response of an arctic watershed during a period of global warming. *Journal of Geophysical Research* 97(D3):2811-2820.
- Kane, DL, and LD Hinzman. 1988. Permafrost hydrology of a small arctic watershed. *Proc. Fifth International Permafrost Conference*. Tapir Publishers, Trondheim, Norway. pp. 590-595.
- Kane, DL, RE Gieck, and LD Hinzman. 1990. Evapotranspiration from a small Alaskan Arctic watershed. *Nordic Hydrology* 21(4/5):253-272.
- Kane, DL, LD Hinzman, CS Benson, and GE Liston. 1991a. Snow hydrology of a headwater arctic basin. 1. Physical Measurements and Process Studies. *Water Resources Research* 27(6):1099-1109.
- Kane, DL, LD Hinzman, and JP Zarling. 1991b. Thermal response of the active layer in a permafrost environment to climatic warming. *Cold Regions Science and Technology* 19(2):111-122.
- Kane, DL, RE Gieck, G Wendler, and LD Hinzman. In Press. Snowmelt at a small Alaskan arctic watershed. 2. Energy related modeling results. *Nordic Hydrology*.
- Ramanathan, V. 1988. The greenhouse theory of climate change: a test by an inadvertent global experiment. *Science* 240:293-299.
- Schlesinger, ME, and JFB Mitchell. 1987. Climate model simulations of the equilibrium climatic response to increased carbon dioxide. *Reviews of Geophysics* 25:760-798.
- Woo, MK. 1990. Consequences of climatic change for hydrology in permafrost zones. ASCE. *Journal of Cold Regions Engineering* 4(1):15-20.
- Woo, MK, R Heron, and P Marsh. 1982. Basal ice in high arctic snowpacks. *Arctic and Alpine Research* 14(3):251-260.



# Sea Surface Temperature and the Subsequent Freshwater Survival Rate of Some Salmon Stocks: A Surprising Link Between the Climate of Land and Sea

David J. Blackbourn

**ABSTRACT:** Previous consideration of the relationship between climate and the survival rate of Pacific salmon eggs and fry has been confined to effects of large variation in the ambient freshwater environment; *eg*, stream discharge, temperature, turbidity. This analysis shows sea surface temperatures during the last year of life of maturing adult salmon are also strongly associated with the subsequent survival rate of salmon eggs and fry in fresh water, presumably through development of the future eggs or sperm. In several stocks of three species of North American salmon, the association between the "marine" climate and egg survival is stronger than, or additive to, any estimated climatic association in fresh water. This apparent and surprising link between fresh water and the distant ocean has some interesting and complex implications for management of future salmon production.

The various species of Pacific salmon (*Oncorhynchus* sp.) spend from 6 months to several years of the early part of their lives in fresh water before they leave for the ocean. The first 3 to 6 months of this period are spent as eggs "incubating" in the gravel of the spawning area in cold, well-oxygenated water. Fewer than 10 percent, and often fewer than 1 percent, of the eggs laid by an adult female salmon develop and leave fresh water as juveniles, and much of the mortality occurs during spawning and incubation (Salo 1991).

When attempting to account for this annual variation early in the life cycle, it is natural that local and contiguous biological and physical processes are usually assumed to be the main agents of mortality. Therefore, in previous studies most attention has been focused on effects of unusually large numbers of spawners and/or on flooding of incubation sites by heavy rain and high river discharge. Both of these factors tend to disturb spawners, move gravel after spawning, and increase the silt content of the gravel; all to the detriment of the developing eggs, some of which may also be exposed or buried in less than optimum locations. Eggs laid in very shallow water are subsequently vulnerable to another physical factor during incubation, extremely cold water.

During a study of the migration timing of pink salmon back to the Fraser River, it was noted that, over several years the subsequent fresh water survival (FWS) rate of the eggs was strongly and surprisingly correlated with the speed of passage of the adult salmon into the terminal fisheries. Also, both of these phenomena were strongly correlated with coastal marine sea surface temperatures (SST) a few months before spawning.

These results implied that SST, migration behavior, or both, had some effect on the quality of salmon eggs or sperm, and/or on adult spawning behavior. Simple models of statistical relationships between SST and the migration timing behavior and terminal pre-spawning mortality of adult salmon have been described elsewhere (Blackbourn 1987, In Prep).

This paper describes an attempt to test the generality of the apparent relationship between FWS for Fraser River pink salmon and SST. I report comparisons between FWS rate in some stocks of Pacific salmon and environmental data from various periods in the final adult year:

- Early in the year and far out in the Gulf of Alaska,
- From periods a month or two prior to spawning, and
- During incubation.

A measure of competitive or "crowding" factors on FWS, such as number of spawners or eggs is also included in the analyses.

Recent trends in near-shore SST and in spawner number for many North American salmon stocks have been similar and increasing. Therefore, to avoid the confounding effect of autocorrelation between these factors, I also examine the extents to which SST data account for significant variation in FWS rate in addition to that accounted for by spawner/egg number and other environmental data.

Fresh-water survival data from four salmon stocks from British Columbia are analyzed from two pink and two sockeye stocks. One stock of each species uses natural spawning conditions and the other stocks spawn under conditions of controlled flow and optimal gravel size in spawning channels. Data from both types of incubation are analyzed to investigate the possible existence of a partial, "universal", pre-spawning SST effort on egg or sperm quality, with and without the confounding effects of other potential agents of annual variation in FWS rate, such as river discharge or inter-gravel particle (silt) size.

## **Data Sources**

---

The salmon data in this paper come from unpublished sources (see Acknowledgments).

The fresh-water survival (FWS) rate data cover various periods in the life history of the stocks. An estimate of numbers of eggs laid is calculated by extrapolation from estimates of average fecundity (number of eggs per female) and is known as the potential egg deposition (PED) in common to all four salmon stocks. In the case of (wild) Atnarko River pinks, the FWS rate is short-term and is based on the percentage of live, of the total of live plus dead eggs and recently hatched juveniles (fry), in the gravel in January, or about 4 months after spawning.

A slightly longer period is covered by FWS rate in the two stocks from spawning channels, Seton Creek pinks and Weaver Creek sockeye. Here FWS rate refers to the number of fry estimated as migrating out of the spawning channel in March as a percentage of the PED in October (in both cases), about 6 months earlier. FWS rate data covering a much longer period are the only kind available for Great Central Lake (GCL) sockeye. In this stock, the number of juveniles in the lake in September about 1 year after spawning is taken as a percentage of the PED.

Some of the British Columbia shore SST data used here have been published in Canadian Data Reports of Hydrography and Ocean Sciences; for example in Giovando (1983). Offshore SST data from the Bering Sea and Gulf of Alaska up to 1982 were obtained from unpublished records of Dr. D. McLain of the Pacific Environmental Group, NMFS, Monterey, California. Since 1982 most of the offshore SST data originates from reports (the "Oceanographic Monthly Summary" and the "15-Day SST Mean") published by the U.S. National Weather Service, NOAA, Washington DC, USA.

British Columbia rainfall and air temperature data are published in the series "Monthly Record-Meteorological Observations in Western Canada" by the Canadian Atmospheric Environment Service, Downsview, Ontario, and in the "British Columbia Climate Summary" from the regional office of the same service.

## **Analyses**

---

Simple and multiple least squares regressions were used to identify associations among environmental data, spawner or egg number, and measures of FWS rate from four stocks of wild or enhanced pink and sockeye salmon. Results are considered significant where  $P \leq 0.05$ . Percentages of the FWS rates are not transformed, as this parameter for stocks of each "incubation type" has fairly low variance in most cases, with little overlap between types. Thus, the data do not greatly violate the assumption of normality in distribution.

Fresh water environmental variables in the analyses are the closest available in time and space to the spawning grounds or channels. Coastal SST data are mean monthly values from stations and periods close to the final marine migration areas of the stocks and also, where appropriate, from the outer coastal areas.

Gulf of Alaska SST data from the brood year are mean monthly values from "Marsden" squares of 5° latitude by 5° longitude and are included in the analyses as follows:

- **Time:** Data from every month from November (adult return year minus one) to June (return year) are considered as potentially appropriate from the inferred location of the stocks according to models of return

timing in pink and sockeye salmon (Blackbourn 1984, 1987). Within these limits, those months or combinations of months of SST data with the highest single regression coefficients versus the FWS rate for each stock are shown in the results.

- **Place:** The stock-specific distribution of North American salmon at sea early in their last year is unknown, although it has been inferred for some stocks, particularly for Fraser River pinks and sockeye (Blackbourn 1984, 1987; Takagi *et al* 1981). From models in the latter papers, it is assumed that pink salmon stocks would be distributed in the southeastern Gulf of Alaska between 40° and 50° N and between 125° and 150° W. Therefore, monthly SST data from this area are used in primary analyses with pink FWS rate data. Similarly, SST data from a large area across the central Gulf between 45° and 55° N and between 135° and 160° W are used in initial comparisons with sockeye FWS rate data.

SST data showing the strongest coefficients when compared to FWS rate data were used in multiple regression analyses with all other factors, including: coastal SST; fresh water environmental data just before, during, or after spawning; and spawner or egg number. In some of the time series there are fairly strong time-series trends and, thus, strong cross-correlation between them, particularly between coastal SST and spawner or egg number in some stocks. In the absence of any model that fits the spawner/egg data with low variance, the best evidence for a real or potential effect of brood-year SST on FWS rate in such cases is taken to be significant additional variation accounted for when SST data are also used. In all analyses the variation is that proportion adjusted for the total degrees of freedom in each combination. A more extensive analysis of these relationships in a larger number of salmon stocks has been described by Blackbourn (1991).

To maximize the degree of biological insight gained, no formal protocol for dealing with successive correlation analyses (Walters 1990) is followed in this study or in Blackbourn (1991). In such a protocol it is recommended that the degrees of freedom be decreased for each successive "case" (here, stock, month or SST "area") investigated. To do so would rapidly exhaust the number of stocks for which it could be used, especially in those stocks with relatively short data records (see Blackbourn 1991).

## Results

---

In all four stocks of salmon discussed here, the effect of SST alone in accounting for variation in FWS rate is significant (Table 1). This is also true for 16 of 18 stocks in a larger study (Blackbourn 1991). In addition, in all four cases the negative relationship between SST and FWS rate is stronger than that between FWS rate and (a) spawner or egg number or (b) local environmental data during incubation.

Table 1  
FACTORS FROM THE FINAL ADULT YEAR OF SALMON THAT ACCOUNT FOR VARIATION IN  
FRESH-WATER SURVIVAL RATE OF STOCKS OF WILD AND SPAWNING-CHANNEL SALMON

Data Period	N	Area	FWS Rate	% of Adjusted Variance of FWS Rate Accounted for in:					
				Simple Regression			Multiple Regression		
				Factor	Sign	% AR <sup>2</sup>	Factor	% AR <sup>2</sup>	P
<b>Atnarko River Pinks (Wild)</b>									
1974-	10	Central	P.E.D. to live	1. Number of spawners	Neg	48	1 + 4	74	0.004
1989		Coastal	eggs and fry	2. Incub air temps	Pos	0	1 + 5	64	0.012
		British	in January	3. Incub river disch	Pos	0	1 + 4 + 5	77	0.007
		Columbia		4. Coastal SST July (Central BC)	Pos	10	1 + 2 + 5	59	0.040
				5. Gulf of Alaska SST	Neg	59			
				Jan-Mar 45-50°N, 145-150°W					
				Feb-Apr 45-50°N, 140-145°W					
<b>Seton Creek (Fraser River) Pinks (Spawning Channel)</b>									
1967-	12	South-	P.E.D. to	1. Number of eggs laid		0	3 + 4	77	0.001
1989		Central	outmigrant fry	2. Incub air temp	Pos	12	2 + 3	72	0.002
		Interior		3. Coastal SST July-Aug	Neg	27	2 + 3 + 4	86	0.000
		British		W. Vancouver Island			1 + 3 + 4	85	0.000
		Columbia		4. Gulf of Alaska SST	Neg	72	1 + 2 + 3 + 4	91	0.000
				May-Jun 45-50°N, 140-150°W					
<b>Great Central Lake Sockeye (Wild)</b>									
1978-	11	Southwestern	P.E.D. to lake	1. Number of spawners	Neg	21	4 + 5	51	0.023
1988		Vancouver	juveniles	2. Incub air temps	Neg	0	3 + 5	49	0.029
		Island (BC)		3. Near-coastal SST June	Neg	38	2 + 4 + 5	58	0.028
				4. Coastal SST July	Neg	36	3 + 4 + 5	53	0.043
				W. Vancouver Island					
				5. Gulf of Alaska SST	Neg	38			
				Mar-Apr 50-55°N, 145-155°W					
<b>Weaver Creek (Fraser River) Sockeye (Spawning Channel)</b>									
1965-	25	Southwestern	P.E.D. to	1. Number of eggs	Neg	46	5 + 6	74	0.000
1989		British	outmigrant fry	2. Female length	0	0	1 + 6	72	0.000
		Columbia		3. Incub air temp	Neg	0	1 + 5 + 6	83	0.000
				4. Coastal SST Aug-Oct	Neg	15	1 + 4 + 5 + 6	82	
				E. Vancouver Island					
				5. Coastal SST Aug	Neg	47			
				W. Vancouver Island					
				6. Gulf of Alaska SST	Neg	61			
				Jan-Feb 45-50°N, 130-145°W					

For three stocks, SST data from the Gulf of Alaska early in the final year account for more variation in FWS rate than do the later coastal data. In GCL sockeye the effect is of similar power for both types of SST data (Table 1). However, the comparisons are not balanced in that SST data from only one or two coastal locations along the migration routes are considered in each case and there is no search for strongest coefficients, whereas only those Gulf of Alaska SST data with the highest coefficients with FWS rate are used in the final comparisons.

Factor combinations from multiple regression analyses result in significant added variation in all four stocks (Table 1). In three stocks, the combination of two or three factors accounts for more than 70 percent of adjusted total variation ( $P < 0.01$ ); in GCL sockeye, three-factor combinations account for more than 50 percent of past variation in FWS rate ( $P = 0.028$ ).

Boundaries of SST areas with the strongest coefficients with FWS data for stocks of three salmon species show some, but not complete, separation (Blackbourn 1991), and distribution of "best" SST areas for each species shows an interesting parallel feature. Despite large differences in period of data record and location of spawning stream, several stocks of the same species have very similar "best" areas and times in the Gulf of Alaska (Figures 1 and 2).

Results for Seton Creek pinks confirm the earlier work with data for pinks from the whole Fraser River watershed in that there is a strong relationship between coastal SST data and FWS rate (Table 1) and, in this case, in that there is a still stronger relationship with earlier SST data from the Gulf of Alaska.

There appears to be little or no difference in the partial effect of early SST on FWS rate whether salmon stocks use natural or controlled spawning areas (Table 1).

## **Discussion**

---

These comparative analyses include data from diverse physical and biological variables. The underlying precision and accuracy of the methods used to produce these salmon data are fairly well known except for Atnarko River pinks. For example, those used for Weaver Creek sockeye are described by Woodey (1984). Paradoxically, it may be a strength in that the expected outcome of analysis of heterogeneous biological and physical data might be expected to reveal few, if any, significant associations between SST and FWS. It is probable that the consistent statistically significant associations among these data reflect some real underlying connection (see Blackbourn 1991).

The hypothesis of a previous effect of brood-year SST on FWS rate in two incubation types is supported by these analyses. The overall additive

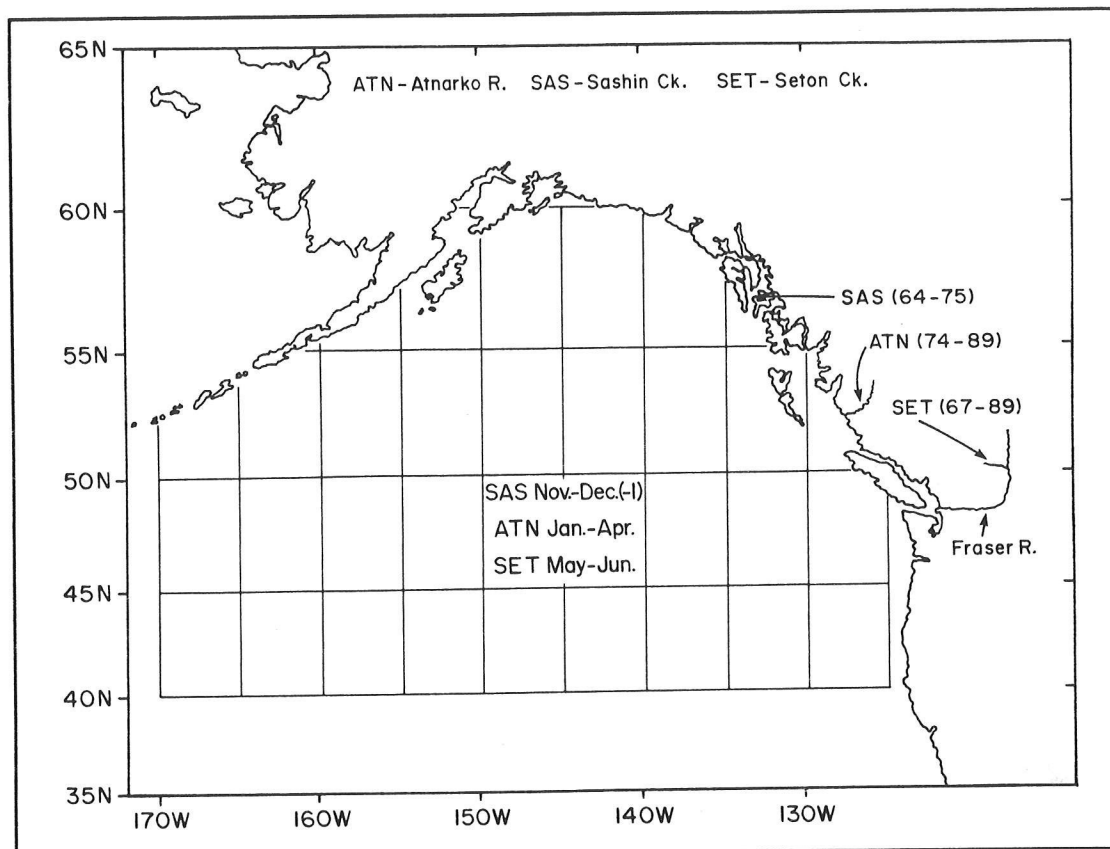


Figure 1. Sources of SST data that show the strongest correlation with the fresh-water survival rate of three stocks of pink salmon.

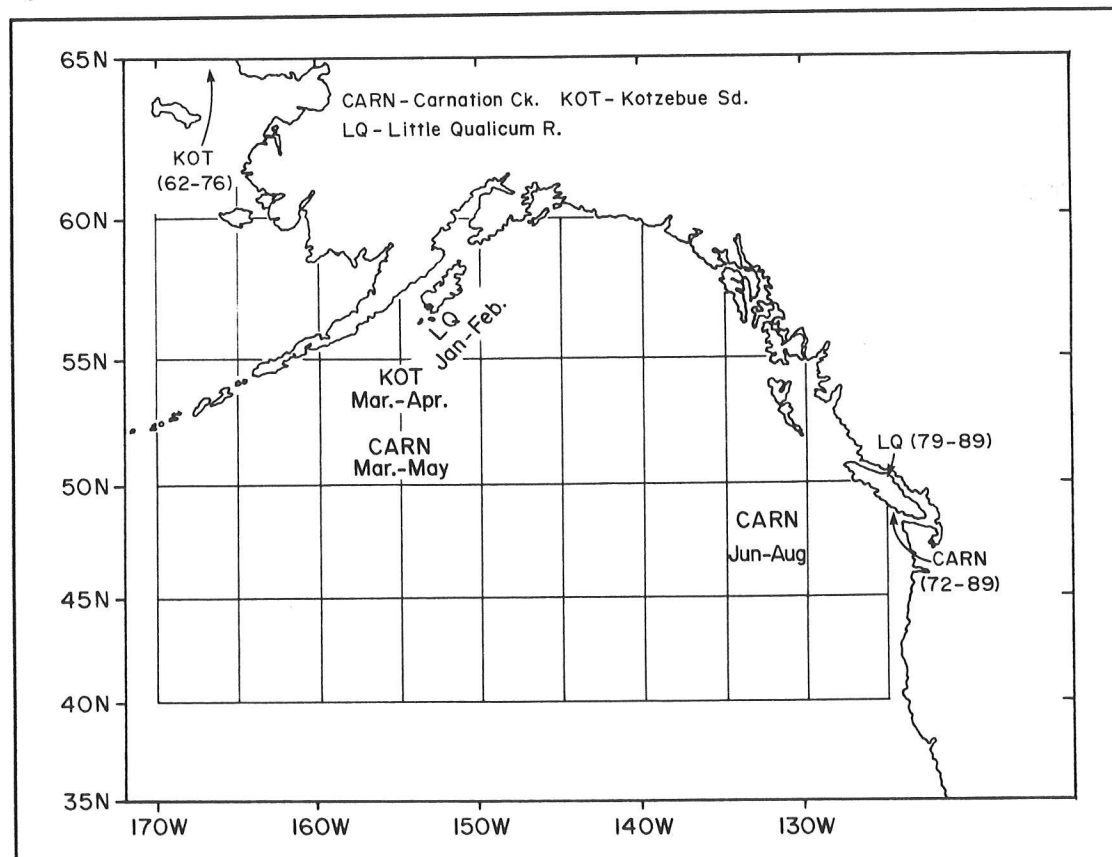


Figure 2. Sources of SST data that show the strongest correlation with the fresh-water survival rate of three stocks of chum salmon.

effect of SST on FWS rate in the multiple regression analyses is demonstrated by its occurrence in all four of these stocks and in all of which more than one factor is related to FWS rate. The particular effect of brood-year SST should be further tested by more intensive studies, particularly in those stocks for which detailed data on spawner and egg number and from the incubation environment can be readily measured. The effect of SST could be partially and experimentally investigated on fish held well before spawning at various sites along the migration path or perhaps held at fish farms with laboratory facilities.

These salmon stocks are of great economic importance. Therefore, in addition to more research, some consideration should be given in the management of such stocks to the application of:

- Final-year oceanic SST data when setting pre-season goals for spawner number.
- Coastal SST data when adjusting those goals during, or perhaps even before, the fishing season.

If these effects are real, and whether or not SST is an index for some other environmental effect on gamete quality, the short-term effect of SST may be predictable. For example, in a year that is warmer than average, a larger than average number of spawners may be necessary to obtain an average number of fry the following spring. However, because the FWS rate for a stock may also be negatively related to spawner or egg number (Table 1), the specific relationship between all these factors must be carefully considered for each stock before changes in goals for spawner number can be recommended.

Although results of the multiple regression analyses are statistically more noteworthy, from an ecological point of view results of the simple regression analyses of the effect of SST data are extremely interesting. First, in three of the four stocks, coastal SST data from locations and places thought, or in some cases known, to be appropriate to particular stocks do show moderate to strong relationships with FWS rate data for those stocks; *eg*, data from Amphitrite Point (western Vancouver Island) in July for the (very early) GCL sockeye and, for the late-summer returning Weaver Creek sockeye, data from Amphitrite Point in August and from Chrome Island (Georgia Strait) from August to October (Table 1).

Results of simple regression analyses of Gulf of Alaska SST data months before spawning are also intriguing. Areas from which SST data show the strongest relationship with FWS rates of pink and sockeye stocks are generally within the boundaries originally thought likely to show such results; *ie*, the southeastern and central Gulf of Alaska. Perhaps the most interesting result of all is that stocks of pinks and chums from widely separated spawning locations and different time-periods have very similar locations and periods for their "best" Gulf of Alaska SST data. These results give some credence to the idea that subtle effects of the ocean

environment on the freshwater survival rate of salmon via gamete development may be real and, in some cases, as important or much more important than the more obvious local fresh water environmental factors. This type of transfer of the oceanic "history" of the salmon into fresh water represents a new form of link between two completely different environments.

The possible warming of the ocean and rivers in the next 50 years due to increased amounts of "greenhouse" gases is already of concern to salmon biologists. The potential warming has been considered important to both freshwater and marine phases of the life cycle of salmon; and present and potential fresh water and ocean temperatures are investigated for each phase respectively, particularly for vulnerable stocks in the southern part of the range for each species.

Consideration of data such as those discussed in this paper add a further concern. The time and place of future changes in ocean climate may be important not only to such salmon parameters as marine survival rates, marine growth rates, fecundity, migration timing and routes, *etc.*, but also to the subsequent fresh water survival rates of the eggs of returning adults. In this respect it may be important to remember that, in the recent past, SST anomalies have been of different strengths and even of the opposite sign in various parts of the northeastern Pacific and the Gulf of Alaska. If the future ocean climate contains a similar amount of temporal and spatial heterogeneity, then the future fresh water survival rate of a particular stock may not be entirely directed by environmental trends at or near the spawning location. Also, to judge by these results, future trends in fresh water survival rate of stocks of different species (*eg.* pinks and chums) at the same spawning locations could be environmentally mediated to a different degree or even in a different direction.

## **Acknowledgments**

---

For provision of unpublished salmon data I am gratefully indebted to the following people from the Canada Department of Fisheries and Oceans:

- > Atnarko River pinks — R. Hilland
- > Seton Creek (Fraser River) pinks — D. Hickey
- > Great Central Lake sockeye — K. Hyatt
- > Weaver Creek (Fraser River) sockeye — D. Harding

I thank L. Giovando and H. Freeland, Department of Fisheries and Oceans, for recent unpublished sea surface temperature data from British Columbia shore stations, and Dr. D. McLain (now of NOAA), Monterey, California, for the use of his unpublished SST data.

## References

---

- Blackbourn, DJ. 1984. Sea surface temperature and return timing in North American Pacific Salmon. pp 111-119 in *1983 Northeast Pink and Chum Salmon Workshop*, K Fresh and S Schroeder (eds). Orcas Island, WA, January 1983.
- \_\_\_\_\_. 1987. Sea surface temperature and the pre-season prediction of return timing in Fraser River sockeye salmon (*Oncorhynchus nerka*). pp 296-306 in *Sockeye salmon (*Oncorhynchus nerka*) population biology and future management* (HD Smith, L Margolis, and CC Wood, eds). Can. Spec. Publ. Fish. Aquat. Sci. 96.
- \_\_\_\_\_. 1991. Brood-year sea surface temperature and the subsequent freshwater survival rate of wild and enhanced stocks of North American pink, chum, and sockeye salmon. pp 122-138. in *Proc. 15th Northeast Pacific Pink and Chum Salmon Workshop* (B White and I Guthrie, eds), Parksville, BC, Canada, February 27 to March 1, 1991.
- \_\_\_\_\_. In Prep. The climate of the Northeast Pacific and the migration of Fraser River sockeye salmon: Some recent mysteries.
- Freeland, HJ. 1990. Sea surface temperatures and salinities along the coast of British Columbia: Regional evidence for a warming trend. *Can. J. Fish. Aquat. Sci.* 47(2):346-350.
- Giovando, LF. 1983. Observations of seawater temperature and salinity at British Columbia shore stations, 1980. *Can. Data Rep. Hydrogr. Ocean Sci.* 9:133.
- Salo, EO. 1991. Life history of chum salmon (*Oncorhynchus keta*). In *Pacific Salmon life histories* (C Groot and L Margolis, eds). University of British Columbia Press, Vancouver, BC.
- Takagi, K, KV Aro, AC Hartt, and MB Dell. 1981. *Distribution and origin of pink salmon (*Oncorhynchus gorbuscha*) in offshore waters of the North Pacific Ocean*. Int. N. Pac. Fish. Comm. Bulletin 40.
- Walters, CJ. 1990. A partial bias correction factor for stock-recruitment parameter estimation in the presence of autocorrelated environmental effects. *Can. J. Fish. Aquat. Sci.* 47(3):516-519.
- Woodey, JC. 1984. Escapement estimation in the management of Fraser River sockeye salmon. pp 121-132 in *Proceedings of the workshop on stream indexing for salmon escapement estimation* (PEK Symons and M Waldichuk, eds) West Vancouver, BC, February 2-3, 1984. Can. Tech. Rep. Fish. Aquat. Sci. 1326.

# Climate Change and Salmonid Production in the North Pacific Ocean

Robert C. Francis

Extreme catches of northeastern Pacific salmon seem to be frequent rather than rare events. Throughout the 1960s and early 1970s, record high catches were realized for stocks originating in streams of Washington, Oregon, and California, while record low catches occurred in the valuable commercial salmon fisheries of Alaska. A major shift in relative fortunes took place beginning in the late 1970s. Recent production of salmon has been so high in Alaska that prices have fallen drastically and much of the product cannot be sold profitably. Conversely, salmon production along the West Coast has fallen so low that the Pacific Fishery Management Council recently considered an option that would eliminate ocean sport and commercial harvest in 1992 from California to Washington. Both sudden declines and increases in salmon production have been either blamed on or credited to a number of natural and anthropogenic factors, "the environment" always being mentioned but in a rather nebulous manner. These recent issues, however, highlight the critical need to understand the long-term effects of the marine environment on the production of northeastern Pacific salmonid stocks and fisheries.

Climate fluctuations and their subsequent oceanic impacts are becoming recognized as important phenomena affecting low-frequency (interdecadal) shifts in large marine ecosystems, resulting in subsequent shifts in marine fisheries production. A recent NOAA plan (NOAA 1989) indicates that, with respect to long-term (interdecadal) shifts in fishery production, a major question that needs to be addressed is: How are large-scale atmospheric and oceanic processes linked to major changes in fish community structure? That is the focus of a research project being conducted, under the support of Washington Sea Grant, by Stephen Riser (University of Washington Department of Oceanography), Warren Wooster (University of Washington School of Marine Affairs) and me. Our specific biological focus is on Pacific salmon for a number of reasons that will be explained later. In general, however, we are attempting to understand the causes and marine biological manifestations of interdecadal shifts in North Pacific atmosphere and ocean regimes.

This paper contains three sections. The first presents an overview of the northeastern Pacific in terms of its component large marine ecosystems and their defining physics and biology. The second attempts to answer the question, why salmon? And the third presents a very rough and

highly speculative model of how atmosphere, ocean, and marine biological production are linked in the North Pacific, resulting in low-frequency and not necessarily in-phase shifts in fisheries production of the major regions.

## Large Marine Ecosystems of the Northeastern Pacific

Physical oceanographers have identified specific domains in the upper zone of the northeastern Pacific Ocean where water properties are influenced predominantly by seasonal heating and cooling, precipitation, evaporation, and wind mixing (Ware and McFarland 1989). Four of these are critical to the structure and dynamics of northeastern Pacific fisheries production.

The **Transitional Domain** (Figure 1) is one of the main oceanic features of the North Pacific. It lies between the subarctic and subtropical gyres and extends from Japan to North America (Roden 1991). The domain, which lies between the subarctic boundary and the Central Subarctic Domain, is defined on both its northern and southern boundaries by strong salinity and temperature fronts extending from the surface to a depth of about 250 meters (Roden 1975, 1991; Percy 1991). The eastward zonal flow in this region is referred to as the Subarctic Current (Figure 1). In the western Pacific this region is defined by the confluence

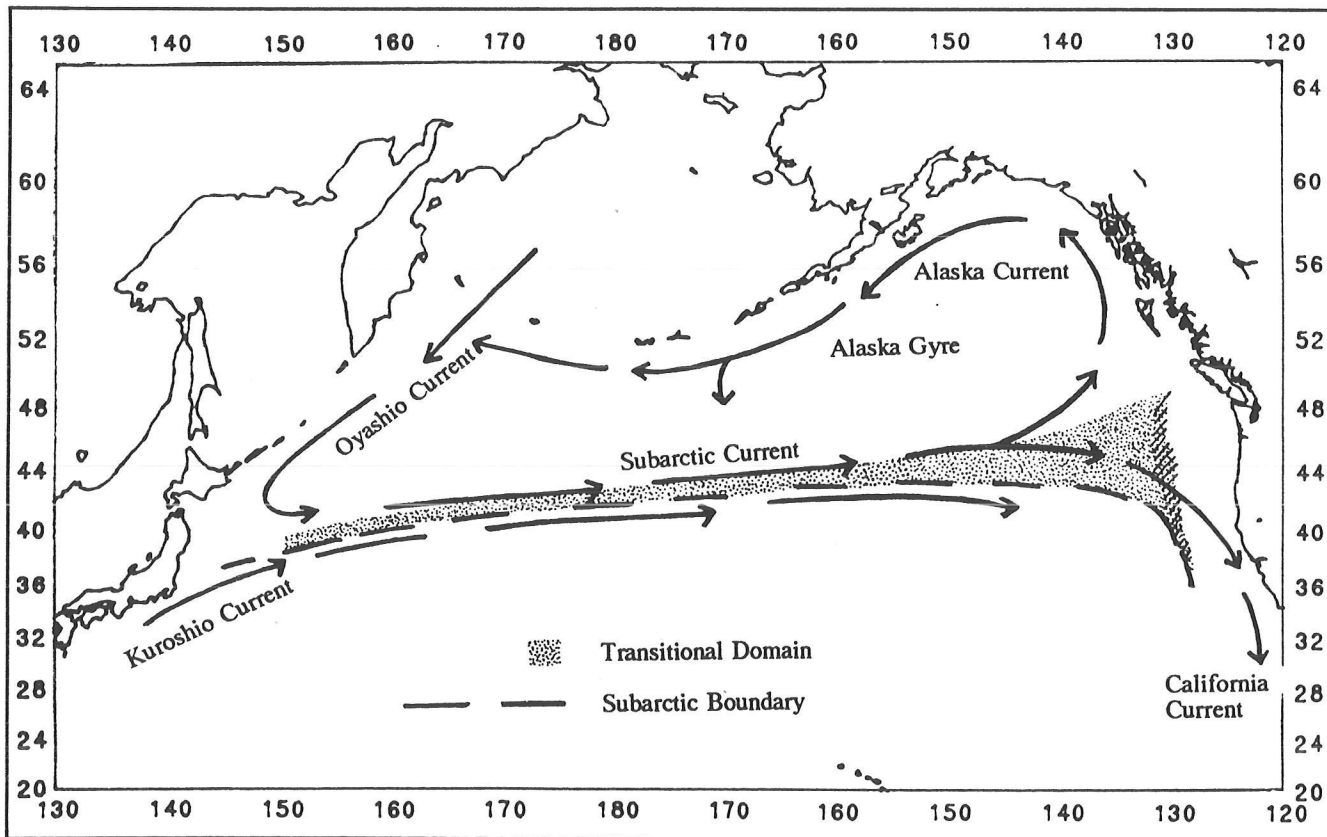


Figure 1. Relevant large-scale upper-level physical oceanography of the Subarctic North Pacific.

of the Oyashio and Kuroshio currents. Conditions influencing formation of the Subarctic Boundary and Subarctic Current are extremely variable (Favorite *et al* 1976; Kawasaki 1983). In the northeastern Pacific, the eastward flowing Subarctic Current separates into two streams about 800 kilometers off shore. One branch (Alaska Current) veers northward and flows into the Gulf of Alaska; the other branch flows southward to form the California Current. This frontal structure, strong eastward zonal flow, and bifurcation at the North American coast are major physical factors that define the other three oceanic domains critical to northeastern Pacific fisheries production (Ware and McFarland 1989). In the summer, large concentrations of flying squid have been harvested by Asian pelagic drift-net fisheries operating in the Transitional Domain.

The **Coastal Upwelling Domain** (California Current) lies off the coast of Washington, Oregon, and California and is a subarctic water mass contained within the southern component of the Subarctic Current bifurcation. This domain is defined by wind-driven equatorward surface flow in the spring and summer resulting in episodic upwelling of cold nutrient-rich water and poleward surface flow in the autumn and winter, during which time downwelling prevails (Percy 1991). The transition from poleward to equatorward flow occurs abruptly in the spring and the reverse transition occurs somewhat less abruptly in the autumn. This domain is dominated by a unique assemblage of pelagic species common to most of the major eastern boundary current regions of the world.

The **Coastal Downwelling Domain** (Alaska Current) lies off the coast in the Gulf of Alaska and is a subarctic water mass contained within the northern component of the Subarctic Current bifurcation. This domain seems to exhibit considerably larger interannual fluctuations than seasonal fluctuations in flow (Reed and Schumacher 1987). At present, it is not clear whether or how the dynamics and intensity of the Alaska Current respond to a very large annual signal in wind and precipitation in the Gulf of Alaska, which is dominated in summer by the North Pacific High and in winter by the Aleutian Low and its accompanying intense cyclonic pressure systems (Royer 1983). Waters contained within the Coastal Downwelling Domain support major salmon, groundfish, crustacean, and herring fisheries.

The **Central Subarctic Domain** lies in the central Gulf of Alaska and is defined by the Alaska Gyre, which rotates in a cyclonic direction. According to Brodeur and Ware (1992), upwelling occurs in the core of the gyre because of a wind-induced divergence in the upper oceanic layer, thus making the domain relatively productive for an oceanic region (Brodeur and Ware 1992). The Central Subarctic Domain serves as an oceanic pasture for many of the Pacific salmon stocks harvested along the northeastern Pacific coast from Alaska to California.

For our research, one of the most striking features associated with the interactions between domains is that a number of physical variables associated with atmospheric conditions (*eg*, temperature, coastal upwelling) and the biological responses of fish in the Alaska and California currents are out of phase (Tabata 1991; Hollowed and Wooster 1991). In our initial work, we have found similar responses in salmonid production (Figure 2). Furthermore, Wickett (1967) and Chelton (1983) speculate that the strengths of the Alaska and California currents apparently fluctuate out of phase. That is, when one of the currents is stronger than normal, the other is weaker. They hypothesize that these north-south shifts in the bifurcation of the subarctic current could be forced by physical factors at or upstream of the bifurcation. Tabata (1991), on the other hand, indicates this "apparent" out-of-phase relationship could be partially due to the influence of in-phase coastal currents that extend from south of the coast of California to Canada. Linked to this is the hypothesis that the fronts that define the Transitional Domain are highly variable in their location. Kawasaki (1983) indicates that in the western Pacific the stream axis of the Kuroshio Current shifts dramatically from year to year and has a significant impact on long-term fluctuations in abundance of Far Eastern sardine. Fulton and LeBrasseur (1985) show evidence of extreme northward shifting of the eastern extension of the Subarctic Boundary in response to anomalous warming events.

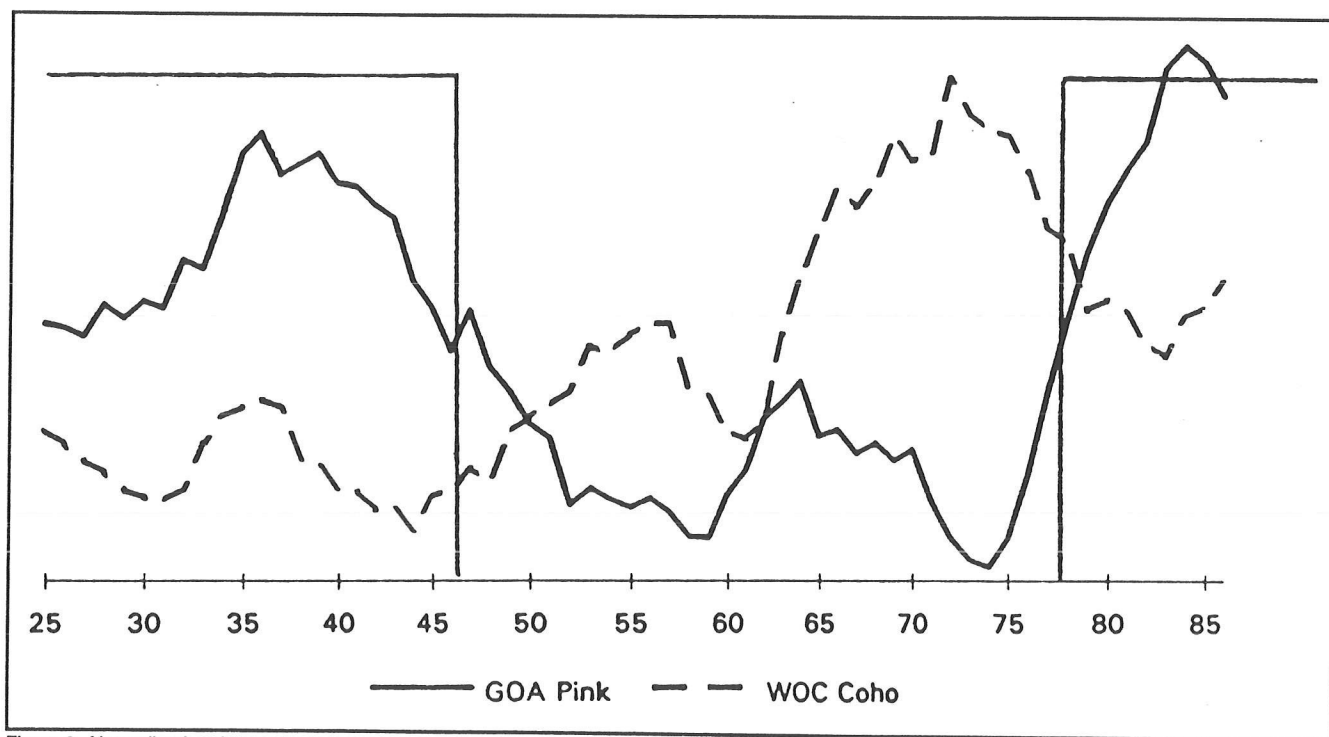


Figure 2. Normalized and smoothed (5-year running mean) pink salmon catch in the Gulf of Alaska and coho salmon catch in the Washington/Oregon/California region.

## Why Salmon?

---

Pacific salmon are unique in the northeastern Pacific pelagic ecosystem in that their life histories depend on and integrate the physical dynamics of all four of the domains described in the previous section. In addition, the five principal salmonid species (pink, chum, sockeye, coho, and Chinook) have very different marine life histories. Pink, chum, and sockeye are considered oceanic, spending a major part of their marine life histories in the Central Subarctic Domain, whereas some stocks of coho and Chinook may remain in coastal waters for their entire marine life. In addition, because of a long history of high-valued exploitation, accurate records of salmonid harvest exist for most of the region for more than a century.

The most important aspects of biological production, with particular reference to salmonids, involve major long-term (interdecadal) fluctuations and synchrony in these trends between different oceanic domains of the northeastern Pacific, as well as between distant regions of the Pacific. Combined with this is the fact that the dynamics of salmon production for a particular domain seem to reflect low-frequency couplings of atmospheric and oceanic processes. This is described in the next section.

Examination of the time series of total landings of Pacific salmon throughout the North Pacific (Shepard *et al* 1985) shows landings peaked in the late 1930s and early 1940s, dropped off in the late 1940s through early 1970s, and peaked again in the late 1970s and 1980s. Areal breakdowns of Pacific salmon catch statistics reveal these peaks were due mainly to high catches of sockeye salmon in western Alaska (primarily Bristol Bay), pink salmon in central and southeastern Alaska, and Asian chum salmon. All three of these species are considered oceanic, occupying the Central Subarctic Domain for a significant part of their marine life histories. Ware and McFarland (1989) estimate the mean salmonid biomass of the Central Subarctic Domain has increased from a low of 480,000 metric tons between 1956 and 1972 to 820,000 metric tons between 1973 and 1984.

Abundance of coastal salmonid species, including coho and Chinook, which predominate in the coastal region from southeastern Alaska to California, as well as stocks of southern chum, was out of phase with the trends for oceanic salmonids (Figure 2). Catches of coho, Chinook, and southern chum were relatively high during the 1960s and 1970s and then declined beginning in the late 1970s. Rogers (1987) hypothesizes that there is either a competitive interaction between southern and northern stocks or an inverse relationship between oceanic conditions favorable for survival. Similar relationships have been discussed by others (*eg*, Peterman and Wong 1984).

## **A Speculative Model**

---

In an attempt to tie together the multidisciplinary nature of our Sea Grant-sponsored research project, we have arrived at a very rough and highly speculative model of how atmosphere, ocean, and marine biological production are linked in the North Pacific, resulting in low frequency and not necessarily in-phase shifts in fisheries production of the major domains. Hollowed and Wooster (1991) hypothesize two mean states of winter atmospheric circulation in the North Pacific — termed Type B and Type A (Figure 3, upper right and lower right panels).

Type B is characterized by (Figure 3, upper right panel):

- A strong winter mean Aleutian Low (AL) with its center located to the east,
- Enhanced southwesterly winds in the northeastern Pacific,
- A more southerly bifurcation of the Subarctic Current,
- Enhanced northward flow at the bifurcation, resulting in increased advection of subarctic water into the Alaska Current,
- Decreased advection into the California Current,
- Positive SST anomalies (+T) throughout the northeastern Pacific and a negative SST anomaly in the central North Pacific (centered on 40°N) (Figure 3, upper left panel).

Type A is characterized by (Figure 3, lower right panel):

- A weak winter mean Aleutian Low (AL) with its center located in the western North Pacific,
- Enhanced westerly winds in the NE Pacific,
- A more northerly bifurcation of the Subarctic Current,
- Enhanced southward flow at the bifurcation resulting in increased advection of subarctic water into the California Current,
- Decreased advection into the Alaska Current,
- Negative sea surface temperature (SST) anomalies (-T) throughout the northeastern Pacific and a positive SST anomaly in the central North Pacific (centered on 40°N) (Figure 3, lower left panel).

The middle panel of Figure 3 shows normalized and smoothed mean Kodiak winter (November-March) air temperature and Gulf of Alaska pink salmon (the dominant species) catches. What is striking is the astounding correlation of overall pattern between these two time series. We hypothesize that abrupt shifts in both winter temperature (winter Gulf of Alaska atmospheric and oceanic temperatures highly correlated) and salmon production (reflected in catch statistics) are related to abrupt shifts between these two mean states of the North Pacific atmosphere and

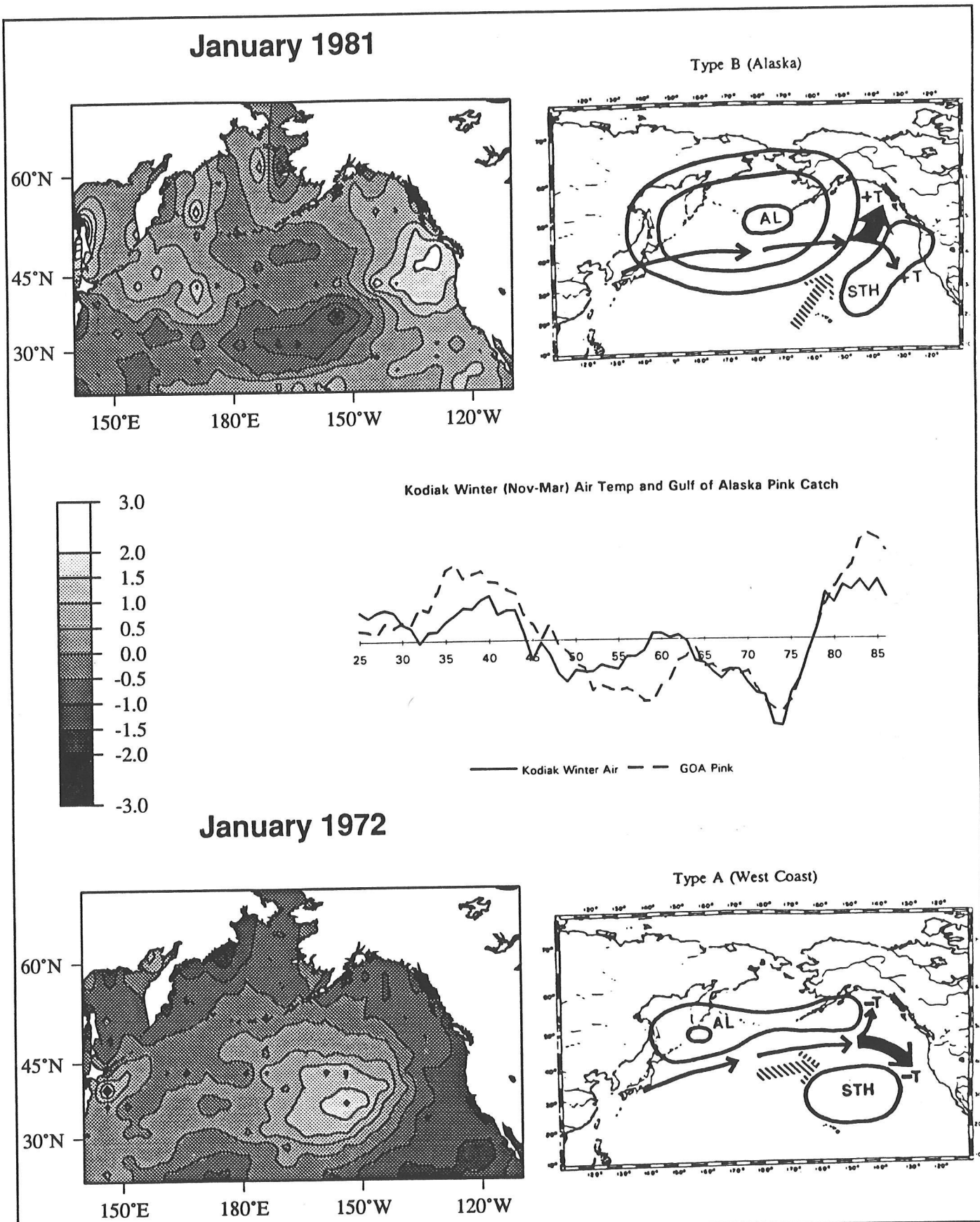


Figure 3. Two hypothesized states of winter atmospheric and oceanic circulation in the North Pacific (after Hollowed and Wooster 1991).  
(Color copy of this figure is available from the author.)

ocean. Hollowed and Wooster (1991) further point out that over the last 60 years the switch from Type-A state to Type-B state has always occurred at the time of significant El Niño events (eg, 1925-26, 1940-41, 1957-58, 1976).

Figure 4 further illustrates how these circulation patterns might relate to long-term trends in northeastern Pacific salmonid production. In the top panel we have plotted:

- Hollowed and Wooster's time series of Type-B and Type-A states from 1925 to 1985,
- Normalized and smoothed Kodiak Island winter air temperature,
- Extreme high and low values of the Central North Pacific (CNP) winter atmospheric pressure index (Cayan and Peterson 1989), which is highly correlated with both the Pacific-North American (PNA) teleconnection pattern (Horel and Wallace 1981) and the intensity of the winter Aleutian Low.

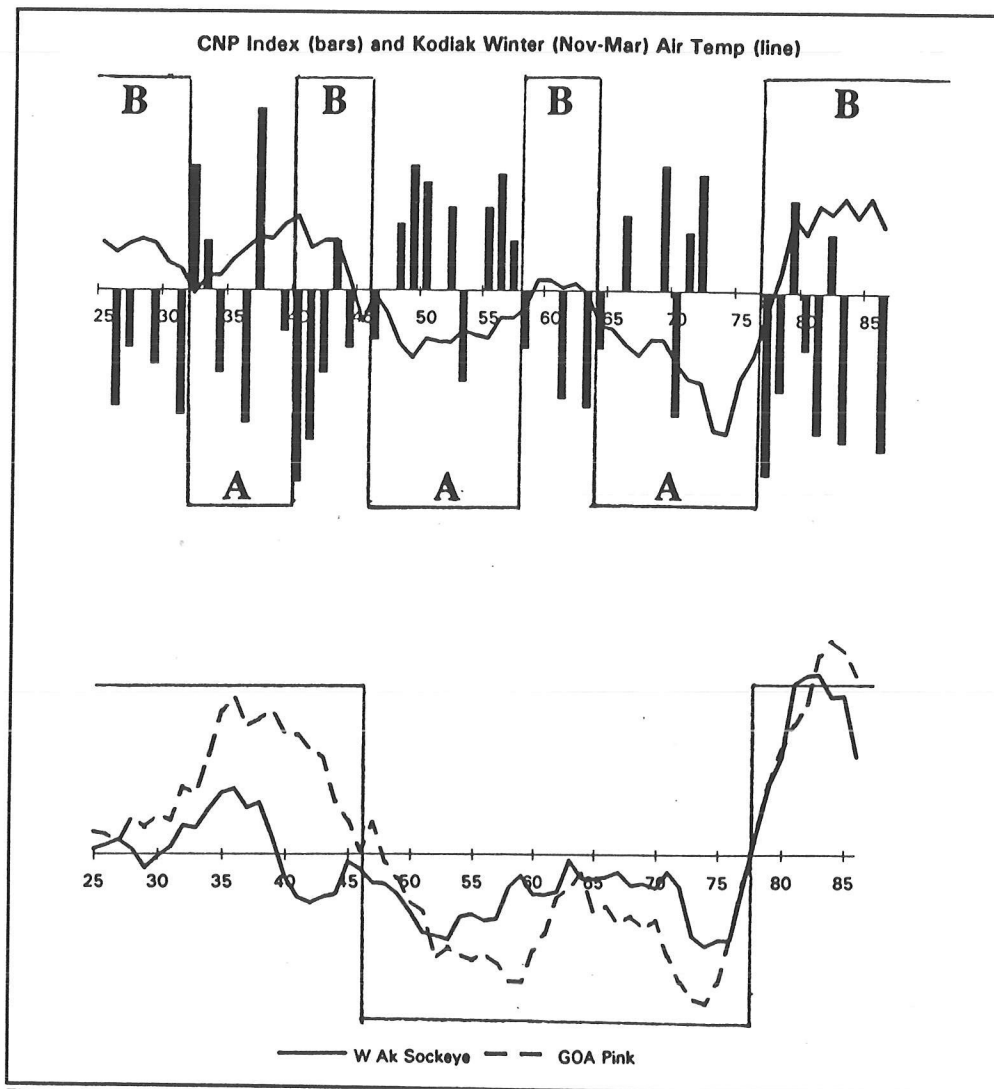


Figure 4. Relationships between Type A/B circulation, Central North Pacific Index, normalized and smoothed Kodiak winter air temperature, western Alaska sockeye salmon catch, and Gulf of Alaska pink salmon catch.

In the bottom panel of Figure 4, we have plotted normalized and smoothed western Alaska sockeye and Gulf of Alaska pink salmon catches, which are the predominant species caught in these two regions. Not only are the long-term patterns similar, but they also show striking correspondence to winter temperature patterns in the upper panel and, in turn, to hypothesized atmosphere/ocean patterns represented by the CNP index and the Type A/B oscillations. Patterns in Alaska salmon production also tend to indicate longer periods of oscillating “warm” and “cool” regimes (early 1920s to late 1940s/early 1950s, early 1950s to mid-1970s, mid-1970s to present). Finally, the hypothesized out-of-phase behavior of the long-term production dynamics of the Alaska Current (GOA Pink) and California Current (WOC Coho) production domains is shown in Figure 2.

## **Epilogue**

---

As an epilogue to what I presented at the 1992 PACLIM meeting, I would like to report on some further developments in this research project that resulted directly from having the chance to meet at PACLIM with multidisciplinary scientists working on other aspects of this same problem. This was my first PACLIM meeting and I was impressed with the general theme of a continuous scientific process, with ideas, concepts, and dialogues being carried on between scientists from one year to the next.

Sus Tabata emphasized that I had somewhat misinterpreted his paper (Tabata 1991) concerning possible mechanisms that might cause the relative intensities of the California and Alaska Currents to be out of phase. He pointed my attention to the role of the coastal currents and undercurrents in the California Current system and how their in-phase relationships might affect apparent out-of-phase relationships in the California-Alaska Currents. This, in turn, links to a discussion with Tim Baumgartner who interprets the intensification of these coastal counter currents and weakening of the California Current as “poleward expansions of tropical influences”.

Tom Murphree and George Kiladis opened my eyes to atmosphere/ocean connections between the equator and North Pacific and the importance of the Western Pacific Warm Pool and Subtropical Jet to those connections. Based on discussions with Tom and George and readings they suggested, I have now learned that:

- The extratropical atmospheric response to anomalies in the tropical Pacific are strongest and most clearly defined in response to tropical warm episodes during the Northern Hemisphere winter,
- Subtle dynamics of the Western Pacific Warm Pool, associated with the ENSO cycle, may have a profound effect on Northern Hemisphere winter circulation, and

- The strong extratropical teleconnection during ENSO events generally occurs when the SST in the far western Pacific is anomalously warm (or at least not too cold).

Closing the circle somewhat, three of the four hypothesized shifts from Type-A to Type-B states in the North Pacific given in Figure 4 (1925/26, 1941/42 and 1976/77) coincide with ENSO winters reported by Hamilton (1988) to have the highest SST in the far western Pacific.

## References

---

- Brodeur, RD, and DM Ware . 1992. Interannual and interdecadal changes in zooplankton biomass in the subarctic Pacific Ocean. *Fisheries Oceanography* (1).
- Cayan, DH., and DH Peterson. 1989. The influence of North Pacific atmospheric circulation on streamflow in the west. pp. 375-398 in DH Peterson (ed), *Aspects of Climate Variability in the Pacific and Western Americas*. AGU Geophysical Monograph 55.
- Chelton, DB. 1983. Commentary: Short-term climatic variability in the Northeast Pacific Ocean. pp. 87-99 in WG Pearcy (ed), *The Influence of Ocean Conditions on the Production of Salmonids in the North Pacific*. OSU Sea Grant Publ. ORESU-W-83-001.
- Favorite, F, AJ Dodimead, and K Nasu. 1976. Oceanography of the subarctic Pacific region, 1960-71. *Int. North Pac. Fish. Com. Bull.* 33. 187 pp.
- Fulton, JD, and RJ LeBrasseur. 1985. Interannual shifting of the subarctic boundary and some biotic effects on juvenile salmonids. pp. 237-252 in WG Wooster and DL Fluharty (eds), *El Niño North*. Wash. Sea Grant Publ. WSG-W085-3.
- Hamilton, K. 1988. A detailed examination of the extratropical response to tropical EL Niño/Southern Oscillation events. *J. of Climatology* 8: 67-86.
- Hollowed, AB, and WS Wooster. 1991. Year class variability of marine fishes and winter ocean conditions in the Northeast Pacific Ocean. ICES Variability Symp. Paper No. 33, Session 3.
- Horel, JD, and JM Wallace. 1981. Planetary-scale atmospheric phenomena associated with the Southern Oscillation. *Month. Weath. Rev.* 109: 813-829.
- Kawasaki, T. 1983. Why do some pelagic fisheries have wide fluctuations in their numbers? Biological basis of fluctuations from the viewpoint of evolutionary ecology. pp. 1081-1111 in GD Sharp and J Csirke (eds), *Proceedings of the Expert Consultation to Examine Changes in Abundance and Species Composition of Neritic Fish Resources*. San Jose, Costa Rica. April 1983. FAO Fish. Rep. 291 (3).
- NOAA. 1989. Recruitment Fisheries Oceanography. Program Development Plan.
- Pearcy, WG. 1991. Biology of the transition region. pp. 39-56 in J Wetherall (ed), *Biology, Oceanography, and Fisheries of the North Pacific Transition Zone and Subarctic Frontal Zone*. NOAA Tech. Rep. NMFS 105.
- Peterman, RM, and FYL Wong. 1984. Cross correlations between reconstructed ocean abundances of Bristol Bay and British Columbia sockeye salmon (*Oncorhynchus nerka*). *Can J. Fish. Aquat. Sci.* 41: 1814-1824.
- Reed, RK, and JD Schumacher. 1987. Physical oceanography. pp. 57-76 in DW Hood and ST Zimmerman (eds), *The Gulf of Alaska: Physical Environment and Biological Resources*. Alaska Office, Ocean Assessment Division, NOAA, Washington, DC.

- Roden, GI. 1975. On the North Pacific temperature, salinity, sound velocity and density fronts and their relation to the wind and energy flux fields. *J. Phys. Ocean.* 5: 557-571.
- \_\_\_\_\_. 1991. Subarctic-subtropical transition zone of the North Pacific: Large-scale aspects and mesoscale structure. pp. 1-38 in J Wetherall (ed), *Biology, Oceanography, and Fisheries of the North Pacific Transition Zone and Subarctic Frontal Zone*. NOAA Tech. Rep. NMFS 105.
- Rogers, DE. 1987. Pacific salmon. pp. 461-476 in DW Hood and ST Zimmerman (eds), *The Gulf of Alaska: Physical Environment and Biological Resources*. Alaska Office, Ocean Assessment Division, NOAA, Washington, DC.
- Royer, TG. 1983. Annual and interannual variability of temperature and salinity in the Gulf of Alaska with emphasis on coastal waters. pp. 244-255 in WG Pearcy (ed), *The Influence of Ocean Conditions on the Production of Salmonids in the North Pacific*. OSU Sea Grant Publ. ORESU-W-83-001.
- Shepard, MP, CD Shepard, and AW Argue. 1985. Long-term trends in the contributions of salmon from different geographical areas to the commercial fisheries of the North Pacific. *Can Tech. Rep. Fish. Aquat. Sci.* 1376.
- Tabata, S. 1991. Annual and interannual variability of baroclinic transports across Line P in the Northeast Pacific Ocean. *Deep Sea Research* 38: 5221-5245.
- Ware, DM, and GA McFarland. 1989. Fisheries production domains in the Northeast Pacific Ocean. *Can. Spec. Publ. Fish. Aquat. Sci.* 168: 359-379.
- Wickett, WP. 1967. Ekman transport and zooplankton concentration in the North Pacific Ocean. *J. Fish. Res. Bd. Can.* 24: 581-594.



# Year-to-Year Changes of Vertical Temperature Distribution in the California Current Region: 1954 to 1986

Jerrold G. Norton and Douglas R. McLain

Studies by Enfield and Allen (1980), McLain *et al* (1985), and others have shown that anomalously warm years in the northern coastal California Current correspond to El Niño conditions in the equatorial Pacific Ocean. Ocean model studies suggest a mechanical link between the northern coastal California Current and the equatorial ocean through long waves that propagate cyclonically along the ocean boundary (McCreary 1976; Clarke 1983; Shriver *et al* 1991). However, distinct observational evidence of such an oceanic connection is not extensive. Much of the supposed El Niño variation in temperature and sea level data from the coastal California Current region (Figure 1) can be associated with the effects of anomalously intense north Pacific atmospheric cyclogenesis, which is frequently augmented during El Niño years (Wallace and Gutzler 1981; Simpson 1983; Emery and Hamilton 1984). This study uses time series of ocean temperature data to distinguish between locally forced effects, initiated by north Pacific atmospheric changes, and remotely forced effects, initiated by equatorial Pacific atmospheric changes related to El Niño events.

## Data Series

Seven time series of monthly mean values from 1953 to 1986 were developed for correlation studies. These were five series of average regional ocean temperature at 0, 50, 100, 200 and 300 meter depths and two series of sea level atmospheric pressure (SLP): one from Darwin, Australia (12.4°S x 130.9°E), and the other from 45°N x 165°W in the northeastern Pacific (Figure 2).

For the ocean temperature series,  $1.9 \times 10^4$  ocean temperature profiles were extracted from the U.S. Navy Fleet Numerical Oceanographic Center Master Oceanographic Observation Data Set (version 4) for the study region and sorted into six subareas (Figure 1). Monthly mean anomaly values were computed from the profile information and divided by the standard deviation of the monthly means at each depth and for each subarea. This allows intercomparison of depths and equal weighting between subareas. Unit magnitude of standardized anomaly (1 sdu) is about 1.0°C above 50 meters, 0.6°C at 100 meters, and 0.5°C below 150 meters.

In: K.T. Redmond and V.L. Tharp, Editors. 1993. Proceedings of the Ninth Annual Pacific Climate (PACCLIM) Workshop, April 21-24, 1992. California Department of Water Resources, Interagency Ecological Studies Program, Technical Report 34.

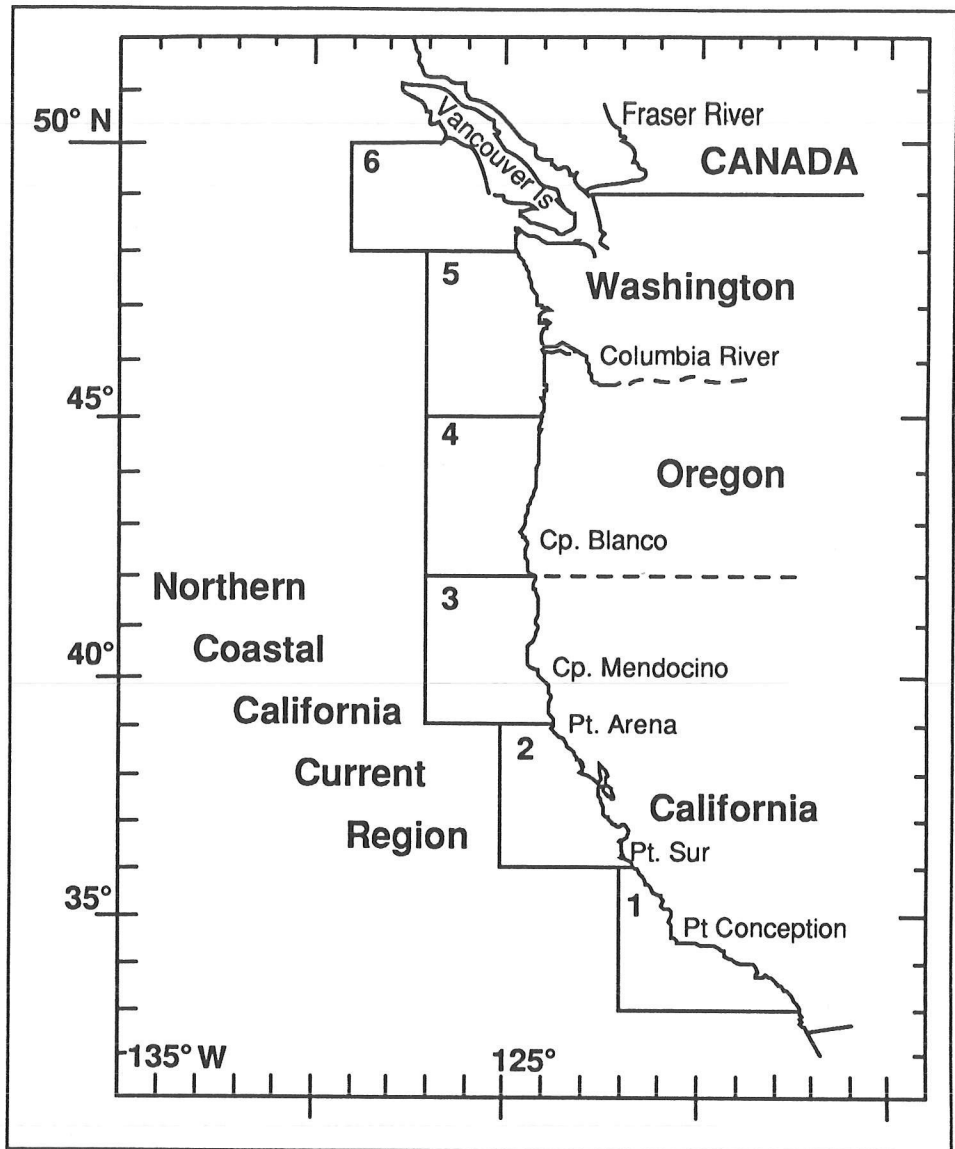


Figure 1. Location of the subareas where standardized monthly temperature anomaly values were computed.

The standardized anomalies for the six subareas were averaged to give a single monthly anomaly value, representative of the entire northern coastal California Current region. Monthly anomalies for the entire region were then averaged to give a single standardized anomaly value ( $A_{z,yr}$ ) for the 6-month (September through February) fall and winter seasons. This value was computed for each depth ( $z$ ) and year ( $yr$ ). The above data-averaging processes focuses analysis on environmental events of greater than a 6-month period. Equal weighting of the six subareas brings emphasis to large-scale processes that tend to have areawide coherence. The year designation for the fall/winter period ( $yr$ ) is that of the fall.

The SLP at Darwin, Australia, is a frequently used indicator of Indonesian Low pressure system development and strength of the equatorial trade winds (Trenberth 1984). The rationale for using this indicator of equatorial Pacific forcing is that an increase in SLP at Darwin is one of the early steps in a sequence of processes that may lead to anomalous warming or

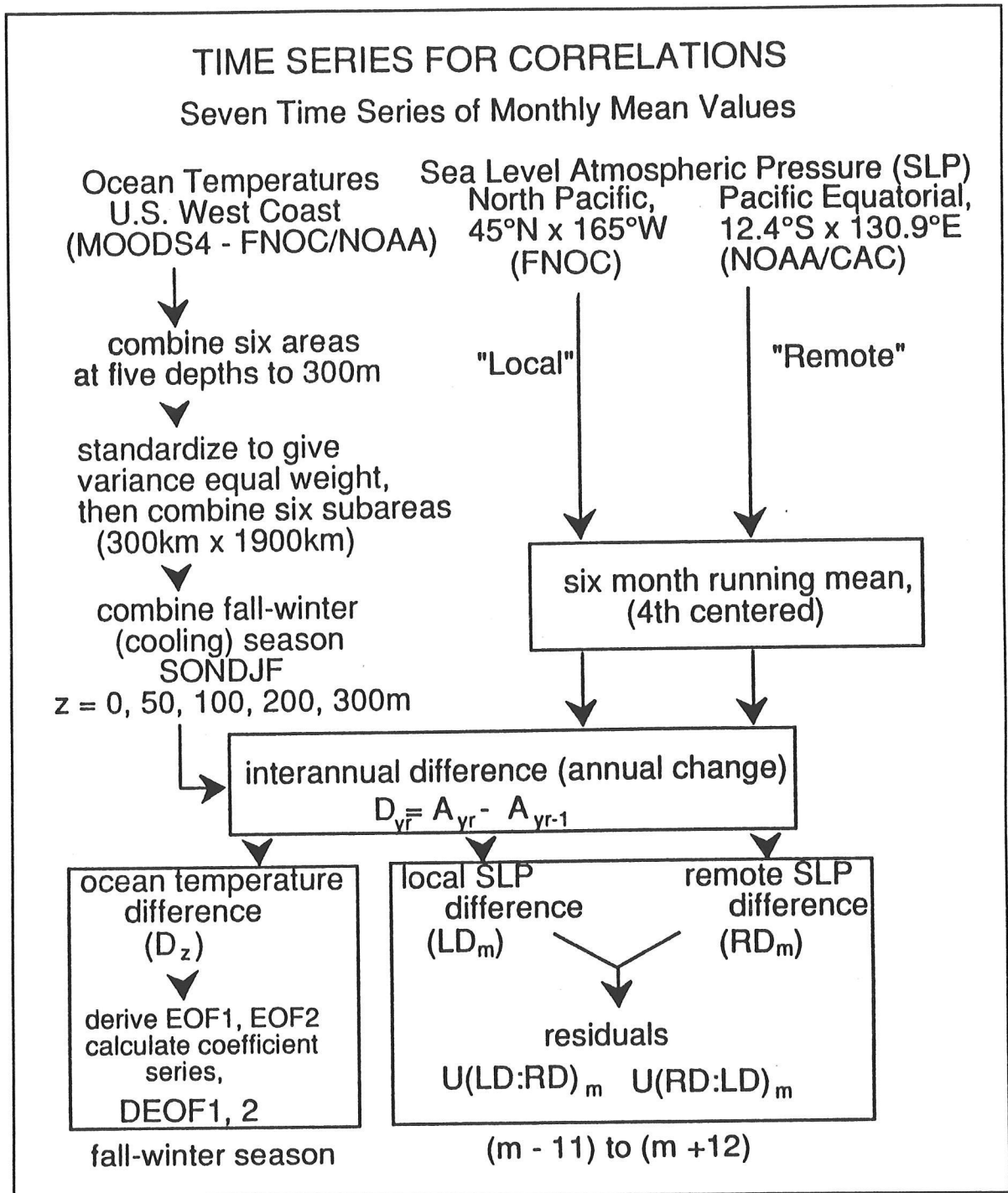


Figure 2. Summary of computations to derive time series for correlation tests. All series used were either inter-annual differences of 7 monthly mean series ( $D_z$ ,  $RD_m$ ,  $LD_m$ ) or derived from them (DEOF1,  $U(LD:RD)_m$ , etc).

cooling in the eastern equatorial Pacific. Monthly mean values for Darwin SLP were derived by averaging all daily values for the month. The series was then smoothed with a 6-month running mean, with the resulting mean values assigned to the fourth month. All "Pacific equatorial" or "remote" forcing indicators were derived from this smoothed series.

The monthly mean SLP at 45°N x 165° W in the northeastern Pacific was selected as an indicator of Aleutian Low cyclogenesis and large-scale local forcing. This location is not the center of greatest seasonal development of the Aleutian Low, but it is near the center of maximum seasonal variation (Horel and Wallace 1981). It is also one of the four locations used by Horel and Wallace (1981) to describe the Pacific-North American (PNA) teleconnection pattern. The monthly SLP at this location was derived by averaging the 6-hourly analyzed pressure fields produced at Fleet Numerical Oceanographic Center (63 x 63 northern hemisphere grid) for each month. The resulting series of monthly means was treated identically to the Darwin series. All "north Pacific" or "local" process indicators were derived from this smoothed series. Figure 2 summarizes the procedures used in deriving the series used in correlations.

Interannual changes or interannual difference indicators of ocean temperature, remote forcing, and local forcing are used in the correlation analyses. The interannual differences were computed for the current year (yr) by subtracting the parameter value for the previous year (yr-1), for example, for a particular annual value of ocean temperature change:

$$D_{z,yr} = A_{z,yr} - A_{z,yr-1}.$$

The five ocean temperature difference series are labeled "D<sub>z</sub>" and the local and remote difference series are labeled "LD" and "RD," respectively (Figure 2).

If there are specific vertical patterns of ocean temperature change associated with remote and local forcing, they should be evident in Empirical Orthogonal Functions derived from the D<sub>z</sub> matrix (Figure 3). The first two EOFs of D<sub>z</sub> will be given physical interpretation drawn from correlations between the series of expansion coefficients (DEOF1 and DEOF2) and indicators of atmospheric forcing. The 50-meter series (D<sub>50</sub>) was excluded from this part of the analysis to weight the EOFs equally with respect to depth interval, since distribution of anomaly over depth appears to be important in distinguishing between event type (Norton *et al* 1985a,b).

As noted, atmospheric teleconnections may link changes in SST in the equatorial Pacific to SLP over the north Pacific. This physical relationship causes the local and remote interannual difference indicators (LD, RD) to be correlated, especially in winter. To correct the LD and RD series for the atmospheric teleconnection, each was linearly regressed on the other, on a month-to-month basis, and the residual series used in correlation tests. The residual values represent the variability in the dependent variable unexplained by the independent variable. These series are referred to as "remote index residuals" or "U(RD:LD)" and "local index residuals" or "U(LD:RD)".

This approach may not show exact relationships between variables or remove all effects of the atmospheric teleconnection and its possible feedbacks but, like the other data manipulations described, it requires

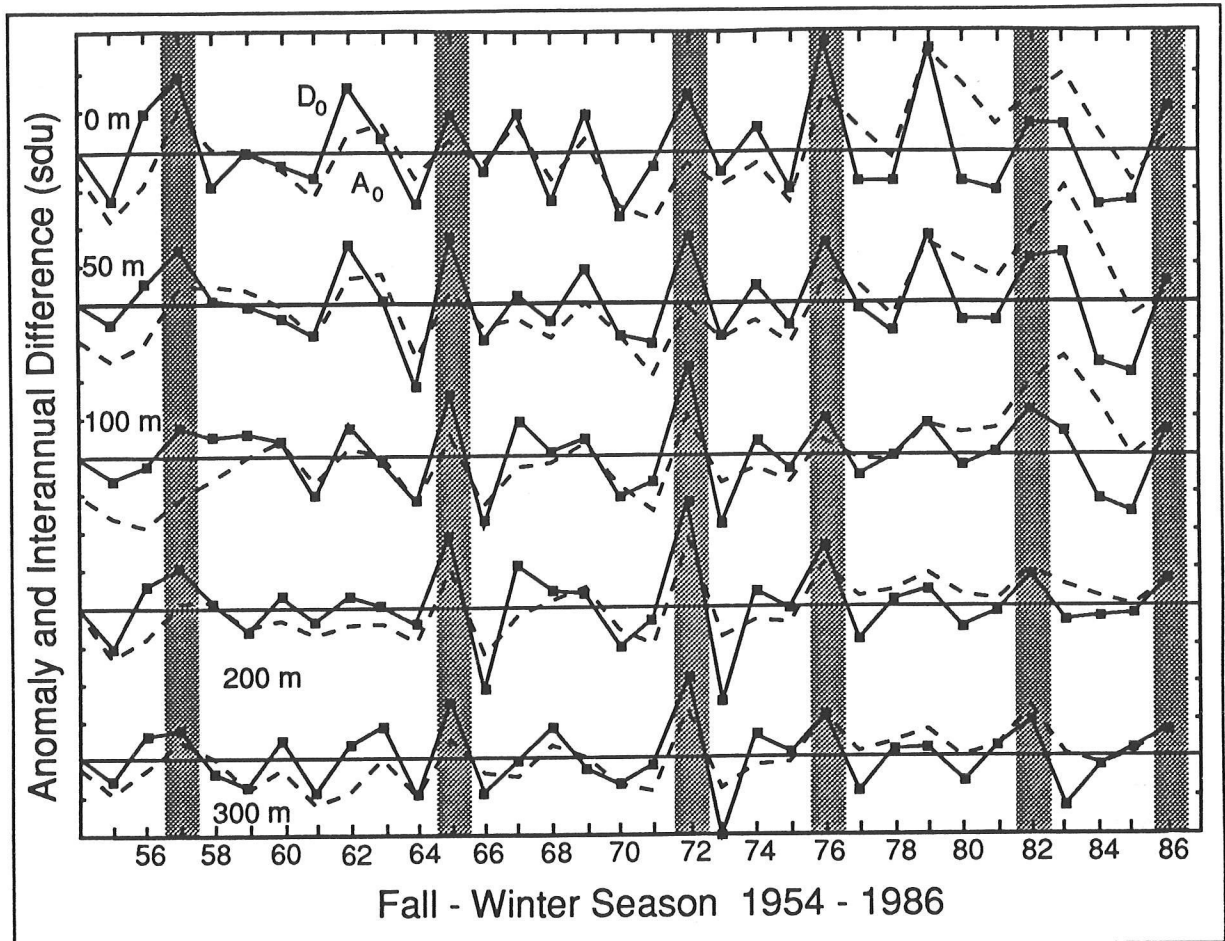


Figure 3. Time series of 6-month average subsurface temperature anomalies and inter-annual differences in the study region.

Solid lines indicate inter-annual temperature change for fall/winter combined ( $D_2$ ).  
 Dotted lines indicate combined standardized temperature anomalies ( $A_2$ ).  
 Horizontal lines mark zero anomaly and zero inter-annual change.  
 Zero value lines are two standard deviation units apart.  
 Shading indicates El Niño years.

minimal assumptions about the nature of the connecting processes. In the case of U(LD:RD), some correction is made for effects of the atmospheric teleconnection, but the interpretation of U(RD:LD) is less direct.

## Results

In years when coherent ocean temperature changes extend from the surface to 300 meters depth, remote forcing from the equatorial Pacific is indicated (Figure 4). Correlation coefficients ( $r$ ) between time series of year-to-year ocean temperature change along the West Coast and the indicator of Pacific equatorial atmospheric conditions (RD) were as large at 100 meters and below ( $r > 0.7$ ,  $p < 0.01$ ) as at the surface (Figure 4a). Figure 3 shows that during 1954 to 1986, the warming events that were coherent over the upper 300 meters occurred only during moderate to strong El Niño years (Quinn *et al* 1987). For fall/winter warming events that appear more closely related to local, north Pacific forcing, correlation coefficients were greater in magnitude at the surface ( $r < 0.7$ ) than at 100 meters and below (Figure 4b). At the ocean surface, lags of up to 6 months

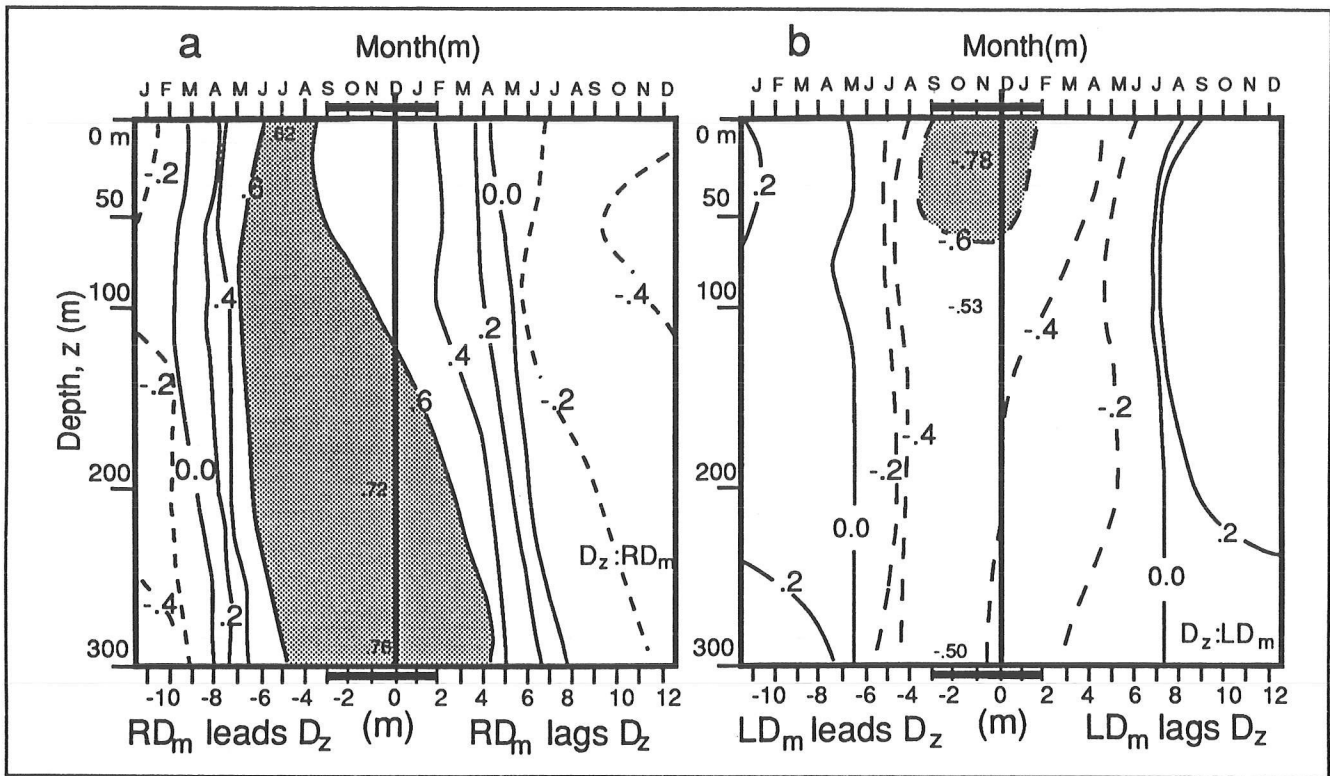


Figure 4. Distribution of correlation coefficients,  $r$ , when fall/winter (solid horizontal bar) ocean inter-annual temperature change series,  $D_z$ , are correlated with the remote (a) and local (b) inter-annual atmospheric pressure change series. Variation in RD and LD is from January ( $m=-11$  leads in yr) through December ( $m+12$  lags in year+1) of the following year. The vertical line marks December of the event year ( $m=0$  lags). Solid and dashed contours at  $r=0.2$  intervals show positive and negative correlation, respectively. For  $|r| > 0.4$  and  $p < 0.05$ . Areas where  $|r|$  is greater than or equal to 0.6 and  $p < 0.01$  are shaded. Positive anomalies in the remote indicator (a) and negative anomalies in the local indicator (b) are correlated with anomalously high temperatures in the study region.

in maximum correlation were found for equatorial Pacific forcing (Figure 4a), while lags of 3 months or less were characteristic of local forcing (Figure 4b).

The first two EOFs accounted for more than 92.5 percent of the variance of the  $D_z$  time series (Figure 5). The first EOF accounts for 79.1 percent of the variance and has nearly uniform component loading over depth (upper panel, Figure 5a). In Figure 5a, a broken line traces the correlation of DEOF1 with the atmospheric forcing indices (LD, RD). From these correlations it appears that EOF1 is related to both the local and remote indices. However, when series residuals,  $U(LD:RD)$  and  $U(RD:LD)$ , were correlated with DEOF1 (solid lines), only the correlation with the remote forcing index residual [ $U(RD:LD)$ ] remained significant with  $p < 0.05$  (greater than shaded area in Figure 5a, lower panel).

In Figure 5 the shaded areas represent the range of  $r$  values required for  $p < 0.05$  when the range of effective degrees of freedom is between  $n$  and  $n^*$ . Here  $n$  is the number of values in the correlated series and  $n^*$  is the effective number of degrees of freedom as determined by the method of Chelton (1983).

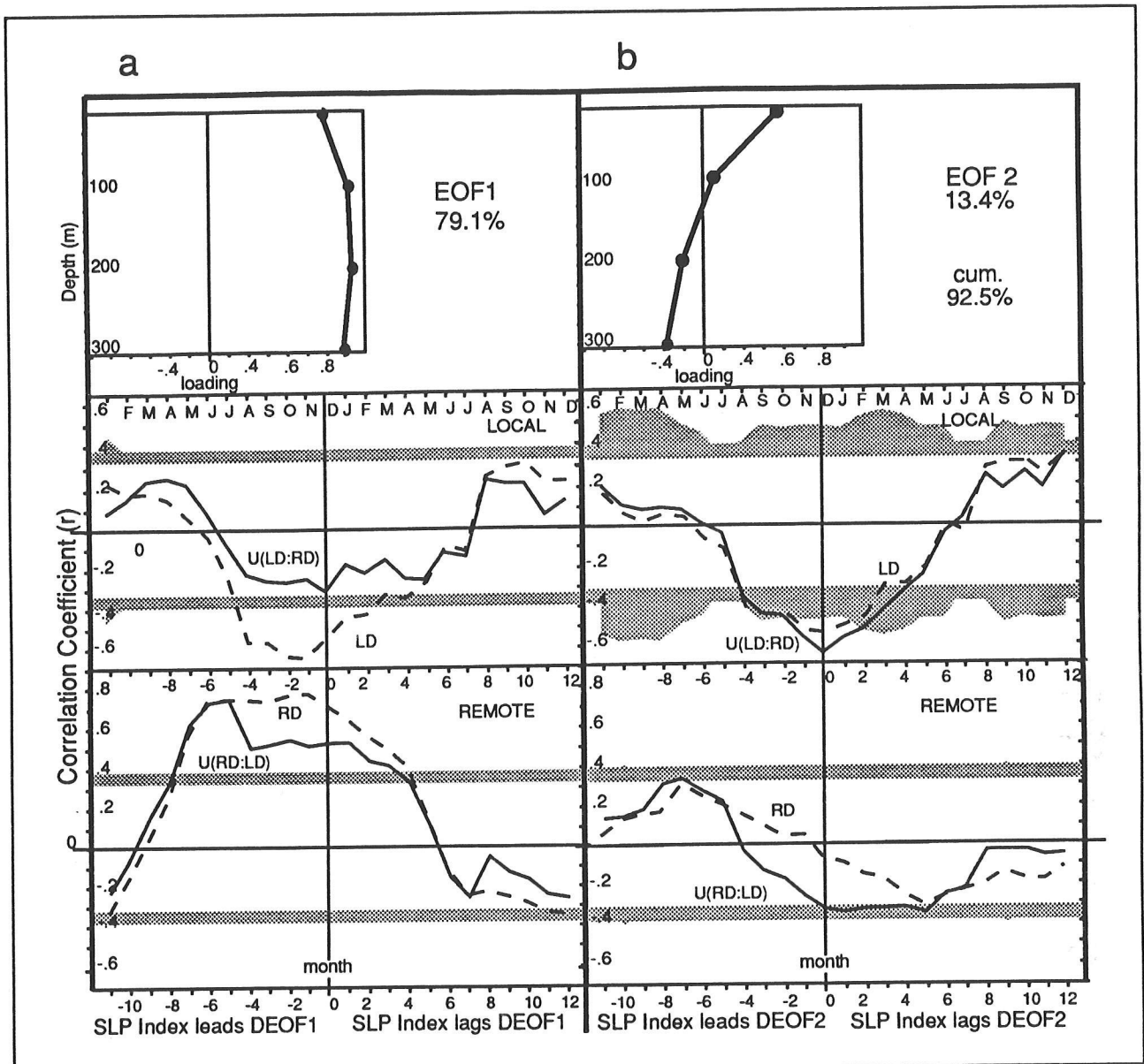


Figure 5. Depth variation in component loading of EOF1 (panel a) and EOF2 (panel b)

Variation derived from  $D_z$  is shown in the upper panels.

Percentage of variance explained by each EOF is on the upper right of each panel.

Broken lines in the middle and lower panels show the correlation of the time variation of coefficients of EOFs 1 and 2 (DEOF1 and DEOF2) to the atmospheric forcing indices  $LD_m$  and  $RD_m$ .

Correlation with the residuals  $U(LD:RD)_m$  and  $U(RD:LD)_m$  are shown by the solid lines.

Monthly leads and lags are the same as for Figure 4.

If  $r$  values exceed the upper bounds of the shaded area,  $p < 0.05$  is indicated.

The second EOF accounts for 13.4 percent of the variance in  $D_z$  and reverses sign at depths below 100 meters (Figure 5b). This suggests that warming at 0 and 100 meters might be accompanied by cooling at 200 and 300 meters. The local, north Pacific, atmosphere appears to be important in forcing this variational mode, as shown by significant correlation in December in the middle panel of Figure 5b. The correlation coefficients for October (yr) through February (yr+1) clearly exceed the  $p=0.05$  level (shaded) for correlations with both local forcing indices [ $LD$ ,  $U(LD:RD)$ ].

## Discussion

---

The results show that northern coastal California Current warming episodes associated with Pacific equatorial events are detected by interannual temperature change at 100 meters and below, and warming associated with north Pacific influences are more likely to be detected in the surface layers, rather than at depth. The pattern of the deep signal is qualitatively consistent with effects expected from remote forcing through the ocean. Complex modal structures associated with coastal-trapped waves contribute to a signal that may be more pronounced at depth due to vertical propagation accompanying horizontal propagation (McCreary 1984; Romea and Allen 1983).

A summary of the temporal relationships of Pacific Basin events and processes associated with a typical El Niño warming are compared with results of the present study in Figure 6. In the upper panel, heavy dashed lines represent temporal relationships established by Horel and Wallace (1981), Cane (1983), Rasmusson and Wallace (1983), and Trenberth (1989). A physical interpretation of the interannual difference is that it represents change in the system over the differencing interval, or the processes that change the variable value during the differencing interval. These interpretations are illustrated by comparing the upper and lower panels of Figure 6.

The lower panel shows that the interannual change of remote forcing (RD) most highly correlated with ocean temperature change ( $D_z$ ) corresponds to the period of increasing SLP at Darwin during El Niño generation (top broken line). This correspondence implies that the interannual difference represents the accumulated effects of processes occurring over the differencing interval, *ie*, accumulated increase in sea level atmospheric pressure. This is qualitatively consistent with modeling results based on long wave theory (McCreary 1976, 1984; Shriver *et al* 1991).

Regional ocean temperature change and local forcing (LD) appear in phase, as shown by the upper and lower solid lines in Figure 6. However, phase shifts of less than 6 months might not be fully detected (resolved) in the present data treatment because of the high autocorrelation between consecutive values.

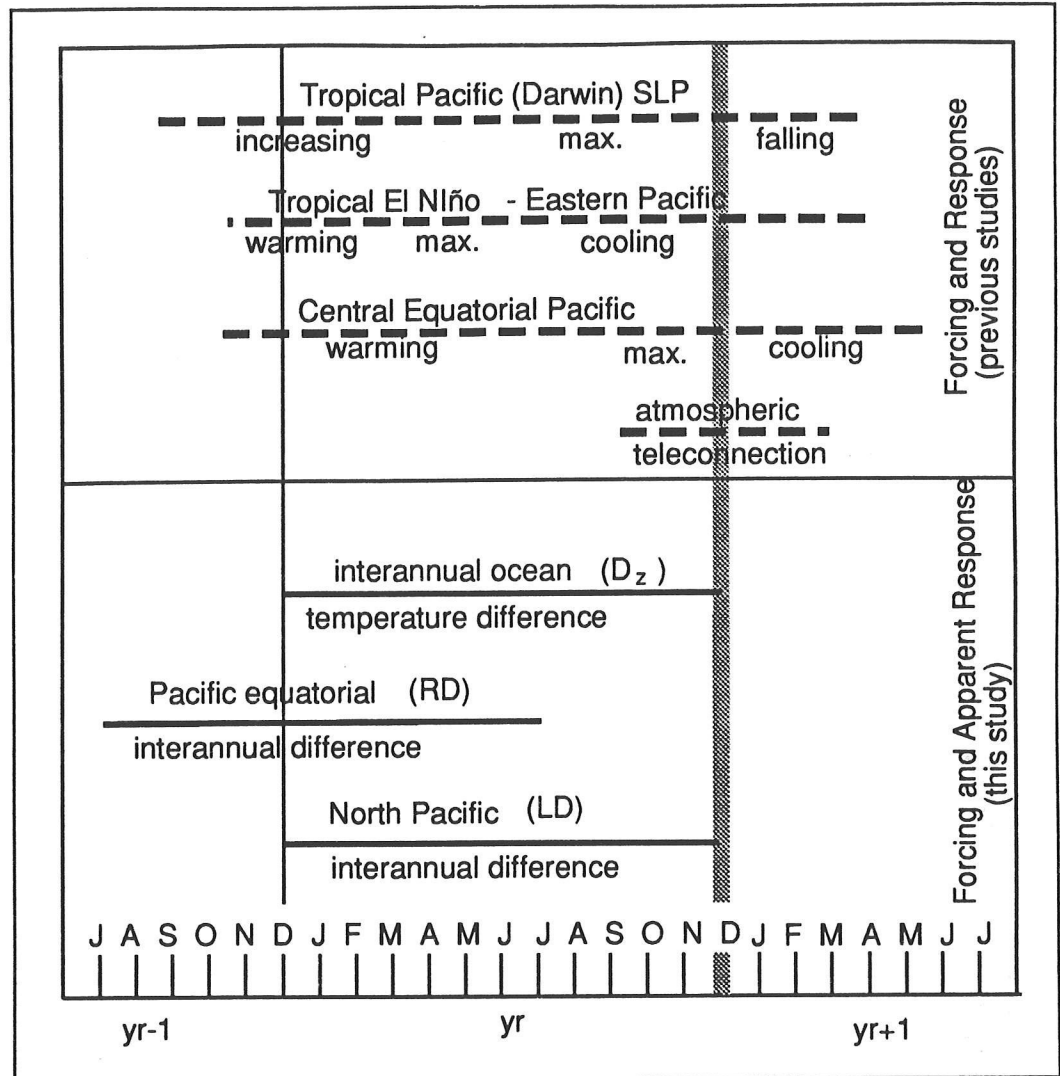


Figure 6. Comparison of temporal relationships for the "typical" tropical El Niño event (top) and results of this study (bottom). Intervals of increase, maximum and decrease in SLP at Darwin, temperature change in the eastern and central equatorial Pacific, and corresponding Aleutian Low augmentation are shown by bold broken lines in the upper panel. Solid lines summarize present results from Figures 4 and 5. The upper solid line shows the ocean temperature differencing interval; the vertical shaded line shows its temporal designation. The lower two solid lines show the difference intervals of remote (SLP at Darwin) and local (North Pacific SLP) indicators that are most highly correlated with  $D_z$ . Solid horizontal lines show the time intervals that will have greatest influence on the  $D_z$ , RD, and LD values.

**Note**

This paper is an abbreviated version of a manuscript by Norton and McLain that will be published elsewhere. A copy of the extended version is available from the authors.

## References

---

- Cane, MA. 1983. Oceanographic events during El Niño, *Science* 222:1189-1194.
- Chelton, DB. 1983. Effects of sampling errors in statistical estimation, *Deep-Sea Res.* 30:1083-1103.
- Clarke, AJ. 1983. The reflection of equatorial waves from oceanic boundaries, *J. Phys. Oceanogr.* 13:1193-1207.
- Emery, WJ, and K Hamilton. 1984. Atmospheric forcing of interannual variability in the northeast Pacific Ocean, *J. Geophys. Res.* 90:857-868.
- Enfield, DB, and JS Allen. 1980. On the structure and dynamics of monthly mean sea level anomalies along the Pacific coast of North and South America, *J. Phys. Oceanogr.* 10:557-578.
- Horel, JD, and JM Wallace. 1981. Planetary atmospheric phenomena associated with the Southern Oscillation, *Mon. Wea. Rev.* 109:813-829.
- McCreary, JP. 1976. Eastern tropical response to changing wind systems: with application to El Niño, *J. Phys. Oceanogr.* 6:632-645.
- \_\_\_\_\_. 1984. Equatorial Beams, *J. Mar. Res.* 42:395-430.
- McLain, DR, RE Brainard, and JG Norton. 1985. Anomalous warm events in eastern boundary current systems, *Calif. Coop. Oceanic Fish. Invest. Rep.* 26:51-64.
- Norton, JG, DR McLain, RE Brainard, and DM Husby. 1985a. El Niño event off Baja and Alta California and its ocean climate context. In Niño effects in the eastern subarctic Pacific Ocean, WS Wooster and DL Fluharty eds., pp. 44-72, Washington Sea Grant Program, University of Washington, Seattle.
- Norton, JG, DR McLain, DM Husby, and RE Brainard. 1985b. Kelvin wave activity during recent California El Niños, *Eos Trans. AGU* 66:1295.
- Quinn, WH, VT Neal, and SE Antunez de Mayolo. 1987. El Niño occurrences over the past four centuries, *J. Geophys. Res.* 92:14449-14461.
- Rasmusson, EM, and JM Wallace. 1983. Meteorological aspects of the El Niño/Southern Oscillation, *Science* 122:1195-1202.
- Romea, RD, and JS Allen. 1983. On vertically propagating coastal Kelvin waves at low latitudes, *J. Phys. Oceanogr.* 13:1241-1254.
- Shriver, JF, MA Johnson, and JJ O'Brien. 1991. Analysis of remotely forced oceanic Rossby waves off California, *J. Geophys. Res.* 96:749-757.
- Simpson, JJ. 1983. Large-scale thermal anomalies in the California current during the 1982-1983 El Niño, *Geophys. Res. Lett.* 10:937-940.
- Trenberth, KE. 1989. TOGA and atmospheric processes. In Understanding climate change, A Berger, RE Dickinson, and John W Kidson eds., American Geophysical Union Geophysical Monograph 52, pp. 117-125, American Geophysical Union, Washington, DC.
- Wallace, J, and D Gutzler. 1981. Teleconnections in the geopotential height field during the northern hemisphere winter, *Mon. Wea. Rev.* 109:784-812.

# An Objective Classification of Climatic Regions in the Pacific and Indian Oceans

Henry F. Diaz and Timothy J. Brown

**Abstract:** We have applied a number of objective statistical techniques to define homogeneous climatic regions for the Pacific Ocean, using COADS (Woodruff *et al* 1987) monthly sea surface temperature (SST) for 1950-1989 as the key variable. The basic data comprised all global 4°x4° latitude/longitude boxes with enough data available to yield reliable long-term means of monthly mean SST. An R-mode principal components analysis of these data, following a technique first used by Stidd (1967), yields information about harmonics of the annual cycle of SST. We used the spatial coefficients (one for each 4-degree box and eigenvector) as input to a K-means cluster analysis to classify the gridbox SST data into 34 global regions, in which 20 comprise the Pacific and Indian oceans. Seasonal time series were then produced for each of these regions. For comparison purposes, the variance spectrum of each regional anomaly time series was calculated. Most of the significant spectral peaks occur near the biennial (2.1-2.2 years) and ENSO (~3-6 years) time scales in the tropical regions. Decadal scale fluctuations are important in the mid-latitude ocean regions.

We present the results of our studies in applying a number of objective statistical techniques to define homogeneous climatic regions over the world oceans (see Diaz and Brown 1992). The variable used is COADS monthly sea surface temperature for 1950 through 1989. Reasons for exploring the nature of "climatically homogeneous" oceanic regions are twofold. First, from the point of view of climate monitoring and climate change detection efforts, it is useful to divide the ocean into smaller units. Second, it might be advantageous to study a number of air/sea interaction processes on regional scales. It is also of interest to compare SST changes in the different ocean basins. We will focus here only on the Indo-Pacific Ocean region.

## Methodology

Using 4-degree latitude/longitude area boxes from the COADS data set (Woodruff *et al* 1987), an R-mode principal component analysis (PCA) was performed using the calendar month 1950-1989 long-term mean SSTs in each box as the variables, with a minimum requirement of five years of data within the 40-year period in each box. The use of the R-mode PCA technique in climate classification was first published by Stidd (1967) to classify the precipitation climate of Nevada, and also by Skaggs (1975) to study the 1930s drought in the United States.

K-means cluster analysis (Hartigan 1975) was then used to classify the gridbox SST data, using as input the spatial coefficients from the first two

eigenvectors of the monthly mean SST. Initially, a total of 1,939 4-degree boxes for the world oceans were used as input to the clustering algorithm, with an initial prescribed seed of 15 groups. Boxes in certain inland seas, and areas with relatively sparse data coverage were manually edited out of the final regional configuration, eliminating 123 boxes, for a final total of 1,816 4-degree boxes yielding 34 regional clusters over the world oceans (20 regions in the Indo-Pacific sector). In general, distinct regions were derived for each hemisphere and ocean basin. The resulting cluster patterns were visually examined to determine if the physical boundaries were climatologically consistent, and various tests were performed to ascertain the temporal coherence of the constituent boxes for each region. This involved, for instance, comparing the distribution of the departure values of the individual 4-degree boxes and calculating the mean inter-box correlation within each region.

### Analysis Results

Figure 1 shows a map of the 20 cluster regions that were classified using the procedure described above, and Table 1 presents a few basic summary statistics for each region. In general, as expected, the largest regions are in the tropics. Seasonal values for the 4-degree boxes within each region were averaged together (with cosine of latitude weighting to account for the differences in area) to form regional time series. Figures 2-4 illustrate these results for three ocean areas: two in the tropics and one in mid-latitudes.

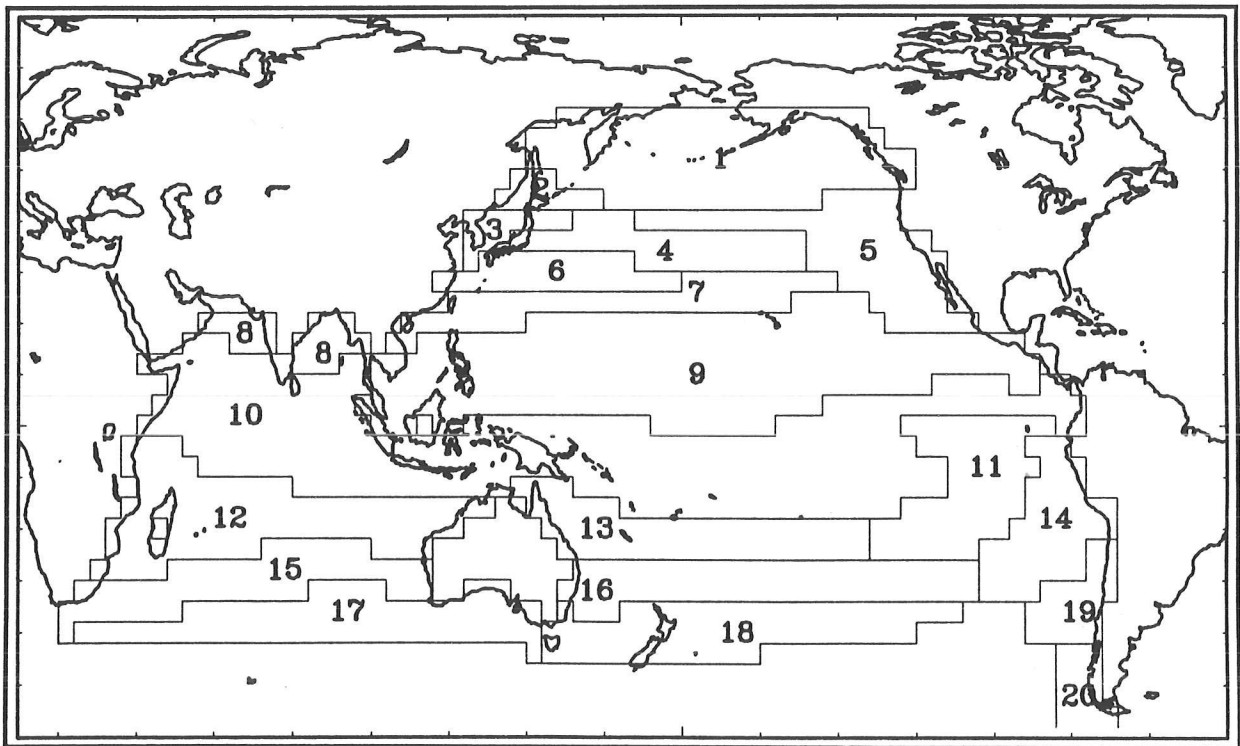


Figure 1. Map illustrating the regional SST boundaries.

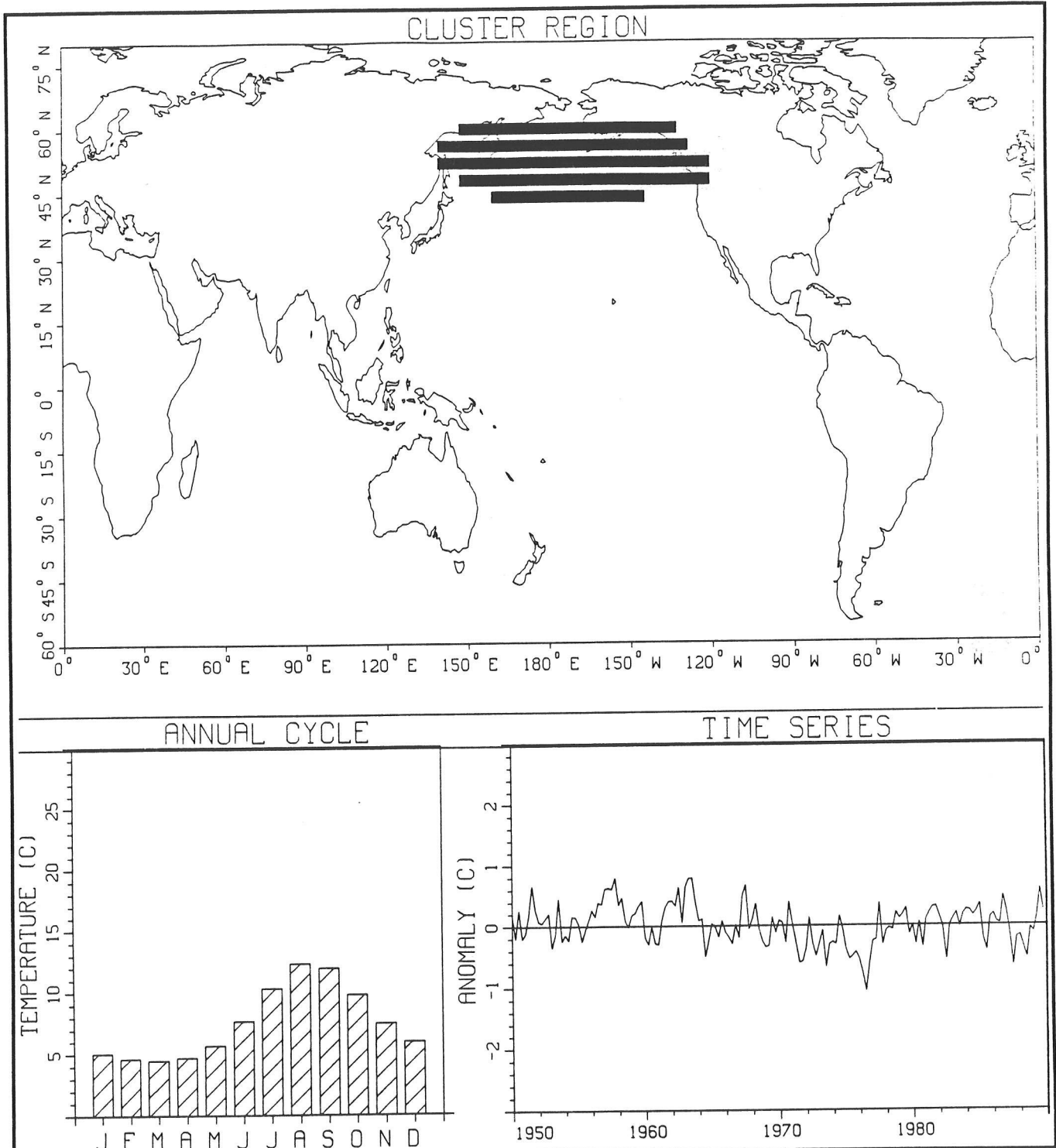


Figure 2. Time series of SST anomalies for the northern North Pacific region (region 1 in Figure 1) indicated by the shaded bars. Figure also shows the seasonal cycle of monthly mean SSTs averaged over the entire region.

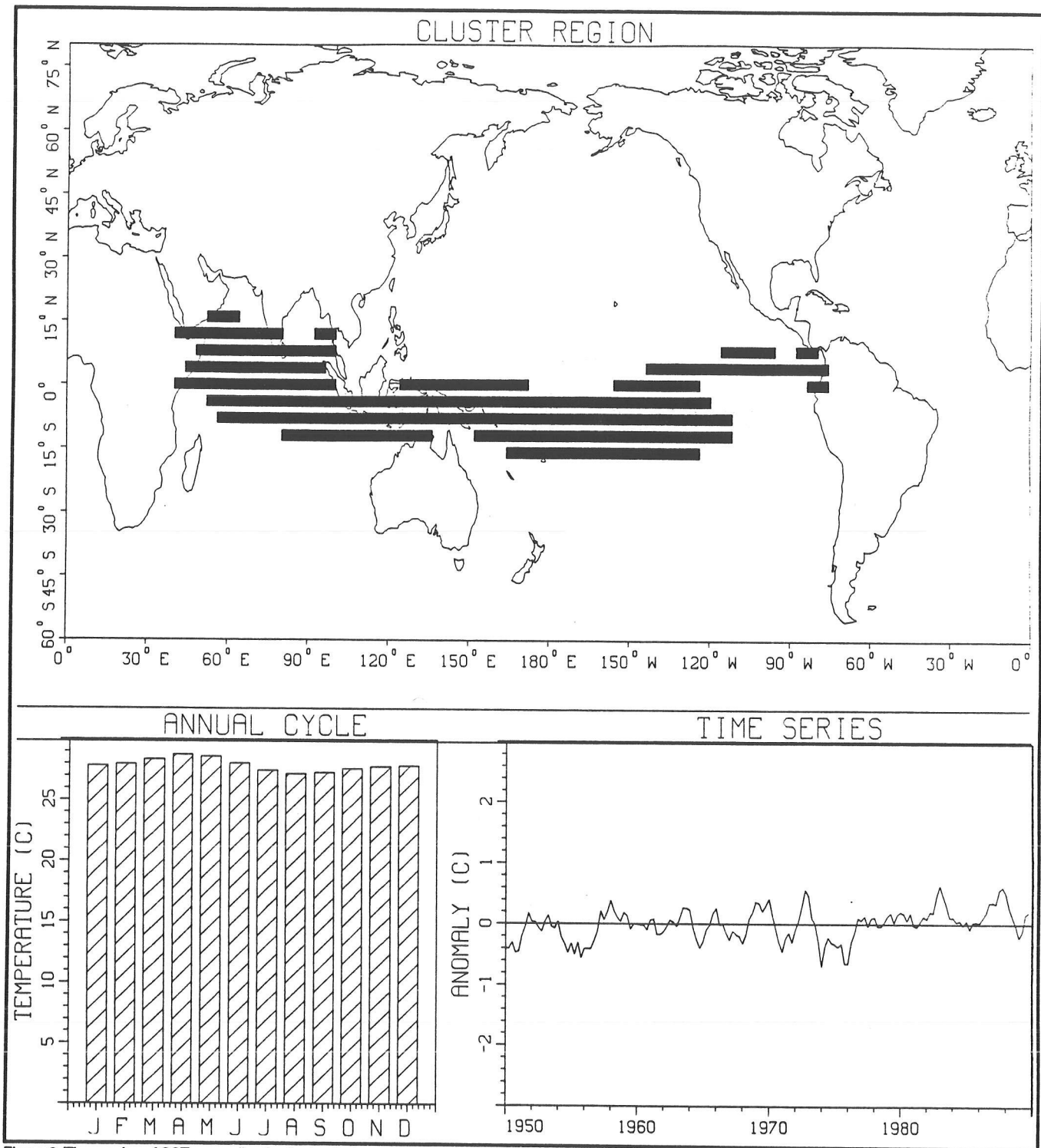


Figure 3. Time series of SST anomalies for the tropical warm pool region (region 10 in Figure 1). Figure also shows the seasonal cycle of monthly mean SSTs averaged over the entire region.

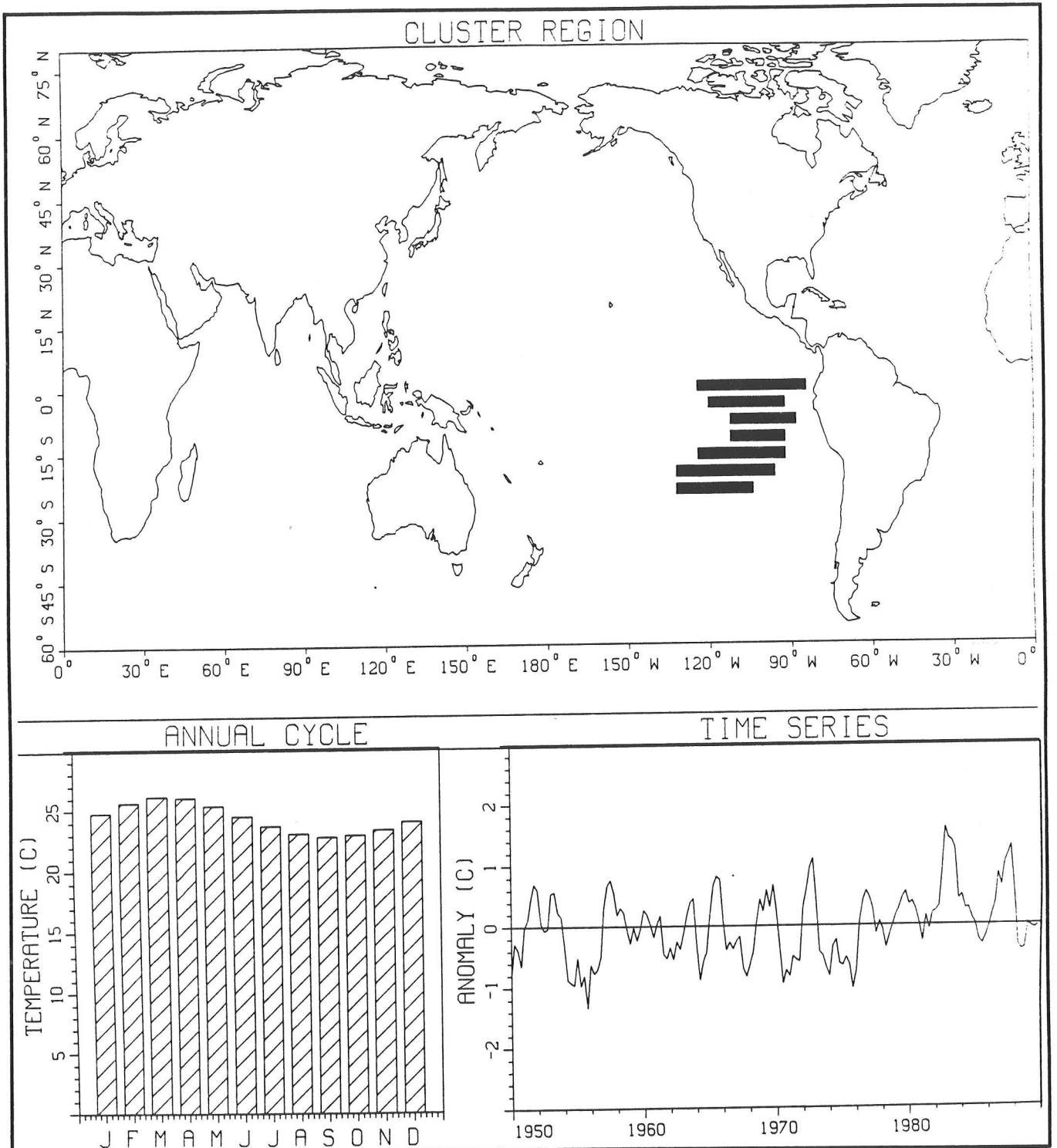


Figure 4. Time series of SST anomalies for an El Niño-sensitive area of the eastern tropical Pacific (region 11 in Figure 1). Figure also shows the seasonal cycle of monthly mean SSTs averaged over the entire region.

For the northern North Pacific region (see Table 1, region 1), seasonal temperature anomalies exhibit a cooling trend of about 0.4°C/decade, although SSTs in the 1980s were steady there, apart from typical interannual variability. Region 10, the large tropical region that encompasses parts of both the Indian and Pacific oceans, has the highest annual mean SST of any of the 34 global regions thus classified. It displays a small (though statistically significant) linear trend over the last four decades of about a tenth of a degree Celsius per decade. Most of the increase in SST is associated with a period of above-average SST beginning in the late 1970s. The other tropical region discussed here (region 11) is strongly affected by the El Niño/Southern Oscillation phenomenon. It has an upward SST trend of about the same magnitude as region 10, but because of its greater interannual variability, the change is not statistically significant.

Table 1  
SELECTED SUMMARY STATISTICS BASED ON  
ANNUAL SST MEANS (°C) FOR EACH CLASSIFIED REGION IN THE INDIAN AND PACIFIC OCEANS

*See Figure 1.*  
The ordinary least squares trend (OLS) is given in °C/decade, and its t-value is shown as an indicative measure of statistical significance.

Region	Mean	S.D.	OLS Trend	t-Value
1	7.56	0.58	-0.37	-6.89
2	8.14	0.63	-0.36	-5.57
3	15.65	0.54	-0.27	-4.49
4	18.92	0.41	-0.23	-5.45
5	17.72	0.26	-0.01	-0.40
6	23.21	0.24	-0.08	-2.69
7	25.36	0.16	-0.02	-0.80
8	27.78	0.24	0.13	4.97
9	27.51	0.21	0.06	2.45
10	27.86	0.23	0.10	3.90
11	24.32	0.49	0.12	1.79
12	25.75	0.28	0.17	6.25
13	25.53	0.21	0.06	2.19
14	20.61	0.57	0.16	2.20
15	20.74	0.33	0.20	6.19
16	20.82	0.22	0.03	0.85
17	15.74	0.27	0.11	3.25
18	15.55	0.24	-0.05	-1.62
19	16.00	0.35	0.05	1.10
20	9.70	0.68	-0.16	-1.81

Principal component analysis using the 20 regional time series of 160 seasonal values (SST anomalies) as input indicates the first four (significant) eigenvector patterns account for 57 percent of the regional seasonal SST variance. We note that spatial patterns of the first two global regional eigenvectors (Diaz and Brown 1992) are similar to the second and third eigenvectors of SST anomaly calculated by Parker and Folland (1991) for the period since 1901 — their first eigenvector representing the long-term trend in the (adjusted) SST record. The temporal coefficients of our first global regional eigenvector closely follow the variations in global mean SST anomalies during this time ( $r = 0.79$ ).

For comparison purposes, the variance spectrum of each regional anomaly time series was calculated. Most significant spectral peaks occur near the biennial time scale (2.1-2.2 years) and in the ENSO frequency band (~3-6 years). We have summarized these results in Figure 5, which illustrates the frequency bands in the SST variance spectrum containing significant power. For instance, in regions 10 and 11, primary peaks in the seasonal variance spectrum of SST anomalies (peaks under 2 years excluded) are in the biennial and ENSO frequency band. For the northern North Pacific region, both decadal scale and ENSO variability are found.

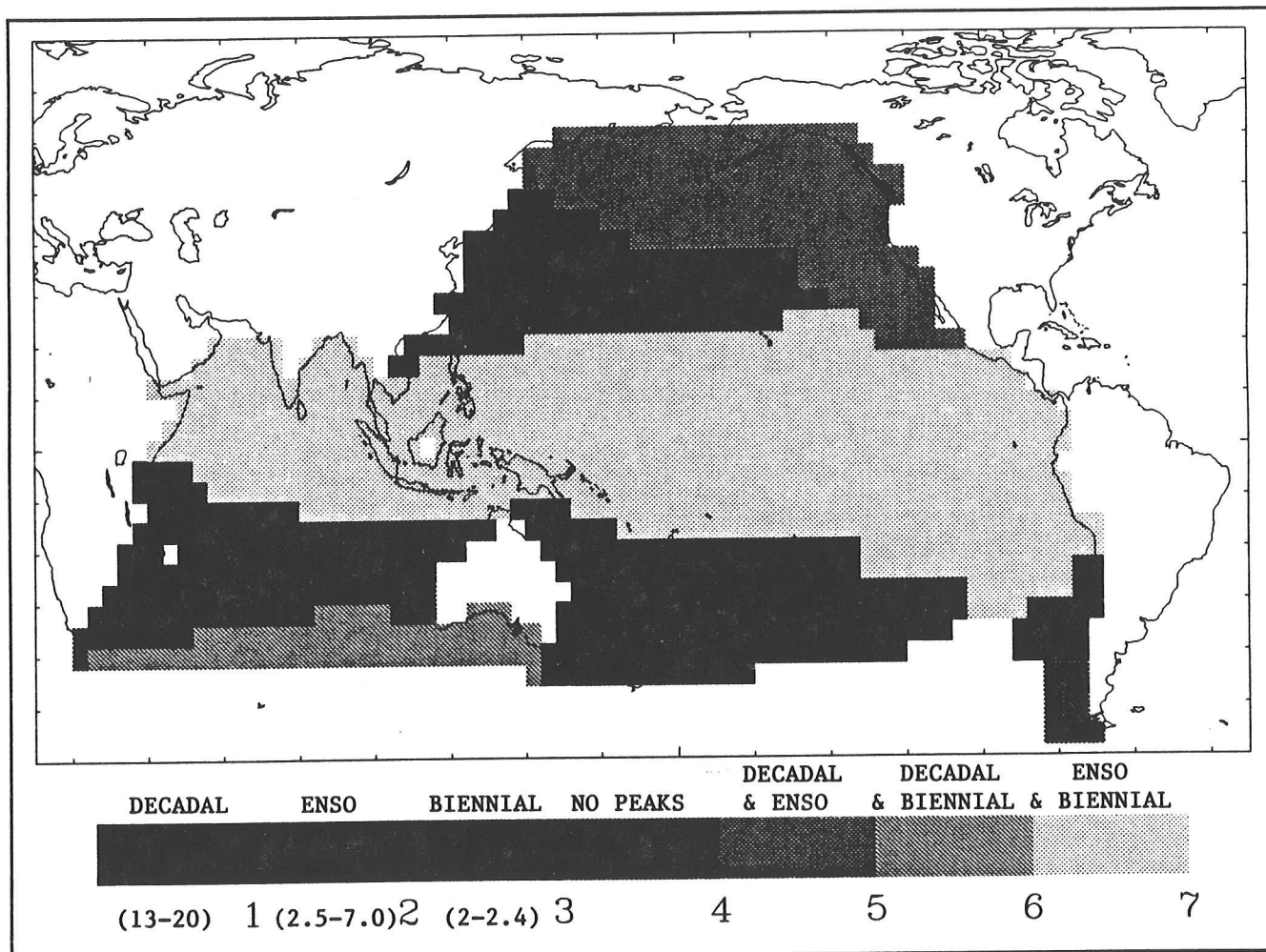


Figure 5. Map illustrating the characteristic time scale of temporal variability in the 20 Indo-Pacific regions.

## Summary

The approach used here to objectively classify climate regions over the ocean departs from the usual methodology, which has relied on similarity of the interannual variability (as measured by the cross-correlation between area time series) to define spatially "homogeneous" regions. Here we have focused on similarity of the annual cycle of SST and applied a clustering algorithm to objectively classify oceanic SST. The results are

useful for monitoring SST changes in upwelling areas along the West Coast of the Americas, the warm water pool in the equatorial Pacific and Indian oceans, *etc.*

Analysis of the variance spectrum of seasonal SST anomalies during the past 4 decades for our area of study illustrates regional differences in their characteristic time scale of variability. In general, the tropical ocean regions exhibit strong biennial and ENSO scale variability, whereas the extratropical regions contain greater variance at decadal time scales.

## **Acknowledgments**

---

This work is part of an effort by several NOAA units, with funding from NOAA's Climate and Global Change Program, to develop a global climate perspectives system for climate diagnostics research and climate change detection efforts.

## **References**

---

- Diaz, HF, and TJ Brown. 1992. Application of statistical techniques for the regionalization of marine surface temperatures. Preprints, 12th AMS Conference on Prob. and Stat. in the Atmos. Sci., Toronto, Canada. pp. J20-J21.m
- Hartigan, JA. 1975. *Clustering Algorithms*. J. Wiley & Sons, NY. 351 pp.
- Parker, DE, and CK Folland. 1991. Worldwide surface temperature trends. *In* ME Schelesinger (ed.) *Greenhouse-Gas-Induced Climatic Change: A Critical Appraisal of Simulations and Observations*. Amsterdam, Elsevier. pp. 173-193.
- Skaggs, RH. 1975. Drought in the United States, 1931-40. *Annals of the Assoc. of Amer. Geogr.* 65:391-402.
- Stidd, CK. 1967. The use of eigenvectors for climatic estimates. *J. Appl. Meteor.* 6:255-264.
- Woodruff, SD, RJ Slutz, RL Jenne, and PM Steurer. 1987. A comprehensive ocean-atmosphere data set. *Bull. Amer. Meteor. Soc.* 68:1239-1250.

# ENSO and Precipitation Variability Over Mexico During the Last 90 Years

George N. Kiladis and Henry F. Diaz

Latin America has been shown to be susceptible to climatic anomalies during El Niño/Southern Oscillation (ENSO) events (*eg.* Aceituno 1988; Ropelewski and Halpert 1987; Kiladis and Diaz 1989). While these studies have emphasized ENSO-related rainfall and temperature anomalies over Central and South America, less work has been done on the climatic effects of ENSO over the Mexican region.

In this study we are investigating interannual and intraseasonal fluctuations in temperature and precipitation over the southwestern United States and Mexico since the turn of the century. We are particularly interested in the effects of ENSO on the interannual variability over this region. This report focuses on the association between ENSO and interannual variability of precipitation over Mexico.

## Data and Methodology

We use a station network of records from the Global Historical Climatology Network, obtained from the National Climate Data Center in Asheville, North Carolina. These data are in monthly summary format and start in January 1900. Much of the temperature and precipitation data for Mexico obtained in this set was compiled and quality checked by Douglas (1982) from archived sources in Mexico.

The station data were interpolated to a regular latitude/longitude grid at 2.5-degree spacing (Figure 1). Climatic regions were determined based on an analysis of the seasonal cycle in precipitation over the study region (see Diaz and Brown, this volume). First an R-mode principal component analysis was performed using the 1900-1988 monthly mean precipitation at each gridpoint. Loadings from the first two eigenvectors of the monthly mean precipitation were then used as input into a K-means cluster analysis (Hartigan 1975) to group the gridpoints. In general, the amplitude and phase of the first two harmonics of the long-term mean seasonal cycle determine the first two eigenvectors, thus stations are grouped on the basis of similarity to their neighboring gridpoints. The climatic regions obtained are shown in Figure 1. It should be emphasized that these regions are not grouped on the basis of their coherent fluctuation over time, but only on the basis of similarity of their mean seasonal cycles.

In: K.T. Redmond and V.L. Tharp, Editors. 1993. Proceedings of the Ninth Annual Pacific Climate (PACCLIM) Workshop, April 21-24, 1992. California Department of Water Resources, Interagency Ecological Studies Program, Technical Report 34.

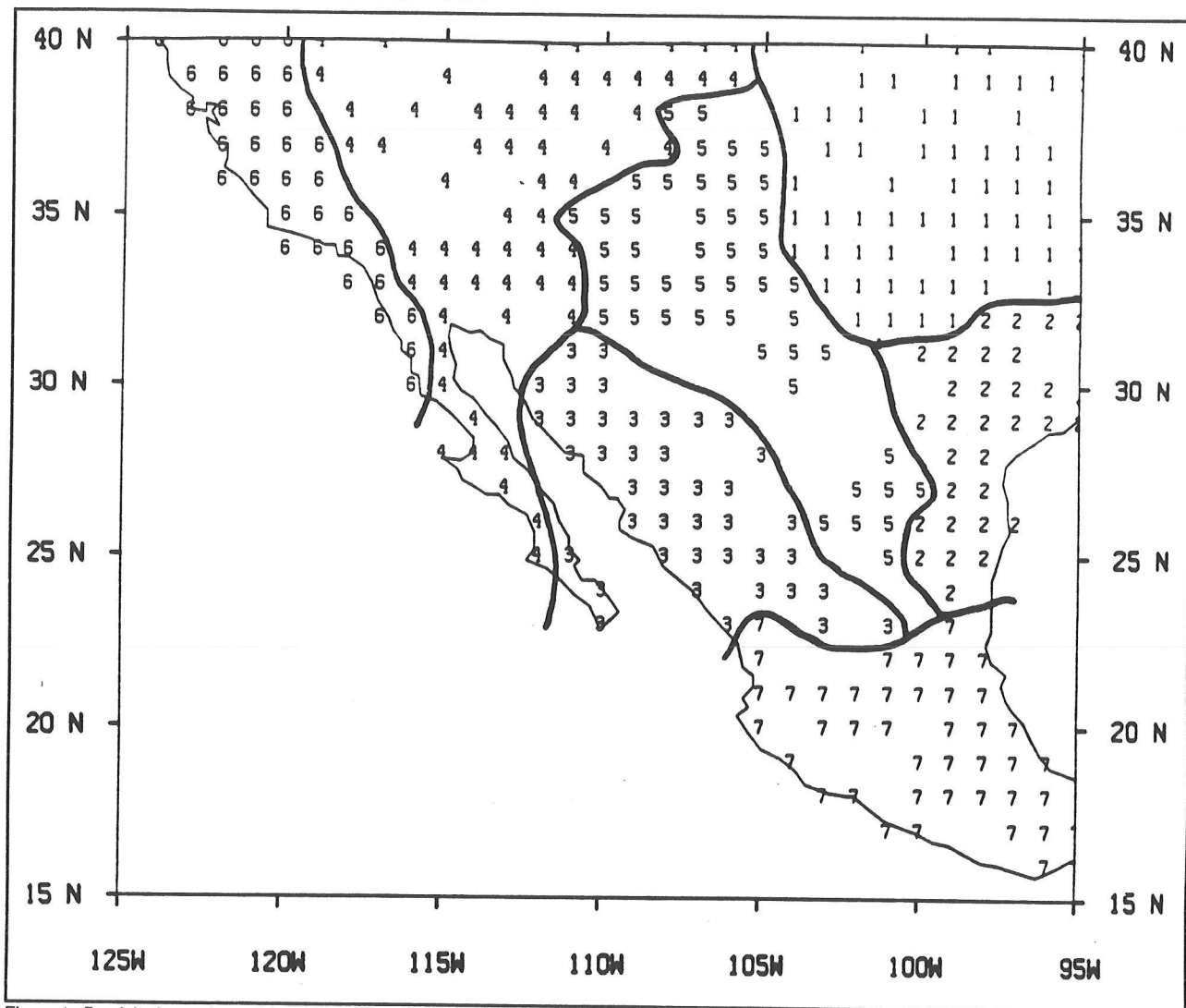


Figure 1. Precipitation regions of the southwestern United States and Mexico as determined by the K-means cluster analysis method based on the seasonal cycle of gridded precipitation data.

- 1 Southern Plains
- 2 Gulf Coastal
- 3 Sierra Madre
- 4 Sonora
- 5 Chihuahua
- 6 Pacific
- 7 Southern Mexico

Seven climate regions are defined using this technique. For example, the Pacific region (area 6) has a winter precipitation maximum and a summer minimum. The southern Mexico region (area 7) has a monsoon type climate, with maximum precipitation in May-September and a minimum in January. The Sierra Madre region (area 3) has a bimodal precipitation regime, with a main monsoonal maximum in July-August and a secondary maximum during December-January, when this region is affected by low latitude disturbances in the subtropical westerly flow from the Pacific. Precipitation over the southern Mexico and Sierra Madre divisions appears to be significantly modulated by ENSO conditions in the tropics and is the focus of this discussion.

Extreme ENSO years in Table 1 were taken from Kiladis and Diaz (1989) and are based on a combination of a sea surface temperature (SST) index and the Southern Oscillation Index (SOI). The SST index represents the integrated seasonal SST anomaly within 4 degrees of the equator from 160°W to the South American coast, based on COADS ship data. The SOI is the standard normalized Tahiti minus Darwin pressure index, which is a measure of the strength of the sea level pressure signal associated with ENSO (Ropelewski and Jones 1987). To qualify as an event, the SST anomaly had to be positive for at least three consecutive seasons, and be at least 0.5°C above the mean for at least one of these seasons, while the seasonal SOI had to remain below -1.0 for the same duration.

Table 1  
LIST OF YEAR ZEROS OF WARM AND COLD EVENTS  
(From Kiladis and Diaz 1989)

Warm Events		Cold Events	
1902	1953	1903	1942
1904	1957	1906	1949
1911	1963	1908	1954
1913	1965	1916	1964
1918	1969	1920	1970
1923	1972	1924	1973
1925	1976	1928	1975
1930	1982	1931	1988
1932	1986	1938	
1939	1991		
1951			

The warm event (El Niño) years shown in Table 1 are called year zero of the events, and are defined, as in Rasmusson and Carpenter (1982), as the year when the SOI changes sign from positive to negative, and when central and eastern equatorial Pacific SST anomalies become strongly positive. Cold event (La Niña) year zeros are defined as having the opposite characteristics. Thus we have included only the first year of multiyear events and ignored successive years, regardless of their magnitudes. Year+1 refers to the year following the start of the event, when remote ENSO teleconnections tend to be maximized.

## Results

Figure 2 shows a superposed epoch analysis of year 0 through year+1 warm and cold event precipitation anomalies for the Sierra Madre region. These two time series were obtained by averaging the integrated Sierra Madre monthly precipitation anomalies (in millimeters) for all warm event years and then for all cold event years separately, then smoothing the respective composite series with a 3-month running mean (see Bradley *et al* 1987). The plot shows that summer monsoon precipitation over the western plateau of Mexico is not strongly affected by ENSO, but that, on average, late fall and early winter precipitation is above normal during

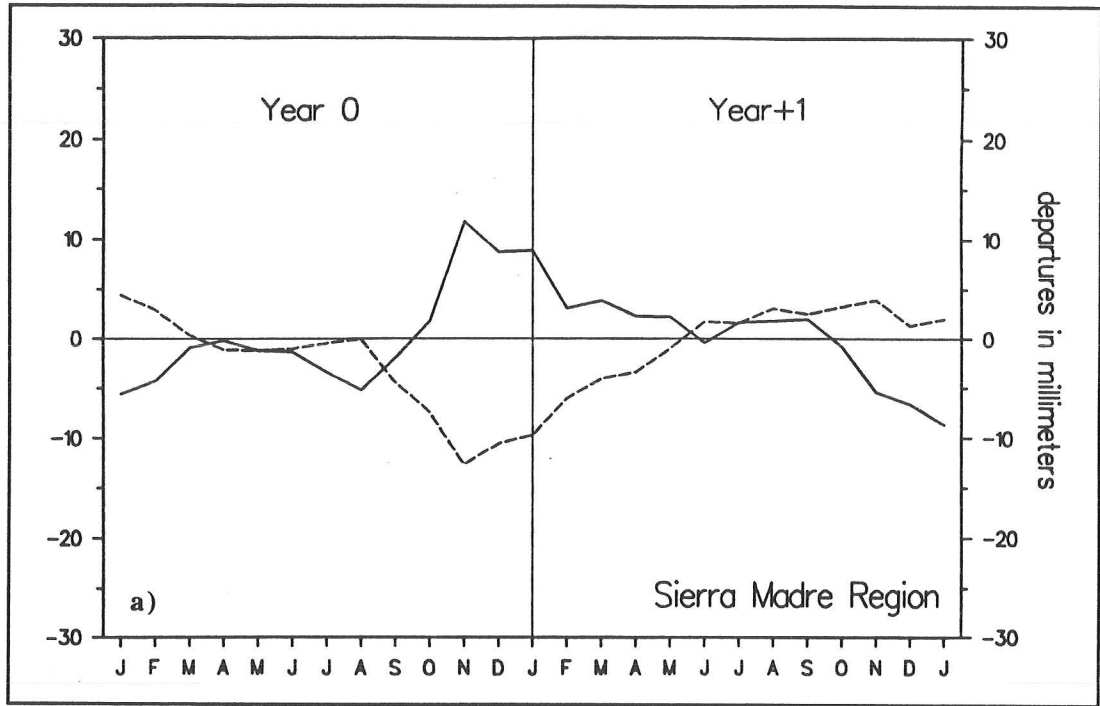


Figure 2. Superposed epoch analysis of warm (solid line) and cold (dashed line) event precipitation anomalies in the Sierra Madre region.

The anomalies have been smoothed by applying a 3-month running mean to the original monthly mean data. Warm and cold event years were taken from Table 1.

warm events and below normal during cold events. This signal reflects a strengthening of the subtropical westerly circulation tied to anomalously strong warm event convection in the equatorial Pacific. Not surprisingly, this particular signal is shared by the Sonora, Chihuahua, and Gulf coast divisions (not shown), which are also under the influence of a strengthened subtropical jet during warm events and a weakened jet during cold events. Although the 1991-92 warm event winter season was not included in the composite, this was an excellent example of this signal, with extremely high precipitation in the northern desert of Mexico, the southwestern United States, and Texas.

The magnitude of monthly anomalies for the Sierra Madre barely exceeds 10 mm per month at most, which is not a large amount of precipitation, but this region is normally quite dry during November through March, averaging less than 25 mm per month. Thus the ENSO signal can account for a substantial portion of the variance in precipitation during winter and, in fact, is responsible for many of the extreme precipitation events during this time of year. This is illustrated in Figure 3a, where individual November-March precipitation departures from the mean are plotted from 1900 through 1988. The winter Sierra Madre precipitation has a consistent ENSO signal, such that nearly all warm events are associated with above-normal precipitation and, without exception, cold events are characterized by below-normal precipitation. What's more, many of the extremely wet winters in the Sierra Madre occurred in association with warm events.

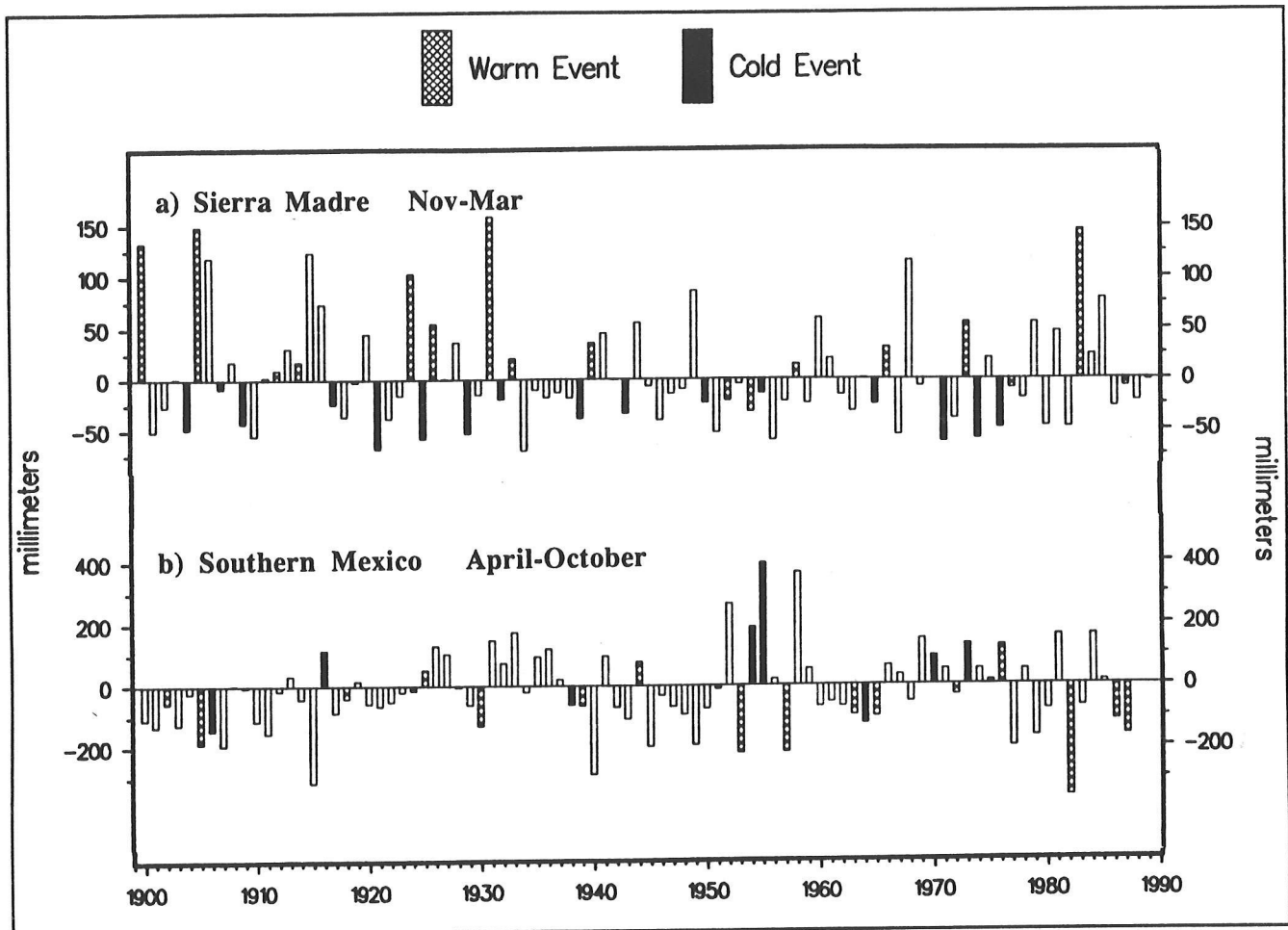


Figure 3. Time series of seasonal precipitation anomalies for November-March in the Sierra Madre and for April-October in Southern Mexico.

Departures are in millimeters/season.

The years in (a) are plotted according to the year zeros listed in Table 1 and refer to the year in which November falls. Warm and cold years in (b) are listed in Table 2.

Similar plots (not shown) were constructed for the southern Mexico region, using the warm and cold event years from Table 1. These plots showed that warm events were, on average, drier than normal and cold events were wetter than normal over southern Mexico; however, the consistency of the signal between events was less impressive than that for the Sierra Madre. We believe the source of this unreliability between ENSO and precipitation over southern Mexico is due to the irregular timing of ENSO onset between events during year 0. Because warm and cold event onset can often occur late in the calendar year (see Fu *et al* 1986), many year 0 designations in Table 1 likely were not necessarily associated with anomalously high SST and convection in the eastern Pacific.

With this in mind, we decided to look at monsoon precipitation during periods of anomalous SST over the central and eastern equatorial Pacific, regardless of whether a year was classified as a warm or cold event as defined by the criteria above. June through August seasons when the integrated SST index described above was greater than  $0.8^{\circ}\text{C}$  or less than  $-0.8^{\circ}\text{C}$  were chosen for this analysis. These years are given in Table 2.

Table 2  
MONSOON SEASONS OF EXTREME SEA SURFACE TEMPERATURE IN THE  
EASTERN EQUATORIAL PACIFIC

*Integrated June-August SST anomaly from 160°W-90°W greater than 0.8°C or less than -0.8°C.*

Warm SST		Cold SST	
1902	1957	1906	1955
1905	1963	1909	1964
1918	1965	1916	1970
1925	1972	1924	1973
1930	1976	1938	1975
1939	1982	1954	1988
1944	1986		
1951	1987		
1953			

Figure 4 shows a superposed epoch plot for April-October southern Mexico precipitation, using the above- and below-normal SST years from Table 2. These show clearly the tendency for precipitation to be deficient during periods of high SST from about April through October of year 0, followed by slightly above-average precipitation until February. Cold SST events show nearly opposite characteristics for a similar period.

The consistency of the southern Mexican precipitation signal to Pacific SST is shown in Figure 3b, where high monsoon season SST is coded as “warm event” and low SST as “cold event”. Of 17 warm SST years, 14 had below-normal precipitation, while 8 of 12 cold SST years had above-normal precipitation — anomalies consistent with the composite signal in Figure 4.

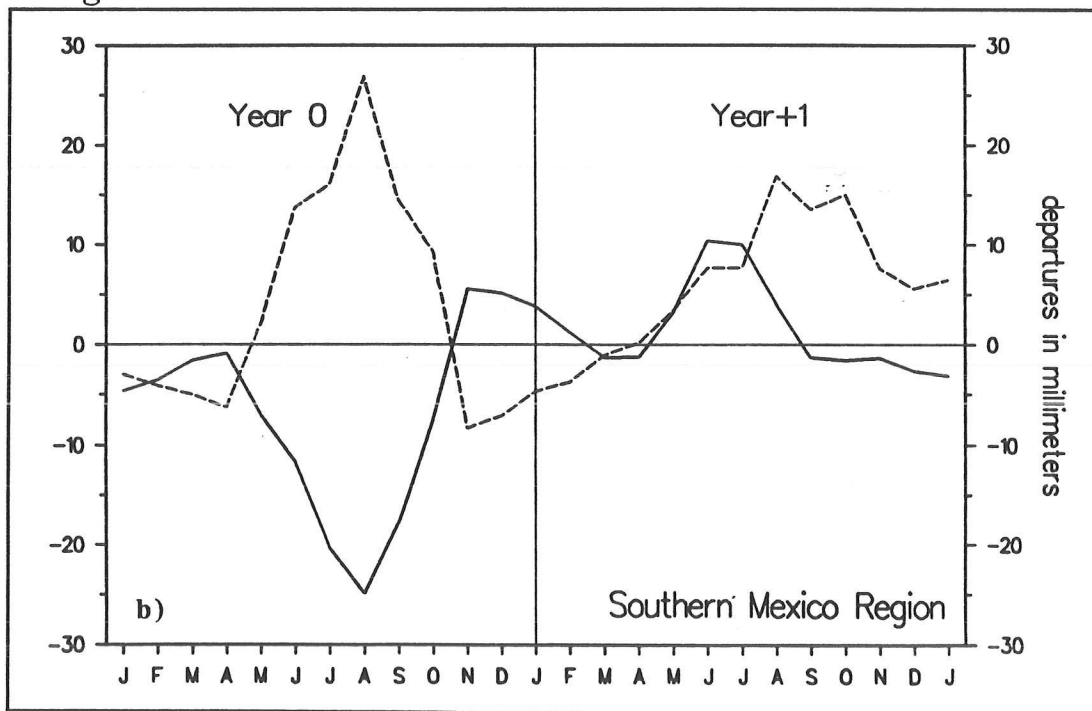


Figure 4. Superposed epoch analysis of warm (solid line) and cold (dashed line) event precipitation anomalies in the Southern Mexico region. The anomalies have been smoothed by applying a 3-month running mean to the original monthly mean data. Warm and cold event years were taken from Table 2.

## Summary

---

Both warm and cold ENSO events have a detectable influence on precipitation over Mexico, although the effect varies for different parts of the country. In the "composite" warm event, the Sierra Madre (and, as it turns out, the whole of north-central Mexico) receives higher-than-normal amounts of precipitation during winter, a signal that is in phase with that over the southeastern United States. This is related to a more active subtropical flow, induced by anomalously strong equatorial convection over the eastern Pacific. During June through August periods of anomalously high SST in the eastern equatorial Pacific, a condition presumably related to active convection in that region, the monsoon rainfall over southern Mexico tends to be weaker than normal. This is likely related to the southward displacement of ITCZ convection over the warmer-than-normal ocean to the south and west of Mexico (*eg*, Douglas 1982). Cold events tend to be characterized by opposite patterns. These signals are fairly robust in that anomalies during most individual events share the same sign as the composite events.

It should be emphasized that, as opposed to the Sierra Madre region, the anomaly amounts over southern Mexico are not large with respect to the total climatological precipitation over this region. On average during April through October, the warm SST years had 88 mm less precipitation than the mean, while cold SST years averaged only 73 mm above the mean, compared to a mean seasonal precipitation of 1175 mm. Thus, while the signal is consistent and individual years can have significant departures related to SST (*eg*, 1953, 1957, 1982 warm years; 1954, 1955 cold years), the net effect of ENSO on monsoon precipitation and agriculture over southern Mexico would appear to be negligible in most cases, with only the most extreme events (such as 1982-83) having a more significant impact.

## Acknowledgments

---

This work is funded by NOAA's Climate and Global Change Program. We thank Jon Eischeid for graphics and data support.

## **References**

---

- Aceituno, P. 1988. On the functioning of the Southern Oscillation in the South American sector. Part I: Surface climate. *Monthly Weather Review* 116:505-524.
- Bradley, RS, HF Diaz, GN Kiladis, and JK Eischeid. 1987. ENSO signal in continental temperature and precipitation records. *Nature* 327:497-501.
- Douglas, AV. 1982. The Mexican summer monsoon of 1982. *Proceedings of the Seventh Annual Climate Diagnostics Workshop*, U.S. Department of Commerce, NOAA, pp.70-79.
- Fu, C, HF Diaz, and JO Fletcher. 1986. Characteristics of the response of sea surface temperature in the central Pacific associated with warm episodes of the Southern Oscillation. *Monthly Weather Review* 114:1716-1738.
- Hartigan, JA. 1975. *Clustering Algorithms*. J. Wiley & Sons, NY. 351 pp.
- Kiladis, GN, and HF Diaz. 1989. Global climatic anomalies associated with extremes in the Southern Oscillation. *Journal of Climate* 2:1069-1090.
- Rasmusson, EM, and TH Carpenter. 1982. Variations in tropical sea surface temperature and surface wind fields associated with the Southern Oscillation/El Niño. *Monthly Weather Review* 110:354-384.
- Ropelewski, CF, and MS Halpert. 1987. Global and regional scale precipitation patterns associated with the El Niño/Southern Oscillation. *Monthly Weather Review* 115:1606-1626.
- Ropelewski, CF, and PD Jones. 1987. An extension of the Tahiti-Darwin Southern Oscillation index. *Monthly Weather Review* 115:2161-2165.

# Changes in Frost Frequency and Desert Vegetation Assemblages in Grand Canyon, Arizona

Robert H. Webb and Janice E. Bowers

**Abstract:** The effect of decreasing frost frequency on desert vegetation was documented in Grand Canyon by replication of historical photographs. Although views by numerous photographers of Grand Canyon have been examined, 400 Robert Brewster Stanton and Franklin A. Nims views taken in the winter of 1889-1890 provide the best information on recent plant distribution. In Grand Canyon, where grazing is limited by the rugged topography, vegetation dynamics are controlled by climate and by demographic processes such as seed productivity, recruitment, longevity and mortality. The replicated photographs show distribution and abundance of several species were limited by severe frost before 1889. Two of these, brittlebush (*Encelia farinosa*) and barrel cactus (*Ferocactus cylindraceus*), have clearly expanded their ranges up-canyon and have increased their densities at sites where they were present in 1890. In 1890, brittlebush was present in warm microhabitats that provided refugia from frost damage. Views showing desert vegetation in 1923 indicate that *Encelia* expanded rapidly to near its current distribution between 1890 and 1923, whereas the expansion of *Ferocactus* occurred more slowly. The higher frequency of frost was probably related to an anomalous increase in winter storms between 1878 (and possibly 1862) and 1891 in the southwestern United States.

The distributional limits of many desert plants may be determined by unusual climatic conditions. Because many of the columnar cacti and leguminous shrubs and trees that characterize the Sonoran Desert are sensitive to frost, the northern limits of that desert have been defined in terms of frost frequency (Shreve 1911; Turnage and Hinckley 1938; Hastings 1963). Rare, catastrophic freezes may cause widespread mortality of Sonoran Desert plants (Turnage and Hinckley 1938; Bowers 1981), particularly seedlings or juveniles not protected by nurse plants (Niering *et al* 1963).

Desert plant assemblages are also sensitive to grazing by domestic livestock. Grazing is so pervasive across the North American desert that it is often difficult to separate the effects of climate from those of grazing. For instance, domestic livestock grazing has been blamed for widespread conversion of grasslands to shrublands (Bahre 1991) and promotion of exotic or unpalatable species (Burgess *et al* 1991), although climatic variability or change could have been responsible for many of the changes (Hastings and Turner 1965). Sites that have been protected from grazing typically are small and relatively inaccessible (*eg*, Schmutz *et al* 1976; Turner 1990).

Large tracts of ungrazed desert are extremely rare; rarer still are those where vegetation has been or can be monitored for many decades. One such area is the bottom of Grand Canyon, where impassable cliffs

prevent movement of grazing animals, and spectacular scenery has encouraged a rich history of photography useful in reconstructing past vegetation (Figure 1). Over the past several years, we have replicated hundreds of historical photographs. This paper reports on changes in desert vegetation that have been documented by matched views.

Photography was extremely important to early river runners, who wanted to document their exploits or finance their expeditions by selling photographs (Fowler 1989). Photographers on early Grand Canyon explorations included Jack Hillers of Major John Wesley Powell's second expedition (1872); Timothy O'Sullivan and William Bell of the Wheeler Expedition (1871-73); Ben Wittick, who explored on his own (1883-85); Franklin A. Nims and Robert Brewster Stanton of the Colorado River Survey (1889-90); Raymond Cogswell, who ran the Colorado River with Julius Stone (1909); the Kolb brothers (1911); and Eugene C. LaRue, who was the photographer of a U.S. Geological Survey expedition (1923). Of this wealth of photographic documentation, the most useful from the standpoint of interpreting desert vegetation are the many views taken by Nims and Stanton.

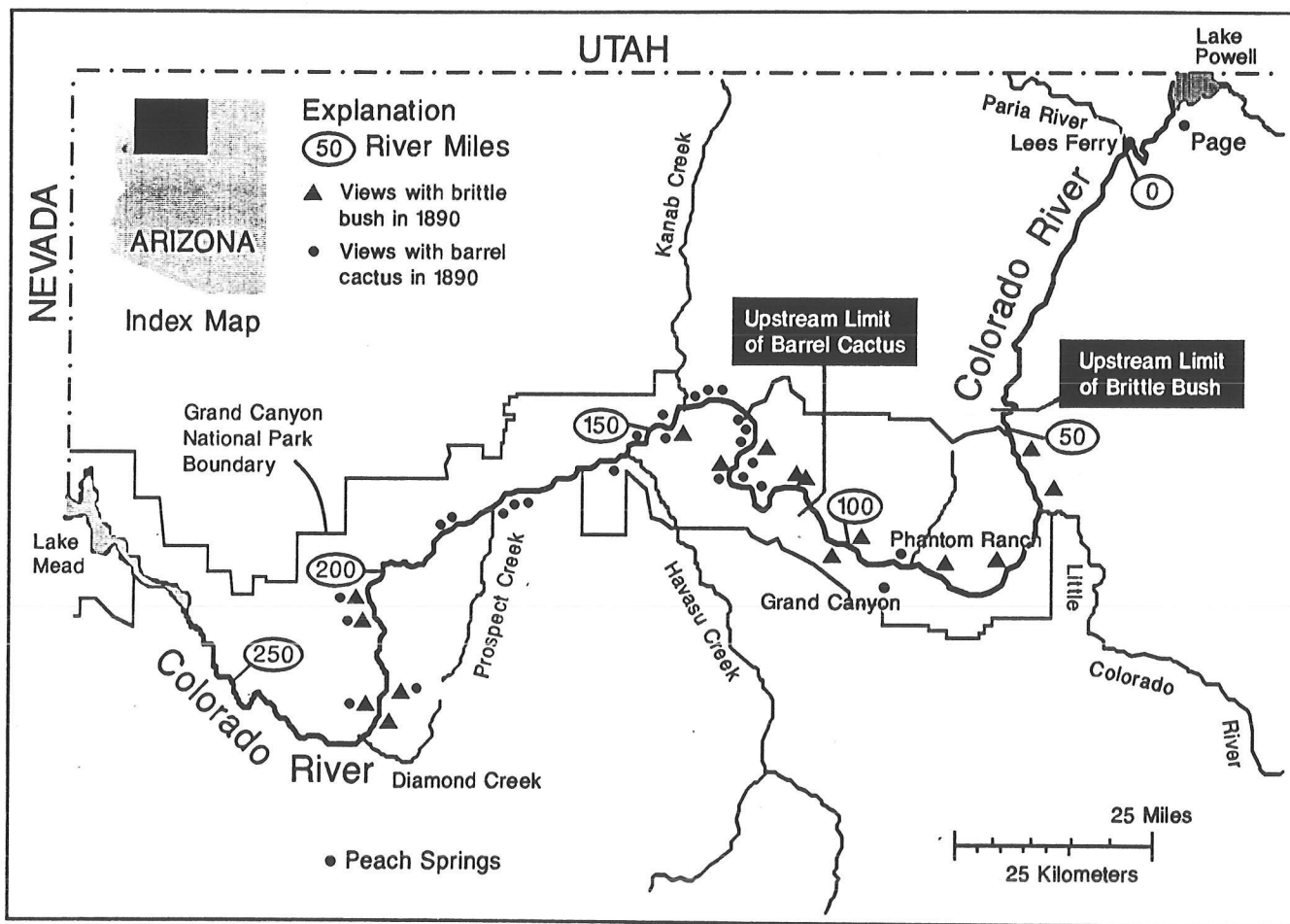


Figure 1. Map of the Grand Canyon.

## The Stanton Photography

---

In 1889, Frank M. Brown, an ambitious investor, formed a company to ascertain the feasibility of a railroad route through the canyons of the Colorado River in Utah and Arizona (Smith 1965; Smith and Crampton 1987). Brown hired Robert Brewster Stanton as chief engineer and Franklin A. Nims as photographer for the project. During the first expedition, in the summer of 1889, Brown and two crew members drowned in two separate accidents, and the mission was aborted after traveling only 50 km into Grand Canyon. Stanton returned to lead a second expedition that began in November 1889. Between December 28, 1889, and March 1, 1890, he and his crew successfully traversed Grand Canyon without additional loss of life.

During the first expedition, Stanton had attempted an instrumental survey of the proposed railroad route. Because the time required for surveying was excessive, Stanton relied on photography to document the feasibility of the route during the second expedition. Unfortunately, Nims, the photographer, was injured in a fall and had to be evacuated after the expedition had traveled only 25 km into Grand Canyon (Smith 1967); Stanton, who had no previous photographic experience, assumed the photographer's duties. Altogether, Nims and Stanton exposed 446 views on 6-1/2 by 8-1/2 inch negatives between the current site of Glen Canyon Dam and the top of Lake Mead, a distance of 400 km. They frequently made upstream and downstream views from the same point.

## Methods

---

In the winters of 1990-1992, we replicated 400 of the views made on Stanton's second expedition. We worked in the winter so as to capture vegetation in the same state of dormancy as depicted in the 1889-1890 views. Supplemental information was obtained from replication of several views of desert vegetation by LaRue in 1923. Of the views we replicated, 241 showed desert vegetation along the river corridor and could be evaluated for changes in species composition and plant density. By comparing the relative positions of plants and stable foreground rocks, we were also able to identify individual shrubs and trees that had persisted *in situ* for one hundred years (Figures 2 and 3). The resolution of the 1889-1890 views varied considerably; in some, only foreground plants could be identified with any certainty. In any given pair of replicates, therefore, we interpreted only the area that was clearly visible in both photographs.

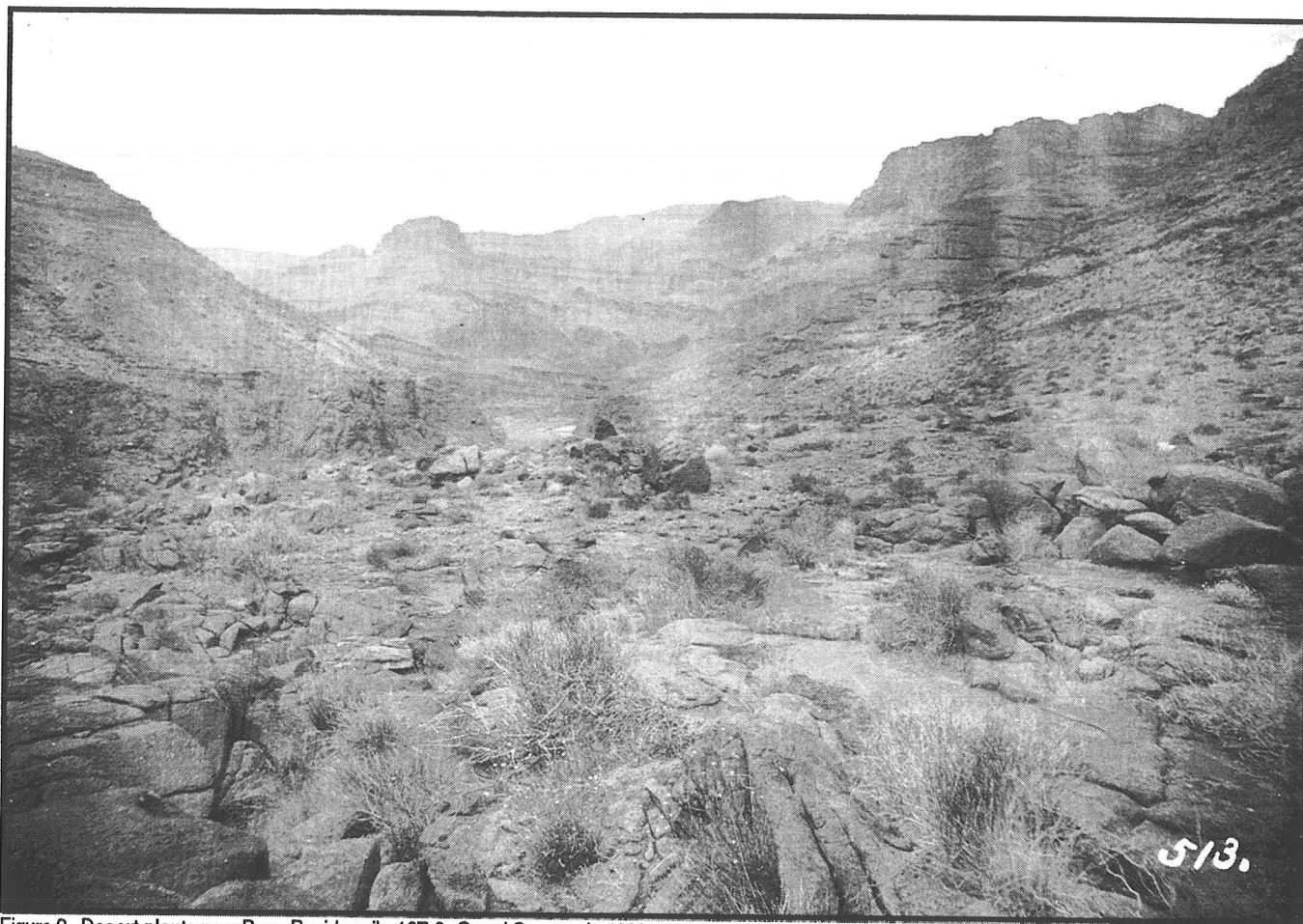


Figure 2. Desert plants near Bass Rapids, mile 107.6, Grand Canyon, in 1890.

Desert vegetation assemblages through much of Grand Canyon were dominated by Mormon tea (*Ephedra* sp.), which is the most common shrub in the foreground of this view. No brittlebush (*Encelia*) appear in this view, which has a resolvable depth of field of about 50 meters. (Photograph by Robert Brewster Stanton, Number 513, taken February 17, 1890, courtesy of the Still Picture Branch, National Archives.)

## Stability of Geomorphic Surfaces

The bedrock and substrate associated with desert plant assemblages is remarkably stable in Grand Canyon. During the last century, our camera stations recorded only a few rockfalls, mainly along the first 45 kilometers of river corridor. Sand dunes, present at a small minority of camera stations, can be mobile. Otherwise, the stability of bedrock outcrops and the persistence of even small rocks has allowed us to eliminate change in substrate as a possible cause for change in the desert plant assemblages.

## Stability of Desert Plant Assemblages

Many species of desert plants in Grand Canyon are long-lived and form stable assemblages. Individuals of about 40 species were found to persist for one hundred years or more. For example, more than a thousand individuals of *Ephedra torreyana* and *E. nevadensis*, the most pervasive dominants along the river corridor, appear in the 1890 views; of these, more than 70 percent have persisted throughout the intervening century.



Figure 3. Desert plants near Bass Rapids, mile 107.6, Grand Canyon, in 1991.

In 1991, this site was dominated by frost-sensitive *Encelia*, the silvery, hemispheric shrub that appears throughout the view. Two of the *Ephedra* in the foreground have persisted the intervening century. (Photograph by Dave Edwards, Stake 1755a, February 14, 1991.)

Because we encountered *E. torreyana* and *E. nevadensis* most often in sterile condition, when they are difficult to distinguish, we discuss them collectively here. Other long-lived species included creosote bush (*Larrea tridentata*), Anderson thorn bush (*Lycium andersonii*), and cat-claw (*Acacia greggii*). Densities of these species did not appear to change substantively between 1890 and 1990. Our replicated photographs suggest that five species of caespitose (non-rhizomatous) grasses are also capable of persisting for one hundred years.

### Changes in Brittlebush

Brittlebush (*Encelia farinosa*) is a common shrub of rocky slopes in the Mojave and Sonoran deserts. The plants are drought-deciduous and retain their leaves in all but the coldest winters. In Grand Canyon, *E. farinosa* is common between mile 42.5 and Lake Mead (Phillips *et al* 1987; Figure 1); in many areas, it is a dominant. The bright, silvery leaves and distinctively forked flower stalks make *Encelia* easy to identify in photographs.

Across much of its range, the species experiences a predictable drought in late spring and early summer. Extreme summer drought is required to produce significant mortality (J.R. Ehleringer, University of Utah, pers. comm., 1992). In all likelihood, a more frequent cause of mortality is catastrophic frost. The low temperature or number of hours below freezing required to kill *Encelia* is uncertain; leaf and apical stem damage has been recorded at  $-4^{\circ}\text{C}$  (Turner *et al* unpublished data), and plants were killed to the ground at  $-8.3^{\circ}\text{C}$  (Turnage and Hinckley 1938). In neither case did temperatures remain below freezing for 24 hours. Along the Colorado River, an *Encelia* population at the upstream limit of the species suffered 70 percent mortality on north-facing slopes (Larry Stevens, National Park Service, pers. comm., 1991) following temperatures of at least  $-6^{\circ}\text{C}$  in February 1989 and December 1990.

In 1890, *Encelia* was uncommon along the river corridor; it is visible in only 17 Stanton views. Today, the species is common; in 1990-1992, we noted *Encelia* in the vicinity of 137 camera stations and captured it in 80 of our views. At many of these 80 stations, the increase in density is striking (Figures 2 and 3). Only one camera station had *Encelia* visible in 1890 but not in 1990. Using a contingency table analysis that compared the presence/absence of *Encelia* in 1890 and 1990s views, the probability that *Encelia* would occur in only 17 of 80 views was extremely low (Chi-square distribution;  $P < 0.001$ ).

Stanton first recorded *Encelia* at mile 52, close to the current upstream limit of the species in Grand Canyon. Moreover, seeds of *Encelia* were found in a 1,500 YBP packrat midden in a tributary at mile 65 (Cole 1985). This suggests to us that the recent increase in *Encelia* does not represent a species invading a favorable habitat. Rather, we hypothesize that the paucity of *Encelia* in the Stanton photographs resulted from extensive mortality in an already well-established population. The most likely cause of this population decline was catastrophic frost. No dead plants of *Encelia* are visible in 1890 views, which suggests the catastrophic event (which may have taken the form either of a single severe freeze or of persistent frequent freezes) occurred many years before 1890.

Of the 17 sites that had *Encelia* in 1889-1890, ten faced south or southwest. Several views depict individuals between large boulders, many of which were black or covered with dark desert varnish. These warmer microhabitats apparently provided refugia from catastrophic frost. After 1890, *Encelia* re-establishment occurred rather quickly; the species appears in 1923 photographs at a site where it was not present in 1890. It is worth noting that *Encelia* apparently occupied an empty niche when it expanded, as many 1890 photographs show bare ground where the 1990s photographs show a relatively dense cover of *Encelia*. The proliferation of *Encelia* in less than 33 years is consistent with a decrease in what probably was persistently frequent severe freezes before the turn of the century.

## Changes in Barrel Cactus

Barrel cactus (*Ferocactus cylindraceus*, formerly *F. acanthodes*) is common along the Colorado River between about mile 110 and Lake Mead. This cylindrical cactus, which is 1 to 3 meters tall, is readily identifiable in historical and modern views because of its shape and stature; we could discern individuals located as much 300 meters away from the camera station. The northerly limit of *F. cylindraceus*, like that of its congeners in the Mojave and Sonoran deserts, is determined by frost (Nobel 1980). Damage to chlorenchyma cells occurs at  $-8.4^{\circ}\text{C}$  in plants that have been cold-hardened (Nobel 1982). Damage is minimized by spine coverage at the apex. Apical spine coverage increases somewhat with plant height, thereby increasing cold-temperature tolerance as the plants age (Nobel 1980). Adult plants are probably not at risk during extreme frost; instead, seedling and juvenile individuals are killed (Nobel 1984). Seedling establishment is also limited by prolonged drought (Jordan and Nobel 1981).

Like *Encelia*, *Ferocactus* appears to have been well established in its current distribution by 1890; Stanton first captured it about 32 kilometers downstream of the current upstream limit. Seeds of *Ferocactus* were found in packrat middens dated at 8,500 to 19,000 YBP that were collected at the western end of Grand Canyon (Phillips 1977). The most striking change shown in the replicated photographs is a dramatic increase in *Ferocactus* density along the entire river corridor. On average, 128 percent more individuals were visible in the 1990-1992 views than in the 1889-1890 views. In a paired-sample t-test comparison, the mean difference between 1889-1890 and 1990-1992 views was 7.9 individuals ( $P < 0.000$ ). In 47 replicates showing *Ferocactus*, only 6 views from 1890 had more individuals than the 1990-1992 views. Although *Ferocactus* commonly appears in 1923 views, the density in 1923 was lower than in 1990-1992. As with *Encelia*, we suspect catastrophic frost drastically reduced the *Ferocactus* population sometime during the late 19th century. The absence of *Ferocactus* carcasses in the Stanton views suggests this occurred well before his 1890 expedition.

A comparison of replicated views shows that *Encelia* was well established by 1923, whereas *Ferocactus* was not. This lag in re-establishment may have resulted from their different reproductive strategies. *Encelia*, a prolific seed producer dispersed in part by wind, is well-suited for colonization of recently disturbed habitats or otherwise empty niches. Plants reach maturity at an early age, and, given a sequence of years favorable for establishment, populations can expand rapidly. In the vicinity of Tucson, Arizona, conditions favorable to *Encelia* germination occurred seven times between 1985 and 1992, a relatively frequent rate for a desert perennial (Bowers, unpublished data). *Ferocactus*, on the other hand, matures more slowly and produces fewer seeds, which are largely dispersed by animals. It encounters favorable germination conditions rather rarely, in only 8 of 18 years in the Mojave Desert (Jordan and

Nobel 1979). This species would, therefore, spread slowly from an initial occupation site.

### Changes in Other Cacti and Succulents

---

Ten species of cacti were recorded in the Stanton views. Like *Ferocactus*, many of these are limited by frost, and, as would be expected, many have shown large increases during the past century. A second species of barrel cactus, *Echinocactus polycephalus*, was present at 23 camera stations in 1990-1992. Of these views, 13 from 1990-1992 showed *Echinocactus* whereas only 3 from 1890 showed it. At one site where *Echinocactus* was clearly visible, 3 individuals were present in the 1890 view (one persisted the century) whereas 11 new individuals were present in a 1991 view. Little is known of the environmental tolerances of *Echinocactus*, although it likely has tolerances similar to *Ferocactus*.

Among other succulents that have increased are *Opuntia erinacea*, *O. basilaris*, and *Echinocereus engelmannii*. Ocotillo (*Fouquieria splendens*), which occurs today between mile 157 and Lake Mead (Phillips *et al* 1987), is also limited in its northward distribution by low temperatures, but this species did not appear in enough views to make an adequate comparison of change.

### Alternative Hypotheses for Observed Changes

---

It is possible that when Stanton traveled the Colorado River in 1890, *Encelia* and *Ferocactus* had only recently appeared in Grand Canyon. If so, the individuals shown in his photographs represent pioneers rather than relicts of formerly well-established populations. The absence of dead plants of either species is congruent with this hypothesis. Using photographs alone, we are unable to distinguish between pioneers and relicts; however, the scattered occurrence of both species along the river corridor in 1890 and preservation of evidence of these species in packrat middens as old as 19,000 YBP suggest the remnants of a decimated population rather than the forerunners of an advancing species. If the latter were the case, we would expect to see more plants in the downstream views than in the upstream ones, since downstream populations would have had more time for reproduction and establishment. Based on the limited number of photographs available, this does not seem to be the case.

Changes in climatic variables other than frost could have affected the density of *Encelia* and *Ferocactus* between 1890 and 1990. For example, extended summer drought could have reduced the density of *Encelia*. Yet, although the amount of summer precipitation in the region did decrease after 1942 (Hereford and Webb 1992), species that are more mesophytic than *Encelia*, particularly *Ephedra*, changed very little. Anomalously high rainfall is also a possibility (large floods occurred regionally in the late

1800s), but, again, other species that presumably would have responded favorably to the increased moisture were unchanged.

### **Anecdotal Evidence of Change in Frost Frequency**

---

Grand Canyon forms a nearly ideal conduit for cold-air drainage during winter months on the Colorado Plateau. As a result, winter temperatures in the bottom of Grand Canyon are extremely variable. At Phantom Ranch, winter lows typically are above freezing but rarely approach  $-18^{\circ}\text{C}$ . The lowest low temperature in the 20-year record at this station is  $-23^{\circ}\text{C}$ , measured in January 1971 (Sellers *et al* 1985). At Lees Ferry, the lowest low temperature is  $-16^{\circ}\text{C}$ , recorded in 1963. The low temperature of  $-14^{\circ}\text{C}$  in January 1971 at Lees Ferry suggests the severe freeze recorded downstream at Phantom Ranch was somewhat localized. Low temperatures during the period around 1890 are unknown for these stations.

Instrumental weather records do not allow evaluation of frost frequency before and after 1890. Lees Ferry, Arizona, the longest record of relevance, began in 1916. Long-term records from the region are restricted, with perhaps the most appropriate being Fort Mojave, Arizona, which was established in 1863 about 200 kilometers southwest of Grand Canyon in the valley of the lower Colorado River. However, this site, near present day Bullhead City, was abandoned in 1938, which does not allow an evaluation of change in frost frequency. Anecdotal evidence is the only type of information available to verify a climatic change that is suggested by change in desert plants in Grand Canyon.

For the continental United States, average temperatures have increased since the 1800s (Kalnicky 1974). In the western United States, the late 1800s were characterized by periodic severe winters that may be related to anomalously frequent El Niño conditions, particularly between 1878 and 1891 (Quinn *et al* 1987). Between 1862 and 1910, abnormally large winter storms caused floods on most of the rivers in the southwestern United States (Webb 1985; Webb and Baker 1987); typically, such storms are followed by severe cold. On the Great Plains, the winter of 1886 claimed at least 35 percent of rangeland cattle during intense and frequent blizzards (Stegner 1953). In northern Nevada, half of the cattle died in the abnormally cold and snowy winter of 1889-1890 (Young and Sparks 1985). Stanton recorded this cold weather in his diary of the 1889-1890 Grand Canyon expedition (Smith and Crampton 1987).

One indication of the severity of winters in the late 1800s and early 1900s is the freezing of the Colorado River at Lees Ferry. Ferryman, and later hydrographers, recorded freezes because of their effects on passage across the river or measurement of streamflow. The most severe documented freeze was in 1878, when the river was frozen from bank to bank below the Paria River for more than two weeks, allowing wagons to be driven across the river (LaRue 1925, p. 13). Other, less notable freezes of

the river occurred in January of 1866, 1880, and 1925. The record of ice effects on the gaging station of the Colorado River at Lees Ferry (Figure 4) suggests a change in frost frequency at this site after the early 1930s that is coincident in a change from predominantly meridional to zonal flow over the Northern Hemisphere (Dzerdzevskii 1969; Kalnicky 1974; Balling and Lawson 1982). Meridional circulation is required to advect arctic air masses into the Southwest.

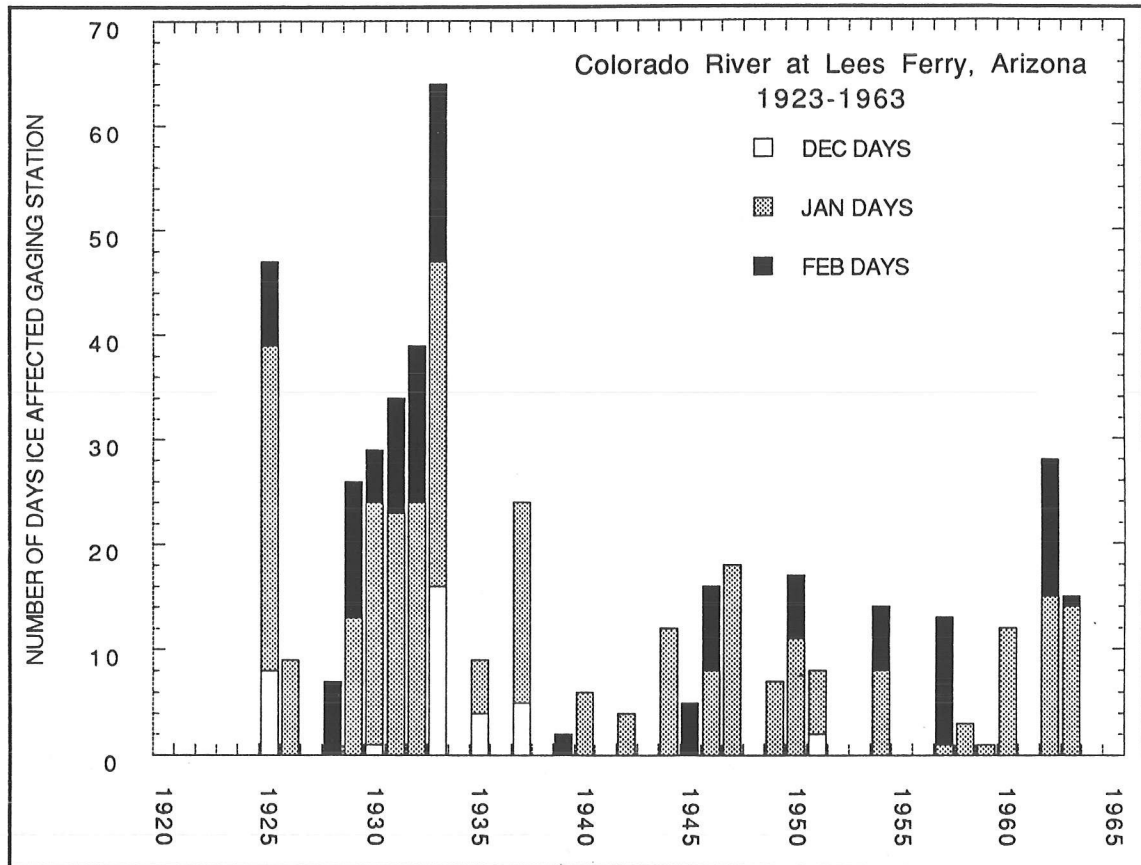


Figure 4. Days of ice at stream-gaging station, Colorado River at Lees Ferry, Arizona, 1923-1963. Closure of Glen Canyon Dam in March 1963 ends this unique record. Data from annual reports on streamflow for the Colorado River basin (eg, U.S. Geological Survey, 1961).

## Conclusions

In the last century, desert plant assemblages have changed significantly along the Colorado River in Grand Canyon National Park. The distribution and abundance of certain climatically insensitive species, such as *Ephedra*, have changed little. Most of the *Ephedra* individuals observed in the 1890 photographs have persisted throughout the intervening century. Other species, particularly *Encelia farinosa*, *Ferocactus cylindraceus*, and *Echinocactus polycephalus*, have increased in abundance since 1890. Occurrence of these species near their current distributional limits in 1890 indicates that they were suppressed sometime before that year; moreover, most *Encelia* visible in the 1890 photographs occurred on southerly-facing slopes or among groups of dark-colored boulders.

The suppression could have occurred during one event, such as the catastrophic freeze of 1878, but more likely the cause was a greater frequency of freezing weather than now occurs in Grand Canyon. Instrumental weather records do not exist for the critical period between settlement of the region and 1890; anecdotal evidence indicates the changes are related to a decrease in the frequency of severe frost after the turn of the century.

## Acknowledgments

---

The authors thank T.S. Melis, T. Wise, M. Murov, L. Hymans, D. Edwards, R. Rondeau, and the numerous others who assisted with the field work for this project. We especially thank the Still Picture Branch of the National Archives, Washington, D.C., for help in obtaining high-quality reproductions of the original photography. J.L. Betancourt and G. Bolton, U.S. Geological Survey, and D. Sandquist, University of Utah, reviewed a draft of this manuscript. This work was partly funded by the U.S. Bureau of Reclamation under the Glen Canyon Environmental Studies Program.

## References

---

- Bahre, CJ. 1991. *A legacy of change: Historic human impact on vegetation of the Arizona borderlands*. Tucson, University of Arizona Press, 231 pp.
- Balling, RC, and MP Lawson. 1982. Twentieth century changes in winter climatic regions. *Climatic Change*. 4:57-69.
- Bowers, JE. 1981. Catastrophic freezes in the Sonoran Desert. *Desert Plants*. 2:232-236.
- Burgess, TL, JE Bowers, and RM Turner. 1991. Exotic plants at the Desert Laboratory, Tucson, Arizona. *Madroño* 38:96-114.
- Cole, KL. 1985. Past rates of change, species richness, and a model of vegetational inertia in the Grand Canyon, Arizona. *American Naturalist* 125:289-303.
- Dzierdzewski, BL. 1969. Climatic epochs in the twentieth century and some comments on the analysis of past climates. In HE Wright, Jr., ed., *Quaternary geology and climate*. 16 of the Proceedings of the 7th Congress, International Quaternary Association. Washington, DC, National Academy of Sciences Publication 1701:49-60.
- Fowler, DD. 1989. *The western photography of John K. Hillers*. Washington, DC, Smithsonian Institution Press, 166 pp.
- Hastings, JR. 1963. *Historical change in the vegetation of a desert region*. Tucson, University of Arizona, unpublished Ph.D. dissertation.
- Hastings, JR, and RM Turner. 1965. *The changing mile*. Tucson, University of Arizona Press, 317 pp.
- Hereford, R, and RH Webb. 1992. Historic variation in warm-season rainfall on the Colorado Plateau, U.S.A. *Climatic Change*, in press.
- Jordan, PW, and PS Nobel. 1979. Infrequent establishment of seedlings of *Agave deserti* (Agavaceae) in the northwestern Sonoran Desert. *American Journal of Botany* 66:1079-1084.

- \_\_\_\_\_. 1981. Seedling establishment of *Ferocactus acanthodes* in relation to drought. *Ecology* 62:901-906.
- Kalnicky, RA. 1974. Climatic change since 1950. *Annals of the Association of American Geographers*. 64:100-112.
- LaRue, EC. 1925. *Water power and flood control of Colorado River below Green River, Utah*. U.S. Geological Survey Water-Supply Paper 556, 176 pp.
- Niering, WA, RH Whittaker, and CH Lowe. 1963. The saguaro: A population in relation to environment. *Science* 142:15-23.
- Nobel, PS. 1980. Influences of minimum stem temperatures on ranges of cacti in southwestern United States and central Chile. *Oecologia* 47:10-15.
- \_\_\_\_\_. 1982. Low-temperature tolerance and cold hardening of cacti. *Ecology* 63:1650-1656.
- \_\_\_\_\_. 1984. Extreme temperatures and thermal tolerances for seedlings of desert succulents. *Oecologia* 62:310-317.
- Phillips, AM III. 1977. *Packrats, plants, and the Pleistocene in the lower Grand Canyon*. Tucson, University of Arizona, unpublished Ph.D. dissertation.
- Phillips, BG, AM Phillips III, and MAS Bernzott. 1987. *Annotated checklist of vascular plants of Grand Canyon National Park*. Grand Canyon Natural History Association Monograph No. 7, 79 pp.
- Quinn, WH, VT Neal, and SE Antunez de Mayolo. 1987. El Niño occurrences over the past four and a half centuries. *Journal of Geophysical Research* 92:14449-14461.
- Schmutz, EM. 1976. An ecological survey of Wide Rock Butte in Canyon de Chelly National Monument, Arizona. *Journal of the Arizona Academy of Sciences* 11:114-125.
- Sellers, WD, RH Hill, and M Sanderson-Rae. 1985. *Arizona climate, the first hundred years*. Tucson, University of Arizona Press, 143 pp.
- Shreve, F. 1911. The influence of low temperature on the distribution of giant cactus. *Plant World* 14:136-146.
- Smith, DL. 1965. *Down the Colorado*. Norman, University of Oklahoma Press, 237 pp.
- \_\_\_\_\_. ed. 1967. *The photographer and the river, 1889-90*. Santa Fe, Stagecoach Press, 75 pp.
- Smith, DL, and CG Crampton, eds. 1987. *The Colorado River survey*. Salt Lake City, Howe Brother Books, 305 pp.
- Stegner, W. 1954. *Beyond the hundredth meridian*. Boston, Houghton Mifflin Company, 438 pp.
- Turnage, WV, and AK Hinckley. 1938. Freezing weather in relation to plant distribution in the Sonoran Desert. *Ecological Monographs* 8:530-550.
- Turner, RM. 1990. Long-term vegetation change at a fully protected Sonoran Desert site. *Ecology*. 71:464-477.
- Webb, RH. 1985. *Late Holocene flooding on the Escalante River, south-central Utah*. Tucson, Arizona, University of Arizona, Ph.D. dissertation, 204 pp.
- Webb, RH, and VR Baker. 1987. Changes in hydrologic conditions related to large floods on the Escalante River, south-central Utah. In V Singh (ed). *Regional Flood-Frequency Analysis*. Dordrecht, The Netherlands, D. Reidel Publishers, pp. 306-320.
- US Geological Survey. 1961. *Surface water supply of the United States, 1960. Part 9, Colorado River basin*. U.S. Geological Survey Water-Supply Paper 1713, 520 pp.
- Young, JA, and BA Sparks. 1985. *Cattle in the cold desert*. Logan, Utah State University Press, 255 pp.

## Relationships Between ENSO Events and San Francisco Rainfall, 1949-1991

Jan Null

As California entered its sixth consecutive year of drought, the onset of a positive sea surface temperature anomaly in the equatorial Pacific and other indicators of a developing ENSO event were observed. This brought the following question from the media, water officials, and the public: What effect will El Niño have on the current rainfall season in general and on the intraseasonal distribution of rain in particular?

To answer the question, the historical San Francisco rainfall record was examined in relationship to previous ENSO events. This record was chosen because it is the longest consecutive rainfall record in northern California, has been tested for homogeneity, and is a record for which an extensive daily database has recently been developed (Null 1991). Earlier works (Fu *et al* 1986) looked at the "typing" of ENSO events since 1940 (Figure 1), and the work of Schonher and Nicolson (1989) studied the relationship between seasonal rainfall for large areas of California and ENSO events since 1950.

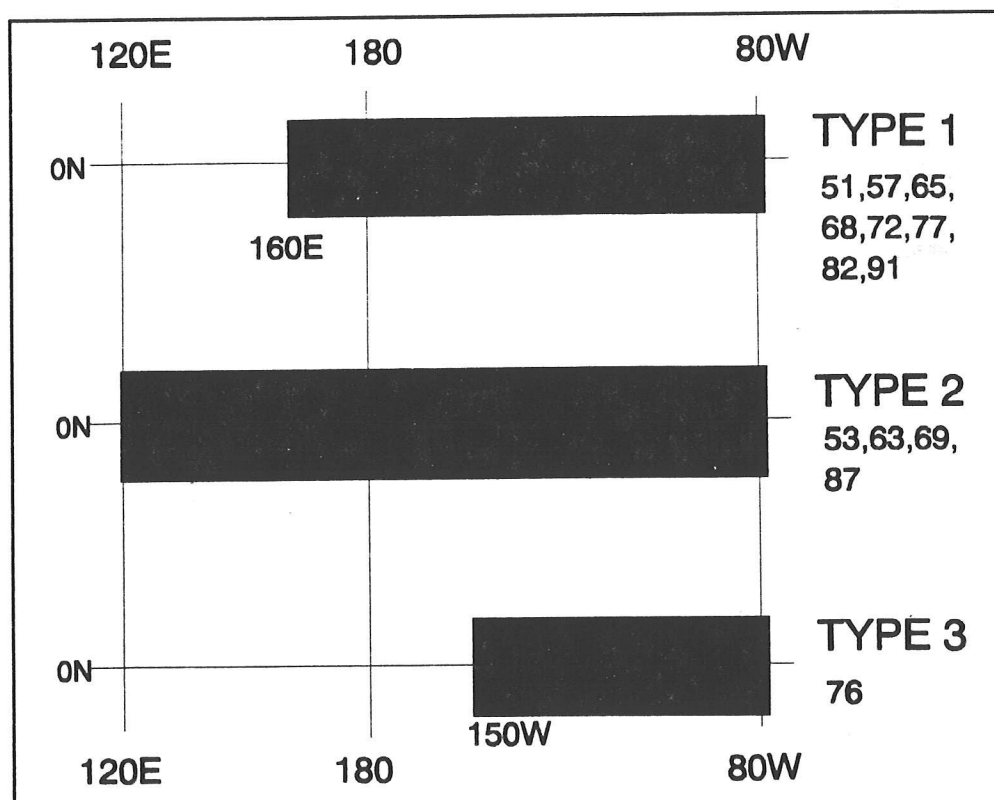


Figure 1. ENSO Type (Fu *et. al*/1986)  
Years indicated are beginning of July 1 to June 30 season.

The goal of this research was to do an introductory examination of the daily, monthly, and seasonal San Francisco rainfall record and their relationships to ENSO events (Figure 2). While no firm conclusions can be drawn until a more thorough statistical analysis of the data is completed, several interesting characteristics of the eight Type 1 ENSO seasons (1951, 1957, 1965, 1968, 1972, 1977, 1982 and 1991) are noted.

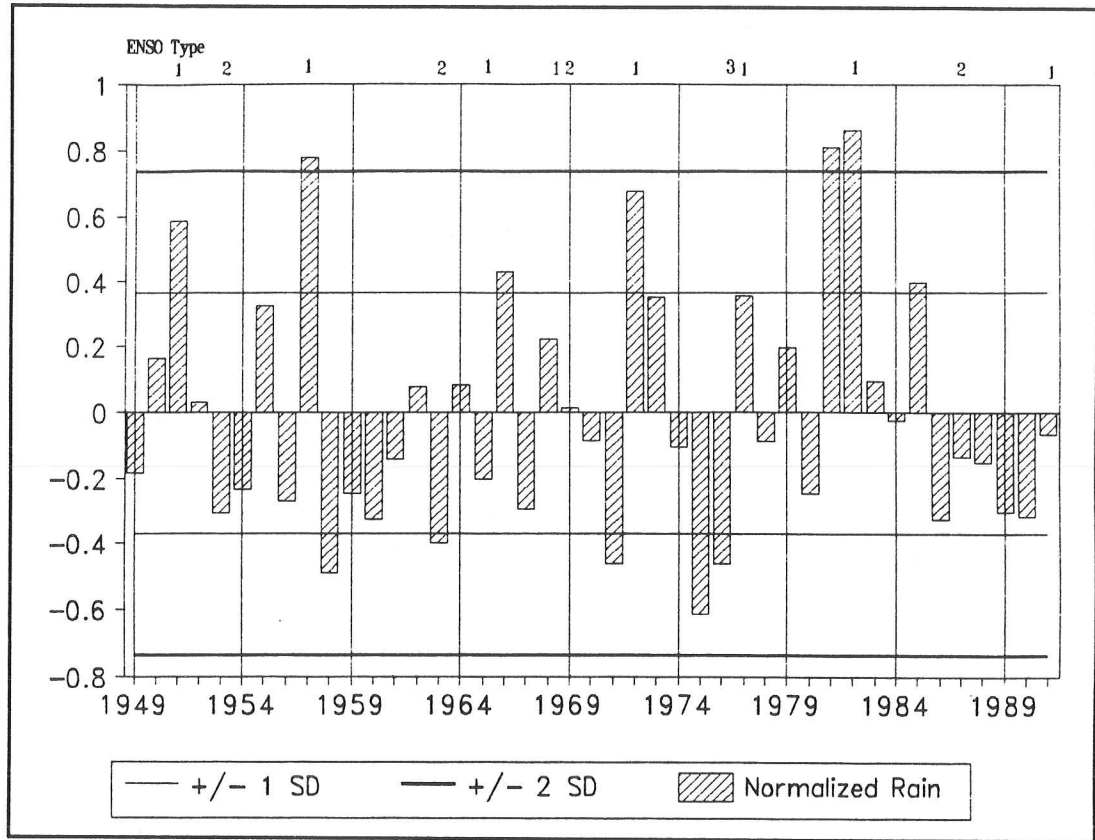


Figure 2. Normalized Rainfall

## Monthly Analysis

The strongest signal that is apparent is for a positive monthly precipitation anomaly during February, when five of the eight Type 1 ENSO seasons were much above normal and one other was above normal (Table 1). January and March also showed a wet bias during Type 1 ENSO events, with three of the eight seasons being much above normal. For January, two additional seasons were above normal, and March had two above the mean.

## Intraseasonal Analysis

As would be expected from the monthly data, there was also a strong positive relationship between ENSO events and intraseasonal rainfall of January through March (Table 2). Of the eight Type 1 seasons, January

Table 1  
RELATIONSHIP OF ENSO TYPE 1 TO MONTHLY RAINFALL

	October	November	December	January	February	March	April
Mean	1.18	2.88	3.54	4.37	3.15	3.13	1.38
Std Dev	1.37	2.33	2.39	2.68	2.29	2.26	1.35
1951	0.81 -	3.33 +	7.92 ++	10.69 ++	2.62 -	4.90 +	1.08 -
1957	3.46 ++	1.13 -	3.60 +	4.38 -	7.78 ++	8.22 ++	5.47 ++
1965	0.01 -	4.79 +	3.51 -	3.27 -	2.72 -	0.80 -	0.36 -
1968	0.62 -	2.67 -	3.91 +	7.74 ++	7.26 ++	1.01 -	1.74 +
1972	5.41 ++	6.40 ++	3.53 -	9.38 ++	6.32 ++	2.63 -	0.02 -
1977	0.17 -	2.22 -	3.30 -	6.94 +	4.14 +	5.90 ++	4.21 ++
1982	2.79 ++	5.62 ++	2.22 -	5.77 +	8.06 ++	9.04 ++	3.48 ++
1991	2.35 +	0.50 -	2.32 -	2.09 -	6.34 ++	4.14 +	0.38 -

- Greater than 1 standard deviation below mean  
 - Less than 1 standard deviation below mean  
 + Less than 1 standard deviation above mean  
 ++ Greater than 1 standard deviation above mean

Table 2  
RELATIONSHIP OF ENSO TYPE 1 TO INTRASEASONAL RAINFALL

	Jan.-Mar.	Feb.-Mar.	Jul.- Dec.	Jan.- Jun.	Season
Mean	10.65	6.28	7.99	12.53	20.52
Std Dev	4.99	3.78	4.11	5.65	7.56
1951	18.21 ++	7.52 +	12.58 ++	19.98 ++	32.56 ++
1957	20.38 ++	16.00 ++	9.66 +	26.82 ++	36.48 ++
1965	6.79 -	3.52 -	8.82 +	7.51 -	16.33 -
1968	16.01 ++	8.27 +	7.29 -	17.80 +	25.09 +
1972	18.33 ++	8.95 +	15.93 ++	18.43 ++	34.36 ++
1977	16.98 ++	10.04 ++	6.68 -	21.19 ++	27.87 +
1982	22.87 ++	17.10 ++	11.35 +	26.82 ++	38.17 ++
1991	12.84 +	10.75 ++	5.59 -	13.61 +	19.20 -

- Greater than 1 standard deviation below mean  
 - Less than 1 standard deviation below mean  
 + Less than 1 standard deviation above mean  
 ++ Greater than 1 standard deviation above mean

through March was much above normal six times and above the mean another time. February through March was slightly above normal three times and much above normal three times.

Examining the second half of the season (January through June) shows a very strong positive precipitation anomaly, with five much above normal and two others slightly above. The first half (July through December) signature was weaker, being much above the mean during two of the Type 1 ENSO events and slightly above another three. For the entire season, four of the eight events were much above normal and two more were slightly above.

## Daily Analysis

Along with the positive anomalies for the monthly data, the daily rainfall amounts yielded a much above-normal number of rainy days during ENSO seasons (Table 3). During the eight Type 1 ENSO events, five exceeded a standard deviation above the mean number of all rain events and another was slightly above. The number of days with more than a half inch of rain was greater than the mean during two of the eight seasons and much above normal four times.

Table 3  
RELATIONSHIP OF ENSO TYPE 1 TO DAILY RAINFALL

	Days > Trace	Days $\leq 0.50"$	Days $\geq 0.50"$
Mean	67	52	14
Std Dev	14	10	6
1951	90 ++	70 ++	20 ++
1957	97 ++	65 ++	32 ++
1965	54 -	43 -	11 -
1968	93 ++	77 ++	16 +
1972	84 ++	59 +	25 ++
1977	81 +	57 +	24 ++
1982	97 ++	70 ++	27 ++
1991	59 -	42 -	17 +

- Greater than 1 standard deviation below mean  
 - Less than 1 standard deviation below mean  
 + Less than 1 standard deviation above mean  
 ++ Greater than 1 standard deviation above mean

## Analysis

There are strong signatures of above normal rainfall during seasons with corresponding ENSO Type 1 events, which are the strongest events. There appeared to be the strongest relationship between these ENSO events and above-normal San Francisco seasonal rainfall during January through March. This carries over into the total number of rainy days, though there is no preference for days with greater amounts of rain as opposed to lighter events.

This is typically the time of year when ENSO events peak (*ie*, there is the greatest positive SST anomaly), resulting in increased convection in the subtropical Pacific and a northward displacement of the subtropical jetstream. At the same time, the polar jet is near its southernmost position, with a net result of a pattern very conducive for heavy California rainfall events.

Conversely, a minimum was seen with the Type 3 event in 1976, though with only a single sample it is impossible to draw any conclusions. The Type 2 events were similarly sparse, with only four events during the 41 seasons of interest. These years were classified by Schonher and Nicholson (1989) as "normal", and all four fall within one-half of a standard deviation of the mean.

While the evidence from ENSO events is not plentiful enough to use as a predictor, it does provide another source of information for decision makers. It also points to the importance of not merely identifying the existence of an ENSO event, but also to determining the "type" of event that it is. The evaluation of additional El Niños, both past and future, will be necessary to draw any firm conclusions as to any significant impact on San Francisco rainfall.

## **References**

---

- Fu, C, HF Diaz, and JO Fletcher. 1986. Characteristics of the Response of Sea Surface Temperature in the Central Pacific Associated with Warm Episodes of the Southern Oscillation. *Monthly Weather Review* 114:1716-1738.
- Null, J. 1991. *Preliminary Analysis of the San Francisco Rainfall Record: 1849-1990*. NOAA Technical Memorandum NWS WR-212. Salt Lake City. National Weather Service.
- Schonher, T, and SE Nicholson. 1989. The Relationship between California Rainfall and ENSO Events. *Journal of Climate* 2:1258-1269.



# Streamflow and La Niña Event Relationships in the ENSO-Streamflow Core Areas

Ercan Kahya and John A. Dracup

The high index phase of the Southern Oscillation (SO), La Niña, has not been given as much attention as its counterpart, the low index phase of the SO, El Niño. One reason may be related to the fact that many similarities exist among El Niño events but not among La Niña events. Thus, the literature mostly contains studies based on composite analysis for El Niño episodes (Philander 1990).

In a global-scale study, Ropelewski and Halpert (1989) found that relationships between the high SO index phase and precipitation anomaly are opposite in sign to the low index phase of the SO relationships. Their study included two regions (the Gulf-northern Mexico and the Great Basin) based on the study of Ropelewski and Halpert (1986) in North America. In a hydrologic perspective, Kahya and Dracup (1993) (hereafter abbreviated as "KD") identified four El Niño/Southern Oscillation (ENSO)-Streamflow core areas (Gulf of Mexico, North East, North Central, and Pacific Northwest) that exhibit a reliable and coherent ENSO/streamflow association (Figure 1). In this study, we focus on the influences of La Niña phenomena on streamflow anomalies in these four areas to explore the SO-related signal over the United States.

## Data Set and Methodology

Monthly virgin streamflow volumes compiled by Wallis *et al* (1991) in the form of CD-ROM are used in this investigation. The data set contains 1,009 high-quality stream gauge records in the United States, each with 41 years of observation (1948-1988). Each record contains nine La Niña events. In determining the relationship between streamflows in the core areas and La Niña events, the following analysis procedures were performed using six event years (1950, 1955, 1964, 1970, 1973, and 1975). In the two cases of two successive La Niña years, only the first year is used for the individual station composite; however, the second years (1956, 1971) and 1988 (if possible) are marked in the index time series.

In our earlier study (KD), the monthly streamflow values were initially expressed in terms of percentiles based on the appropriate log-normal distribution for each month at each station. The ENSO streamflow composite at each station was formed for a idealized 2-year period to make our results comparable to those of Ropelewski and Halpert (1989).

In: K.T. Redmond and V.L. Thorp, Editors. 1993. Proceedings of the Ninth Annual Pacific Climate (PACCLIM) Workshop, April 21-24, 1992. California Department of Water Resources, Interagency Ecological Studies Program, Technical Report 34.

However, the length of the composites was changed to three years when detecting a seasonal signal. (This was especially important in the PNW area.) The episode year in which maximum sea surface temperature anomalies related to El Niño (or La Niña in this study) generally occur in the central and eastern Pacific Ocean was designated by (0); the year that precedes the episode year is designated by (-) and the year that follows is designated by (+). In this convention, ENSO composites of the log-normal streamflow percentiles were constructed for the 24-month period starting with the July preceding the episode, July(-), and continuing through the June following the episode, June(+). These composites were subjected to the fit of the first harmonic. The phase of the first harmonics was assumed to represent the time of maximum relationship between streamflow and ENSO events. The amplitude of the first harmonics represents the magnitude of the relationship. Both quantities were combined into one as a vector and plotted on a map (Figure 1) in order to identify regions that have spatial coherence in terms of timing and magnitude for the streamflow response to the tropical thermal forcing.

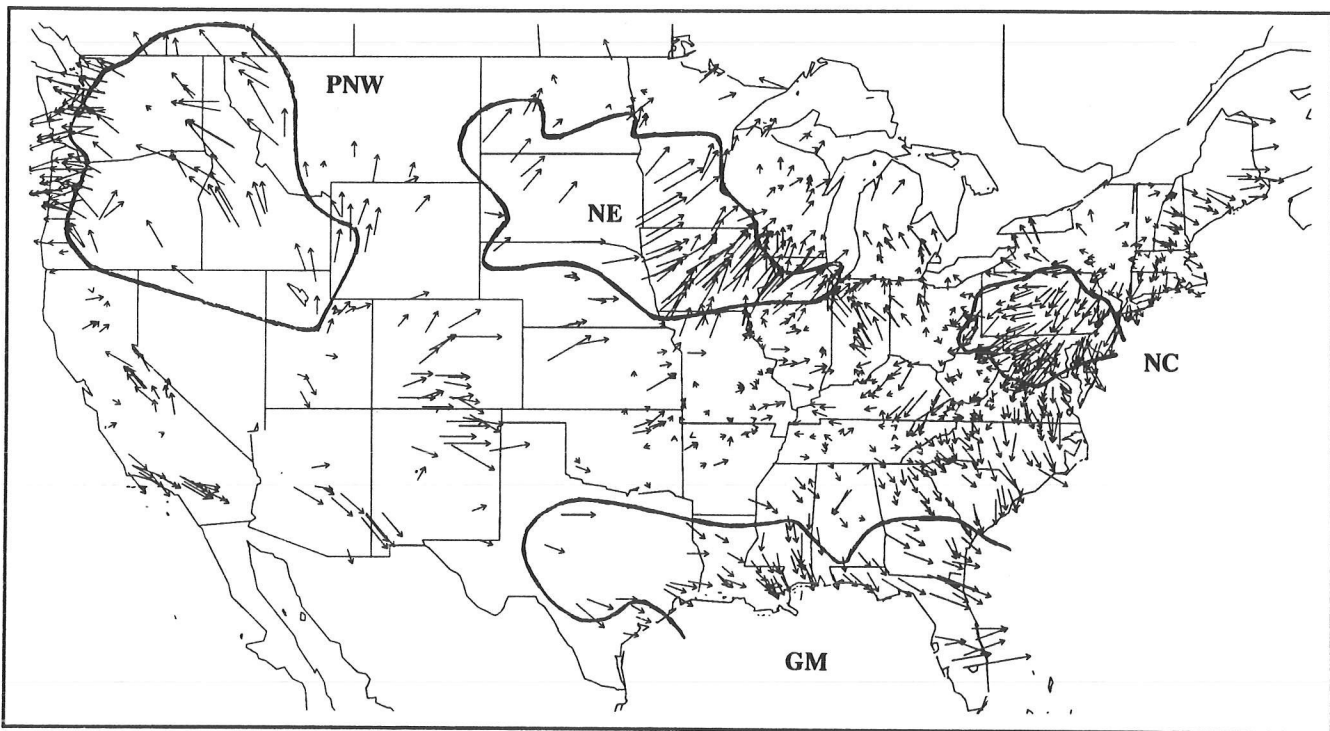


Figure 1. Streamflow station vectors based on the 24-month harmonic fitted to ENSO streamflow composites. Outlined regions of coherent streamflow responses are the core areas. For the direction of arrows, south refers to July(-), north corresponds to June(0), and so on. For the magnitude of arrows, the harmonic arrow belonging to southernmost Florida has a magnitude of 21.6 percent and a phase of December(0), for example. (Adapted from Kahya and Dracup 1992.)

Analysis steps in this study start with those streamflows included in the four core areas. An aggregate La Niña composite for each area is obtained by averaging individual station composites based on three years to detect subjectively a single season. The index time series (ITS) for the region is plotted against the detected season. Finally, ITS is examined for temporal consistency to see whether the La Niña-related streamflow signal is reliable.

## **Results and Discussion**

---

In this section, results are summarized for each of the four areas. Specific information for an area, such as number of stations included, coherence of the first harmonics, and general regional climate, are available in KD.

Since the phenomena of El Niño and La Niña are known to be the extreme state of climate in the equatorial Pacific, it may be plausible to expect their influences on the surface hydroclimatic parameters at middle latitudes to be extreme. It would be advantageous if water resources managers could understand the causes of extreme conditions such as floods and droughts. Therefore, we intend to determine the number of extreme streamflow conditions that were coincident with the occurrence of La Niña events.

The values of an ITS (numbered as a total of 41) are basically the average of log-normal percentiles for months that are included in the corresponding season for each year. Since these index values constitute a distinct population for different seasons, limits for the lowest and the highest will depend on the season and the ITS under consideration. Thus, in this study, the values of an ITS that are lower than 30 percent or higher than 70 percent are not specified as a driest or wettest season average. For that, we found the cumulative distribution of the values of an ITS and calculated the limiting index values for the 10 percent (for the driest conditions) and the 90 percent (for the wettest conditions). In our case, there are always four ITS values that fall below 10 percent and another four that fall above 90 percent.

This analysis attempts to identify a coherent and systematic hydrologic response to the equatorial cold events in the ENSO-streamflow core areas, but the streamflow response to La Niña events may exist elsewhere. Also, the sizes and locations of the core areas may not be right to look for the La Niña-related streamflow response. This may be checked by performing the entire analysis initially based on the La Niña composite.

### Gulf of Mexico (GM)

In the La Niña aggregate composite for the GM area (Figure 2), the 9-month dry period from December(0) to August(+) has been selected as a season with strong La Niña/streamflow relationship. This seasonal signal has similar timing and magnitude with that of ENSO (wet December(0) to April(+) in KD), but has opposite sign. This season also appeared as a dry period in the ENSO aggregate composite (see KD) for the GM. The ITS based on this season is depicted in Figure 3. Seven out of eight episodes affirmed the detected dry season and only one appeared to be extremely dry.

Similarly Ropelewski and Halpert (1989) found that regional precipitation response to La Niña events in the Gulf-northern Mexico region was in the form of dry season, with 16 out of 19 confirmed cases in their 101-year record. In the GM area, Kiladis and Diaz (1989) found a tendency for dry conditions during fall of (-) year that later turns out to be a weak dry signal during winter of (0) year. In the fall of (0) year, the SO-related signal reverses sign, appearing as weak precipitation anomalies. Approaching winter and spring of (+) year, strong wet anomalies dominate the region. These findings refer to El Niño; the opposite is true for La Niña events. Moreover, composite 700-mb height anomalies for six winters (three of

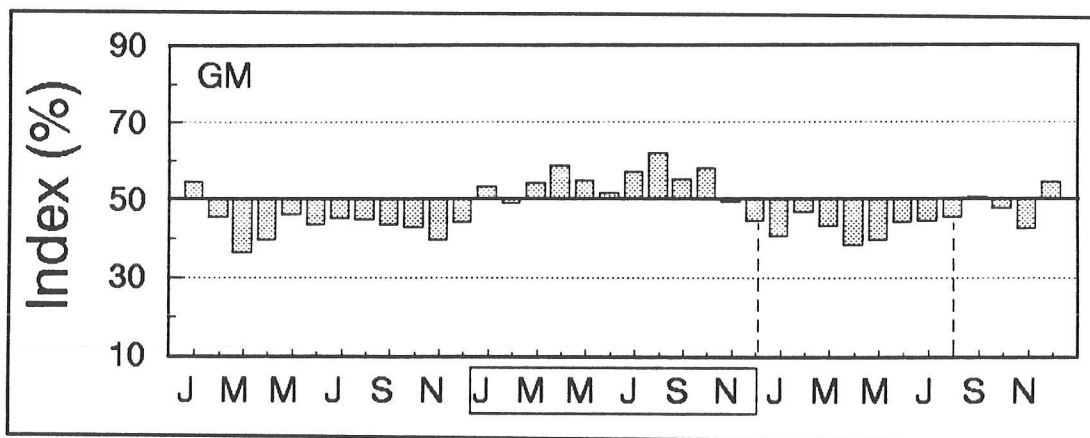


Figure 2. Aggregate La Niña composite based on percentiles of log-normal distribution for the Gulf of Mexico area. Dashed lines delineate the season of possible La Niña-related streamflow responses. Months in the box refer to La Niña or (0) year.

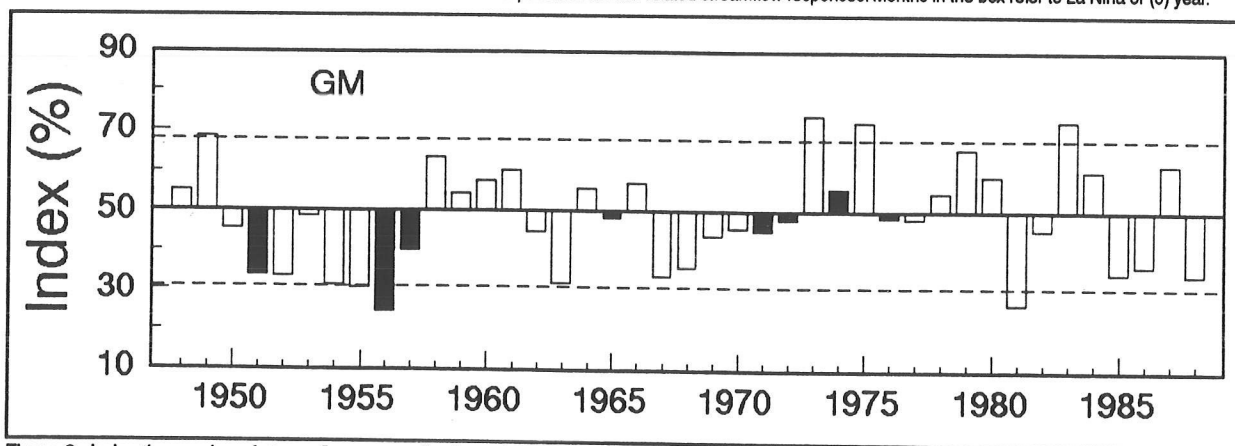


Figure 3. Index time series of streamflow percentiles based on the season chosen in Figure 2 for the Gulf of Mexico area. Signal years are shown by dark bars. Dotted lines indicate the limit for the wettest and driest values.

those indicated as La Niña winters in this study) following dry autumns in the equatorial Pacific (Douglas and Englehart 1981) suggest decreased storm activity in the Gulf of Mexico due to a weakened East Coast trough. This circulation pattern generally bears a warm, dry winter in Florida.

**North East (NE)**

The wet August(0) to February(+) season is an apparent period for the signal timing in the aggregate composite of the North East area (Figure 4). The seasonal ENSO signal with negative anomalies has been previously found during the August(0) to February(+) season in the NE (see KD). The relevant ITS for this area (Figure 5) indicates an acceptable level of consistency, since six of eight cases had above-normal values, one almost neutral, and one major failure case. Two of four extremely wet seasons occurred during La Niña events.

Kiladis and Diaz (1989) indicate a significant SO-related signal for dry conditions for ENSO events (wet conditions for La Niña events) over the North East during summer of (0) year, which is the start of wet streamflow season mentioned above. Their analysis also indicates dry precipitation anomalies during the mature phase. This is in agreement with our results.

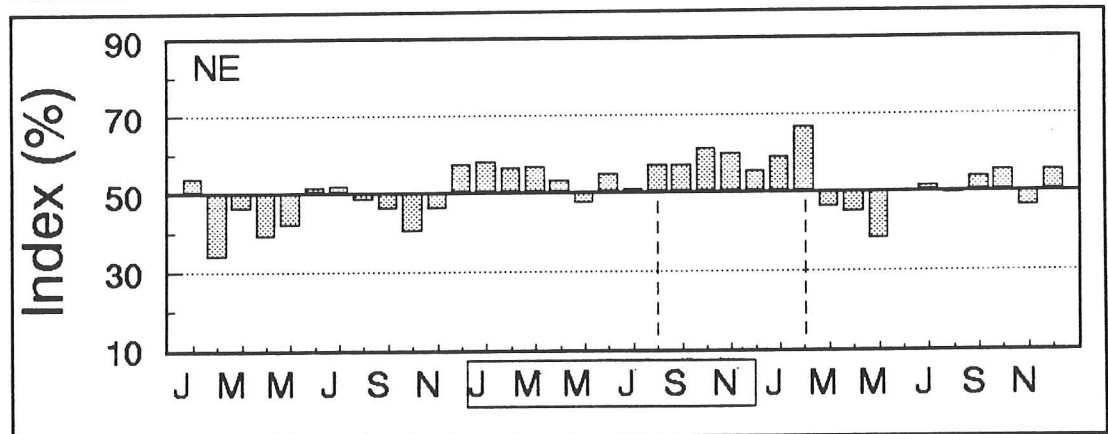


Figure 4. Aggregate La Niña composite based on percentiles of log-normal distribution for the North East area. Dashed lines delineate the season of possible La Niña-related streamflow responses. Months in the box refer to El Niño or (0) year.

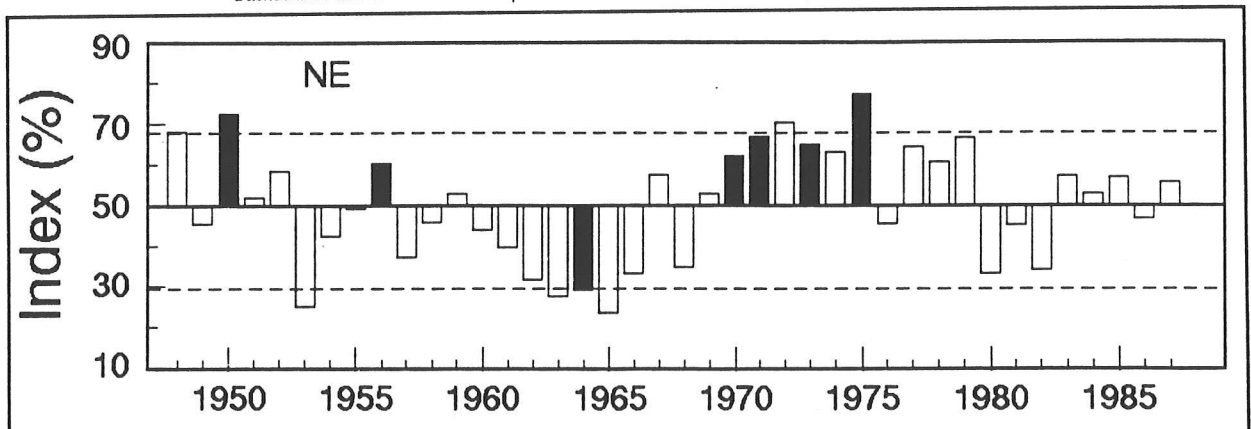


Figure 5. Index time series of streamflow percentiles based on the season chosen in Figure 4 for the North East area. Signal years are shown by dark bars. Dotted lines indicate the limit for the wettest and driest values.

**North Central (NC)**

Figure 6 illustrates typical streamflow anomalies in the evolution period of La Niña phenomena. The sequence of below-average anomalies between July(0) and January(+) has been considered as the response of streamflows in the NC to the tropical cold events. Comparison of this season with the wet April(0) to January(+) season for ENSO events (see KD) shows that initiation of this season was delayed by 3 months and signs of anomalies were reversed. The persistent negative anomalies from January(-) to January(0) in the ENSO composite (see KD) were almost the same as this NC dry season associated with La Niña events. Figure 7 shows the relevant ITS with two positive departures from the median (out of 9 La Niña episodes), confirming the signal by a 0.78 level of consistency. In the study period, three of the four driest seasons occurred during the La Niña years. From a perspective of the occurrence of extreme streamflow conditions, this signal is highly significant.

The results of Kiladis and Diaz (1989) for the NC area indicates dry conditions in the southeastern NC during winter of (+) year and wet conditions in the southwestern NC during spring of (+) year.

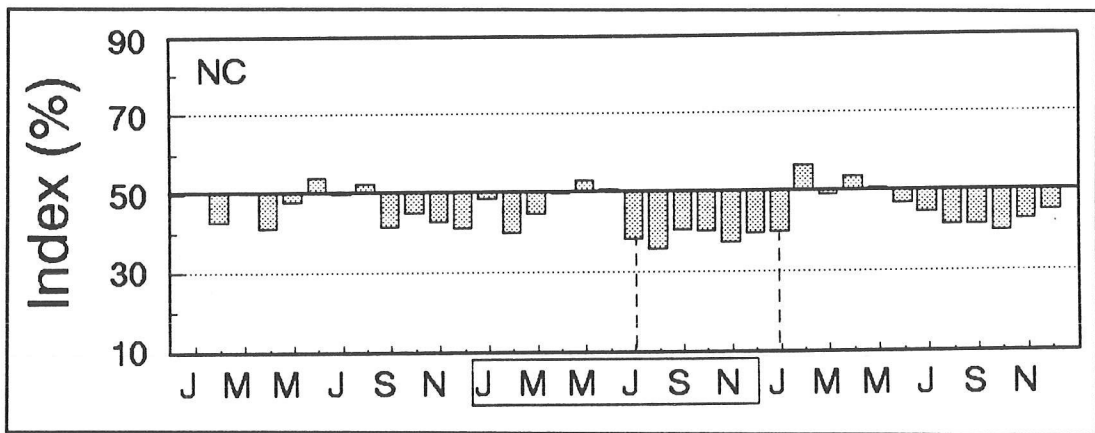


Figure 6. Aggregate La Niña composite based on percentiles of log-normal distribution for the North Central area. Dashed lines delineate the season of possible La Niña-related streamflow responses. Months in the box refer to La Niña or (0) year.

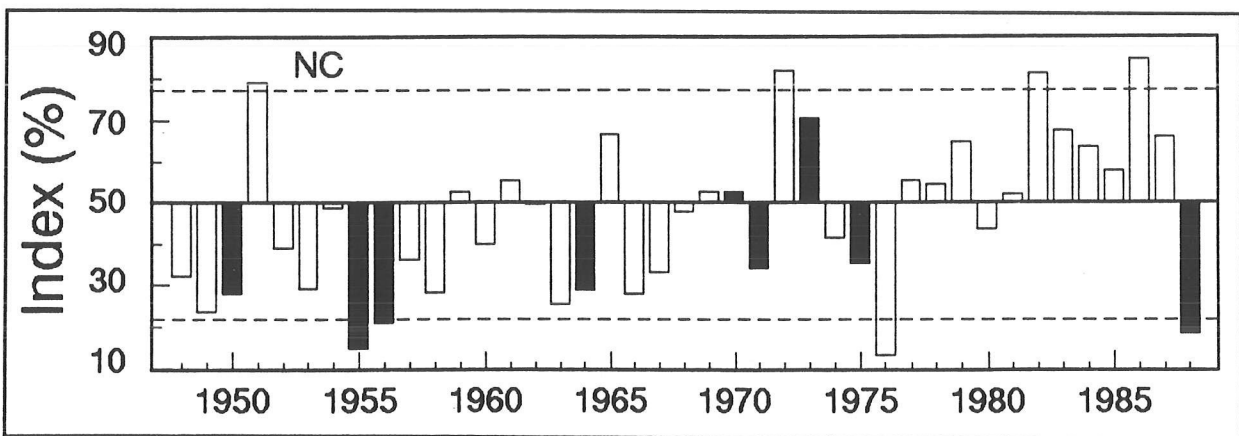


Figure 7. Index time series of streamflow percentiles based on the season chosen in Figure 6 for the North Central area. Signal years are shown by dark bars. Dotted lines indicate the limit for the wettest and driest values.

### Pacific Northwest (PNW)

In the aggregate La Niña composite for the PNW area (Figure 8), the October(0) to August(+) season has been selected from among several alternatives as a period when the La Niña/streamflow relationship is possibly strong and coherent. In the plot of ITS for this season, all seasonal averages associated with La Niña events show an above-normal departure, indicating a highly consistent relationship. All of four extremely wet streamflow occurrences for this season coincided with a La Niña event. Two obvious seasons — October(0) to February(+) and April(+) to August(+) — that could be selected as a response period in Figure 8 revealed reasonable results. The ITS for October-February season (not shown) indicated a high degree of consistency, except one small negative departure (1.7 percent), and the occurrence of two extreme cases. The ITS for the April-August season (not shown) also had eight positive departures out of nine and three extremely wet seasonal occurrences. Redmond and Koch (1991) also found that anomalies of the surface climatic parameters in the PNW region during La Niña events were equally as pronounced as those for ENSO years. The map of Kiladis and Diaz (1989) for the American sector offers some clues for below-normal precipitation in the PNW during the (+) year.

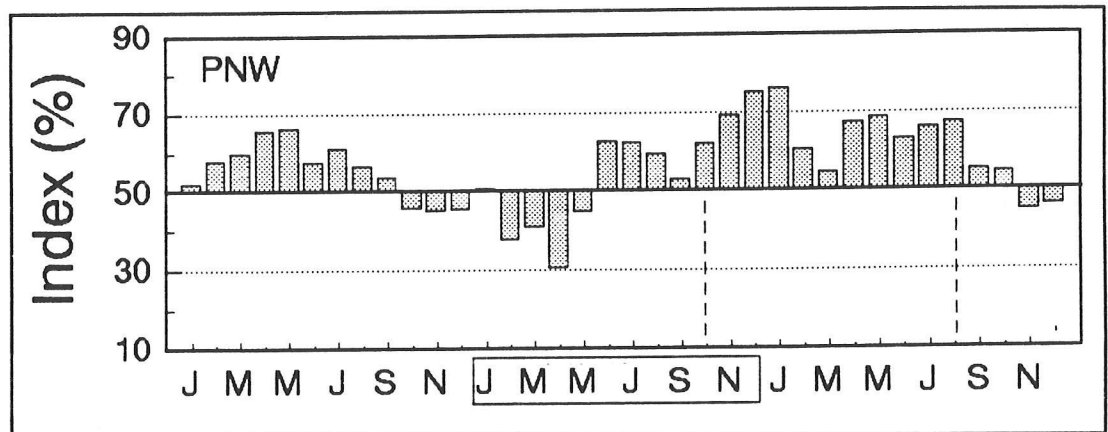


Figure 8. Aggregate La Niña composite based on percentiles of log-normal distribution for the Pacific Northwest area. Dashed lines delineate the season of possible La Niña-related streamflow responses. Months in the box refer to La Niña or (0) year.

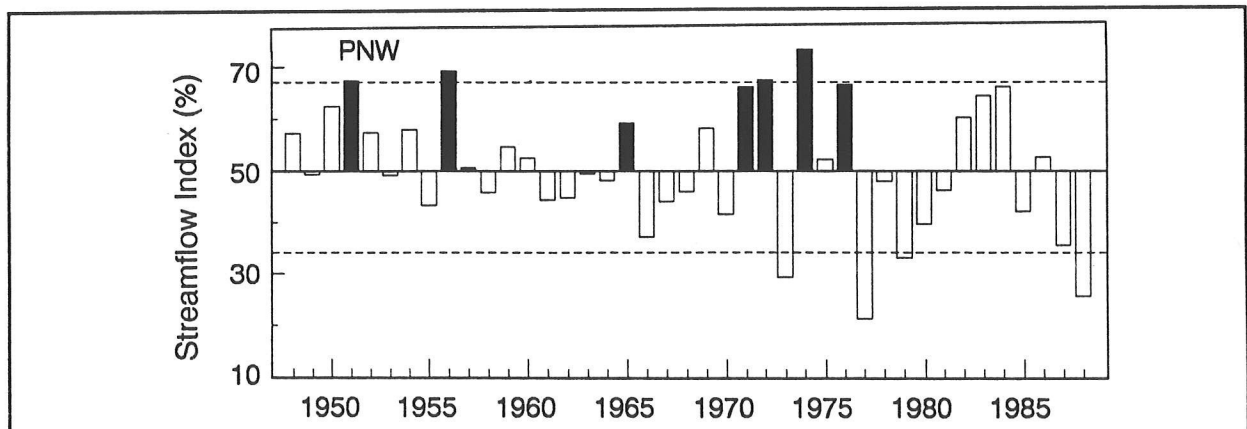


Figure 9. Index time series of streamflow percentiles based on the season chosen in Figure 8 for the Pacific Northwest area. Signal years are shown by dark bars. Dotted lines indicate the limit for the wettest and driest values.

## Conclusion

---

Identification of possible core areas is a major step in seeking predictive utilities for long-range streamflow forecasting in the United States. The core areas that may have had streamflow anomalies associated with ENSO events have been shown to have the same degree of association with La Niña events. The season that reveals the sign and magnitude of the La Niña-related streamflow signal has been detected for each ENSO-streamflow core area. In general, these seasons have almost the same timing, length, and magnitude as those for ENSO events, but the signs of anomalies are reversed.

We have implied the existence of significant mid-latitude streamflow responses to the colder-than-normal sea surface anomalies in the eastern Pacific. Results of this study confirmed the previous climatic studies on the subject from a hydrologic perspective and offered a basis to check the outcomes of atmospheric and hydrologic modeling studies. Since the extremes of the SO have occurred 18 of the 41 years of this study period (44 percent), the relationships specified here and the earlier studies provide some insight for a crude long-range seasonal prediction of streamflow for several regions in the United States.

## References

---

- Douglas, AE, and PJ Englehart. 1981. On a Statistical Relationship between Autumn Rainfall in the Central Equatorial Pacific and Subsequent Winter Precipitation in Florida. *Mon. Wea. Rev.* 109:2377-2382.
- Kahya, E, and JA Dracup. 1992. U.S. Streamflow in Relation to El Niño/Southern Oscillation. *Water Resources Research*, in press.
- Kiladis, GN, and HF Diaz. 1989. Global Climatic Anomalies Associated with the Extremes in the Southern Oscillation, *Journal of Climate* 2:1069-1090.
- Philander, SG. 1990. *El Niño, La Niña, and the Southern Oscillation*. Academic Press, San Diego.
- Redmond, KT, and RW Koch. 1991. Surface Climate and Streamflow Variability in the Western United States and Their Relationship to Large Circulation Indices. *Water Resources Research* 27(9):2381-2399.
- Ropelewski, CF, and MS Halpert. 1986. North American Precipitation and Temperature Patterns Associated with the El Niño Southern-Oscillation (ENSO), *Mon. Wea. Rev.* 114:2352-2362.
- \_\_\_\_\_. 1989. Precipitation Patterns Associated with the High Index Phase of the Southern Oscillation, *Journal of Climate*, Vol. 2, March 1989.
- Wallis, JR, DP Lettenmaier, and EF Wood. 1991. A Daily Hydroclimatological Data Set for the Continental United States, *Water Resources Research*, 27(7):1657-1663.

# A Mechanism for the Link Between Solar-Irradiance Variations and Regional Precipitation

Charles A. Perry

**Abstract:** Although the mechanisms of climatic fluctuations are not completely understood, changes in global solar irradiance show a link with regional precipitation. A proposed mechanism for this linkage begins with absorption of varying amounts of solar energy by tropical oceans, which may aid in development of ocean temperature anomalies. These anomalies are then transported by major ocean currents to locations where the stored energy is released into the atmosphere, altering pressure and moisture patterns that can ultimately affect regional precipitation. Correlation coefficients between annual averages of monthly differences in empirically modeled solar-irradiance variations and annual state-divisional precipitation values in the United States for 1950 to 1988 were computed with lag times of 0 to 7 years. The highest correlations ( $R=0.65$ ) occur in the Pacific Northwest with a lag time of 4 years, which is about equal to the travel time of water within the Pacific Gyre from the western tropical Pacific Ocean to the Gulf of Alaska. With positive correlations, droughts coincide with periods of negative irradiance differences (dry, high-pressure development), and wet periods coincide with periods of positive differences (moist, low-pressure development).

Variations in the total solar irradiance may play an important role in short-term climatic variations. Until documentation of the association of solar-magnetic oscillations to solar-energy output (Kuhn *et al* 1988), there have been no well-documented external-forcing hypotheses to explain climatic cycles that are in the range of 1 to 10 years. Earth-satellite measurements since 1978 have revealed that total solar irradiance has an average variation of at least 0.1 percent over the 11-year period of a sunspot cycle (Willson and Hudson 1988). However, monthly variations of as much as 0.1 percent have occurred. The 10.7-cm solar flux has been measured here on Earth since 1947, and it too shows a pattern of irradiance variations that corresponds with sunspot patterns (Lean and Foukal 1988). Estimates of total solar-irradiance variations between 1874 and 1988 are available, based on an empirical model using past solar activity (Foukal and Lean 1990). Solar irradiance may play an important role in the global climatic system, but the variations in irradiance are small, on the order of  $1 \text{ W/m}^2$  per month, so their effect must be amplified to cause significant climatic variations.

## Proposed Mechanism

One possible medium for amplification of the solar-irradiance variations may be through the transfer of energy from the oceans to the atmosphere. Variations in the temperature of the ocean surface, specifically sea-surface temperatures (SST), have been linked to atmospheric-pressure anomalies (Wallace *et al* 1990). There is evidence that an anomalously

cool SST in the eastern Pacific was responsible for the severe 1988 North American drought (Palmer and Brankovic 1989). Ocean currents serve as the major conveyers of energy from the tropics toward the poles. The mechanism proposed for the coupling of solar irradiance with regional climate through the ocean consists of three components:

- Absorption of solar energy by the transparent tropical oceans in a deep surface layer.
- Transport of that energy from the tropics to the temperate regions by major ocean currents.
- Transfer of that energy into the atmosphere by evaporation processes, which supplies moisture and energy to low pressure systems that cause precipitation.

A difference of only  $1 \text{ W/m}^2$  reaching the Earth's surface and penetrating the ocean can be translated into a measurable change in ocean temperature. About 75 percent of the power reaching the Earth's surface is absorbed in the top 10 meters of clear ocean water (Beer 1983). However, blue light can penetrate to nearly 100 meters. If a  $1 \text{ W/m}^2$  irradiance difference persists over a time span of 1 year, and if it is assumed that 75 percent of that difference in energy is absorbed by the top 10 meters of the ocean (the remainder absorbed below 10 meters), then that 10-meter column of ocean water could have a temperature variation of more than  $0.5^\circ\text{C}$ . Lewis and others (1990) show that solar radiation penetrates to a significant depth (instead of being absorbed at the surface) in the clear waters of the western tropical Pacific Ocean. This explains the discrepancy between observed SST in the western Pacific and those predicted by current ocean/atmosphere models. By occurring over an area of several thousand square kilometers, this variation in the total energy of a very large volume of water could have an effect on the atmosphere above it for a considerable time.

The Pacific Gyre and its minor circulations are the conveyers of absorbed solar energy from the central and western tropical Pacific to locations north and east. If incoming solar energy varied on time scales of months to years, different parts of the gyre would receive varying amounts of energy as water moved through the tropics in its journey around the gyre. During a period of decreased solar irradiance, a part or pool of the tropical ocean would receive less energy and become anomalously cool, whereas increased irradiance would result in an anomalously warm pool. These pools of warmer or cooler water are drawn around the Pacific Gyre like riders on a carousel. A lag time of several years could elapse between the time that energy is absorbed into the tropical ocean and the time the energy is finally released to the atmosphere. By then the pool of ocean water may have traveled thousands of miles. Other factors affect SST, such as cloud cover, atmospheric turbidity, latitude, wind speed, and ambient air temperature, but irradiance variations may play an important role in ocean temperatures below the surface.

Evaporation from the surface of the ocean is the mechanism that may have the greatest amplification of the effect of solar-irradiance variations on climate. The vapor pressure of water increases by about 6 to 7 percent for each 1°C of increase in temperature between 5 and 25°C. For example, a +2°C anomaly in SST has nearly 28 percent more water vapor above it than does a -2°C anomaly. This increase in water vapor could significantly affect precipitation by increasing atmospheric moisture fields from which further amplification of irradiance variations could occur through the dynamic atmospheric processes of storm and precipitation formation.

### **Solar Irradiance and Precipitation Correlations**

---

Annual averages (January to December) of monthly solar irradiance differences were computed from the modeled irradiance values of Foukal and Lean (1990). Correlation coefficients between these annual totals and annual state-divisional precipitation values for the 344 regions in the United States for 1950 through 1988 (NOAA 1989) were computed with lag times of 0 to 7 years. The different lag times were used to examine the time of transport of stored solar energy in the ocean water from the tropical Pacific to the atmosphere over locations in North America.

Correlation coefficients (R) for the 8 lag times and the 344 regions ranged between -0.51 and +0.65. To be significant at the 1 percent level, R must be less than -0.37 or greater than 0.37. The highest correlation coefficient (R=0.65) was obtained in the Pacific Northwest when the annual irradiance averages were lagged 4 years. At this time lag, droughts coincided with periods of lower irradiance averages (decreased energy availability), and greater than average precipitation coincided with periods of higher irradiance averages (increased energy availability). Examples of the correlation between annual irradiance averages lagged 4 years and precipitation averages for two regions are shown in Figure 1. A region of abundant precipitation (the 39-year average is about 200 cm) is shown in Figure 1a, using data from Oregon's coastal region 1. A region of meager precipitation (the 39-year average is about 44 cm) is shown in Figure 1b, using data from southeastern Washington region 10, the Palouse Blue Mountain area.

Correlation coefficients of  $R > 0.60$  were obtained in five other regions in Oregon, eastern Washington, and western Idaho. Coefficients of  $R > 0.50$  were obtained for surrounding regions, including a large region in northern California (Figure 2). Positive correlation coefficients of  $R > 0.50$  also were obtained for the southeastern part of the United States and along the eastern seaboard for the 4-year lag time. This could be a reflection of a long-wave, trough-ridge-trough pattern as forced by Pacific Ocean temperatures. Weak negative correlation coefficients occur in Texas, New Mexico, eastern Montana, northeastern Wyoming, and western North and South Dakota, midway between the areas of positive correlations, supporting the trough-ridge-trough condition.

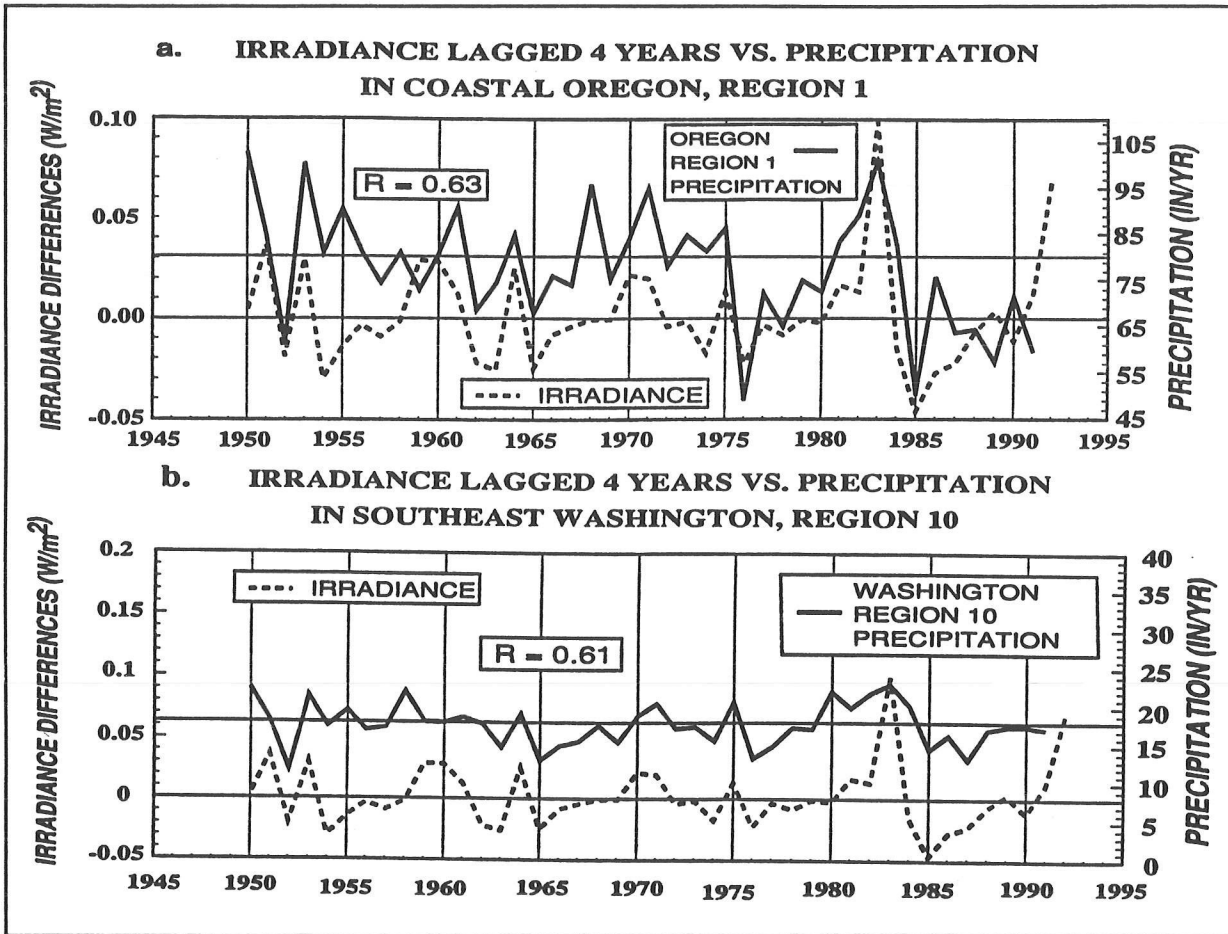


Figure 1. Comparison of annual total of monthly solar-irradiance differences lagged 4 years and annual precipitation for (a) Coastal Oregon, Region 1 and (b) Southeast Washington, Region 10 ( $R$ =Correlation Coefficient).

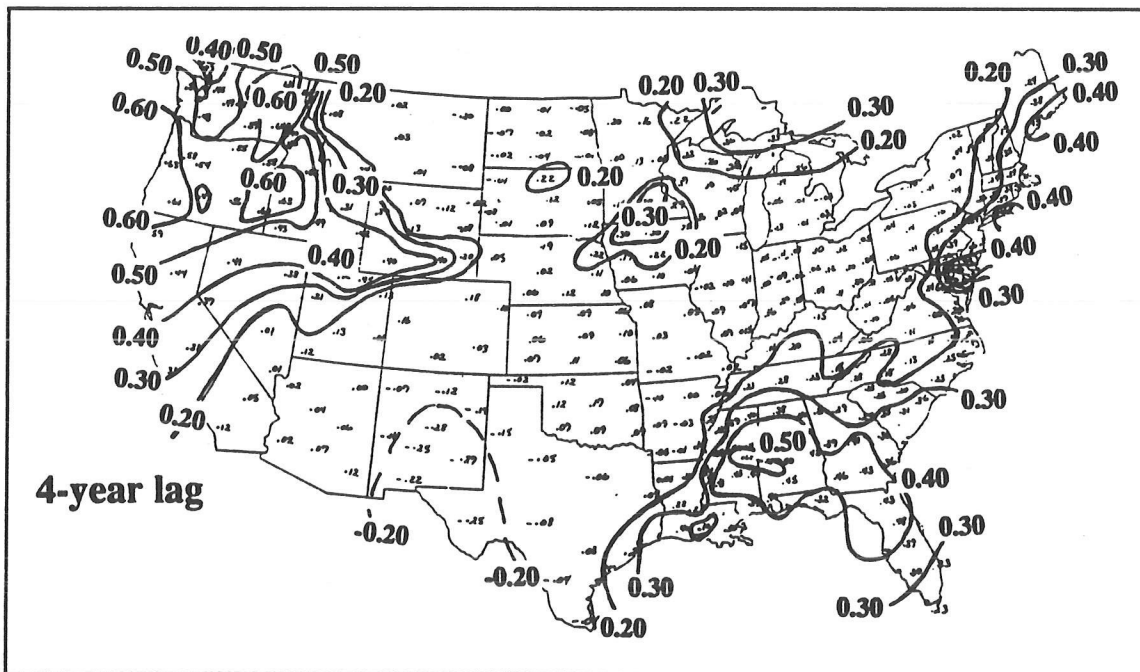


Figure 2. Correlation coefficients between annual regional precipitation and annual averages of monthly irradiance differences for a 4-year lag time, 1950-1988 (1% significance,  $R > 0.37$ ).

The strongest positive correlations were obtained with the 4-year lag time, but significant correlations exist at other lag times, suggesting the influence of other oceanic areas. For example, significant positive correlation coefficients exist for regions in the Desert Southwest for a lag times of 3 years. The 3-year lag positive correlation could be caused by temperature anomalies in water arriving off Baja California after traveling from the western and central tropical Pacific Ocean along the Equatorial Counter Current. Significant positive correlation coefficients are obtained from Texas to Nebraska with a 2-year lag, indicating the possibility of ocean temperature anomalies in the Caribbean Sea and the Gulf of Mexico affecting precipitation in the plains states.

### **Summary and Conclusions**

---

Annual precipitation data for the 344 state-divisional regions in the United States were correlated with solar-irradiance data lagged 0 through 7 years. Annual averages of monthly differences of empirically modeled solar-irradiance values show significant correlations with annual regional precipitation at certain lag times. Periods of increased annual irradiance averages correspond to periods of increased precipitation, whereas periods of decreased averages correspond to decreased precipitation in the Pacific Northwest, when irradiance is lagged 4 years. Travel time for water moving from the warm, western tropical Pacific Ocean to the Gulf of Alaska within the Pacific Gyre also is about 4 years, further evidence for an oceanic transfer mechanism.

These significant correlations may be due to a solar-climate mechanism that involves a combination of the processes of absorption, transport, and transfer of varying amounts of energy from the Sun to the oceans and back to the atmosphere. Large quantities of energy in the visible spectrum can be injected into ocean below the mixing layer. This energy then is transported by major ocean currents to locations where the energy flux becomes upward into the atmosphere. The effects of solar-irradiance variations may be amplified by the 7 percent increase in the vapor pressure of water for every 1°C increase in ocean temperature. The energy is transferred to the atmosphere and becomes available for formation of storms that produce precipitation.

The persistent drought in the western states from 1985 to 1991 may be related to a period of decreasing solar irradiance between 1981 and 1987. The correlation between solar-irradiance values and West Coast precipitation in the last 38 years indicates the possibility of greater than average precipitation occurring 4 years after the strong increases in solar irradiance observed during 1988.

## **Acknowledgments**

---

I thank J. Lean for providing the modeled solar irradiance data and G. Reid for critical comments on a preliminary manuscript. This work is a cooperative effort between the U.S. Geological Survey and the University of Kansas.

## **References**

---

- Beer, T. 1983. *Environmental Oceanography*. Pergamon Press, Oxford. 206p.
- Foukal, P, and J Lean. 1990. An empirical model of total solar irradiance variation between 1874 and 1988. *Science* 247:556-559.
- Kuhn, JR, KG Libbrecht, and RH Dicke. 1988. The surface temperature of the sun and changes in the solar constant. *Science* 242:908-911.
- Lean, J, and P Foukal. 1988. A model of solar luminosity modulation by magnetic activity between 1954 and 1984. *Science* 240:906-908.
- Lewis, MR, M Carr, GC Feldman, W Esaias, and C McClain. 1990. Influence of penetrating solar radiation on the heat budget of the equatorial Pacific Ocean. *Nature* 347:543-545.
- National Oceanic and Atmospheric Administration. 1989. *Climatological data for the United States*. National Climatic Center. Asheville, NC.
- Palmer, TN, and C Brankovic. 1989. The 1988 U.S. drought linked to anomalous sea surface temperature. *Nature* 338:54-57.
- Wallace, JM, C Smith, and Q Jiang. 1990. Spatial patterns of atmosphere-ocean interaction in the northern winter. *Journal of Climate* 3:990-998.
- Willson, RC, and HS Hudson. 1988. Solar luminosity variations in solar cycle 21. *Nature* 332:810-812.

# A Preliminary Description of Climatology in the Western United States

John O. Roads, Shyh-Chin Chen, Kyozo Ueyoshi,  
James Bossert, and Judith Winterkamp

**ABSTRACT:** We describe the climatology of the western United States as seen from two 1-month perspectives, January and July 1988, of the National Meteorological Center large-scale global analysis, the Colorado State University Regional Atmospheric Modeling System (RAMS), and various station observation sets. An advantage of the NMC analysis and the RAMS is that they provide a continuous field interpolation of the meteorological variables. It is more difficult to describe spatial meteorological fields from the available sparse station networks. We assess accuracy of the NMC analysis and RAMS by finding differences between the analysis, the model, and station values at the stations. From these comparisons, we find that RAMS has much more well-developed mesoscale circulation, especially in the surface wind field. However, RAMS climatological and transient fields do not appear to be substantially closer than the large-scale analysis to the station observations. The RAMS model does provide many other meteorological variables, such as precipitation, which are not readily available from the archives of the global analysis. Thus, RAMS could, at the least, be a tool to augment the NMC large-scale analyses.

In a previous paper, Roads *et al* (1991) discussed the forecast accuracy of the National Meteorological Center's medium-range forecasts of near-surface meteorological elements such as temperature, relative humidity, and wind speed in terms of the NMC global analysis. Although these global analyses are most applicable for global perspectives, we are interested in more regional scales. Here, we expect the large-scale analyses to only grossly simulate various regional effects, especially in regions that are strongly influenced by topography. This brings up the question as to just how useful or accurate the large-scale analysis is at regional scales.

At regional scales, a mesoscale model, which is overlying mesoscale topography and which is forced at the boundary and initialized with a large-scale analysis, could provide an even better representation of the regional climate. Feasibility of the regional modeling approach has recently been demonstrated for the western United States by Giorgi and Bates (1989) using the Penn State/NCAR mesoscale model. A number of papers also discuss how we might develop a regional assimilation with a limited-area model and other observations, such as various station observations (see, *eg*, Stauffer and Seaman 1990; Stauffer *et al* 1991). Development of this kind of capability will become even more important as we begin to assimilate some of the observations associated with the modernized weather service systems.

In a similar manner, a regional model initialized and forced at the horizontal boundaries by general circulation model (GCM) variables (see, *eg*, Dickinson *et al* 1989; Giorgi 1990) might provide more detailed spatial

representation of climatic change than is available from statistical interpolations (eg, Wigley *et al* 1990) or simple linear interpolations of the large-scale GCM output to the regional scale. We must be worried, though, that a regional climatology that is statistically or dynamically interpolated from an inaccurate large-scale climatology may not be any closer to the truth than a regional climatology that is linearly interpolated from the inaccurate large-scale climatology. That is, even though detailed regional climatology may be different from the large-scale coarse climatology, we do not know if this difference makes it any better.

Therefore, to assess the accuracy of the NMC analysis and to test the regional model interpolation hypotheses, we examine here a regional climatology from the perspective of the large-scale NMC analysis and from the perspective of the large-scale NMC analyses that is filtered through the regional modeling system of the CSU RAMS mesoscale model in comparison to individual station observations. In particular, we examine how well the model can simulate temperature, relative humidity, wind, and precipitation at individual stations. We examine the climatological spatial variations as well as the day-to-day transient variations.

## Analysis

---

We use the NMC global analysis on a 2.5-degree global grid (available from the National Center for Atmospheric Research) and on constant pressure surfaces at 1000, 850, 700, 500, 400, 300, 250, 200, 150, 100, 70 mbs. Variables in this analysis are virtual temperature, relative humidity, wind speed and direction, geopotential, and surface pressure (see Roads *et al* 1992). Over the region of interest, there are only 117 analysis grid points (denoted by X in Figure 1a). This large-scale analysis is horizontally interpolated to the higher resolution model grid using bilinear interpolation. The values on the horizontal pressure grid are then interpolated in the vertical to the staggered vertical grid of the RAMS model (described below), as well as to the surface, as well as to constant height levels (every 500 meters) above sea-level.

## Model

---

As described by Bossert *et al* (1992 a, b, c), the CSU-RAMS mesoscale model is a highly flexible modeling system capable of simulating a wide variety of mesoscale phenomena, including regional climatology. Recent model developments are described in Tremback *et al* (1986); Cotton *et al* (1988); Tremback (1990); and Tripoli (1992). The model framework for the present study incorporates a 3-dimensional, terrain-following, hydrostatic version of the code. The domain's topography, shown in Figure 1, is derived from a 5-minute northwestern hemispheric topographic dataset. A silhouette averaging scheme is used to preserve realistic topography heights. These height data are then interpolated to the model grid described below.

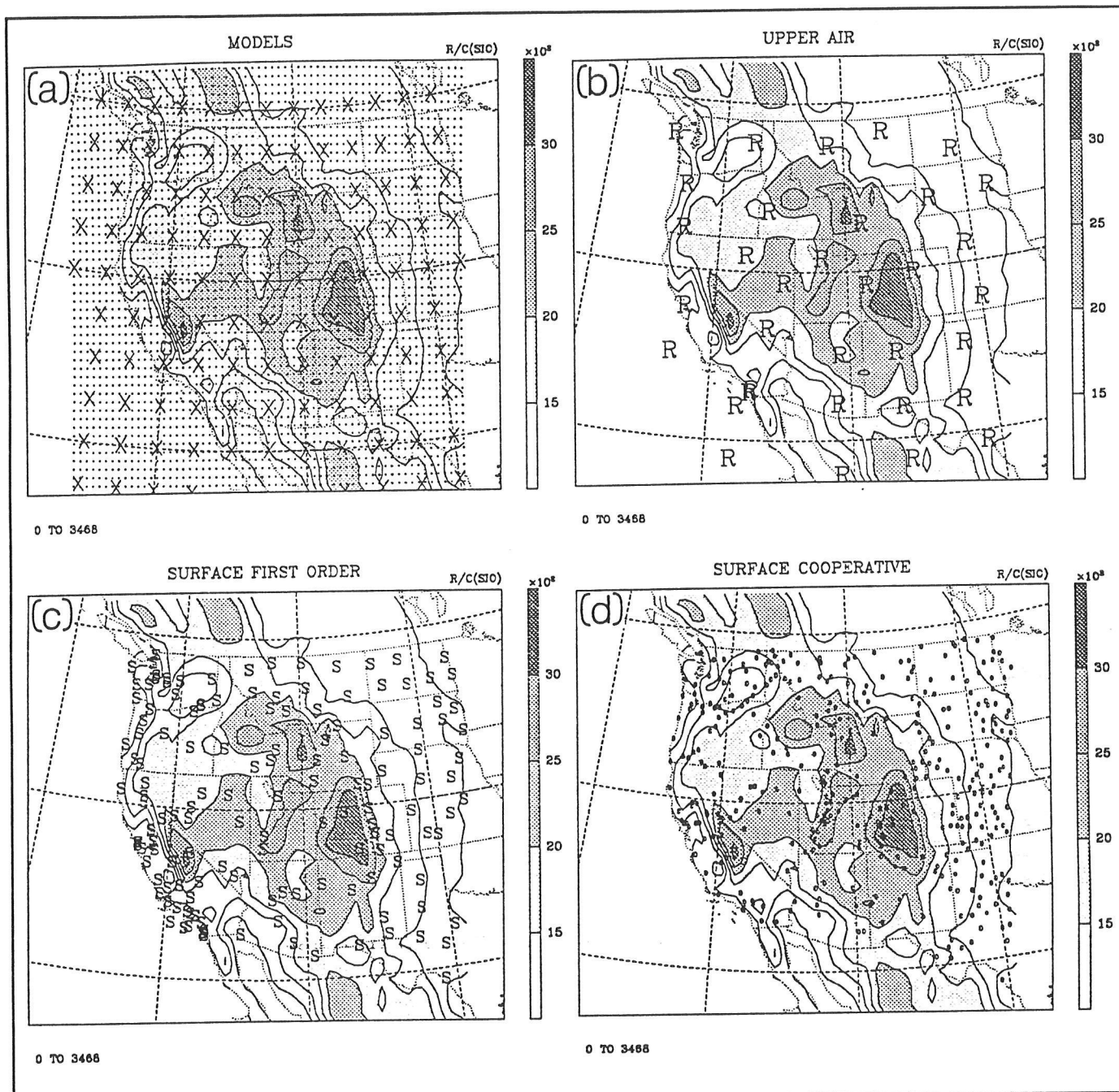


Figure 1. Topography, grid point, and station locations. Topography shown with 500-meter interval. Only areas with elevations higher than 1500 meters are shaded.

- (a) Analysis grid points are shown by X. Model grid points are shown by dots.
- (b) Rawinsonde station locations are shown by R.
- (c) First order summary of day station locations are shown by S.
- (d) Cooperative station locations are shown by o.

The topography is smoothed to only contain wavelengths greater than or equal to 4 grid points. In the vertical, we use 21 staggered levels, with a resolution of 300 meters near the surface and 1000 meters at the top of the model (Figure 2). The model's geographical domain (Figure 1) covers the region from 127.5W to 97.5W and 27.5N to 52.5N. The model has 0.5 degrees horizontal resolution at the tangent point of the polar

stereographic grid at 40.0N and 112.5W (at this midpoint the grid points are 55.5 kilometers apart in the north-south direction and 40 kilometers apart in the east-west direction). There are 61 by 51 horizontal model grid points (denoted by dots in the upper-left panel of Figure 1). Horizontal boundary conditions around the domain are updated each time-step by linearly interpolating between each successive 12-hour large-scale analysis. These boundary conditions were nudged in with weights changing from 0.5 at the outermost boundary to 0 within 5 grid points.

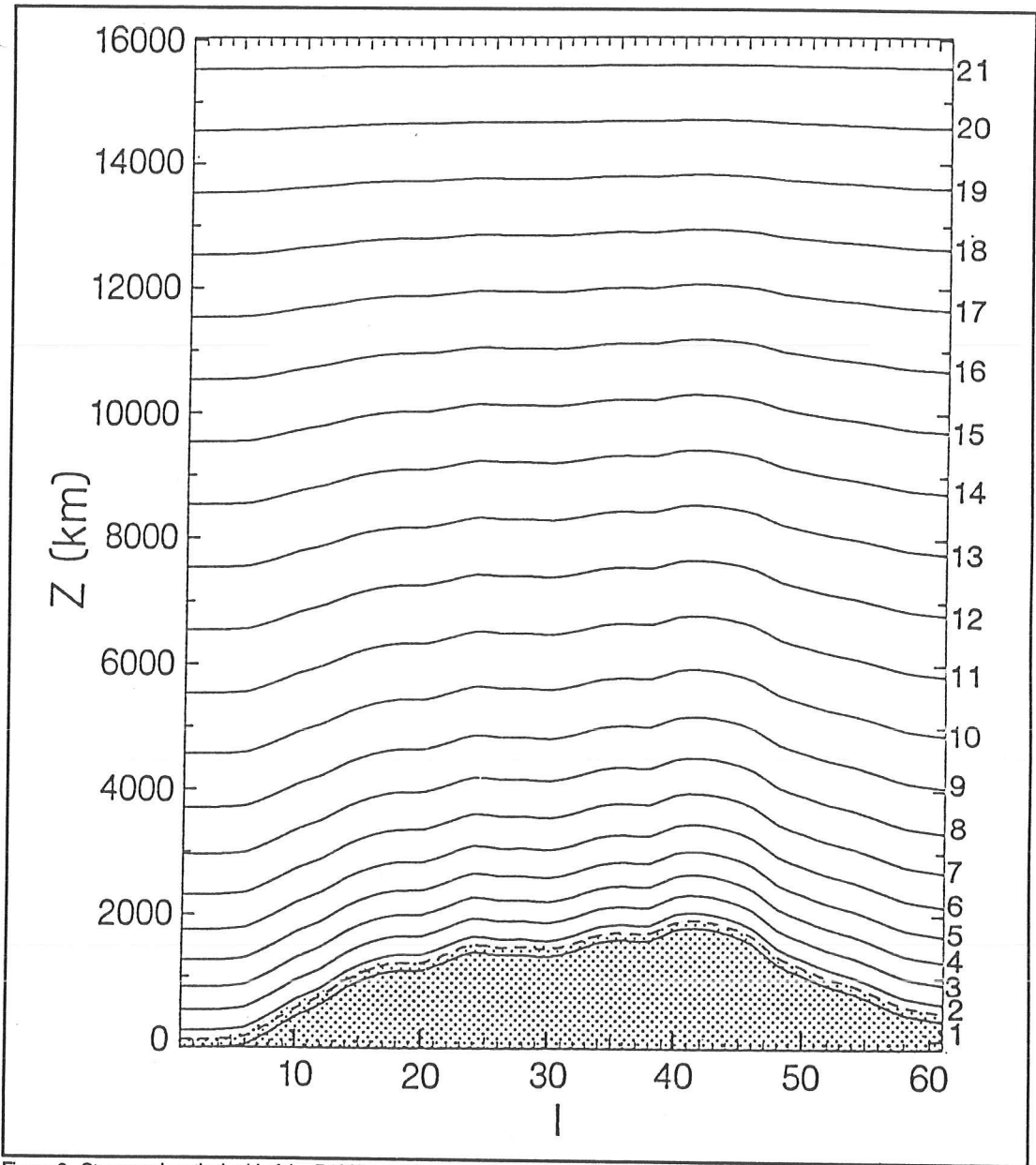


Figure 2. Staggered vertical grid of the RAMS model averaged over the  $j$  grid points. That is, we show here an average W-E cross section. The first model level is below the surface; the second model level is 145 meters above the surface over the ocean (slightly less over the mountain peaks).

## **Station Observations**

---

All station observations were obtained from the National Climatic Data Center. For verification above the surface, we use the rawinsonde stations. The United States maintains more than 169 stations at scattered global locations (mainly the contiguous 48 states), but less than 35 apply to the chosen western region (station locations are denoted by R in Figure 1b). Data from these rawinsonde stations are initially interpolated to 25 standard pressure levels and then vertically interpolated to the model's vertically staggered grid points as well as to a uniform vertical grid above sea level.

The principal surface stations are first order stations at which temperature, relative humidity, resultant wind speed and wind direction, precipitation, and other meteorological observations are taken. The United States maintains about 470 such stations, about 147 of which cover the chosen domain (station locations are denoted by S in Figure 1c). Most of these summary of day stations also have hourly information from automatic recording instruments at these certified sites.

There are also cooperative stations at which maximum and minimum temperature and daily precipitation are measured. Some of these stations have been included in NCDC historical climatological network. Over the region of interest there are about 350 such HCN stations (locations denoted by small "o" in Figure 1d). For this study, we use only the HCN stations.

## **Regional Modeling Methodology**

---

A number of methodologies could be used to simulate the regional climatology. The simple one that we apply here is to use the NMC large-scale global analysis as the initial condition and external boundary condition and then allow the interior of the regional model to equilibrate, on short time scales, to the mesoscale circulation forced by the mesoscale topography. We decided on this simplified regional modeling methodology for several reasons.

- It is easy to initialize stable regional circulation with only the NMC analysis.
- We want to compare the resulting model simulations to the station observations, some of which are truly independent of the initializing analysis. Once a regional data assimilation is more fully developed, we will have a better idea how important it is to also initialize with station data (and perhaps other mesoscale data becoming available with modernization of the weather service).
- We want to test the hypothesis that a fine-mesh regional model forced and initialized by a coarse-mesh, large-scale model can better represent

the regional climatology than can a large-scale model or analysis, especially over the mountainous western United States.

For this preliminary assessment, we integrate for only 12 hours from each initial condition. There are several indications (not shown here) that 12 hours is sufficient time for the mesoscale circulation to equilibrate. Also, we discuss here only the daily averages. Although there are some interesting diurnal variations, they are not analyzed here. Station comparisons are made only at the station grid point locations. For simplicity, we only compare daily averages and do not attempt to diagnose the diurnal variation. We average the maximum and minimum or the 0 and 1200 UTC values for this daily value. In a similar manner, we average the maximum and minimum from the cooperative station values to provide an average daily value.

## **Climatology**

---

Climatological temperature fields are shown in Figure 3. During winter, there is a large-scale gradient between the ocean and the adjacent land surface. During summer this gradient reverses and much higher temperatures occur over the land, especially just to the north of the Gulf of California region. Most of the spatial variations can be explained by elevation differences or by inland distance from the Pacific Ocean.

Only small differences are present between the regional model (lower panels, Figure 3) and the NMC analyses (upper panels). In particular, we see the model surface temperature feature of the California Central Valley and Sierras that does not show up in the large-scale analysis, especially during winter. At upper levels (not shown), there is hardly any difference between the NMC analysis and RAMS except the regional model appears to be noisier; most of the noticeable differences occur at the surface.

Relative humidity (Figure 4) shows the characteristic dry structure of the land surface, especially during summer when relative humidity is less than 20 percent over Nevada. There is not much difference between the NMC analyses (upper panels) and regional model (lower panels) except during winter, when relative humidity seems a bit higher just about everywhere. At higher elevations, the regional model maintains this relative moistness during winter but is a bit drier during winter, especially over the ocean. At 6 kilometers (not shown), relative humidity is slightly drier over the ocean than over land, which is the opposite of what occurs at the surface.

Wind climatology is shown in Figure 5. During winter, the NMC (upper left panel) oceanic westerlies tend to split near the coast. Climatological particle tracks north of 40 degrees latitude would move northward over the Coast Ranges and Rocky Mountains and particle tracks to the south would move southward over the mountains. On the leeward side of the mountains, the westerlies once again coalesce into the windiest regions

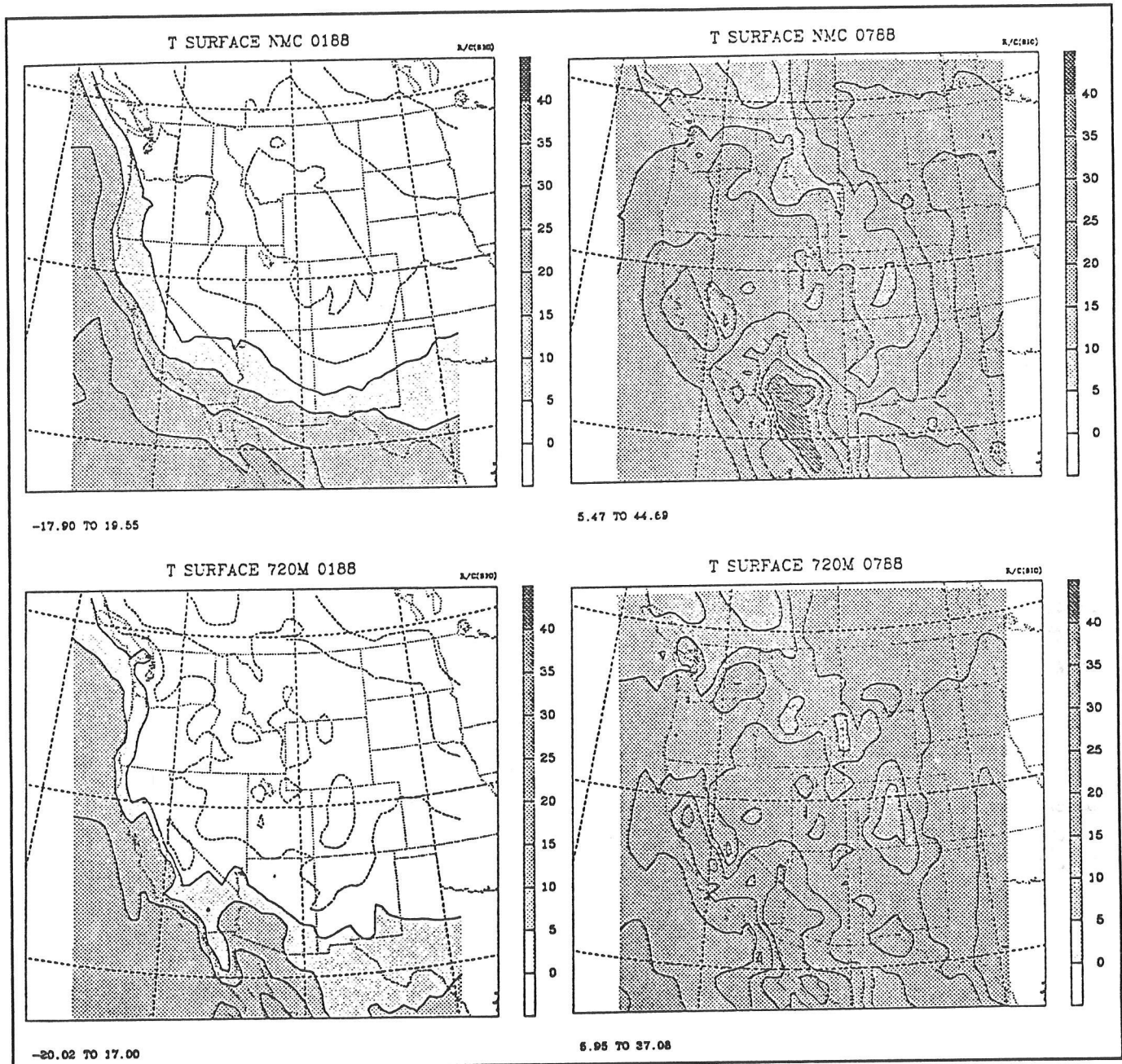


Figure 3. Surface temperature for January and July 1988.  
 Upper panels show temperature from the large-scale NMC analysis.  
 Lower panels show temperature from RAMS.

of the domain. The RAMS appears to have more intense winds in the Wyoming wind corridor. Also, the California Santa Ana winds are more predominant in the RAMS climatology than in the original NMC analysis. At upper levels, the predominant westerlies are similar in the analysis and the RAMS; the RAMS winds are bit noisier, but this may be due to model defects.

During summer (upper right panel, Figure 5) the highest wind speeds occur offshore, west of San Francisco. Northerly winds consistent with summertime strengthening of the Pacific subtropical high occur over the

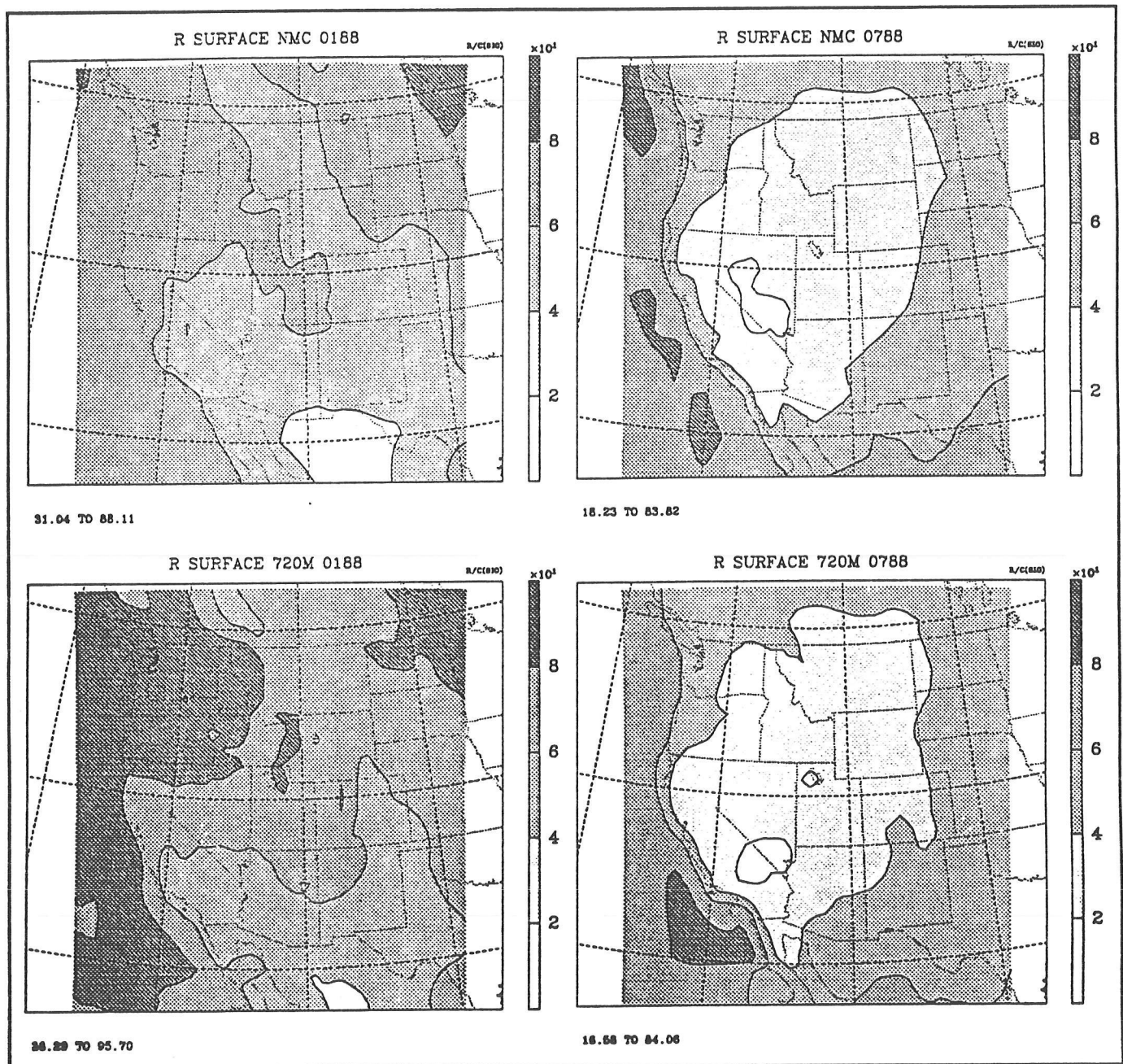


Figure 4. Relative humidity for January and July 1988.  
 Upper panels show relative humidity from the large-scale NMC analysis.  
 Lower panels show relative humidity from RAMS.

entire coastal area. The RAMS model winds (lower right panel) in this region are noticeably different in that the coastal central California northerly jet becomes much narrower and confined to the coastal regions. Similar features are also present in a high resolution study with another model of the Southern California summertime Catalina Eddy (Ueyoshi and Roads 1992). Some strong winds in the lee of the northern Rocky Mountains are comparable in the NMC analysis and RAMS, but the strongest winds appear to originate in the southeastern portion of the model domain. At the upper levels, the weakened upper level westerlies are again comparable in the NMC analysis and RAMS.

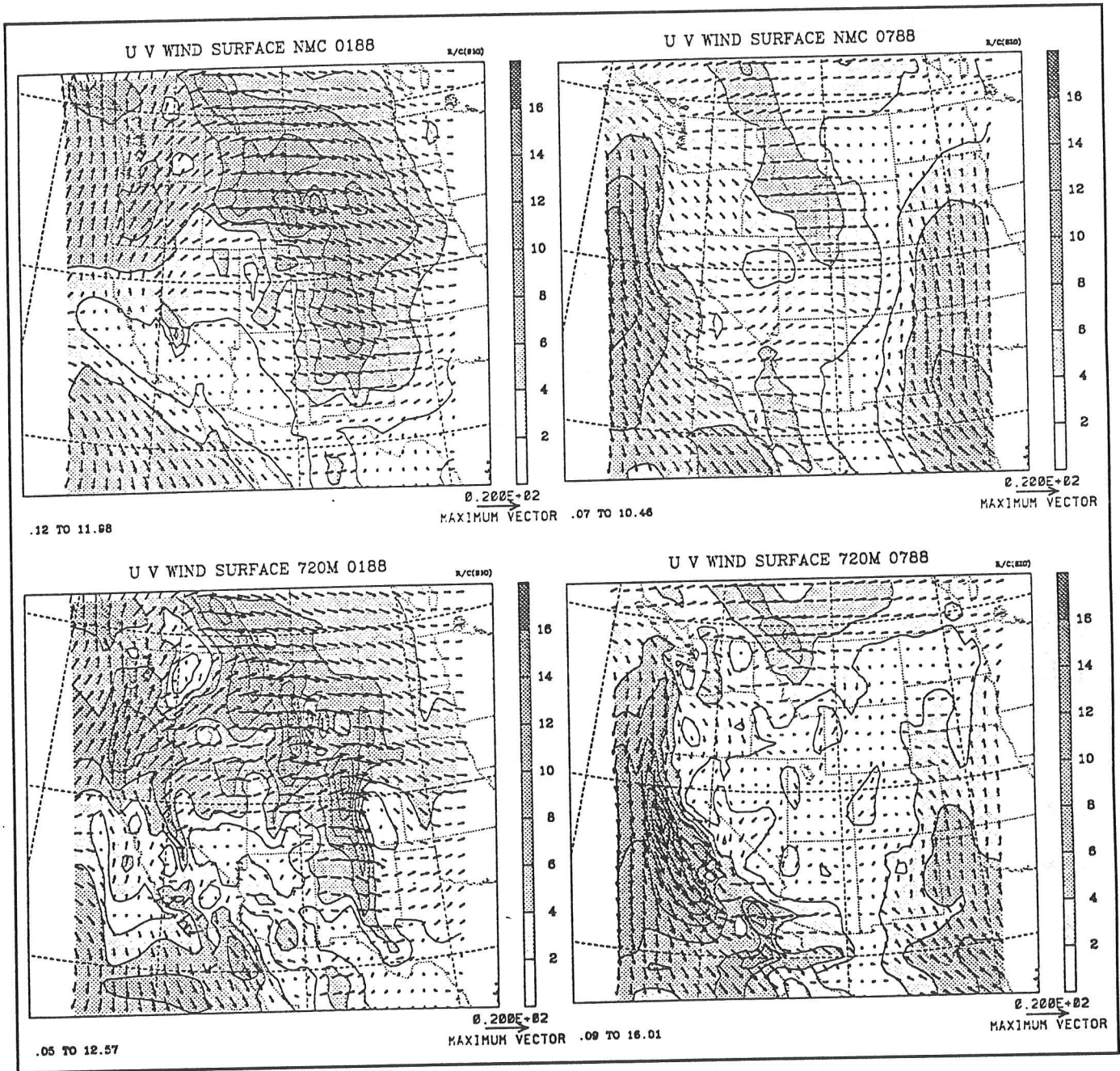


Figure 5. Surface wind speed for January and July 1988.  
 Upper panels show wind speed from the large-scale NMC analysis.  
 Lower panels show wind speed from RAMS.  
 Arrows show wind direction.

Precipitation is not one of the analyzed variables and for now all we can show (Figure 6) is an interpolation of the sparse station observations (HCN and first order stations). Clearly an advantage to having a regional model forced by the large-scale analysis is that the regional model can take the standard meteorological variables available in the standard archives and generate additional relevant variables as needed. Still, the crudely interpolated station dataset does show some correspondence with the RAMS precipitation. During winter the northwestern United States has most of the precipitation, whereas the southwestern and

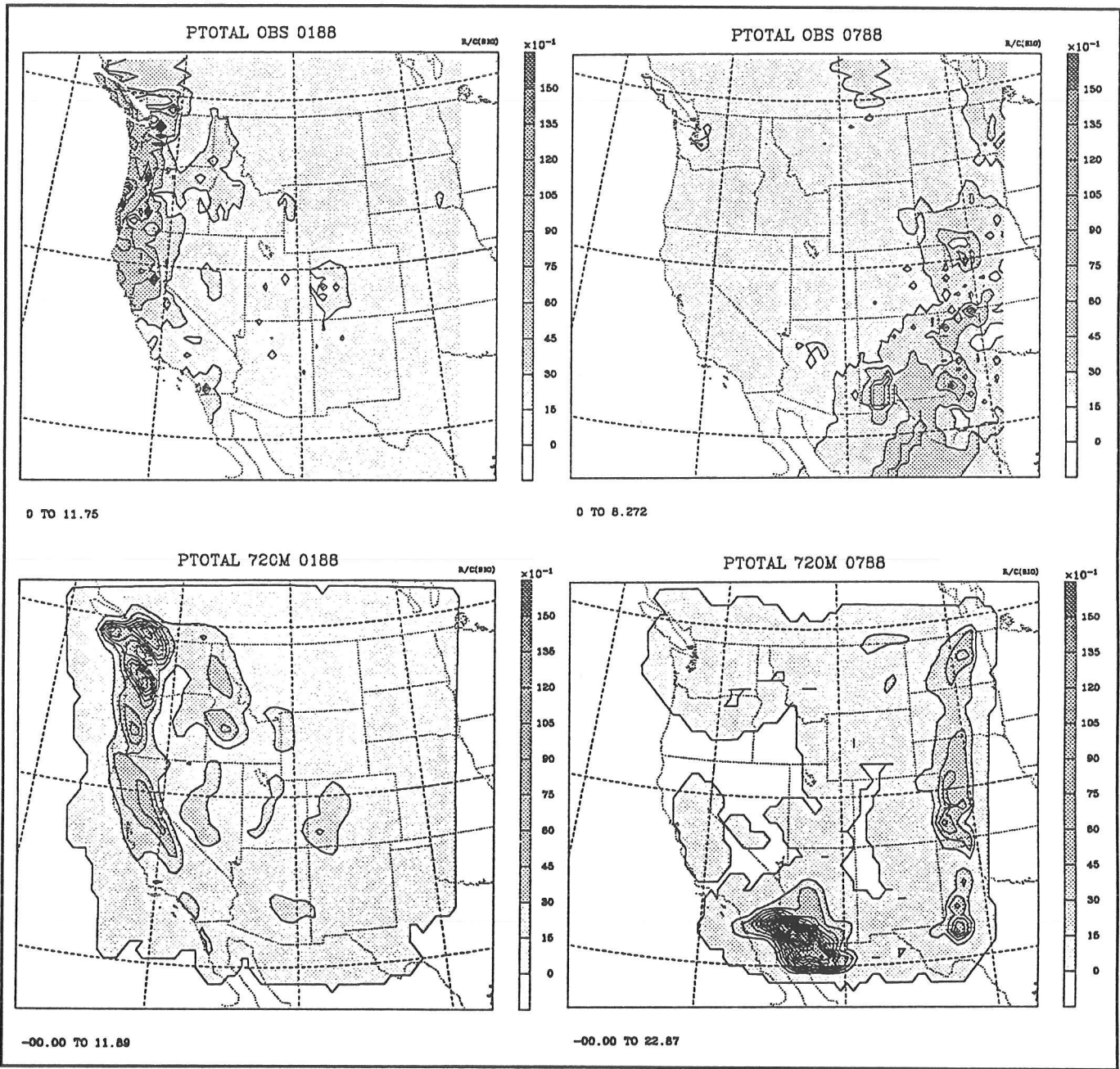


Figure 6. Surface precipitation for January and July 1988.

Upper panels show precipitation from the large-scale NMC analysis.

Lower panels show precipitation from RAMS.

NOTE: Observed precipitation shown in the upper panels is linearly interpolated (iteratively) from about 400 first order and cooperative stations to 3111 grid points.

central United States have most of the summer precipitation (within the boundaries of the model domain). Another feature brought out by the regional model is that during winter most precipitation over the western states falls in the form of snow; rain is dominant only along the extreme West Coast. An irritating feature is the RMS precipitation on the United States/Mexico border during July 1988; the lack of correspondence could be due to lack of Mexican observations in the NCDC datasets or to model defects, we tend to suspect the latter.

## Verification

The large-scale analysis and RAMS appear to be similar, although RAMS has more small-scale features. How realistic are these climatologies and is the regional simulation better? To answer those questions, we now compare the NMC analysis and the regional model simulation with the rawinsonde observations. We examine six characteristics of the climatological field for 3 meteorological variables: temperature ( $T$ ), relative humidity ( $R$ ), and wind ( $U$ ).

The first characteristic is the domain and time averaged values:

$$\bar{A} = \frac{1}{N} \sum_{n=1}^N \bar{A}^n(z)$$

where  $A$  is an arbitrary variable;  $N$  is the number of rawinsonde locations (~35); and  $\bar{A}(z)$  is the ensemble, time, or climatological value at each rawinsonde location,  $n$ , and elevation,  $z$ :

$$\bar{A}^n(z) = \frac{1}{M} \sum_{l=1}^M A_l^n(z)$$

Here  $M$  is the number of events in the ensemble (30 days). The elevation in this case refers to the model vertical grid. The next characteristic is the spatial standard deviation, which measures the level of variability over the domain. This measure is:

$$s = \left( \frac{1}{N-1} \sum_{n=1}^N (\bar{A}^n - \bar{A})^2 \right)^{\frac{1}{2}}$$

The transient standard deviation measures the day-to-day variability taken out by the climatological averages, and is given by:

$$s' = \left( \frac{1}{N-1} \frac{1}{M-1} \sum_{l=1}^M \sum_{n=1}^N (A_l^n - \bar{A}^n)^2 \right)^{\frac{1}{2}}$$

Corresponding error measures are the systematic error:

$$d = \bar{A} - \bar{R}$$

where  $R$  denotes the observed rawinsonde value.

Another error measure is the average RMS difference between the rawinsonde climatology and model climatology:

$$e = \left( \frac{1}{N-1} \sum_{n=1}^N (\overline{A^n} - \overline{R^n} - \overline{A} + \overline{R})^2 \right)^{\frac{1}{2}}$$

Finally, the transient RMS differences are given by:

$$e' = \left( \frac{1}{N-1} \frac{1}{M-1} \sum_{l=1}^M \sum_{n=1}^N (A'_l{}^n - R'_l{}^n)^2 \right)^{\frac{1}{2}}$$

where:

$$A'_l{}^n = A_l{}^n - \overline{A^n}$$

It should be noted here that in the limit of no skill:

$$e \sim \sqrt{2}s \text{ and } e' \sim \sqrt{2}s'$$

Figure 7 shows the comparison of the NMC analysis and RAMS 12-hour simulations to observations from rawinsondes for the wintertime temperature field. From near-freezing values near the surface, temperature decreases to minus 55°C at the isothermal tropopause. The spatial standard deviation is largest near the surface and decreases to a minimum at 12 kilometers. The transient standard deviation has a minimum at 10 kilometers and a slight maximum at the tropopause. The systematic differences between the analysis, model, and rawinsondes are not large, with the model being about 3.5°C too cold near the surface and about 2°C too warm near the top of the model. The model has the largest bias. RMS spatial differences throughout the troposphere between the analysis or RAMS and rawinsondes are smaller than the spatial standard deviation of about 6°C, which indicates the spatial variability is quite realistic. The RMS error is slightly less in RAMS near the surface than in the NMC analysis. However, transient variations are better portrayed by the NMC analysis.

Figure 8 shows results for the relative humidity field. Here the RAMS relative humidity is biased high, which is related to the cold bias (Figure 7). In addition RAMS tends to have a bit larger spatial and transient error variance than the NMC analysis does everywhere (Figures 7-9). However, the NMC analyses and the RAMS RMS errors are quite close to the transient variations, which indicate much less skill at describing this field. Relative humidity is obviously an intrinsically more difficult field to describe.

The zonal wind field (Figure 9) and the meridional wind field show similar results. RAMS is close to the NMC analysis but still slightly worse. This non-improvement in the wind features was somewhat discouraging, since the climatological wind fields (Figure 5) appear, at first glance, to have more reasonable regional features.

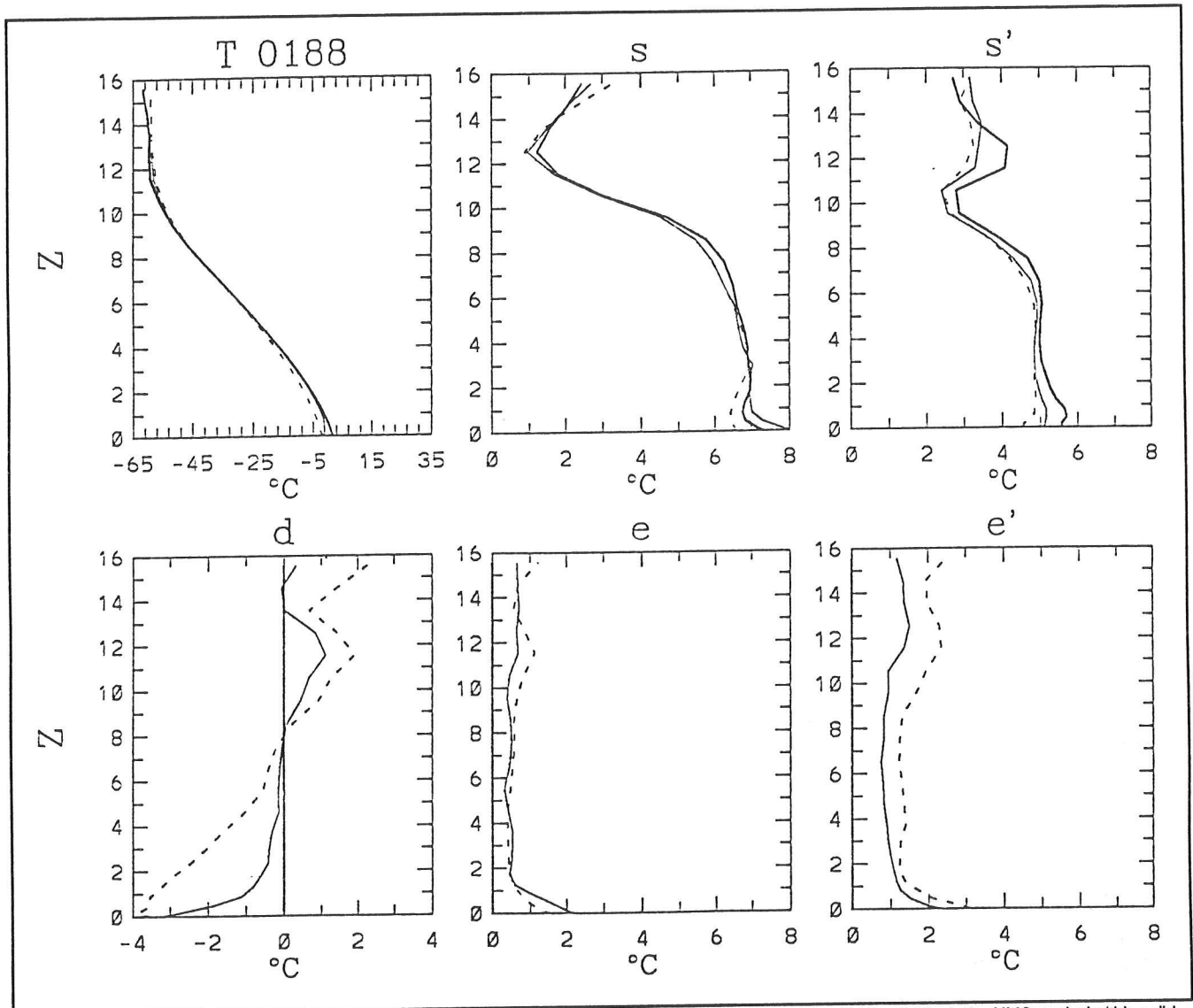


Figure 7. Vertical temperature variations as seen by an average at all rawinsonde locations of the rawinsondes (thick solid line), the NMC analysis (thin solid line) and the RAMS simulation (thin dashed lines).

Upper left = total field.

Upper center = spatial standard deviation ( $s$ ).

Upper right = transient standard deviation ( $s'$ ).

Lower left = average difference ( $d$ ) between the domain averages and the rawinsonde averages.

Lower center = RMS difference (between analysis and rawinsonde or RAMS and rawinsonde) of the spatial values.

Lower right = Transient RMS difference ( $e'$ ).

Tables 1 and 2 show the  $d$ ,  $e$ , and  $e'$  measures at the surface, where we have many additional station measurements. In particular, we inter-compare the values from the first order stations ( $S$ ), the cooperative stations ( $o$ ), the RAMS ( $M$ ), the interpolated surface rawinsonde values ( $R$ ), the NMC analysis ( $X$ ), and the rawinsonde surface observations ( $r$ ). We inter-compare the station values with each other if the stations are within 50 kilometers of each other; no attempt is made to interpolate station locations to finer scales.

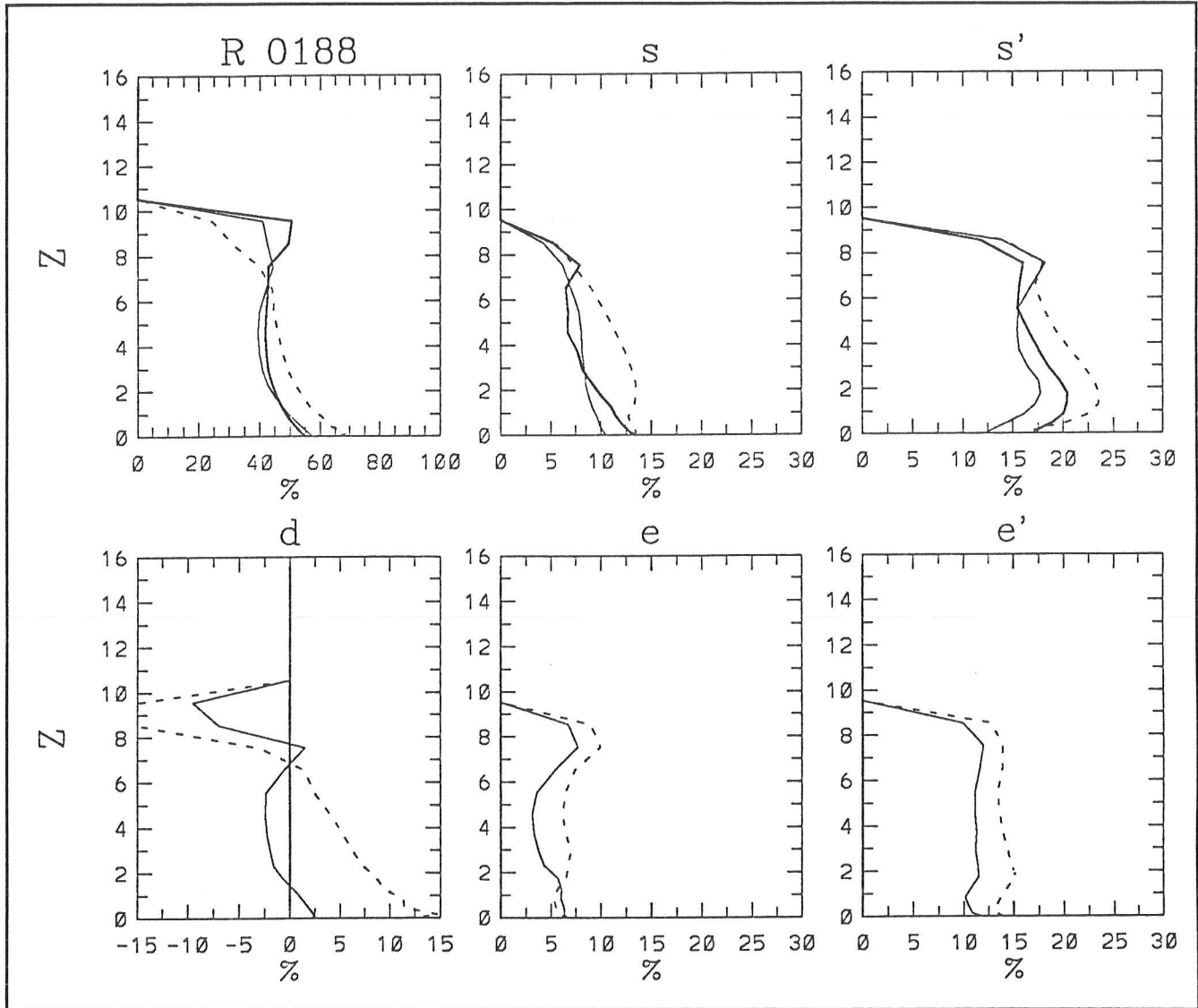


Figure 8. Relative humidity variations as seen by an average at all rawinsonde locations of the rawinsondes (thick solid line), the NMC analysis (thin solid line) and the RAMS simulation (thin dashed lines).

Upper left = total field.  
 Upper center = spatial standard deviation ( $s$ ).  
 Upper right = transient standard deviation ( $s'$ ).  
 Lower left = average difference ( $d$ ) between the domain averages and the rawinsonde averages.  
 Lower center = RMS difference (between analysis and rawinsonde or RAMS and rawinsonde) of the spatial values.  
 Lower right = Transient RMS difference ( $e$ ).

The individual rows and columns of the Tables 1 and 2 refer to values at the first order stations ( $S$ ), the cooperative stations ( $o$ ), the model grid points ( $M$ ), the hourly station values ( $h$ ), the interpolated rawinsonde surface values ( $R$ ), the analysis grid points ( $X$ ), and the measured rawinsonde surface values ( $r$ ). Values in each row refer to the error when measured with respect to values at the stations that name the column. For example consider the first set of differences in Table 1, given by the

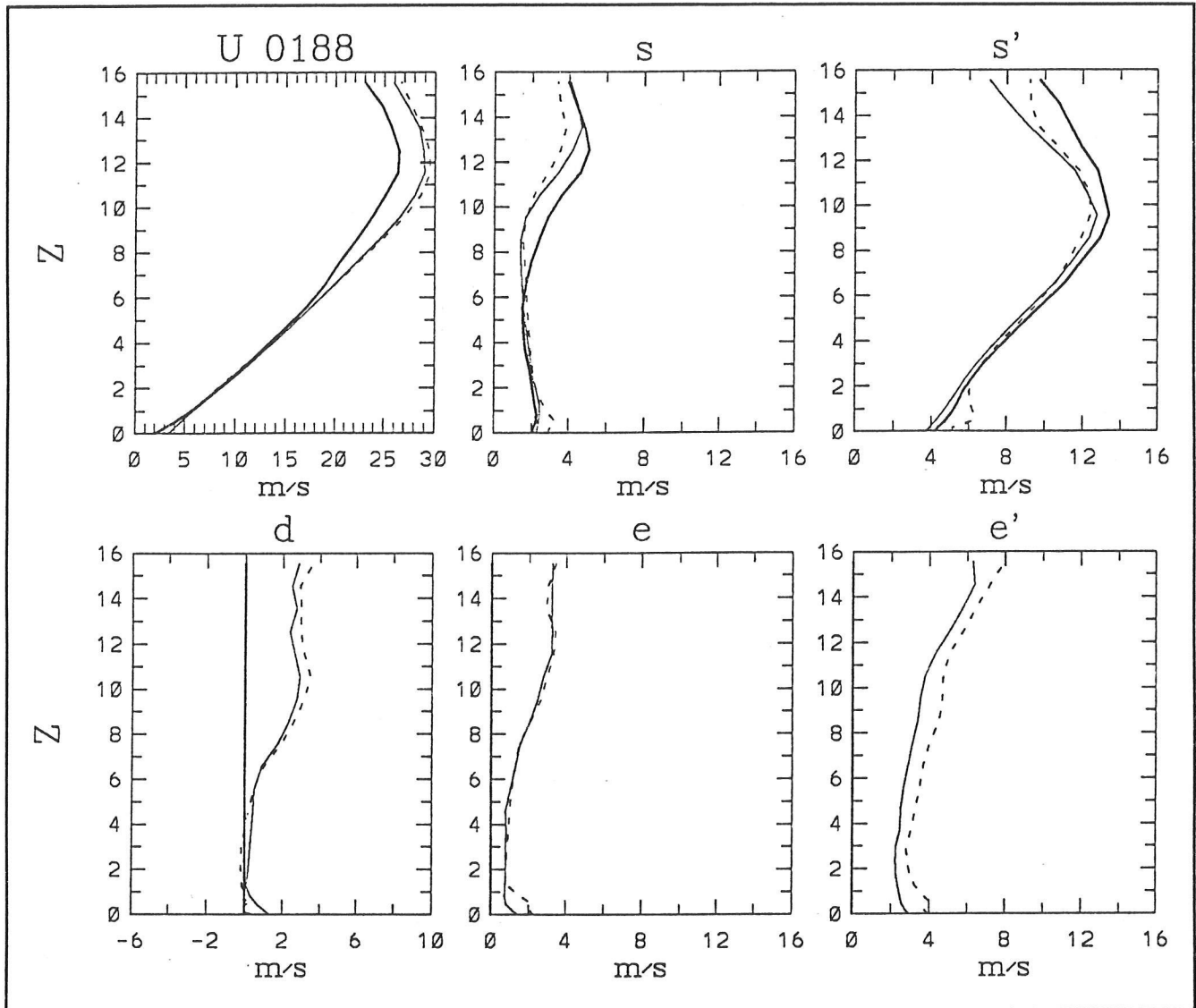


Figure 9. Wind field variations as seen by an average at all rawinsonde locations of the rawinsondes (thick solid line), the NMC analysis (thin solid line) and the RAMS simulation (thin dashed lines).

Upper left = total field.

Upper center = spatial standard deviation ( $s$ ).

Upper right = transient standard deviation ( $s'$ ).

Lower left = average difference ( $d$ ) between the domain averages and the rawinsonde averages.

Lower center = RMS difference (between analysis and rawinsonde or RAMS and rawinsonde) of the spatial values.

Lower right = Transient RMS difference ( $e'$ ).

left panel under the heading "T 0188", which denotes temperature during January 1988. The first column shows the differences with respect to the first order stations. At the first order station locations, the cooperative stations are 0.2 degrees too high, the model is 2.4 degrees too low, the hourly station values are 0.5 degrees too high, the interpolated rawinsonde set is 0.8 degrees too high, the NMC analysis is 2.5 degrees too low, and the measured surface rawinsonde temperature is 0.3 degrees too high.

Table 1  
 SURFACE SYSTEMATIC ERRORS, SURFACE SPATIAL RMS ERRORS, AND SURFACE TRANSIENT ERRORS FOR JANUARY 1988

Meaning of the rows and columns labeled S, o, M, h, R, X, and r is discussed in text.

T 0188 — Temperature (Units = 0.1 degree K)																							
SURFACE SYSTEMATIC ERRORS							SURFACE SPATIAL RMS ERRORS							SURFACE TRANSIENT ERRORS									
S	o	M	h	R	X	r	S	o	M	h	R	X	r	S	o	M	h	R	X	r			
S	0	-2	24	0	-8	25	-3	S	0	10	28	6	16	30	6	S	0	19	33	12	29	32	13
o	2	0	16	0	-13	15	-4	o	10	0	30	10	12	31	5	o	19	0	39	21	42	40	23
M	-24	-16	0	-23	-34	-3	-29	M	28	30	0	28	15	23	26	M	33	39	0	35	30	21	35
h	0	0	23	0	-11	24	-4	h	6	10	28	0	18	32	6	h	12	21	35	0	33	34	8
R	8	13	34	11	0	31	5	R	16	12	15	18	0	22	14	R	29	42	30	33	0	23	29
X	-25	-15	3	-24	-31	0	-25	X	30	31	23	32	22	0	27	X	32	40	21	34	23	0	33
r	3	4	29	4	-5	25	0	r	6	5	26	6	14	27	0	r	13	23	35	8	29	33	0

RH 0188 — Relative Humidity (Units = Percent)																							
SURFACE SYSTEMATIC ERRORS							SURFACE SPATIAL RMS ERRORS							SURFACE TRANSIENT ERRORS									
S	o	M	h	R	X	r	S	o	M	h	R	X	r	S	o	M	h	R	X	r			
S	0	0	0	-1	11	9	0	S	0	0	8	1	5	6	4	S	0	0	15	4	12	11	4
o	0	0	0	0	0	0	0	o	0	0	0	0	0	0	0	o	0	0	0	0	0	0	0
M	0	0	0	0	11	10	1	M	8	0	0	7	6	7	7	M	15	0	0	15	13	10	15
h	1	0	0	0	13	10	1	h	1	0	7	0	5	6	4	h	4	0	15	0	13	11	4
R	-11	0	-11	-13	0	-2	-10	R	5	0	6	5	0	6	7	R	12	0	13	13	0	11	12
X	-9	0	-10	-10	2	0	-8	X	6	0	7	6	6	0	6	X	11	0	10	11	11	0	11
r	0	0	-1	-1	10	8	0	r	4	0	7	4	7	6	0	r	4	0	15	4	12	11	0

U 0188 — Zonal Wind (Units = 0.1 meter/second)																							
SURFACE SYSTEMATIC ERRORS							SURFACE SPATIAL RMS ERRORS							SURFACE TRANSIENT ERRORS									
S	o	M	h	R	X	r	S	o	M	h	R	X	r	S	o	M	h	R	X	r			
S	0	0	-19	2	-15	-26	0	S	0	0	30	4	13	21	4	S	0	0	44	13	33	31	13
o	0	0	0	0	0	0	0	o	0	0	0	0	0	0	0	o	0	0	0	0	0	0	0
M	19	0	0	22	5	-5	21	M	30	0	0	29	20	18	24	M	44	0	0	43	39	27	43
h	-2	0	-22	0	-16	-28	0	h	4	0	29	0	15	21	3	h	13	0	43	0	35	32	13
R	15	0	-5	16	0	-13	15	R	13	0	20	15	0	14	13	R	33	0	39	35	0	29	32
X	26	0	5	28	13	0	28	X	21	0	18	21	14	0	19	X	31	0	27	32	29	0	31
r	0	0	-21	0	-15	-28	0	r	4	0	24	3	13	19	0	r	13	0	43	13	32	31	0

V 0188 — Meridional Wind (Units = 0.1 meter/second)																							
SURFACE SYSTEMATIC ERRORS							SURFACE SPATIAL RMS ERRORS							SURFACE TRANSIENT ERRORS									
S	o	M	h	R	X	r	S	o	M	h	R	X	r	S	o	M	h	R	X	r			
S	0	0	-6	1	-2	0	0	S	0	0	25	3	17	22	4	S	0	0	42	13	32	34	15
o	0	0	0	0	0	0	0	o	0	0	0	0	0	0	0	o	0	0	0	0	0	0	0
M	6	0	0	8	4	5	6	M	25	0	0	27	13	14	24	M	42	0	0	42	32	26	41
h	-1	0	-8	0	-3	-3	-1	h	3	0	27	0	17	24	2	h	13	0	42	0	33	34	13
R	2	0	-4	3	0	1	1	R	17	0	13	17	0	11	17	R	32	0	32	33	0	25	31
X	0	0	-5	3	-1	0	0	X	22	0	14	24	11	0	20	X	34	0	26	34	25	0	31
r	0	0	-6	1	-1	0	0	r	4	0	24	2	17	20	0	r	15	0	41	13	31	31	0

P 0188 — Precipitation (Units = 0.1 millimeter/day)																							
SURFACE SYSTEMATIC ERRORS							SURFACE SPATIAL RMS ERRORS							SURFACE TRANSIENT ERRORS									
S	o	M	h	R	X	r	S	o	M	h	R	X	r	S	o	M	h	R	X	r			
S	0	-3	0	0	0	0	0	S	0	10	16	0	0	0	0	S	0	33	41	0	0	0	0
o	3	0	1	0	0	0	0	o	10	0	13	0	0	0	0	o	33	0	40	0	0	0	0
M	0	-1	0	0	0	0	0	M	16	13	0	0	0	0	0	M	41	40	0	0	0	0	0
h	0	0	0	0	0	0	0	h	0	0	0	0	0	0	0	h	0	0	0	0	0	0	0
R	0	0	0	0	0	0	0	R	0	0	0	0	0	0	0	R	0	0	0	0	0	0	0
X	0	0	0	0	0	0	0	X	0	0	0	0	0	0	0	X	0	0	0	0	0	0	0
r	0	0	0	0	0	0	0	r	0	0	0	0	0	0	0	r	0	0	0	0	0	0	0

Table 2  
SURFACE SYSTEMATIC ERRORS, SURFACE SPATIAL RMS ERRORS, AND SURFACE TRANSIENT ERRORS FOR JULY 1988

Meaning of the rows and columns labeled S, o, M, h, R, X, and r is discussed in text.

T 0788 — Temperature (Units = 0.1 degree K)																								
SURFACE SYSTEMATIC ERRORS								SURFACE SPATIAL RMS ERRORS								SURFACE TRANSIENT ERRORS								
	S	o	M	h	R	X	r		S	o	M	h	R	X	r		S	o	M	h	R	X	r	
S	0	-1	1	4	16	-7	1	S	0	17	33	6	23	46	5	S	0	12	22	10	16	25	10	
o	1	0	-5	4	19	-16	-3	o	17	0	31	14	26	44	9	o	12	0	24	16	20	28	15	
M	-1	5	0	1	13	-10	-1	M	33	31	0	34	20	22	37	M	22	24	0	23	18	17	21	
h	-4	-4	-1	0	12	-10	-2	h	6	14	34	0	25	46	2	h	10	16	23	0	16	26	8	
R	-16	-19	-13	-12	0	-24	-14	R	23	26	20	25	0	36	23	R	16	20	18	16	0	18	15	
X	7	16	10	10	24	0	10	X	46	44	22	46	36	0	53	X	25	28	17	26	18	0	23	
r	-1	3	1	2	14	-10	0	r	5	9	37	2	23	53	0	r	10	15	21	8	15	23	0	

RH 0788 — Relative Humidity (Units = Percent)																								
SURFACE SYSTEMATIC ERRORS								SURFACE SPATIAL RMS ERRORS								SURFACE TRANSIENT ERRORS								
	S	o	M	h	R	X	r		S	o	M	h	R	X	r		S	o	M	h	R	X	r	
S	0	0	12	0	6	10	1	S	0	0	8	1	5	7	2	S	0	0	10	4	7	8	4	
o	0	0	0	0	0	0	0	o	0	0	0	0	0	0	0	o	0	0	0	0	0	0	0	
M	-12	0	0	-12	-4	-1	-9	M	8	0	0	8	7	4	8	M	10	0	0	10	9	6	10	
h	0	0	12	0	6	11	1	h	1	0	8	0	6	7	2	h	4	0	10	0	7	8	3	
R	-6	0	4	-6	0	3	-4	R	5	0	7	6	0	3	7	R	7	0	9	7	0	7	7	
X	-10	0	1	-11	-3	0	-7	X	7	0	4	7	3	0	9	X	8	0	6	8	7	0	7	
r	-1	0	9	-1	4	7	0	r	2	0	8	2	7	9	0	r	4	0	10	3	7	7	0	

U 0788 — Zonal Wind (Units = 0.1 meter/second)																								
SURFACE SYSTEMATIC ERRORS								SURFACE SPATIAL RMS ERRORS								SURFACE TRANSIENT ERRORS								
	S	o	M	h	R	X	r		S	o	M	h	R	X	r		S	o	M	h	R	X	r	
S	0	0	0	0	-3	-7	0	S	0	0	15	5	10	11	8	S	0	0	27	14	20	20	15	
o	0	0	0	0	0	0	0	o	0	0	0	0	0	0	0	o	0	0	0	0	0	0	0	
M	0	0	0	0	-1	-8	2	M	15	0	0	13	20	15	18	M	27	0	0	29	26	19	26	
h	0	0	0	0	-3	-8	1	h	5	0	13	0	10	11	7	h	14	0	29	0	20	21	14	
R	3	0	1	3	0	-5	4	R	10	0	20	10	0	11	7	R	20	0	26	20	0	19	18	
X	7	0	8	8	5	0	9	X	11	0	15	11	11	0	12	X	20	0	19	21	19	0	19	
r	0	0	-2	-1	-4	-9	0	r	8	0	18	7	7	12	0	r	15	0	26	14	18	19	0	

V 0788 — Meridional Wind (Units = 0.1 meter/second)																								
SURFACE SYSTEMATIC ERRORS								SURFACE SPATIAL RMS ERRORS								SURFACE TRANSIENT ERRORS								
	S	o	M	h	R	X	r		S	o	M	h	R	X	r		S	o	M	h	R	X	r	
S	0	0	6	2	-2	0	0	S	0	0	18	6	13	17	9	S	0	0	28	16	28	22	18	
o	0	0	0	0	0	0	0	o	0	0	0	0	0	0	0	o	0	0	0	0	0	0	0	
M	-6	0	0	-2	-5	-7	-1	M	18	0	0	16	16	14	16	M	28	0	0	29	31	19	28	
h	-2	0	2	0	-5	-3	-1	h	6	0	16	0	12	17	7	h	16	0	29	0	28	23	14	
R	2	0	5	5	0	0	3	R	13	0	16	12	0	15	11	R	28	0	31	28	0	25	25	
X	0	0	7	3	0	0	3	X	17	0	14	17	15	0	18	X	22	0	19	23	25	0	21	
r	0	0	1	1	-3	-3	0	r	9	0	16	7	11	18	0	r	18	0	28	14	25	21	0	

P 0788 — Precipitation (Units = 0.1 millimeter/day)																								
SURFACE SYSTEMATIC ERRORS								SURFACE SPATIAL RMS ERRORS								SURFACE TRANSIENT ERRORS								
	S	o	M	h	R	X	r		S	o	M	h	R	X	r		S	o	M	h	R	X	r	
S	0	0	2	0	0	0	0	S	0	3	20	0	0	0	0	S	0	29	73	0	0	0	0	
o	0	0	4	0	0	0	0	o	3	0	15	0	0	0	0	o	29	0	68	0	0	0	0	
M	-2	-4	0	0	0	0	0	M	20	15	0	0	0	0	0	M	73	68	0	0	0	0	0	
h	0	0	0	0	0	0	0	h	0	0	0	0	0	0	0	h	0	0	0	0	0	0	0	
R	0	0	0	0	0	0	0	R	0	0	0	0	0	0	0	R	0	0	0	0	0	0	0	
X	0	0	0	0	0	0	0	X	0	0	0	0	0	0	0	X	0	0	0	0	0	0	0	
r	0	0	0	0	0	0	0	r	0	0	0	0	0	0	0	r	0	0	0	0	0	0	0	

For the most part, these tables show the RAMS model is marginally worse than the NMC analysis, and both the analysis and RAMS model are worse than the various station datasets. There are notable exceptions. For example, during winter (Table 1) the climatological surface temperature errors appear to be marginally lower in the RAMS model than in the NMC analysis; the transient error is larger, however. Similar results occur for the summer simulation (Table 2). Here, the RAMS transient variations as well as spatial variations are slightly better at the surface for temperature. However, the other fields are not modeled any better, and now the model depiction of the precipitation field appears to be quite a bit worse than the cooperative or first order station values. Whether this model depiction is better than the precipitation field associated with the large-scale analysis is unknown; again, precipitation is not a part of the large-scale NMC archives.

## Conclusions

---

In some respects, we were quite pleased with the results. Preliminary comparisons indicate the NMC large-scale, global analysis is doing a perfectly adequate job representing various meteorological characteristics at individual stations in the western United States. The explained variance is quite high, especially for the temperature field, but also for wind and relative humidity.

We were disappointed, though, that the regional modeling system did not do a demonstrably better job than the original large-scale analysis at representing climate in the western United States. We now suspect we cannot rely on simply having a mesoscale model overlying mesoscale topography and forced only by a large-scale analysis. We will also probably need to include individual stations, as well as the NMC large-scale analysis, in a continuous model/data assimilation if we are to get a regional climatology that is a whole lot better than the original large-scale analysis. This kind of work is beyond the scope of work being reported here, but it is being explored by others (*eg*, Stauffer and Seaman 1990; Stauffer *et al* 1991).

One clear advantage to using the regional model was brought out by this comparison. The regional model can develop a smooth geographic representation of precipitation fields, which are not readily available elsewhere. Since precipitation is not needed to initialize the large-scale models, and is in fact a forecast field, it has not been previously archived or stored in any useful format. Another advantage is that the RAMS regional model can distinguish between snow and rain, which will be quite useful eventually when these regional models are coupled to various surface hydrology modules. Other variables, especially derived nonlinear variables, may also be better represented by the regional model fields than by the large-scale analysis.

Finally, since errors of the regional modeling attempt are not substantially less than errors of the original analyses, is it better to interpolate dynamically by forcing a mesoscale model with large-scale GCM output than it is to linearly interpolate the original GCM output? Many papers appear to indicate that a regional model gives substantially better answers and could, therefore, be used to interpolate large-scale GCM future climate simulations to regional scales. From the present results, we cannot yet wholeheartedly agree.

Further details of this work are provided in Roads *et al* (1992b).

## References

---

- Bossert, J, J Kao, J Winterkamp, JO Roads, SC Chen, and K Ueyoshi. 1992a. Regional-scale simulations of the western U.S. climate. Proceedings of the International Conference on Global Climate Change: Its Mitigation Through Improved Production and Use of Energy. Los Alamos National Laboratory, Los Alamos, NM, October 21-24, 1991.
- Bossert, J, J Roads, J Kao, S Chen, and K Ueyoshi. 1992b. Regional-scale simulations of the western U.S. climate. Proceedings of the Third Symposium on Global Change Studies, Atlanta, GA, January 5-10, 1992.
- Bossert, J, JO Roads, CY Jim Kao, SC Chen, and JL Winterkamp. 1992c. Development of a regional-scale climate modeling system: Simulations with a detailed microphysics parameterization. DOE ARM 1991 Science Team Proceedings.
- Cotton, WR, CJ Tremback, and RL Walko. 1988. CSU RAMS: A cloud model goes regional. Proc. NCAR Workshop on Limited-Area Modeling Intercomparison, November 15-18, NCAR, Boulder, CO, 202-211.
- Dickinson, RE, RM Errico, F Giorgi, and GT Bates. 1989. A regional climate model for the western United States. *Climatic Change* 15:383-422.
- Giorgi, F., 1990: Simulation of regional climate using a limited area model nested in a general circulation model. *J. Climate* 3:941-963.
- Giorgi, F, and GT Bates. 1989. On the climatological skill of a regional model over complex terrain. *Mon. Wea. Rev.* 117:2325-2347.
- Roads, JO, K Ueyoshi, S-C Chen, J Alpert, and F Fujioka. 1991. Medium-range fire weather forecasts. *International Journal of Wildland Fire* 1(3):159-176.
- Roads, JO, S-C Chen, J Kao, D Langley, and G Glatzmaier. 1992. Global aspects of the Los Alamos general circulation model hydrologic cycle. *J. Geophys. Res.* 97(D9):10,051-10,068.
- Roads, JO, S-C Chen, K Ueyoshi, J Bossert, and J Winterkamp. 1992b. Development of a regional climatology for the U.S. West. (in preparation)
- Stauffer, DR, and NL Seaman. 1990. Use of four-dimensional data assimilation in a limited-area mesoscale model. part I: experiments with synoptic-scale data. *Mon. Wea. Rev.* 118:1250-1277.
- Stauffer, DR, NL Seaman, and FS Binkowski. 1991. Use of four-dimensional data assimilation in a limited-area mesoscale model, part II: effects of data assimilation within the planetary boundary layer. *Mon. Wea. Rev.* 119:734-754.
- Tremback, CJ. 1990. Numerical simulation of a mesoscale convective complex: Model development and numerical results. Colorado State University, Dept. of Atmospheric Science, Paper No. 465.
- Tremback, CJ, GJ Tripoli, R Arritt, WR Cotton and RA Pielke. 1986. The Regional Atmospheric Modeling System. *Proc. Internat. Conf. Development and Application of Computer Techniques to Environmental Studies*, November, Los Angeles, CA. P Zanetti (ed). Computational Mechanics Publications, Boston. pp 601-607.
- Tripoli, GJ. 1992. A nonhydrostatic mesoscale model designed to simulate scale interaction. *Mon. Wea. Rev.* 120(7):1342-1359.
- Ueyoshi, K, and JO Roads. 1992. Simulation and prediction of the Catalina Eddy. Submitted to *Mon. Wea. Rev.*
- Wigley, TML, PD Jones, KR Briffa, and G Smith. 1990. Obtaining sub-grid-scale information from coarse-resolution general circulation model output. *J. Geophys. Res.* 95:1943-1953.

# **Climatic Impacts of the 1991-92 Western Winter**

---

Kelly T. Redmond

The latest in a series of unusual winters affected the western United States during 1991-92. This report is primarily concerned with the 6 to 8 coolest months, with some consideration of the adjacent summer months. Among the most outstanding features of this period are:

- A sixth year of continued drought in the Sierra Nevada and southern Oregon Cascades
- Severe drought in the Pacific Northwest
- An extremely warm winter in the northern West and western Canada
- Very heavy precipitation in southeastern Alaska
- Very heavy precipitation from southern California to Texas

Much of the winter was characterized by "split flow" west of North America. As it approached the West Coast, the jet stream frequently diverged into a northern branch toward Panhandle Alaska and a second southern branch that dived south along the California coast and then eastward along the US-Mexican border. Repeatedly, storms approaching the West Coast were stretched north-to-south, losing their organization in the process.

## **Regional Climate Anomalies**

---

During October, fires burned large acreages of wild land, destroyed 100 homes in Spokane, and consumed 3,354 homes and 456 apartment units in a major conflagration in Oakland. The Oakland fire killed 23 people and produced insurable losses of 1.5 to 2 billion dollars, the second costliest disaster in United States history (behind Hurricane Hugo). A severe cold outbreak at the end of October brought what turned out to be the coldest temperatures of the winter to large parts of the West.

As the winter progressed, a series of closed, upper low pressure systems drifting south parallel to the California coastline dropped heavy precipitation all along the central and southern coast, and then in the interior as they swung inland near Los Angeles. The lack of a significant upslope component over the Sierra during these periods meant the normally substantial contribution from orographic uplift to snowpack did not occur. The precipitation ratio of Sierra sites to the valley and coastal locations was, therefore, much lower than usual.

During the first half of February, heavy rain inundated southern California. Lake Cachuma, water supply for Santa Barbara, received a foot of rain in one week, and nearby sites received over 16 inches. Maria Ygnacio Creek in Santa Maria County flooded for the first time on record, and other local floods were called the "worst in 50 years". In some central coastal basins, the multi-year drought was declared over. However, since little precipitation fell in the source regions for most of California's water supplies, the drought continued essentially uninterrupted. Los Angeles residents, in the midst of severe localized flooding, struggled to reconcile the seemingly contradictory message that the water covering the furniture was of little value for drought relief.

Statewide precipitation and runoff for California during the past 6 water years (October-September) is shown in Table 1, expressed as a departure in percentage from 100 percent of average. Because of local recycling and evapotranspiration, not all precipitation results in runoff. A reduction in precipitation by one-quarter results in a runoff reduction of one-half.

Statewide	1986-87	1987-88	1988-89	1989-90	1990-91	1991-92	6-Year Average
Precipitation Departure	-39	-18	-14	-31	-24	-14	-23
Runoff Departure	-52	-52	-30	-55	-57	-57	-50

At the Central Sierra Snow Lab (6900 feet) near Donner Summit, snow depth on April 1 was 35 inches (average is 85). The snow was gone by April 25 (average depth 65 inches), two months earlier than the usual date of snow disappearance (June 25). This was a combined result of below-average precipitation and a very warm spring. This was the sixth very warm March and April in the past 7 years, the exception being 1991, the year with the "Miracle March" (Figure 1). Nearby Lake Tahoe dropped to its lowest level on record (Figure 2).

By the end of the water year (September 30), storage in 155 major California reservoirs was 33.6 percent of capacity, compared with 36.6 percent one year previous and an average of 59.8 percent of capacity. During those 6 years, the average runoff as expressed by the Sacramento River Index was 9.96 million acre-feet, one percent higher than the previous 6-year minimum (9.78) from 1929-1934. To the south over the same period, the San Joaquin River Index averaged 2.70 million acre-feet, 81 percent of the previous minimum (3.34) from 1929-1934.

From some perspectives, this 6-year event may be viewed as a short-term climate "change" or fluctuation. Taken as a whole, these six years begin to resemble the types of scenarios used by climate modelers in studies of climate sensitivity. The difference, in this case, is that this is an observed realization in the real atmosphere, and not merely hypothetical. An

example is shown in Figure 3. At Tahoe City on Lake Tahoe, temperatures have been above average for the past 6 years on most days of the year. Maximum temperatures have, in particular, been warmer than usual in the spring and fall. Minimum temperatures have been above average

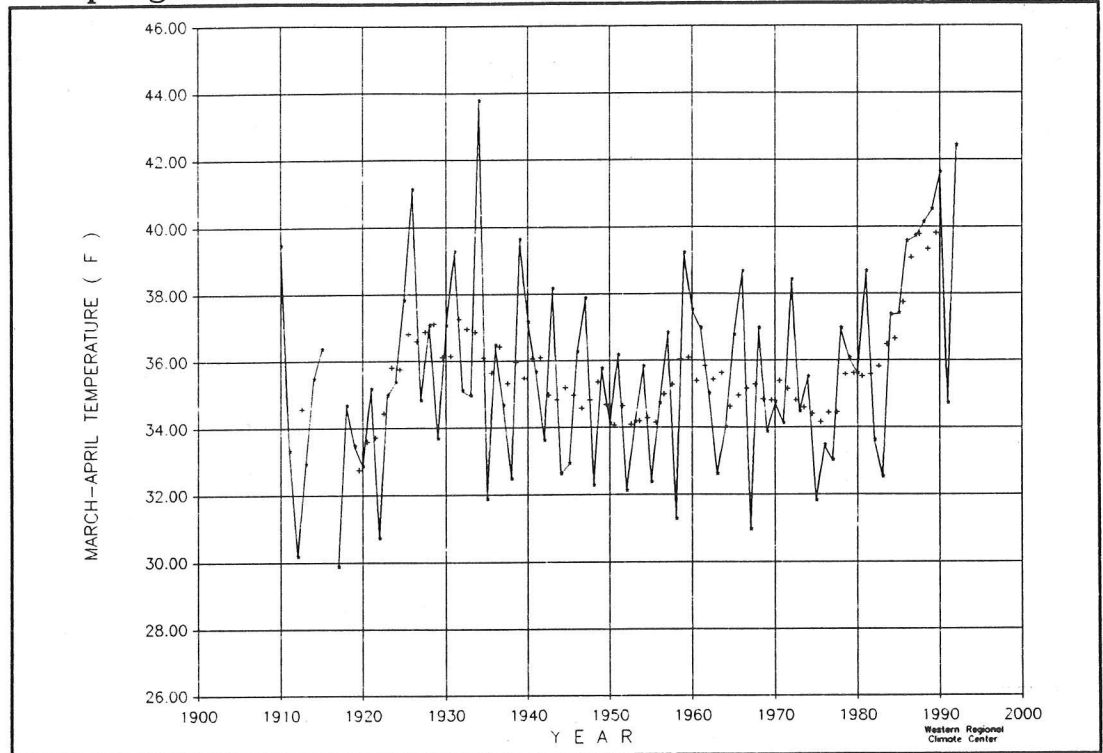


Figure 1. Mean temperature for March and April at Tahoe City, where the Truckee River leaves Lake Tahoe. The "+" symbols show a 6-year running mean.

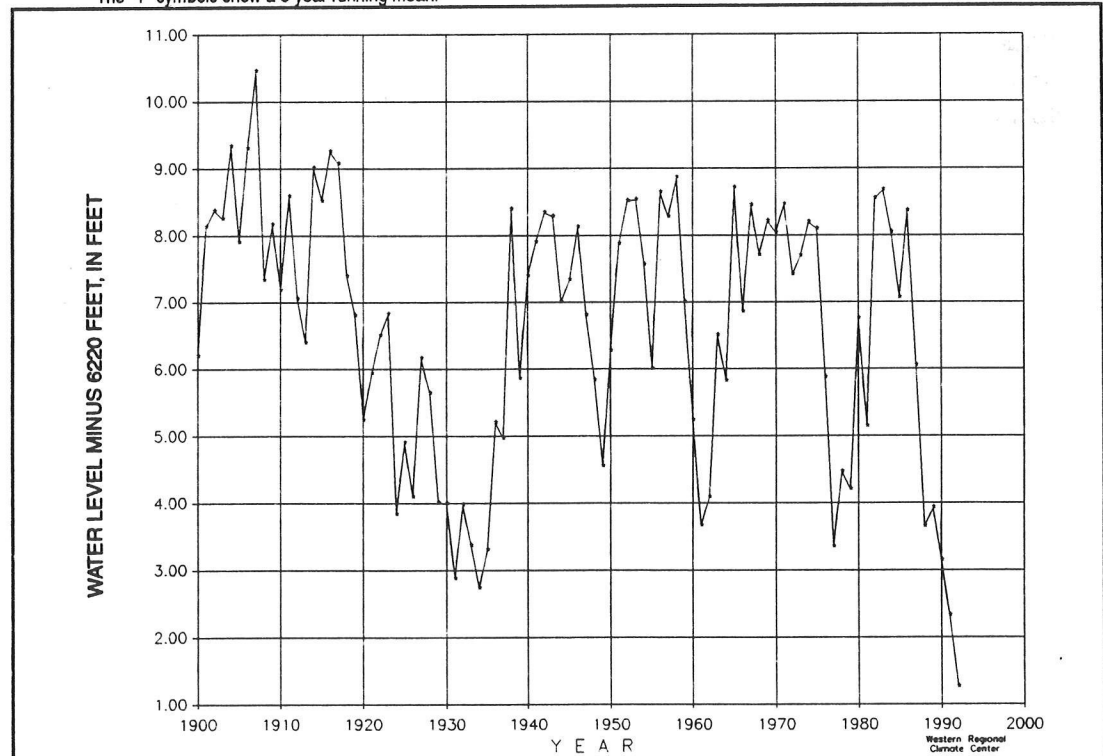


Figure 2. Water level of Lake Tahoe on the last day of August. Units are in terms of elevation minus 6220 feet. Lake rim level is 6223.00 feet (3.00 on diagram).

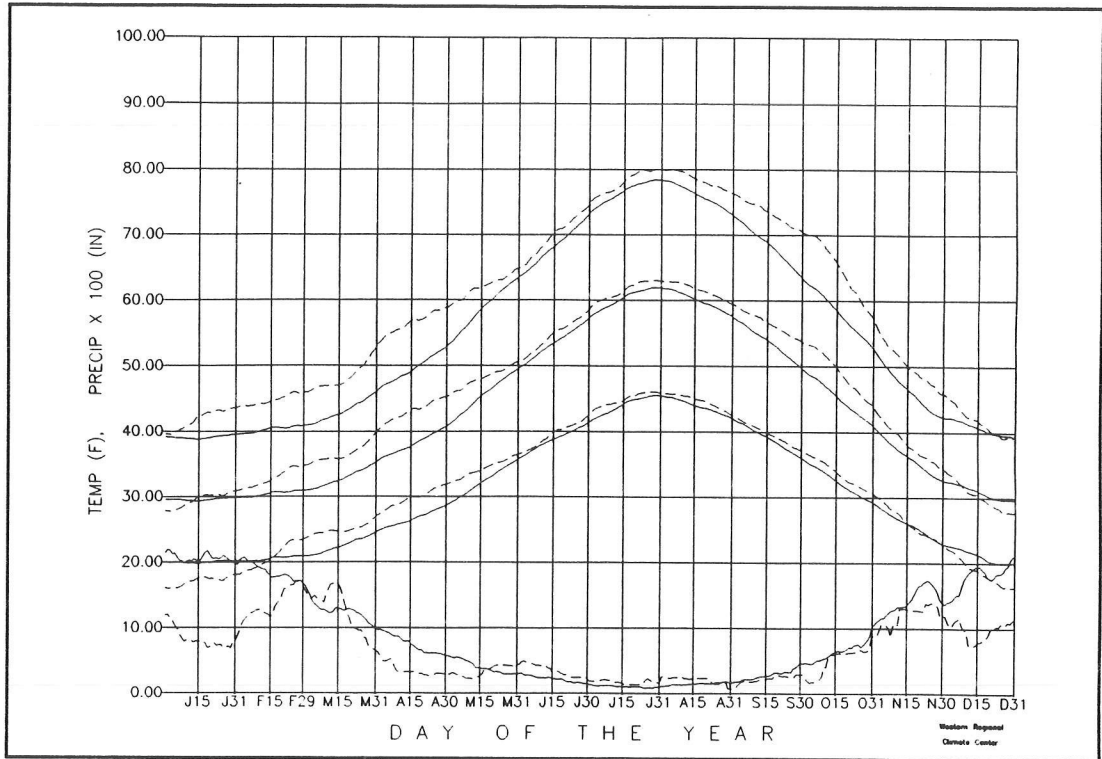


Figure 3. Daily temperature and precipitation climatology for 1951-1986 and for January 1987-September 1992. Daily mean precipitation has been multiplied by 100, so that units are in hundredths of inches. Smoothed with a 29-day filter. Solid Line: (From top) maximum, mean, and minimum for 1951 through 1986. Dashed Line: (From top) maximum, mean, and minimum for January 1987 through September 1992.

through most of the spring, and mean temperatures have been reaching the freezing point more than a month earlier in the spring than before. The figure also shows that precipitation has been below average from early December into late February, leaving a large reduction during the heart of the major precipitation season. The combined precipitation/temperature effects have been (1) reduced precipitation, (2) a higher rain/snow line so that even less snow falls at a given elevation, (3) earlier initiation of snowmelt season, and (4) an earlier start to vegetative growth and attendant consumption of water.

In the northern West, a promising start to the snow accumulation season gave way to steadily falling water supply projections as winter progressed and precipitation-bearing systems moved well to the north. Table 2 shows the percentage of average snowpack for four Pacific Northwest states on different dates as the season progressed. By early May, very little snow was found below 5000 feet elevation in Oregon.

State	Dec23	Jan06	Jan20	Jan30	Feb17	Mar02	Mar24	Apr09	Apr20	May18
Washington	96	84	75	83	79	82	67	56	54	30
Oregon	74	62	57	52	45	40	29	20	17	5
Idaho	106	83	71	72	66	72	60	49	47	17
Montana	119	97	92	93	80	83	75	68	69	40

The steady decrease in snow water percent of average was the result of both dry conditions and very warm temperatures. For example, Government Camp, Oregon, which at 4000 feet is often near the rain/snow level, reported just 114 inches of snowfall from October through March, compared with an average of 241 inches. At Crater Lake, corresponding figures were 223 and 411 inches. In the southern Cascades, Sexton Summit (3836 feet) was considerably warmer than average all winter (Table 3) and noted just 5 days with a mean temperature of freezing or lower, compared with an average of 41 days.

Table 3  
CLIMATE ANOMALIES FOR SELECTED CITIES AND SELECTED ELEMENTS, 1991-92

*Precipitation is in inches. Departures are from 1961-1990 means. Values are in original English units as measured.*

Site	1991					1992						
	Aug	Sep	Oct	Nov	Dec	Jan	Feb	Mar	Apr	May	Jun	Jul
<u>Hilo, Hawaii</u>												
Precipitation (inches)	26.92	9.41	5.15	6.74	15.04	1.33	1.29	3.90	6.62	2.99	9.36	17.63
Departure	+17.58	+0.88	-4.45	-7.77	+3.00	-8.55	-9.00	-9.98	-8.64	-6.92	+3.16	+7.92
Percent	288	110	54	46	125	13	13	28	43	30	151	182
<u>Yakutat, Alaska</u>												
Precipitation (inches)	27.74	42.45	18.70	18.28	19.88	29.84	19.47	37.28	5.48	12.93	13.64	7.84
Departure	+16.20	+23.80	-4.27	+3.76	+4.94	+7.66	+8.80	+6.56	-4.44	+3.27	+6.34	-0.34
Percent	240	228	81	126	133	245	182	348	55	134	187	96
<u>Valdez, Alaska</u>												
Snowfall (inches)	0.0	0.0	6.4	59.9	137.1	85.7	85.7	100.2	38.9	1.9	0.0	0.0
Departure	0.0	-0.2	-3.2	+23.5	+64.7	+29.4	+35.2	+46.7	+19.4	+1.3	0.0	0.0
Accumulated*	0.0	0.0	6.4	66.3	203.4	289.1	374.8	475.0	513.9	515.8	515.8	515.8
Accumulated Departures**	0.0	-0.2	-3.4	+20.1	+84.8	+114.2	+149.4	+196.1	+215.5	+216.8	+216.8	+216.8
<u>Miles City, Montana</u>												
Temperature (degrees F)												
Departure	+4.1	+1.2	-4.0	-1.4	+11.2	+16.0	+12.5	+8.2	+2.5	+7.8	+1.9	-7.7
<u>Government Camp, Oregon</u>												
Snowfall (inches)	0	0	25	40	20	18	9	2	17	0	0	0
Departure	0	0	+18	+6	-32	-41	-31	-46	-13	-7	0	0
Accumulated*	0	0	25	65	85	103	112	114	131	131	131	131
Accumulated Departures**	0	0	+18	+24	-8	-49	-80	-126	-139	-146	-146	-146
<u>Crater Lake, Oregon</u>												
Snowfall (inches)	0	0	33	47	38	44	51	10	18	0	2	0
Departure	0	-4	+11	-21	-45	-38	-21	-75	-25	-19	-2	-1
Accumulated*	0	0	33	80	118	162	213	223	241	241	243	243
Accumulated Departures**	0	-4	+7	-14	-59	-97	-118	-193	-218	-237	-239	-239
<u>Sexton Summit, Oregon</u>												
Temperature (degrees F)												
Departure	+1.0	+8.4	+6.7	+4.0	+4.0	+3.7	+6.3	+8.9	+6.4	+10.7	+4.0	+0.8
<u>Winslow, Arizona</u>												
Temperature (degrees F)												
Departure	-1.9	-1.3	-0.0	-2.4	-2.3	-4.0	+0.7	-0.2	+3.9	-1.2	-3.3	-5.6
<u>Alamosa, Colorado</u>												
Temperature (degrees F)												
Departure	+1.0	+0.5	+0.7	-6.5	-12.8	-14.6	-8.3	-2.0	+6.4	+3.1	-1.0	-2.9

\* Accumulated since the first month.

\*\* Accumulated sum of the departures.

By July 30, the large Owyhee Reservoir in southeastern Oregon had fallen below the outflow pipes, and eight other reservoirs in the northern Great Basin were completely dry. June flow on the Columbia River at The Dalles was 55 percent of average and ranked fourth lowest of 67 years, and for the same month flow on the Willamette River at Salem was 29 percent of average and ranked lowest in 67 years.

Around mid-December 1991, a warm pattern established itself over the northern plains and mountain states, extending along the Rockies to the Yukon. Extremely warm weather dominated for most of the next 22 weeks. Montana recorded its warmest and third driest winter (December-February) since 1895. Miles City averaged 14 degrees F above normal during this period (Table 3), at one point reaching within one degree of the state record of 73 degrees for January.

At the same time, the active storm track moved north to Alaska. Yakutat (Table 3) recorded extremely heavy precipitation for the December-February winter season (68.00", departure +30.21"), for calendar year 1991 (219.48", departure +68.23") and for the 12-month period in Table 3 (253.53", departure +102.28"). Valdez recorded 516 inches of snowfall, where average is just 299 inches. Anchorage recorded its greatest snow depth ever (34 inches) late in January.

Although the winter of 1991-1992 brought much less snow than usual to most of the West, an unusual number of deaths were reported from avalanches. The US Forest Service recorded 23 people were killed in the West and Alaska, compared with the 21-year average of 13 deaths.

South of Alaska, Hawaii usually receives less precipitation during El Niño events. Ironically, because of its porous volcanic soils, short rivers, and lack of reservoirs, this island state can quickly plunge into water-supply deficit when precipitation is less than average for an extended period. From January through May, for example, Hilo received just 16.13 inches (average is 59.26), and from October through May 43.06 inches fell (average is 95.41). Worried water purveyors did receive some relief during the summer.

The only cooler-than-average temperatures noted during the winter were in the Southwest. Maximum temperature at Winslow, Arizona, remained below 50 degrees F for 64 consecutive days, from November 29 to January 30, three days longer than the previous record in 1967-68. To its north, Alamosa became a winter-long oddity, consistently recording very cold temperature departures while nearby stations were near to well above normal. Cloudless skies and a good snow cover allowed radiative cooling to dominate at this high valley site. These same cloudless skies left a skimpy Colorado snowpack, which ensured that the flow of the Colorado River into Lake Powell would be the lowest 6-year total ever recorded. Continuing a steady decline, by July 31 Lake Powell was only 61 percent full.

In March Las Vegas received an astonishing 4.80 inches of rain, 1230 percent of the March average and more than the annual average. This was not an isolated cloudburst but fell on 11 days, and reflected a very wet month throughout the Southwest. The Southwest continued to receive heavy precipitation into the summer monsoon season. By July 25, the following amounts had been recorded since January 1:

	Southwest Precipitation January 1 - July 25 (in inches)	
	<u>1992</u>	<u>Average</u>
Yuma	3.99	1.09
Gila Bend	4.40	2.66
Parker	7.68	1.94
Phoenix	9.54	3.27
Buckeye	10.07	3.04
Flagstaff	16.37	10.74
Payson	19.15	10.17

By this time, most of the United States was in the midst of what was to become the third coldest summer on record, an event popularly ascribed to the Mt. Pinatubo stratospheric aerosol cloud. However, west of the Rockies the summer was near to above normal in temperature. In Great Falls, the shortest growing season on record ended when several inches of snow fell on August 22. The 92-day season had started May 22, and was a full 9 days shorter than the previous short seasons of 1984 and 1989.

## **Relationship to ENSO**

Previous work (Redmond and Koch 1991) has shown that winter surface climate conditions in the West are related to El Niño/Southern Oscillation (ENSO). Using the Southern Oscillation Index (SOI) as an indicator, it was shown that the June-November SOI (of year "t") is related to the temperature and precipitation anomaly field for the subsequent October (year "t") to March (year "t+1") period. These patterns are shown in Figures 4 and 5. A negative anomaly (usually associated with El Niño) implies dry/warm conditions in the Pacific Northwest and wet/cool average conditions in the Southwest. The 1992 June-November SOI averaged -0.95, a large enough anomaly that a signal, if present, could show itself unambiguously. Observed anomalies for October-March 1991-92 are shown in Figures 6 (precipitation) and 7 (temperature). There is close correspondence between the expected and observed patterns, somewhat better than the strength of the relationships would lead us to believe. (SOI accounts for one-fourth to one-third of the precipitation variance in the two "centers of action".)

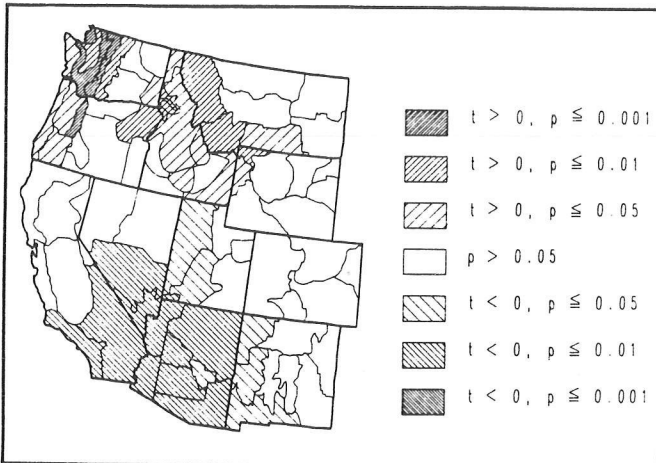


Figure 4. Significance map of October-March precipitation differences between years with average June-November SOI of +0.50 or more (11 cases) minus years with average June-November SOI of -0.50 or less (15 cases). Values shown are significance of t-tests of differences. Data from 51 winters, 1933-34 through 1983-84. (Figure 2 from Redmond and Koch [1991].)

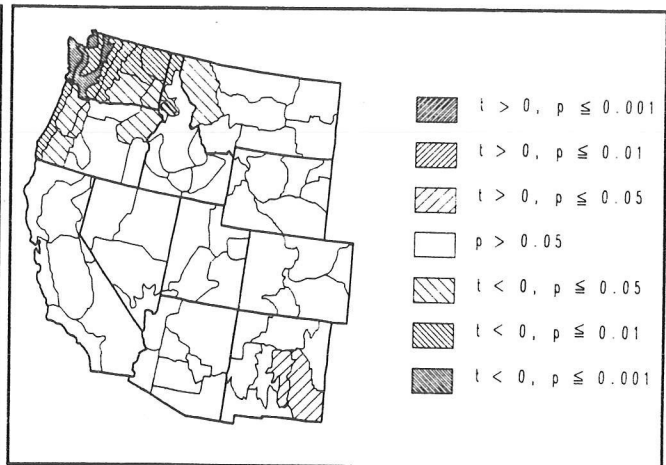


Figure 5. Significance map of October-March temperature differences between years with average June-November SOI of +0.50 or more (11 cases) minus years with average June-November SOI of -0.50 or less (15 cases). Values shown are significance of t-tests of differences. Data from 51 winters, 1933-34 through 1983-84. (Figure 5 from Redmond and Koch [1991].)

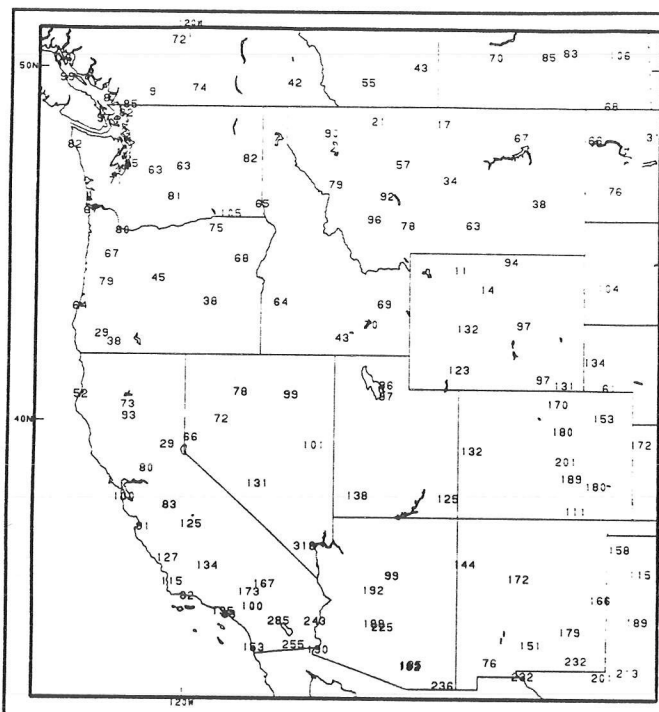


Figure 6. Observed 1991-92 October-March precipitation, expressed as percent of average. (Courtesy of NOAA Climate Analysis Center.)

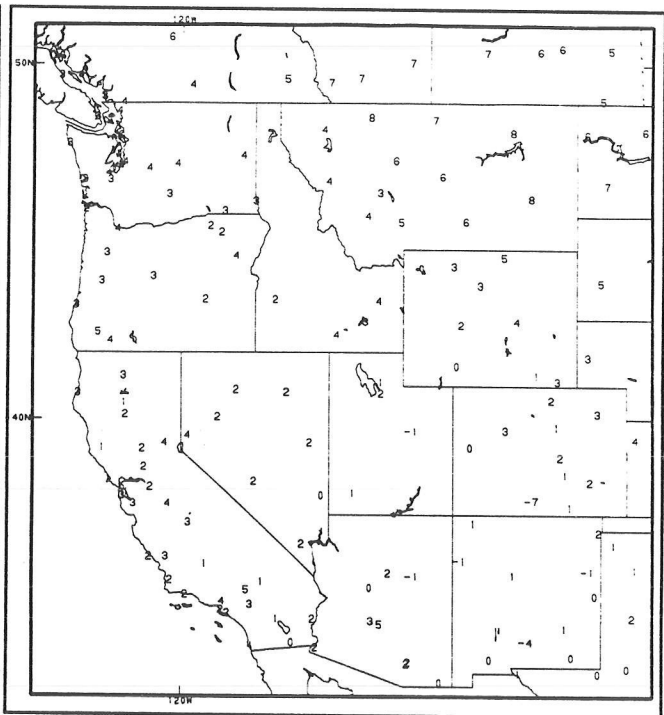


Figure 7. Observed 1991-92 October-March temperature, expressed as departure from average in whole degrees F. (Courtesy of NOAA Climate Analysis Center.)

In both the Pacific Northwest and the Southwest, relationships of SOI with temperature and precipitation act in concert to magnify the effect on snowfall for sites not far from the freezing level. At Crater Lake, for example, years with average SOI values of +0.50 or greater receive 111 inches more snow from October-March than those years with average SOI values of -0.50 ( $p < 0.05$ ) (see Figure 8; the winter of 1991-92, mentioned above, is circled).

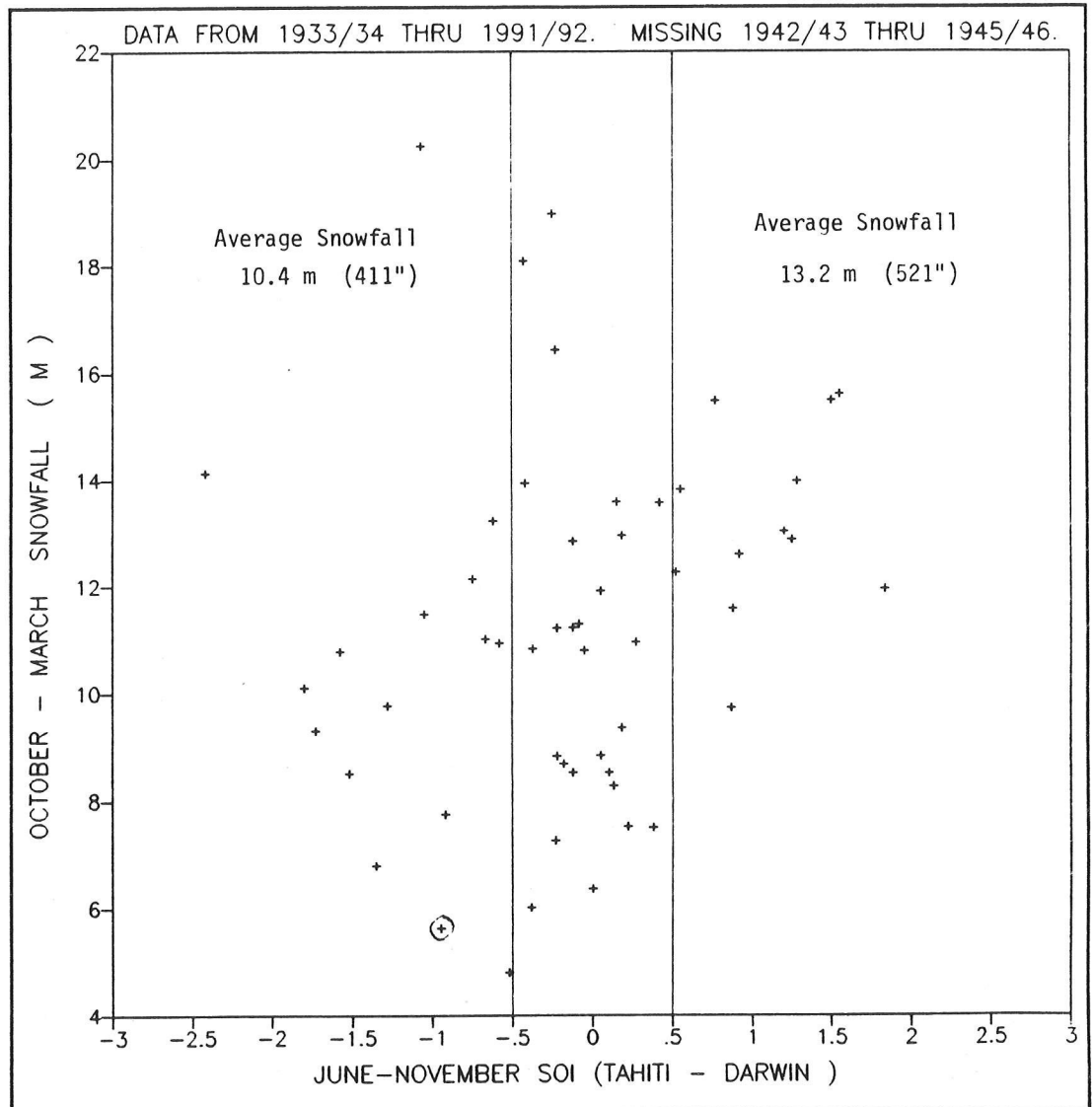


Figure 8. Scatter plot of June-November Southern Oscillation Index (SOI) versus subsequent October-March total snowfall at Crater Lake National Park headquarters. The winter of 1991-92 is circled (SOI = -0.95, snowfall = 5.66 meters).

## Other Impacts

Space does not permit a comprehensive overview of the impacts of the drought and other climate anomalies in the West. Gleick and Nash (1991) summarized the principal effects in California of the Sierra drought; the economic impacts they discussed will increase when the following winter (1991-92) is included.

Major sectors affected by drought and other climate variability in this region include: water resources, transportation, agriculture, forestry, energy, recreation, and fish and wildlife. Many of these areas are tightly interlinked. For example, the endangered winter run of Chinook salmon up the Sacramento River needs cool water to survive. Other constraints require minimum inflow to San Francisco Bay to prevent salinity intrusion, among other reasons. Contents of warm Folsom Reservoir, a popular recreation area near Sacramento, were rapidly drawn down to a

relative puddle at mid-summer to meet legal requirements for minimum Bay inflow, saving the cool, deep water behind Shasta Dam for later release to assist the upstream passage of endangered fish but arousing the ire of Folsom recreation businesses and marinas as the lake disappeared.

Climate variability also affects the health of ecosystems, and their susceptibility to disruptive influences. Natural systems have already adapted to climate variability. However, they have not adapted to additional human-caused forcings, such as tropospheric ozone or acid rain, which cause extra stress when the system is itself already stressed by natural climate fluctuations.

One important impact that is harder to assess is the cumulative effect of six years of almost uninterrupted water deficit in much of the West on the attitudes of its citizens toward water. Ten-year-old children, remembering nothing but drought, may come to value water differently than their parents. A prevailing attitude in much of the arid West has been that, no matter how population grew, sufficient water would be identified and acquired to meet the increased needs. A different attitude has also taken root — that natural resource constraints arising from considerations of quantity, quality, and temporal variability impose limitations on population growth and distribution.

The value of water and the relative value of uses to which it is applied are being assessed anew. This is illustrated in California, where more flexible regulations have made it possible to trade agricultural water rights for municipal uses; that is, for farmers to sell agricultural water to cities, profiting from the sale of water itself rather than from what the water would grow. This reflects a growing realization throughout the West that resource limitations are of fundamental importance in long-term planning and decision-making. The western drought has simply accentuated this point in a forceful, direct, and tangible way.

## **Acknowledgments**

---

This work was supported by the Western Regional Climate Center. Impact information has distilled from a wide variety of reports, publications, newspapers, state and national climate centers, and personal communications.

## **References**

---

- Gleick, PH, and L Nash. 1991. *The societal and environmental costs of the continuing California drought*. Pacific Institute for Studies in Development, Environment and Security. July 1991. [1681 Shattuck Ave, Suite H, Berkeley, CA 94709]
- Redmond, KT, and RW Koch. 1991. Surface climate and streamflow variability in the western United States and their relationship to large-scale circulation indices. *Water Resources Res.* 27:2381-2399.

# Drought Frequency Analysis for California from Observed, Synthetic, and Proxy Data

Frederick Wade Freeman and John A. Dracup

Drought frequency analysis can be performed with statistical techniques developed for determining recurrence intervals for extreme precipitation and flood events (Linsley *et al* 1992). The drought analysis method discussed in this paper uses the log-Pearson Type III distribution, which has been widely used in flood frequency research.

Some of the difficulties encountered when using this distribution for drought analysis are investigated. These difficulties arise because this distribution has been developed from statistics derived from large-sample-size datasets, while streamflow time series data generally contain only a limited number of drought events and, therefore, most drought datasets are of small sample size. For example, the 86-year record (starting in water year 1906) of unimpaired flow data for the 4-River Index, which represents streamflow in Northern California, contains only 19 drought events, 10 of which are minor events with durations of only 1 year. Large-sample-size statistics are typically based on datasets of 30 events or more. The problem the hydrologist faces is that the analysis of recurrence intervals for drought events of severity critical to the management and operation of water delivery systems is often based on datasets of very small sample size. If an adequate amount of data were to become available, then the methods developed for floodflows could be applied to droughts with only moderate adjustments (Lee *et al* 1986).

Two possible responses to the limiting condition of small-sample-size datasets are:

- Development and application of small-sample-size statistics specifically for use in drought frequency analysis, or
- Extension of the flow data record to increase the number of drought events, thus allowing analysis by standard methods such as the log-Pearson Type III distribution.

The first response has been investigated by a number of researchers, including Sen (1980), Lee *et al* (1986), and Nathan and McMahon (1990).

The second possibility, which is explored in this paper, involves expansion of the number of drought events in the time series record for a particular drainage basin. Two options exist for expanding the sample size of drought events for a given drainage basin. They are:

- Use of statistical modeling to generate additional years of synthetic flow data with statistical characteristics similar to the original dataset. These statistical models can be operated until a sufficient number of synthetic drought events have been created to increase sample size for use with large-sample-size statistics. A review of statistical streamflow models capable of generating synthetic droughts has been presented by Lawrance and Kottegoda (1977).
- Augmentation of the observed flow record with proxy flow data reconstructed from regression analysis of paleoclimate records and, in the specific case of this research, from tree-ring chronologies. An example of reconstructing streamflows from tree-rings has been presented by Stockton (1975).

## Methodology and Results

Discussed here is the application of the log-Pearson Type III distribution to various interpretations of the flow data record for the 4-River Index. This distribution is used to relate drought severity to recurrence interval. A limitation of this analysis is that it cannot determine drought duration, although Lee *et al* (1986) have presented an approach for frequency analysis of drought duration that can be employed in conjunction with the method presented here.



Figure 1. The rivers of the 4-River Index and locations of their streamflow gauge stations.

The hydrologic system under investigation is the 4-River Index of the Sacramento River Basin, for which annual unimpaired flow data exist for 1906 through 1991 (data provided by California Department of Water Resources). Figure 1 identifies the rivers constituting the 4-River Index. Tree-ring sampling locations used to reconstruct annual 4-River Index flows for 1560 to 1980 are shown in Earle and Fritts (1986).

Flow data are shown in Figure 2 for the observed, synthetic, and proxy records. Mean flow values are included for each of these three interpretations of the flow record.

Figure 3 shows two interpretations of the observed 86-year record. These interpretations are the theoretical and empirical values for (1) streamflow frequency for each water year and (2) drought frequency for each drought event (generally multi-

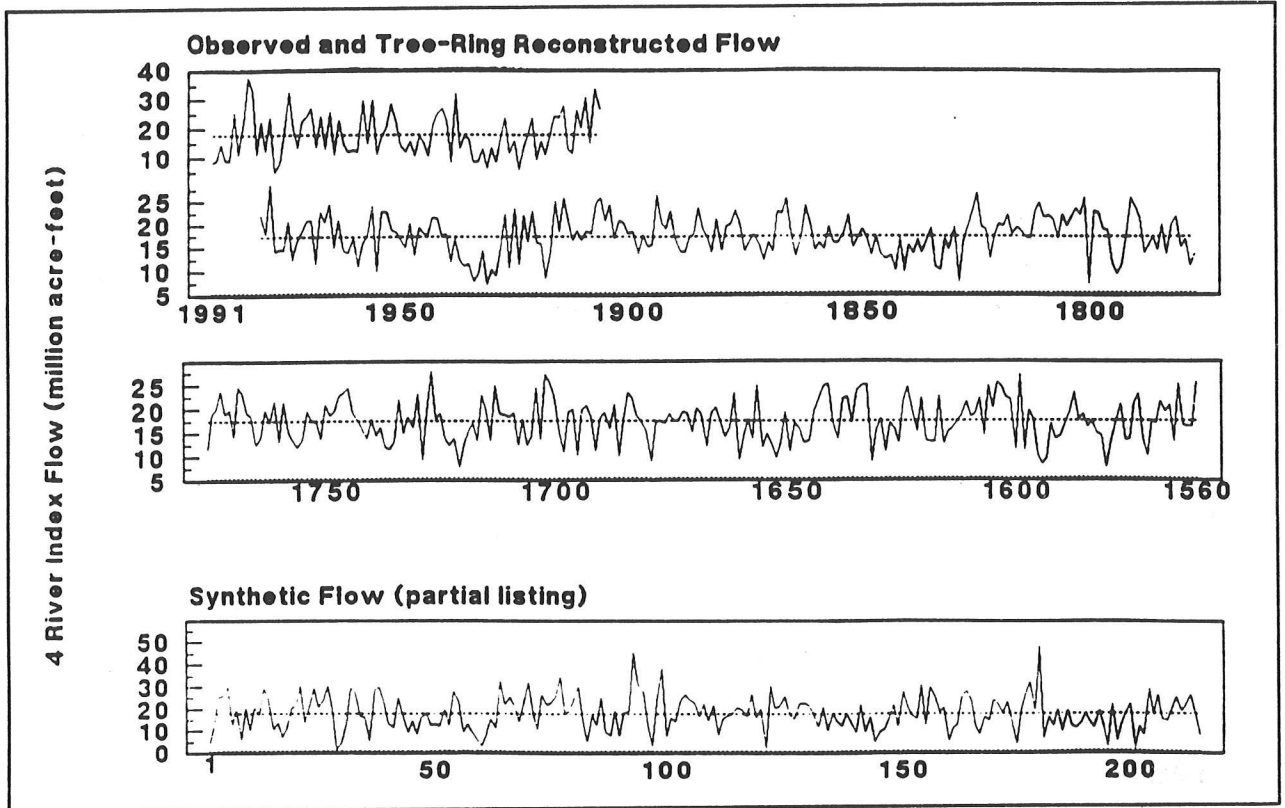


Figure 2. Annual flow data for the 4-River Index from the 86-year observed record (top graph), the 420-year tree-ring reconstructed record (top and middle graphs), and a partial listing of the 10,000-year synthetically generated record (bottom graph). Mean annual flows are 17.81 million acre-feet for the observed and synthetic records and 17.46 million acre-feet for the reconstructed record.

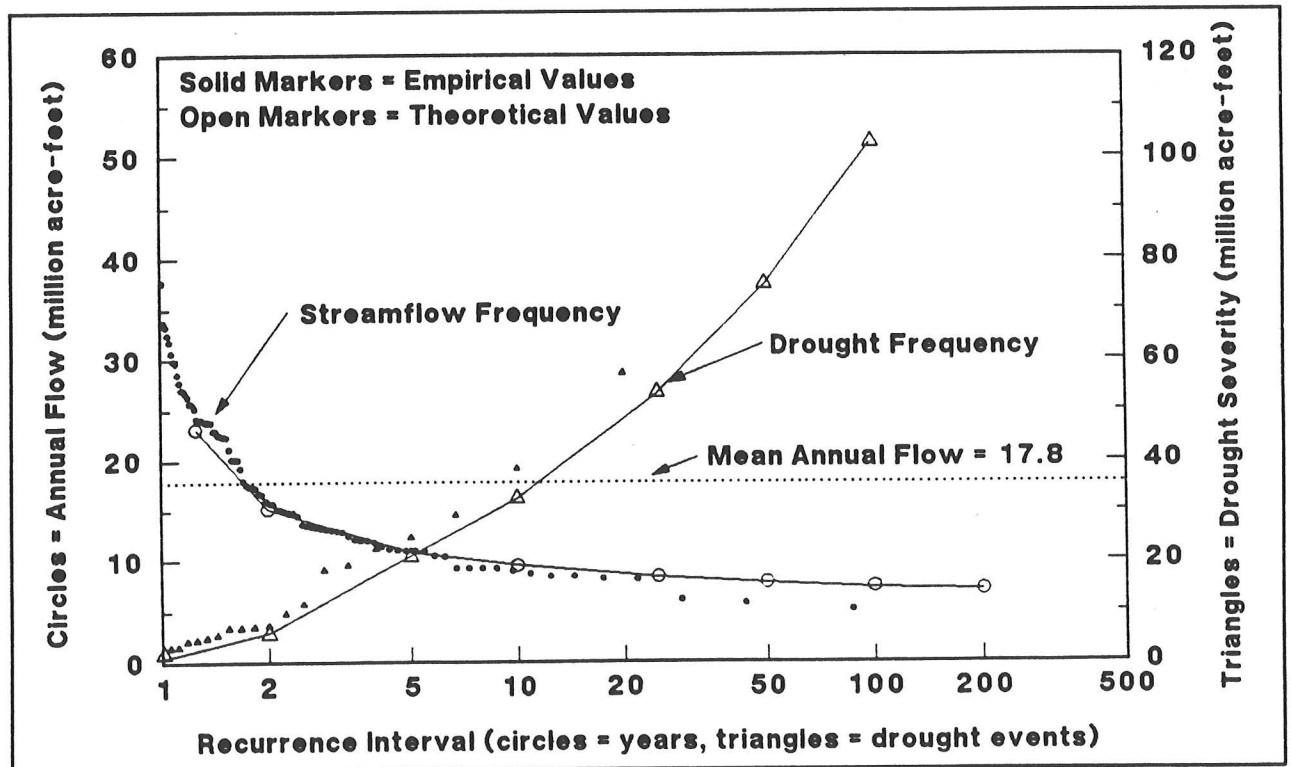


Figure 3. Streamflow and drought frequency analysis for the 4-River Index from observed data. Solid markers represent empirical values determined with equation (1). Open markers indicate theoretical values determined by the log-Pearson Type III distribution. The axes are labeled differently for each curve. Mean annual flow is shown by the dotted line.

year in duration). Theoretical frequencies were computed by the log-Pearson Type III distribution, and the empirical recurrence interval,  $T_r$ , is determined by:

$$T_r = N+1/m \quad (1)$$

(Linsley *et al* 1992), where  $N$  = sample size and  $m$  = rank of each drought event. The curve labeled "streamflow frequency" shows that for a water year similar to 1991 (8.4 million acre-feet, which is 47 percent of the annual mean flow) the theoretical recurrence interval is about 18 years. This is plotted by the open-circle markers. Theoretical values compare well with those computed empirically, which are plotted by the solid-circle markers, with the exception of the three lowest flows, further discussed below.

Two limitations of this application of the log-Pearson Type III distribution are that it applies only to single-year flows and not to multi-year droughts and that it does not account for the non-independence of annual flow data.

The curve in Figure 3 labeled "drought frequency" details an alternative procedure for applying the log-Pearson Type III distribution to the same 86-year record of observed flows to overcome the above-stated limitation. This procedure calculates theoretical frequency curves from the series of drought events, each with a measurable severity and duration (after Dracup *et al* 1980), contained within the observed flow record. The threshold flow defining a drought year is set at 5 percent below the mean annual flow. This curve relates drought severity to recurrence interval. However, a consequence of extracting the series of drought events from the annual flow data is that the series loses its temporal character; that is,  $N$  in equation (1) is no longer a measure of the number of years in the observed flow record but, instead, is a measure of the number of drought events occurring over this observed record. This results in a recurrence interval measured by the number of interceding drought events (all having less severity) and not interceding years. This unit of measure is difficult to use in drought frequency analyses.

This difficulty is overcome by empirically determining a recurrence interval measured in years. This is achieved by determining the average interval between drought event onsets calculated from the total number of droughts occurring over the total record length. For the 4-River Index, 19 drought events have occurred during the 86-year observed record, which is equivalent to 4.53 years between events.

Table 1 summarizes this recurrence interval calculation for a frequency analysis of a drought with a severity of 38 million acre-feet. Column A of Table 1 shows that a recurrence interval of 14 drought events is calculated from the observed frequency curve for a drought of the given severity. The recurrence interval is then converted into units of years,

Table 1  
SUMMARY OF RECURRENCE INTERVALS  
(For a Drought of Severity = 38 Million Acre-Feet)

Data Source	Recurrence Interval from Graphs (in Drought Events)	Length of Record (in Years)	Number of Drought Events	Years Between Onsets (per Drought Event)	Recurrence Interval (in Years)
	A	B	C	D (D=B/C)	E (E=AxD)
Observed	14	86	19	4.53	63
Synthetic	24	10,000	2,233	4.48	108
Proxy	70	420	85	4.94	346

column E, by the use of the empirical return frequency determined in column D. For the observed data, the recurrence interval is 63 years. Synthetic and proxy data have longer recurrence intervals, 108 and 346 years respectively.

Noticeable on both curves in Figure 3 is how the theoretical curve underestimates severity when compared to the empirical data. For the streamflow frequency curve, this is limited to the extreme events, which are water years 1931, 1924, and the lowest year on record, 1977. This behavior may suggest that extreme low flow years follow a different distribution or are caused by a physical mechanism separate from that causing the other low-flow years. For the drought frequency curve, all events are underestimated. This may be due to the small sample size of drought events contained in the observed record.

Figure 4 attempts to improve the accuracy of the theoretical drought frequency curve of Figure 3 when compared to empirical data by displaying curves for expanded versions of the 4-River Index flow obtained from (1) synthetically generated flow values and (2) proxy flow values reconstructed from tree-ring chronologies. The theoretical drought frequency curve from synthetic data accurately reproduces the trend of the empirical data as determined from 2,233 drought events contained within 10,000 years of annual flow data generated from an ARMA(1, 1) statistical model. The ARMA(1,1) model was selected over other autoregressive models because it had the best AIC value (Akaike 1976). This type of model has been described by Box and Jenkins (1970). For clarity, not all 2,233 drought events used to determine the theoretical curve are shown by the solid-triangle markers plotted in Figure 4. The theoretical drought frequency curve for the proxy data from tree-ring reconstructions also accurately reproduces the trend of the empirical data from the 85 drought events within the 420 years of reconstructed flow, with the exception of the single most severe reconstructed drought event of 1928-1939. This 12-year period recorded a total flow deficit of 72.8 million acre-feet and, when plotted, lies far above the theoretical curve. These two theoretical curves better represent the severity of moderate and extreme drought events (events with deficits of about 20 to 60 MAF) than the theoretical drought curve of Figure 3 when compared to the empirical values.

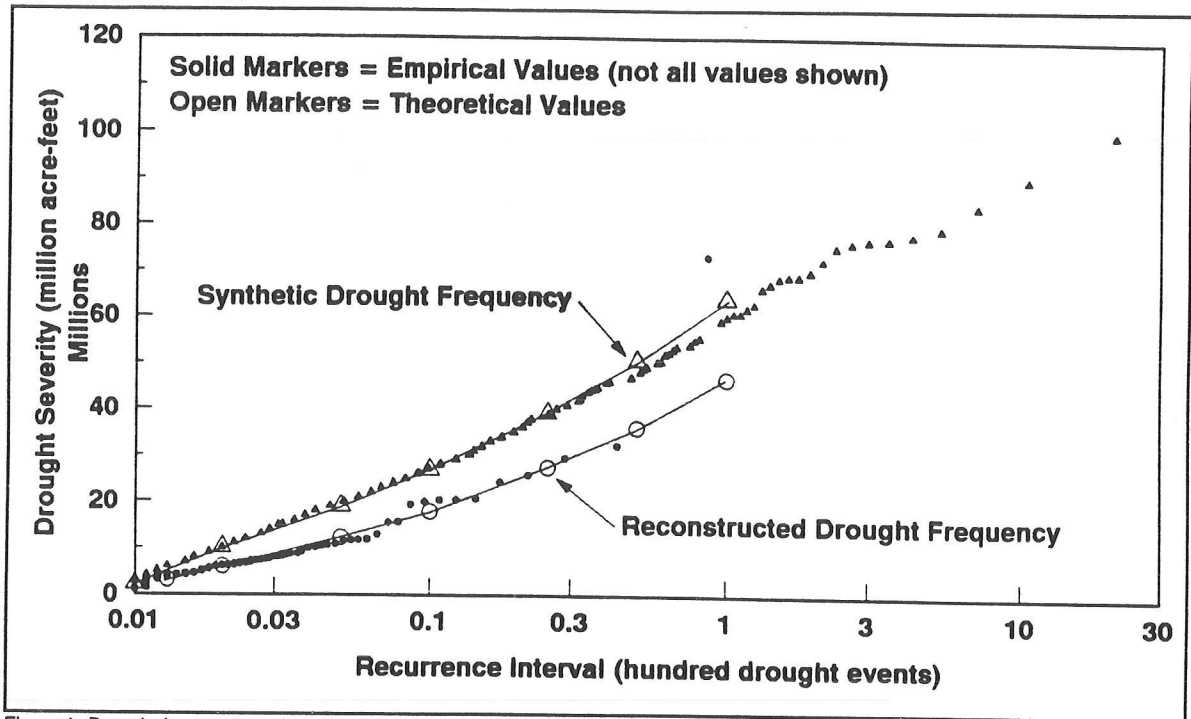


Figure 4. Drought frequency analysis for the 4-River Index from ARMA(1,1) synthetically generated data and tree-ring reconstructed proxy data. Solid markers represent empirical values determined with equation (1). Open markers indicate theoretical values determined by the log-Pearson Type III distribution. The horizontal axis is scaled in drought events.

Figure 4 suggests that analyzing synthetic data from an appropriate statistical model or proxy data from tree-ring reconstructions may provide better frequency analysis from distributions developed for large sample sizes, such as the log-Pearson Type III distribution. However, there are deficiencies in both the synthetic and proxy datasets. The ARMA(1.1) model computes an occasional impossible negative annual flow value. For the analysis presented here, all negative flows were set to zero, although zero or near-zero flows have never been recorded by the 4-River Index, suggesting severity of a drought event containing a zero flow year would be unduly exaggerated. Reconstructed flow from tree-ring data, on the other hand, display less variance than observed flow in that it makes estimates for high or low flows that are less accurate than estimates for flows close to the mean (Earle and Fritts 1986).

The log-Pearson Type III method assumes independence of the input data. To check for independence, lag-one autocorrelation coefficients were determined for each of the four frequency curves presented in Figures 3 and 4. The autocorrelation results are well within the confidence interval in each case and are summarized in Table 2.

Figure 5 compares the two log-Pearson Type III theoretical frequency curves of Figure 4 and the same curve for the observed data from Figure 3. The curve from the observed data provides the shortest recurrence intervals; the proxy data curve provides the longest. The recurrence interval of drought events with severity of 38 million acre-feet is considered as an example (refer to Table 1). This severity is about equal to the first five years (1987-1991) of the current 6-year California drought. This

Table 2  
SUMMARY OF LAG-ONE AUTOCORRELATION COEFFICIENTS

Data Source	Type of Frequency Curve	Curve Location	N (from Eq. 1)	Autocorrelation Coefficient	95% Significance Level
Observed	Annual Flows	Figure 3	86 Years	0.095	-0.190
Observed	Drought Events	Figure 3	19 Events	0.048	-0.446
Synthetic	Drought Events	Figure 4	2,233 Events	0.009	-0.035
Proxy	Drought Events	Figure 4	85 Events	-0.081	-0.192

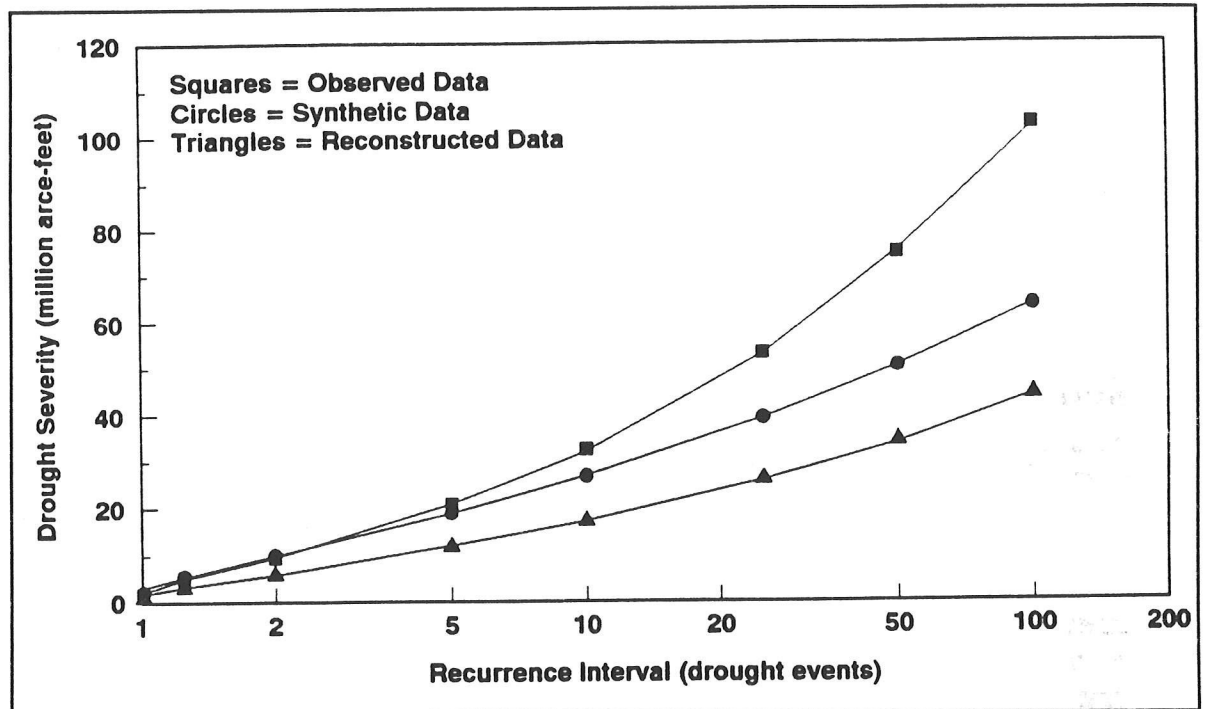


Figure 5. Comparison of theoretical drought frequency curves from Figures 3 and 4 for observed, synthetic, and tree-ring reconstructed (proxy) data for the 4-River Index. The horizontal axis is scaled in drought events.

is the second-worst drought, behind the drought of the 1930s, for the observed and reconstructed records.

The disparity between the observed curve and the synthetic and proxy curves in Figure 5 becomes even greater for larger severities. This suggests the observed dataset is being adversely affected by its small sample size during log-Pearson Type III analysis.

## Conclusions

Frequency curves from both synthetic and proxy data reproduce the trend of the empirical values better than the frequency curve from the observed data. The divergence of the observed data frequency curve from the synthetic and proxy curves may represent the influence of the inappropriate application of the log-Pearson Type III distribution to datasets of limited sample size.

Both synthetic and proxy data-based analyses have advantages and drawbacks. The synthetic data sample size can be expanded as desired; however, it is based on the sample statistics of the observed dataset, which is often of limited temporal duration (86 years for the 4-River Index) and, therefore, may not represent the best available sampling of the population. While tree-ring reconstructed data, on the other hand, may be adversely affected due to a loss of observed variance, the data do have the advantage of being based on the much longer sample size, in this case 420 years of annual flow values. However, analysis of the results presented here suggests the loss of variance in the tree-ring reconstructions maybe sufficient to cause significant overestimation of recurrence intervals, as is apparent from column E of Table 1 for the proxy data, although no quantitative measure of this has been made.

## Acknowledgment

---

Support for this research was provided by the National Science Foundation through the Small Grants for Exploratory Research program contract BCS 9114753.

## References

---

- Akaike, H. 1976. Canonical correlation analysis of time series and the use of an information criterion. In R Mehra and DG Lainiotis (Editors), *Advances and Case Studies in System Identification*, pp. 27-96. Academic Press, New York.
- Box, GEP, and GM Jenkins. 1970. *Time Series Analysis: Forecasting and Control*. Holden-Day, San Francisco.
- Dracup, JA, KS Lee, and EG Paulson. 1980. On the definition of droughts. *Water Resources Research* 16(2):297-302.
- Earle, CJ, and HC Fritts. 1986. *Reconstructing Riverflow in the Sacramento Basin Since 1560*. Prepared by the Laboratory of Tree-Ring Research, University of Arizona, Tucson for the California Department of Water Resources, Sacramento.
- Lawrance, AJ, and NT Kottegoda. 1977. Stochastic modelling of riverflow time series. *Journal of the Royal Statistical Society, A*.140(1):1-47.
- Lee, KS, J Sadeghipour, and JA Dracup. 1986. An approach for frequency analysis of multiyear drought duration. *Water Resources Research* 22(5):655-662.
- Linsley, RK, JB Franzini, DL Freyberg, and G Tchobanoglous. 1992. Chapter 5 in *Water-Resources Engineering*, Fourth Edition. McGraw-Hill, New York.
- Nathan, RJ, and TA McMahon. 1990. Practical aspects of low-flow frequency analysis. *Water Resources Research* 26(9):2135-2141.
- Sen, Z. 1980. Statistical analysis of hydrologic critical droughts, *Journal of the Hydraulics Division, Proceedings of the American Society of Civil Engineers* 106:99-115.
- Stockton, CW. 1975. *Long Term Streamflow Reconstructed From Tree Rings*. University of Arizona Press, Tucson.

# A Multi-Basin Seasonal Streamflow Model for the Sierra Nevada

Daniel R. Cayan and Laurence G. Riddle

Abstract: Linear regression models are constructed to predict seasonal runoff by fitting streamflow to temperature, precipitation, and snow water content across a range of elevations. The models are quite successful in capturing the differences in discharge between different elevation watersheds and their interannual variations. This exercise thus provides insight into seasonal changes in streamflow at different elevation watersheds that might occur under a changed climate.

## Background and Objectives

Related to possible future climate warming, there is concern that the snowmelt runoff portion of the water supply may be reduced. Under the present climate in the western United States, streams in intermediate to high elevations respond to monthly precipitation throughout the year, but only exhibit sensitivity to monthly temperature during the transition seasons, particularly in spring (Riddle *et al* 1991; Aguado *et al* 1992; Cayan *et al* 1992). The magnitude of monthly temperature variability in California is typically about 1-2°C, which is relatively small compared to the temperature change across different elevations (Table 1). The elevation differences produce large contrasts in the timing of streamflow.

Table 1  
MEAN ELEVATIONS, MEAN JANUARY TEMPERATURES, AND  
PERCENT OF MEAN ANNUAL STREAMFLOW  
FOR BASINS USED IN CONSTRUCTING THE MODEL

Basin	Mean Elevation (meters)	January Mean Temperature (°C)	Percent of Mean Annual Streamflow			
			ASO	NDJ	FMA	MJJ
Cosumnes	1121	1.0	1	21	59	18
American	1433	-0.8	2	19	46	33
San Joaquin	2286	-6.1	6	9	29	56
Merced	2743	-8.9	4	5	21	70
Stanislaus	1768	-2.8	3	13	38	46
East Carson	2485	-7.3	7	11	24	58

How would streamflow change with temperature? Since there is a broad range of watershed elevations in the Sierra Nevada (California's major water bearing region), there is an opportunity for a natural experiment to determine the response of runoff to a fairly wide range of temperature.

The approach taken here is to construct a statistical model for seasonal streamflow that incorporates basins having different mean elevations, thereby including fairly large differences in mean temperature. The model constructed is developed from four watersheds with mean elevations ranging from 1100 meters to 2700 meters and encompassing a mean temperature range of about 10°C. This multi-basin statistical approach is possibly a better alternative to determining temperature sensitivity from a single watershed, which, averaged over the basin, is limited to natural seasonal temperature variability of order 1°C (eg, Cayan, *et al* 1992). Projected climate warmings range from 3 to 5°C, well beyond the range of seasonal temperature anomalies used to derive the response of a single watershed streamflow anomaly model. Consequently, such a response may not apply to larger climate changes.

In this study we develop a linear model using multiple basins to simulate variability of seasonal streamflow across elevations and from year to year. Individual models are constructed for three seasons. The skill of this approach is evaluated for each season and for each individual basin. The models are calibrated on data from 1950-1986 and validated using independent data from 1913-1949. Interpretation of the model structures is used to diagnose the various climate influences.

## Data and Processing

---

Most of the data used were averaged or totaled into 3-month seasons used previously by the authors in watershed climate studies (Riddle *et al* 1991; Aguado *et al* 1992; Cayan *et al* 1992). Three of these are used here: November, December, and January (*NDJ*); February, March, and April (*FMA*); and May, June, and July (*MJJ*).

The four primary basins employed in constructing the linear regression models (see Figure 1) were Cosumnes River (estimated at Michigan Bar), American River (estimated at Folsom), San Joaquin River (estimated at Friant), and Merced River (gauged at Happy Isles Bridge). Two additional streams used to verify the model were Stanislaus River (estimated at Melones) and East Carson River (gauged at Markleeville). Cosumnes, American, San Joaquin, and Stanislaus were reconstructed full natural flow estimates from the California Department of Water Resources (DWR), and Merced River and East Carson were from U.S. Geological Survey (USGS) gauge records. All stream records were monthly mean flows and were averaged to obtain seasonal means.

Mean elevation of the basins ranged from 1121 meters (Cosumnes River) to 2743 meters (Merced River), which amounts to a January mean temperature range of about 1 to -9°C (Table 1; see also U.S. Weather Bureau 1943). Distribution of elevations within the American and Stanislaus River basins is graphed in Figure 2.

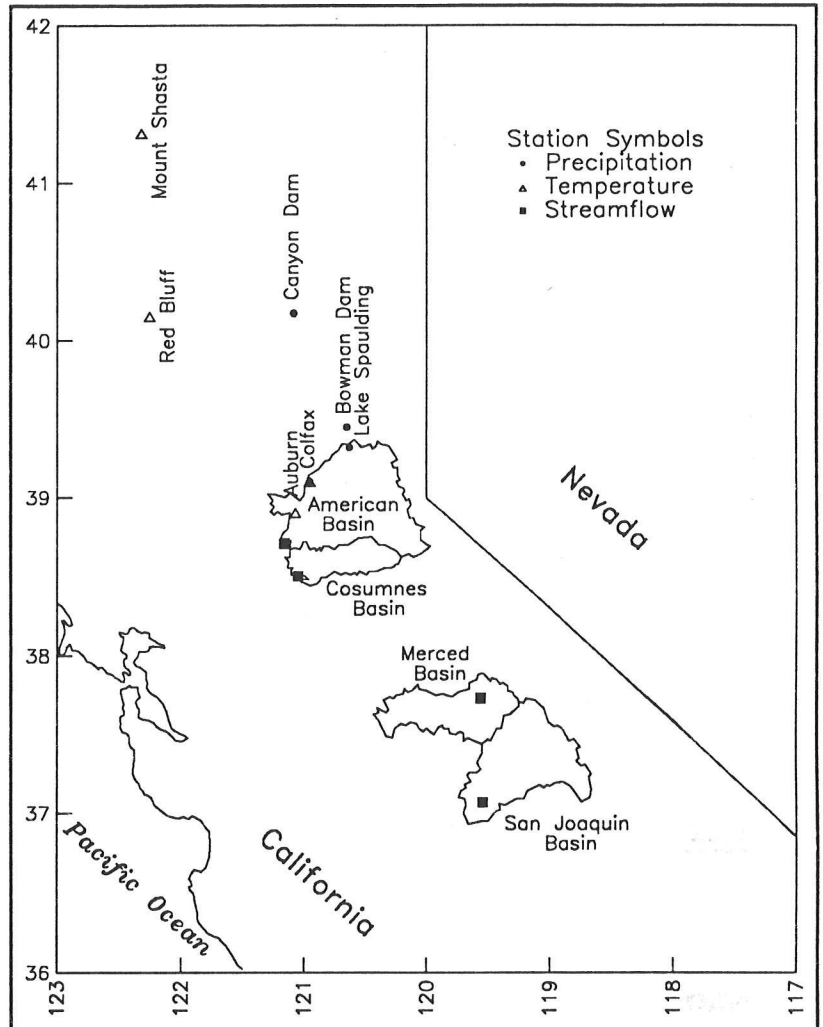


Figure 1. Four primary watersheds, stream gauge locations, and stations employed for precipitation and temperature records.

In terms of daily mean temperature degree days (dd) above  $0^{\circ}\text{C}$ , average seasonal totals for these basin mean elevations range from about 50 to 1000 dd in *NDJ*, from about 130 to 1500 dd in *FMA*, and from about 700 to 2000 dd in *MJJ*. As shown in Figure 3, the average degree day profiles are linear with elevation in *MJJ*, but not in *NDJ* and *FMA*, as the fall-off in dd values at upper elevations is limited by days whose mean temperature falls below  $0^{\circ}\text{C}$ .

Independent data input to the regression models are seasonal total precipitation, seasonal mean temperature, and snow water content, modified by seasonal mean temperature degree days. Seasonal precipitation and temperature used were averages of four stations for two regions, the central and southern Sierra Nevada (Aguado *et al* 1992). The dd values for each basin were derived by first summing the daily mean temperatures greater than  $0^{\circ}\text{C}$  for each day in each season, for each year, for each basin mean elevation. Mean temperatures were from a regional daily time series built from central Sierra Nevada stations (four and six

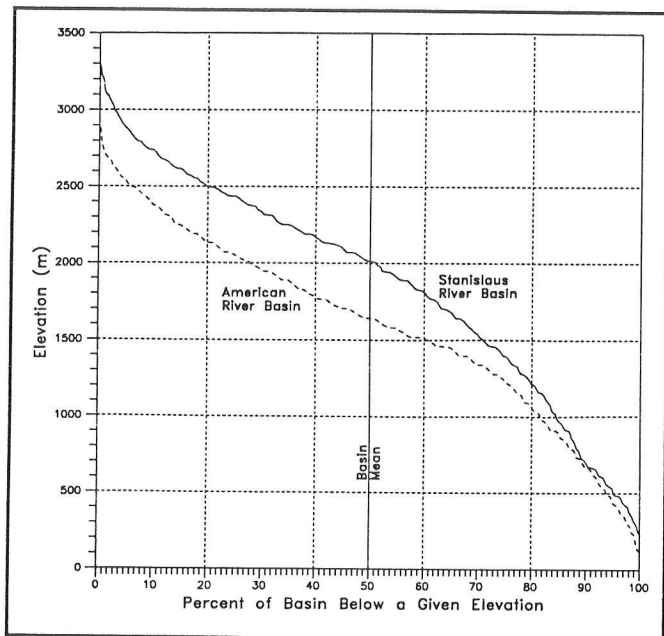


Figure 2. Distribution of elevations (in meters) within American River and Stanislaus River basins from the (NOHRSC) digital elevation model.

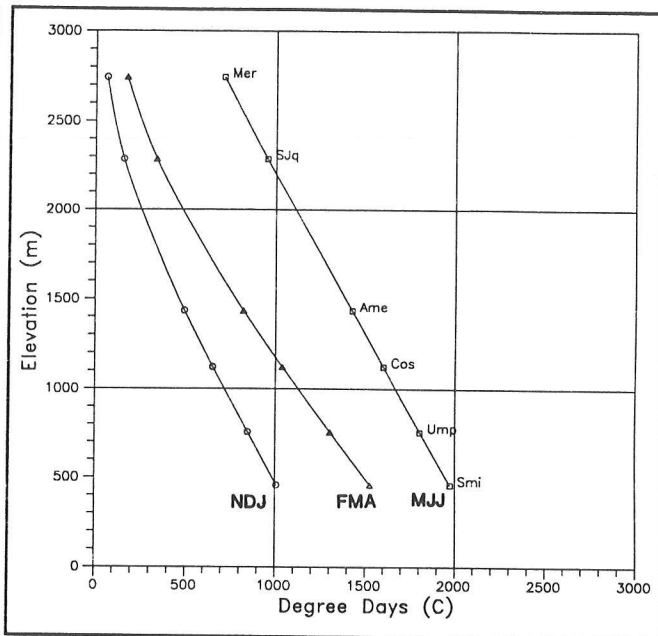


Figure 3. Seasonal mean degree days versus elevation. Each of the six basins is noted on curves according to its basin mean elevation (DWR and USGS mean elevations).

stations for the northern and southern Sierra basins used here). Individual daily mean temperatures were then adjusted from the station mean elevation to the individual basin mean elevations according to the lapse rate in U.S. Weather Bureau (1943). The individual basin totals

$$\left[ \sum_{j=1}^n (T_j > 0) \right]$$
 for the "n" days in each season for each year were then considered to be the degree days for that basin and season.

The snow water content (SWC) was derived for each of the two regions by averaging three snow courses in each (Cayan *et al* 1992). Variability of the regional average SWC is quite representative in view of the strong coherence between stations within the region, illustrated in Figure 4 by the February 1 and April 1 records in the central Sierra Nevada (see also Aguado 1990).

The model relates seasonal streamflow (the dependent variable) to seasonal regional precipitation, seasonal elevation-adjusted mean temperature, and degree-day-weighted snow water content, which we call the snowmelt factor, SN. The seasonal precipitation is the seasonal total for a given year scaled by the long-term mean annual total. This scaling weights precipitation according to its seasonal and interannual variability. October mean streamflow,  $Q_{Oct}$ , is scaled by the mean annual streamflow for its basin and is used as a measure of baseflow going into the wet season. Seasonal mean temperature,  $T$ , is adjusted to the mean elevation for the basin. The snowmelt factor, SN, is the product of snow water content (SWC) and mean temperature degree days. SN is computed by:

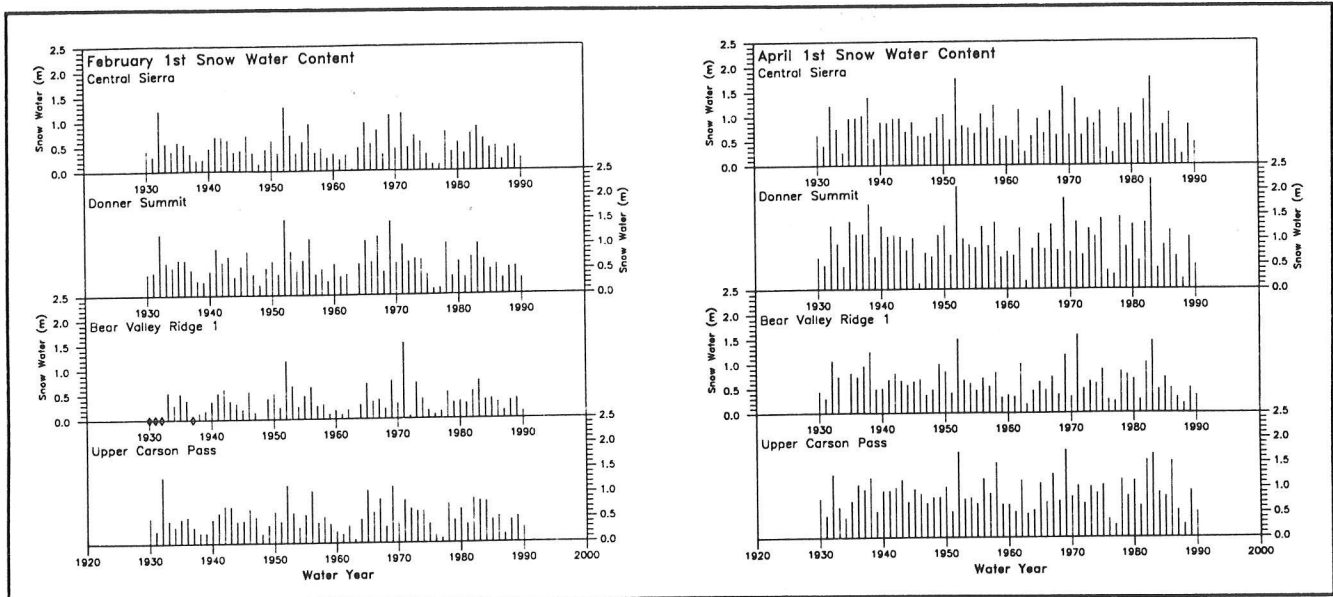


Figure 4. Time history of February 1 (left) and April 1 (right) SWC for central Sierra average and individual snow courses.

$$SN = \left[ \sum_{k=1}^n (T_K > 0) \right] \cdot SWC \quad \text{Equation (1)}$$

where the sum of the daily mean temperatures greater than  $0^{\circ}\text{C}$  from the first through the last day of the season is multiplied by SWC, which has been scaled against the April 1 long-term mean SWC for the basin. The January 1 SWC is used for the *NDJ* snowmelt, April 1 SWC for *FMA*, and May 1 SWC for *MJJ*. In years when either SWC or *dd* was not available, their values were estimated using linear regression from seasonal precipitation and temperature. These estimates were necessary for some of the pre-1930 SWC and for the pre-1948 *dd* values for SWC. The regression models accounted for 69, 82, 70, and 85 percent of the February 1, March 1, April 1, and May 1 SWC. For *dd*, the regression models accounted for 91, 92, and 87 percent of the *NDJ*, *FMA*, and *MJJ* variations.

## Model Formulation

The general form of the streamflow models is:

$$\hat{Q}_i = a_i Q_{Oct} + \sum_{j=ASO}^i b_{ji} T_{ji} + \sum_{j=ASO}^i c_{ji} P_{ji} + \sum_{j=NDJ}^i d_{ji} SN_{ji} \quad \text{Equation (2)}$$

$$i = NDJ, FMA, MJJ$$

Streamflow ( $Q$ ) for a particular season,  $i$  ( $NDJ$ ,  $FMA$ , or  $MJJ$ ), is estimated by summing the contributions of the individual predictors from an initial season,  $j$ , to the season being estimated. Predictor factors are temperature,  $T$ , precipitation,  $p$ , and snow,  $SN$ . Note that the regression includes the temperature and snowmelt values for all four basins, so they are effectively expressed as departures from elevational mean value for each season.

## Results

Just three predictive equations result, which must describe the four training basins plus any others for which independent data can be provided. The overall (all basins taken together) skill of the models (top two rows of Table 2) is relatively high, ranging from about 0.6 to 0.8 for the 1913-1949 independent data. When the simulated seasonal anomalies of the individual basins are evaluated (rows 3-10 of Table 2), lower values are obtained for selected seasons and basins (skill at Merced for  $FMA$  drops to 0.17), but skill is relatively large (0.7 to 0.8) during seasons with highest discharge (see percent of annual streamflow in Table 1.) The skill level generally holds up quite well from the training period to the independent period. Also, when applied to the two basins (Stanislaus and East Carson) not included in the training set (bottom 4 rows of Table 2), skill is relatively high, ranging from about 0.5 to 0.8 during the 1913-1949 period.

Basin	Period (Water Years)	NDJ	FMA	MJJ
All Basins	1950-1986	0.71	0.79	0.84
	1913-1949	0.63	0.80	0.79
Cosumnes	1950-1986	0.66	0.80	0.72
	1913-1949	0.51	0.79	0.38
American	1950-1986	0.72	0.86	0.76
	1913-1949	0.71	0.79	0.48
San Joaquin	1950-1986	0.62	0.72	0.76
	1913-1949	0.73	0.58	0.67
Merced	1950-1986	0.43	0.30	0.80
	1913-1949	0.38	0.17	0.74
Stanislaus	1950-1986	0.66	0.83	0.81
	1913-1949	0.57	0.75	0.66
East Carson	1950-1986	0.50	0.67	0.81
	1913-1949	0.49	0.62	0.77

The simulated seasonal streamflow, along with observed, is plotted in Figures 5, 6, and 7 for the four primary basins used in training the model. From these plots, it is clear that the model holds up quite well in capturing the mean level of streamflow across the basins, as well as the year-to-year variability in each basin. The model is relatively successful in avoiding negative streamflow predictions. This is an improvement over previous versions of the model that did not include the degree-day-weighted snow water content. Presumably, snowmelt allows for years

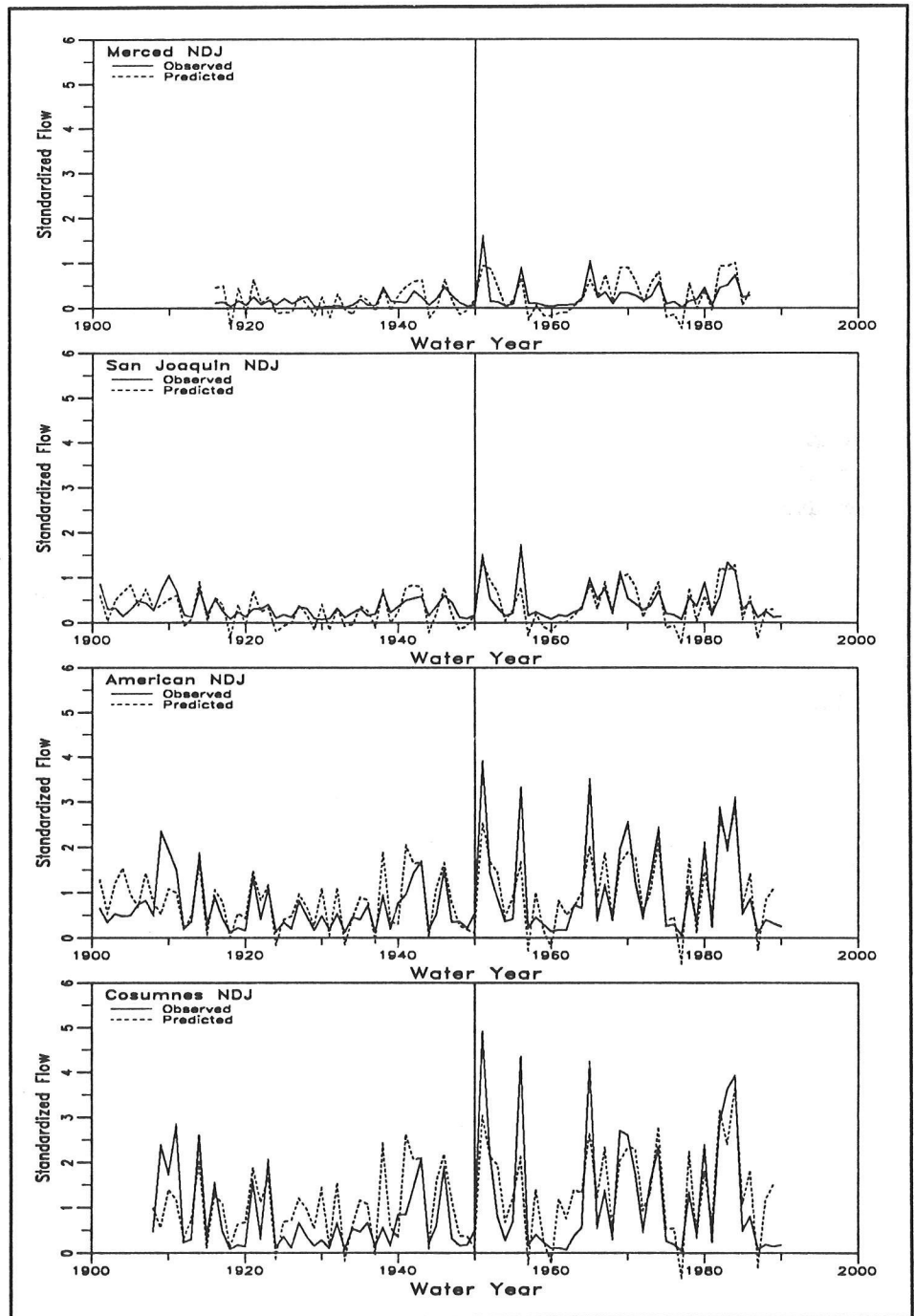


Figure 5. Predicted (dashed) and observed (solid) streamflow for four primary streams for November, December, and January.

that are cool/dry or warm/wet, *etc.*, in ways that precipitation and temperature cannot emulate separately in the linear models.

Two temperature influences appear in the model. The first is the mean temperature itself, whose mean values range over about 10°C from the lowest to the highest basin. The second is the number of degree days that enter the snowmelt term, whose mean values range over 1000 dd in a given season from the lowest to the highest basins. The snowmelt factor

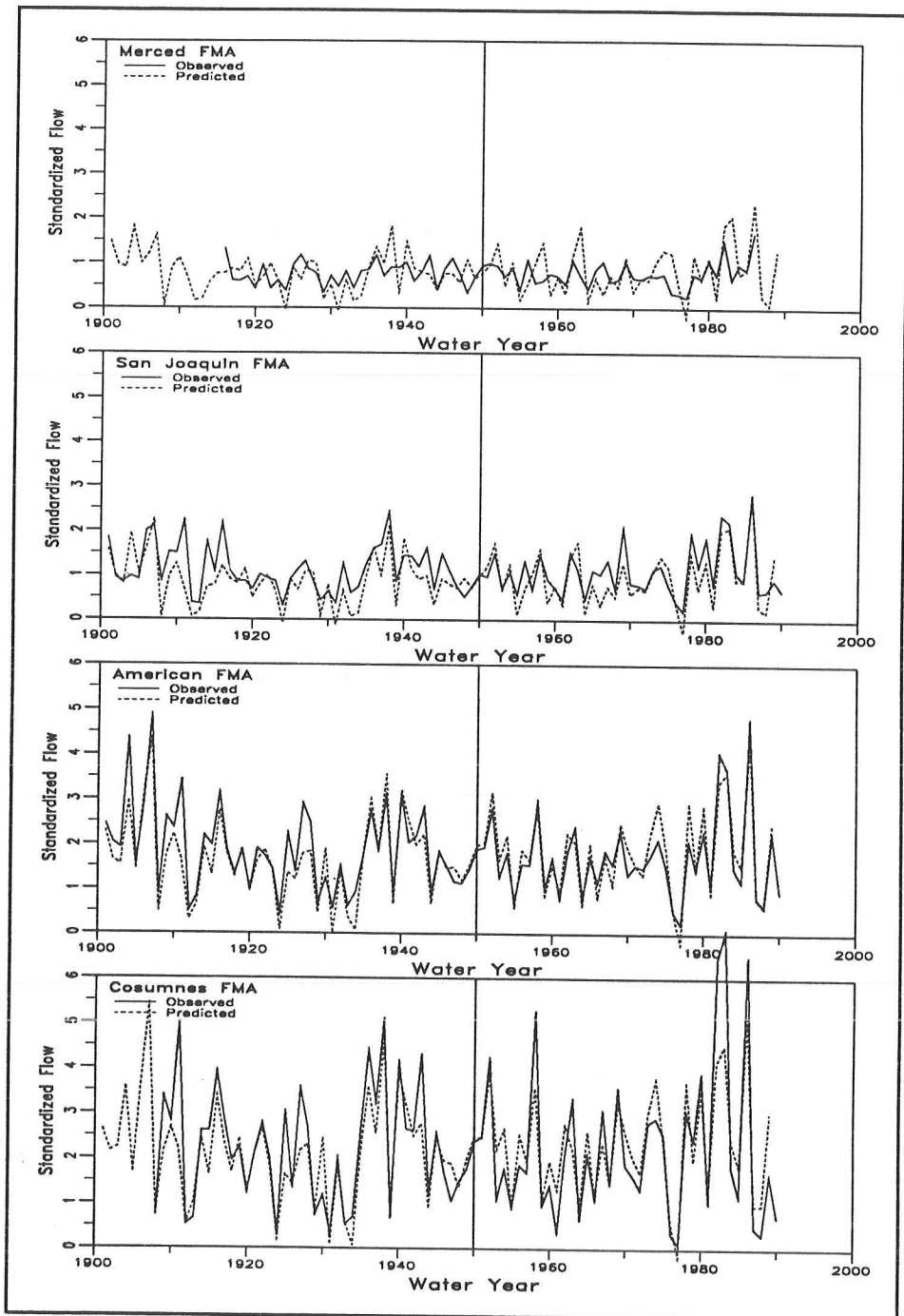


Figure 6. Predicted (dashed) and observed (solid) streamflow for four primary streams for February, March, and April.

(SN) is the larger of the two temperature influences. Inspection of the predictors in Figure 8 indicates that snowmelt is the model element that produces the difference in mean runoff from one basin to the next. The plots in Figures 5-7 show that the models perform reasonably well in simulating mean discharge: from 21 to 5 percent of annual flow in *NDJ*, from 59 to 21 percent in *FMA*, and 18 to 70 percent in *MJJ* (see Table 1.)

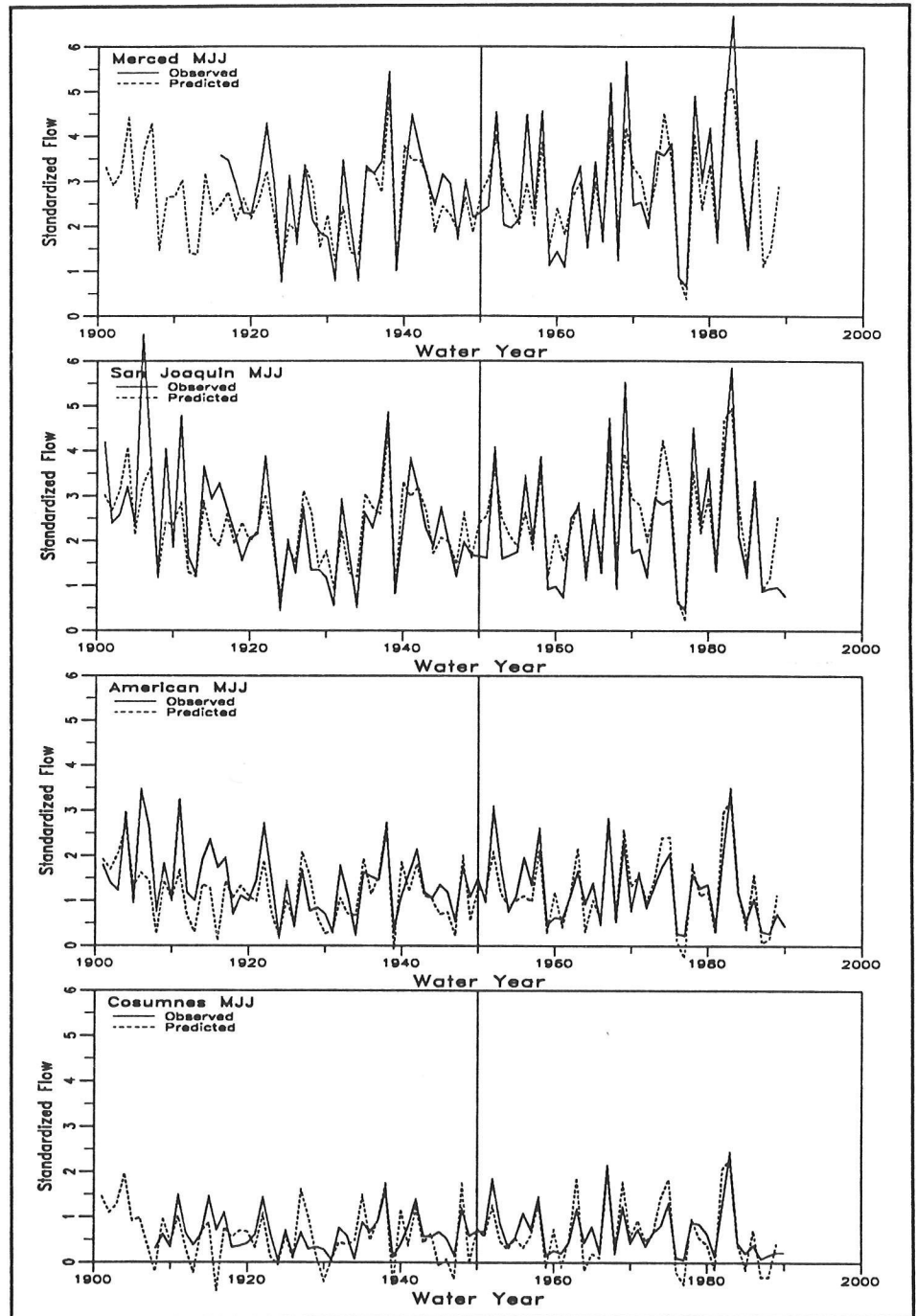


Figure 7. Predicted (dashed) and observed (solid) streamflow for four primary streams for May, June, and July.

The structure of the *NDJ*, *FMA*, and *MJJ* seasonal models is given in Figure 8, which shows the “beta” coefficients obtained by the multiple regression scheme. These are the model coefficients (*a*, *b*, *c*, and *d* in Equation (2)) that would result if all of the variables, including the predictand (streamflow), were normalized by their respective standard deviations. The predictors extracted by the regression procedure were those whose contribution to streamflow variance was significant in the 95 percent confidence level, using an *F* test.

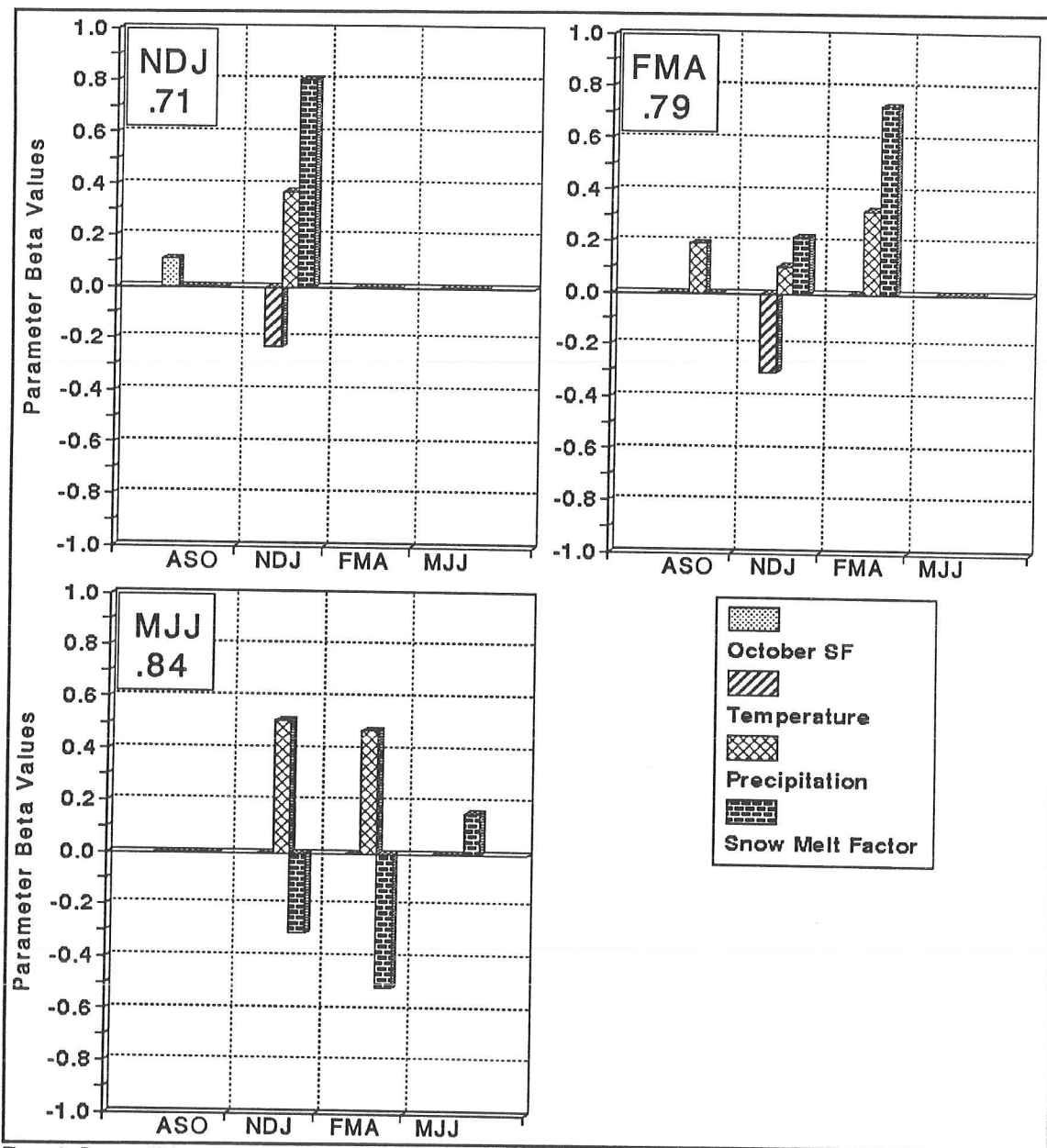


Figure 8. Beta coefficients for each of the three models. These are the contributions by the chosen predictors, given that the predictors and predictand are normalized by their respective standard deviations. Predictors were included if the variances they contributed were significant at the 95% confidence level or greater.

In *NDJ*, the significant predictors are limited to within-season variables, with the exception of a small contribution by October streamflow (a measure of the initial flow during the beginning of the water year). The largest predictors are positive contributions by *NDJ* snowmelt and *NDJ* precipitation. *NDJ* temperature gives a negative contribution (cooler temperatures produce greater flows).

In *FMA*, the model includes both contemporaneous and preceding season contributions to streamflow. Like the *NDJ* model, the largest predictor is a positive contribution from in-season snowmelt, followed by a positive contribution by in-season precipitation. It also draws upon positive contributions by previous season (*NDJ*) snowmelt and precipitation and *ASO* precipitation. Again, *NDJ* temperature makes a negative contribution.

In *MJJ*, the streamflow variations are mostly affected by anomalous conditions from previous seasons. All quite large, these include positive contributions by precipitation in *NDJ* and *FMA* precipitation and negative contributions by snowmelt in *NDJ* and *FMA*. The only in-season contribution is a relatively small, positive contribution by *MJJ* snowmelt. The negative *SN* predictors during *NDJ* and *FMA* represent snowmelt that depletes the snowpack accumulated during winter and early spring, while the positive *SN* predictor in *MJJ* is the contribution to streamflow by snowmelt during late spring and early summer. The lack of a precipitation influence in *MJJ* must stem from the seasonal fall-off in precipitation in spring and summer.

## Conclusions

A multi-basin model has been constructed to simulate the inter-basin and inter-annual variations in streamflow across watersheds representing a wide range of mean elevations in the Sierra Nevada. Besides precipitation, the model includes degree-day-weighted snow water content and basin mean temperatures, which vary over a range of about 10°C for a given season.

The model skill is reasonably high, accounting for 60 percent or more of the variance for most seasons and individual watersheds. The models held up quite well in independent data from the training period and also perform fairly well for independent basins with different elevations. The relatively high skill indicates that seasonal mean climate variables are useful in predicting seasonal streamflow variations. Apparently the spatial coherence of temperature and precipitation anomalies provides a good representation with just a few stations. More important, the multi-basin approach captures essential differences in seasonal flow between basins with different mean elevations.

There is a strong temperature influence, especially in relation to snowmelt. This influence provides the ability to account for large differences

in seasonal flow amounts from low to high elevation watersheds. The most severe shortcoming in the models is for the highest elevation basin (Merced River), where it produces too much discharge in *NDJ* and *FMA* and not enough in *MJJ*. This suggests that the linear relationship with precipitation and snowmelt is not satisfactory over the entire range of elevations. Still, the *MJJ* model skill for the independent period is 0.74 for Merced, so it does capture much of the variability during the time of year with greatest runoff in the high basins.

More tests need to be done, but the models exhibit reasonable skill in simulating differences in flow between basins with large contrasts in elevation. This suggests that they can estimate the effect of seasonal temperature changes, such as those proposed for future greenhouse warming conditions. An increase in temperature of +3°C is roughly equivalent to a decrease in elevation of 500 meters. Via the observed streamflow behavior at several basins, the models clearly show that streamflow response to such a change would depend strongly on season and elevation. This is due to the effect it has on mean temperature and rain vs. snow as snowmelt.

## **Acknowledgments**

---

We thank Gary Hester of the California Department of Water Resources for streamflow and precipitation data and information concerning its application. James Goodridge provided temperature data and an evaluation of the quality of those records. Mike Dettinger, David Peterson, and Maurice Roos provided many useful suggestions and comments. We thank Jean Seifert and Vera Tharp for text processing. Support was provided by the University of California Water Resources Center and by the National Oceanographic and Atmospheric Administration through the Experimental Climate Forecast Center program.

## **References**

---

- Aguado, E. 1990. Elevational and latitudinal patterns of snow accumulation departures from normal in the Sierra Nevada. *Theor. and Appl. Climatol.* 42:177-185.
- Aguado, E, DR Cayan, and LG Riddle. 1992. Climatic fluctuations and the timing of West Coast streamflow. *J. of Climate*, in press.
- Cayan, DR, LG Riddle, and E Aguado. 1992. The influence of precipitation and temperature on seasonal streamflow in California. In review, *Water Resources Research*.
- Riddle, LG, DR Cayan, and E Aguado. 1991. The influence of seasonal precipitation and temperature variations on runoff in California and Southwestern Oregon, *Proceedings of the Seventh Annual Pacific Climate (PACLIM) Workshop*. California Department of Water Resources, Interagency Ecological Studies Program Technical Report 26.
- U.S. Weather Bureau, Hydrometeorological Section. 1943. *Hydrometeorological Report No. 3: Maximum possible precipitation over the Sacramento basin of California*. 225 pp.

# Patterns of Orographic Uplift in the Sierra Nevada and Their Relationship to Upper-Level Atmospheric Circulation

Edward Aguado, Dan Cayan, Brian Reece, and Larry Riddle

**ABSTRACT:** We examine monthly and seasonal patterns of precipitation across various elevations of the eastern Central Valley of California and the Sierra Nevada. A measure of the strength of the orographic effect called the "precipitation ratio" is calculated, and we separate months into four groups based on being wet or dry and having low or high precipitation ratios. Using monthly maps of mean 700-mb height anomalies, we describe the northern hemisphere mid-tropospheric circulation patterns associated with each of the four groups. Wet months are associated with negative height anomalies over the eastern Pacific, as expected. However, the orientation of the trough is different for years with high and low precipitation ratios. Wet months with high ratios typically have circulation patterns favoring a west-southwest to east-northeast storm track from around the Hawaiian Islands to the Pacific Northwest of the United States. Wet months with low precipitation ratios are associated with a trough centered near the Aleutians and a northwest to southeast storm track. Dry months are marked by anticyclones in the Pacific, but this feature is more localized to the eastern Pacific for months with low precipitation ratios than for those with high ratios. Using precipitation gauge and snow course data from the American River and Truckee-Tahoe basins, we determined that the strength of the orographic effect on a seasonal basis is spatially coherent at low and high elevations and on opposite sides of the Sierra Nevada crestline.

The majority of precipitation in the Sierra Nevada results from the passage of mid-latitude cyclones from November through March. Since the range is oriented north-south and the storms normally have a strong west-east component, a significant orographic effect generally results in increases in precipitation with elevation. Although spatial distribution of precipitation anomalies is fairly uniform throughout the range (Aguado 1990), the strength of this orographic effect can vary considerably.

The elevational distribution of precipitation has some important ramifications to water managers. If a larger than normal orographic effect is experienced, there will likely be more precipitation in the form of snow as opposed to rain, leading to a delay in the hydrograph response. Moreover, it has been shown (Aguado *et al* 1992; Cayan *et al* 1992) that the relative importance of temperature and precipitation to the timing of melt varies with elevation. The timing of runoff is important for two reasons:

- It influences the allocation of water for the conflicting purposes of water retention and flood control.
- Timing of runoff is likely to be significantly altered if any of the hypothesized climatic warming scenarios are realized (*eg*, Gleick 1987, 1989; Lettenmaier and Gan 1990).

The primary objectives of this paper are to examine underlying patterns of orographic uplift across a transect of the Sierra Nevada and to relate variability in these patterns to synoptic-scale circulation patterns in the mid-troposphere. We also examine on a seasonal basis whether higher or lower than normal orographic effects tend to occur simultaneously on the windward and leeward basins of the range. Finally, we examine whether seasonal low or high orographic effects are consistent for different elevation bands across the windward and leeward slopes of the Sierra.

## **Data**

---

Determination of the strength of the orographic effects and their relationship to middle tropospheric circulation patterns was based on precipitation data from November through April for 9 stations, 5 from the eastern part of the California Central Valley and 4 from the Sierra Nevada. These data, from 1949 through 1988, were obtained from the National Climate Data Center.

A second set of precipitation and snow-course data from the American and Truckee River basins were used to test spatial consistency of the monthly orographic effects for the cool season (November through March). Nine precipitation gauges and two snow courses were used for the American River basin; three precipitation and five snow-course sites were employed for the Truckee. These precipitation and snow data were obtained from the Centralized Data Exchange Center (CDEC) of the California Department of Water Resources and the Centralized Forecast System (CFS) of the U.S. Soil Conservation Service for water years 1949 through 1991. The snow-course data were used as surrogates for cool season precipitation due to the limited number of precipitation gauges at high elevation and the fact that standard rain gauges are unreliable when precipitation occurs as snow. In most instances, however, these snow courses observe snow cover on only a monthly basis during the snow season. This means any melting of snow cover or occurrence of significant rainfall could cause the snow-course measurements to underestimate the true seasonal precipitation. By comparing April 1 snow-water equivalents to the net cool season snowfall measured by daily, automated snow sensors (pillows), we determined that courses above 2450 meters elevation accurately represented net cool season precipitation. Procedures used to make this determination are detailed in Reece and Aguado (1992).

## **Methodology**

---

The first step in determining intensity of the orographic effect for each month was to obtain the precipitation gauge values for the five Central Valley and four Sierra Nevada locations. Thus, for each month from November through April, the regional mean precipitation for both the Central Valley and the Sierra Nevada was determined. The ratio of Central

Valley to Sierra Nevada regional mean precipitation was then calculated as a measure of the orographic effect we call the "orographic ratio". Separate datasets were assembled for the 40 years of record for each month (*ie*, individual datasets consisted only of data for November, December, *etc*). We then stratified the datasets into terciles of wet, normal, and dry months and plotted them for each of the six months.

We examined the middle tropospheric circulation patterns associated with months that fell into four categories of precipitation and precipitation ratios (*ie*, wet/high, wet/low, dry/high, dry/low). For this portion of the analysis we restricted our data to December through February, since those months contribute the greatest amount of precipitation and would yield the most meaningful composites. The categories were delineated by the following procedure:

For each of the months, December through February, the 14 wettest and driest were selected. These were subdivided into those with the seven highest and lowest precipitation ratios. The result was that for each of the three months, seven cases were included in each of the four categories. Finally, the seven cases for each of the three months were merged into larger datasets containing 21 cases with wet/high ratio, wet/low ratio, dry/high, and dry/low events. For each of the categories, the average monthly 700-mb height anomalies across the Northern Hemisphere were determined and mapped.

Spatial consistency with regard to windward versus leeward sides of the Sierra and low versus high elevations were examined using the precipitation and snow-course data from the American and Truckee basins. First, the ratio of precipitation at each site to the lowest in the basin was calculated for each cool season. A 42-year mean ratio was then calculated for each site.

For each cool season, each site's ratio of precipitation to that of the lowest site was compared to the 42-year ratio (*ie*, the ratio for each cool season was compared to the mean ratio). The mean ratio was calculated for each cool season for each basin, from which ordinal rankings were determined for the seasonal mean ratios. The same procedure was also performed separately for the precipitation gauges and the snow courses so their mean ratios for each cool season could be compared.

### **Central Valley / Sierra Nevada Precipitation Transects**

---

Figure 1 depicts the precipitation ratios (*ie*, the ratio of mean precipitation for the four Sierra Nevada precipitation gauges to the mean of the five from the eastern Central Valley) for the wettest and driest months. For all months considered, there is a considerable range of ratios, with the greatest range occurring for the tercile of dry years.

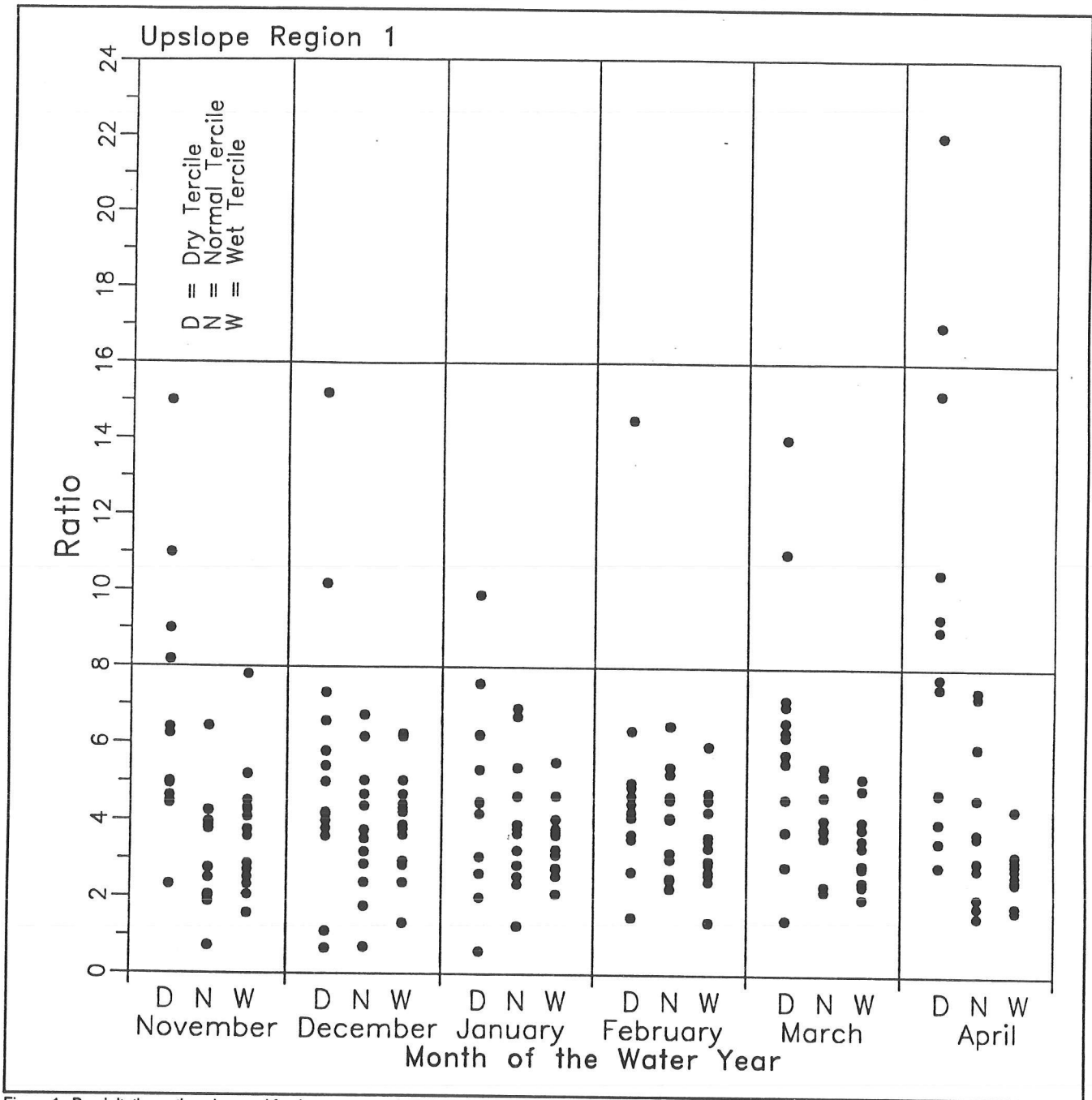


Figure 1. Precipitation ratios observed for the wet, normal, and dry terciles of monthly precipitation.

Extratropical cyclones may traverse a wide range of differing paths across the Pacific Ocean. It has been shown in other areas (eg, Williams and Peck 1962) that the direction of wind relative to the mountain orientation can influence the magnitude of the orographic effect. Moreover, the mean paths of the storms on a monthly basis can be related to middle tropospheric circulation patterns. We therefore composited maps of 700-mb Northern Hemisphere anomalies associated with wet and dry years with low and high precipitation ratios (Figures 2 and 3).

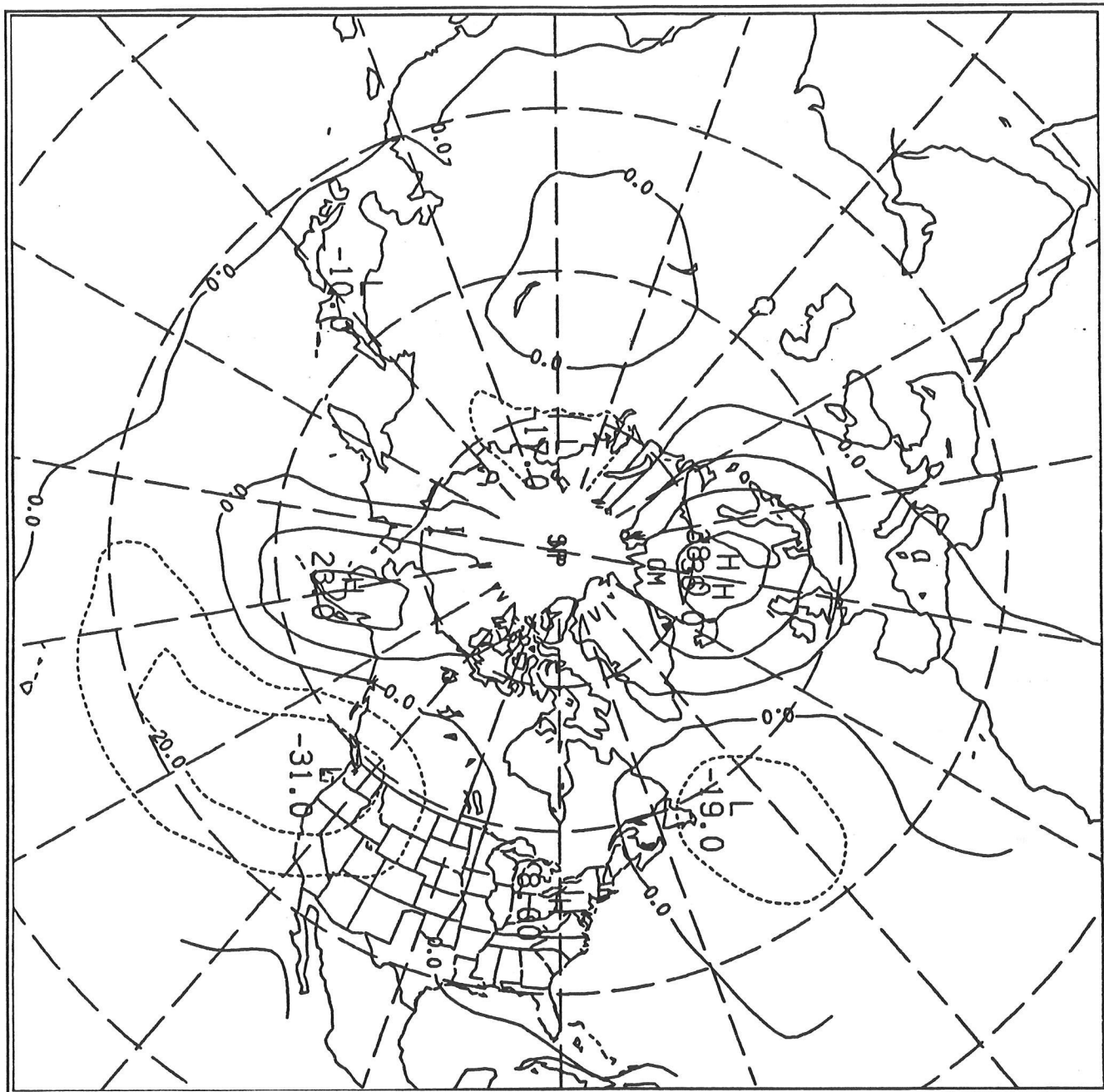


Figure 2. Mean 700-mb height anomalies (in meters) for the wet months with high precipitation ratios.

For the wet months, as expected, a mean low pressure is present in the eastern Pacific. However, the configuration of the troughs is different for months with high (Figure 2) and low (Figure 3) precipitation ratios. In the case of the high ratios, the trough assumes a west-southwest to east-northeast elongation, consistent with a zonal storm track. In contrast, the wet years with low precipitation ratios are marked by a deeper trough centered in the Gulf of Alaska. The trough line stretches southward along the west coast of North America and indicates a more southward progression of the storms. The result here is that the storm path is more oblique to the orientation of the Sierra Nevada, thus lowering its orographic influence on precipitation. All the high and low pressure systems

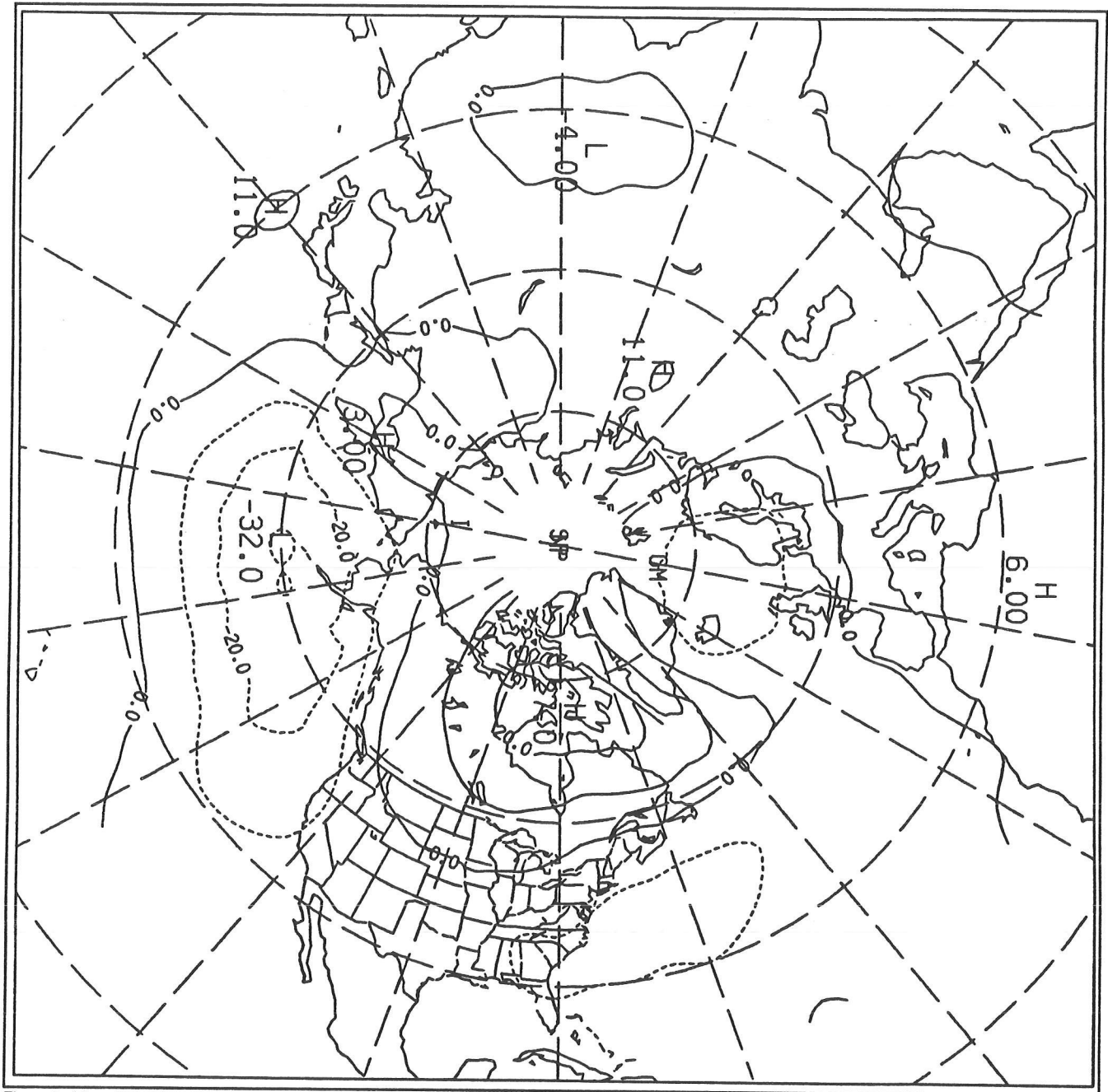


Figure 3. Mean 700-mb height anomalies (in meters) for the wet months with low precipitation ratios.

described contained observation points with anomalies that exceeded the 90 percent confidence level using a 2-tailed t-test. This in fact proved true as well for all the systems described in the following paragraphs.

The average middle tropospheric height anomalies are mapped for dry years with high and low precipitation ratios in Figures 4 and 5, respectively. While both show blocking highs in the Pacific Ocean, there is a major difference in the size and shape of these features. In the case of low-ratio months, the high pressure is more localized and occupies a position over the eastern Pacific and the west coast of North America. To

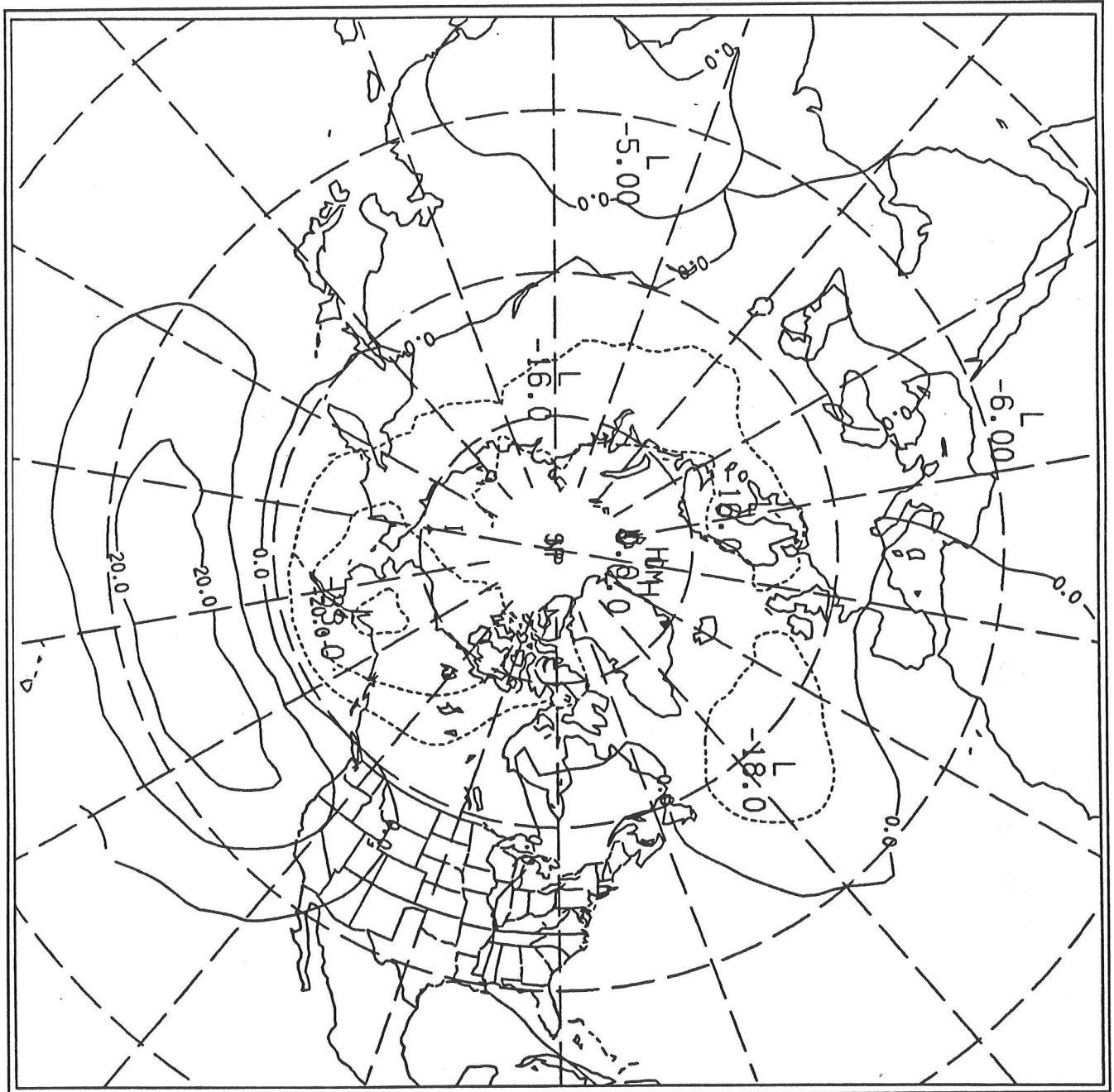


Figure 4. Mean 700-mb height anomalies (in meters) for the dry months with high precipitation ratios.

the west of the anticyclone is a large area of negative height anomalies over much of the central Pacific. This pattern suggests a mean cyclone path from west to east over much of the Pacific, with a northward deflection around the high pressure over the eastern Pacific. This pattern could allow for some storms to pass obliquely over the Sierra Nevada.

In the case of dry years with low precipitation ratios (Figure 4), a large high pressure system occurs with an west-east elongation over most of the Pacific. To the north of the anticyclone is a region of negative height anomalies from eastern Siberia to northwestern Canada. Such a pattern

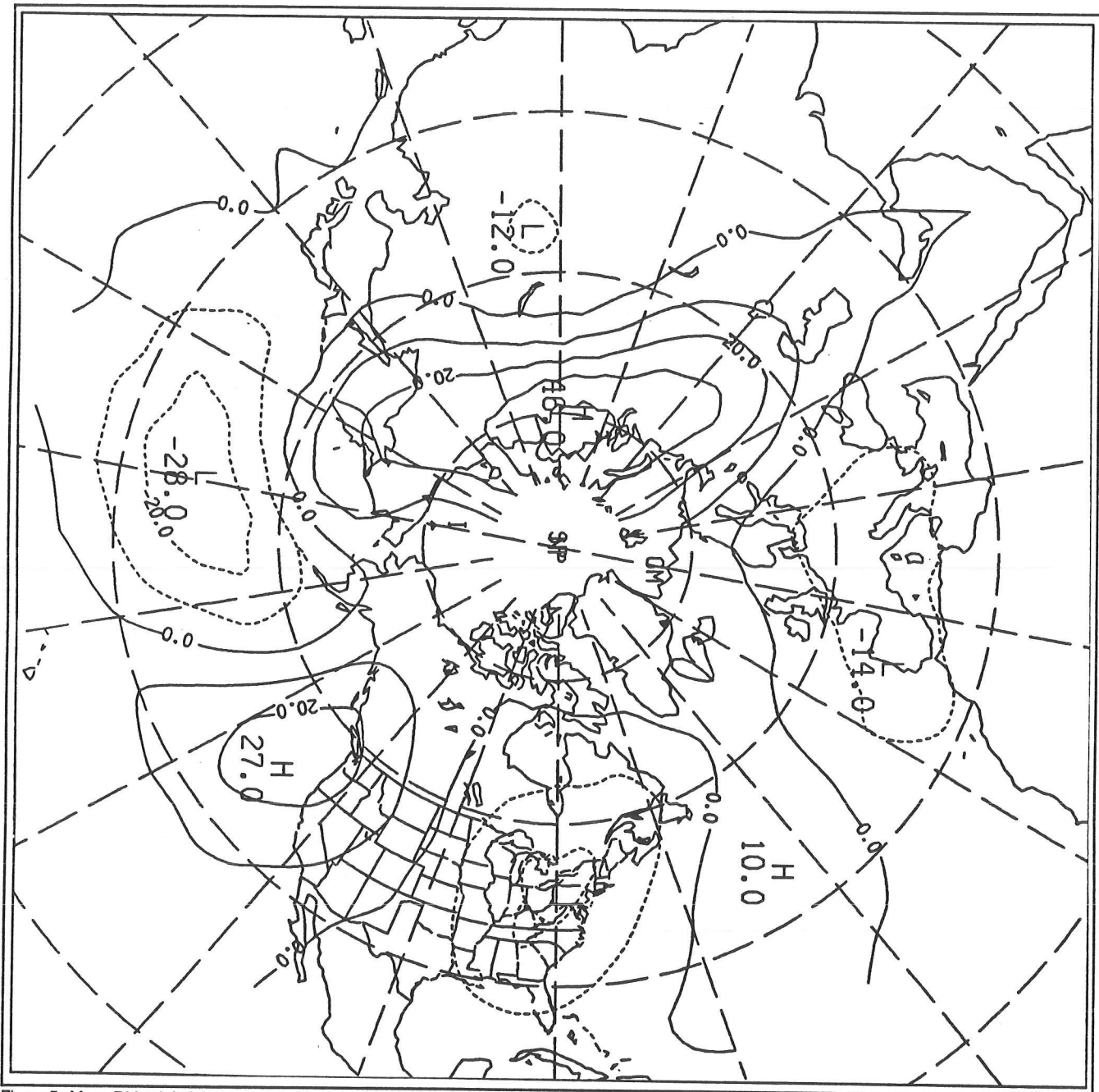


Figure 5. Mean 700-mb height anomalies (in meters) for the dry months with low precipitation ratios.

is consistent with a westerly storm track displaced northward. Under such a scenario, the Sierra Nevada could be receiving some precipitation from the tail end of cold fronts passing across the range.

In summary, Figures 2-5 indicate substantial differences in the middle tropospheric circulation with each of the four categories of precipitation and precipitation ratios. It also appears that those patterns favoring a more west-east storm track tend to enhance the ratio of high- to low-elevation precipitation.

## **Spatial Consistency of Orographic Effects**

---

Figure 6 plots annual percentage change from normal of orographic effects for the American and Truckee-Tahoe basins. It is evident that for most years the mean orographic effect as a percentage of normal is similar on either side of the Sierra. Correspondence between orographic effects on the east and west slopes was further illustrated by a time-series plot (not shown) of the ordinal rankings of annual orographic effects on the American and Truckee-Tahoe basins. In most cases the ordinal ranking of orographic effect was the same or nearly so in both basins.

Figure 7 illustrates the similarity of the annual orographic effects at low and high elevations. In most cases there is a strong similarity in the percentage change from the annual ratios using datasets consisting only of the precipitation gauges (representing lower elevations) and the snow courses (high elevation). A time-series plot (not shown) simultaneously depicting ordinal rankings of the annual precipitation gauge and snow-course values further supports the spatial consistency of annual orographic effects at a wide range of elevations.

## **Conclusions**

---

We have used several decades of data to determine elevational patterns of precipitation from the eastern Central Valley of California to the Sierra Nevada. We used monthly precipitation gauge data to determine "precipitation ratios" representing precipitation on the windward slopes of the Sierra Nevada relative to that in the Central Valley. Individual months were categorized as wet or dry and as having low or high precipitation ratios. Months with the four possible combinations of wetness and precipitation ratios were then associated with maps of the corresponding mean middle tropospheric circulation.

As expected, wet months were associated with the presence of mean low pressure over the eastern Pacific Ocean. However, the shape of the low pressure was different for high- and low-precipitation ratio months. High precipitation ratios tend to occur when the trough over the eastern Pacific is oriented from the west-southwest to east-northeast, suggesting movement of storms from around the Hawaiian Islands. For wet years with low ratios, the low is centered near the Aleutians and the stormtrack assumes a northwest to southeast track.

Dry months were characterized by the presence of positive height anomalies for the corresponding mean 700-mb maps. For those with high precipitation ratios, the region of positive anomalies was large and oriented with a west to east elongation. For dry years with low ratios, there tended to be a smaller region of positive anomalies over the extreme eastern Pacific with a region of negative anomalies to the west. As was the case with wet years, high precipitation ratios seemed to be favored by a more zonal pattern of mean air flow.

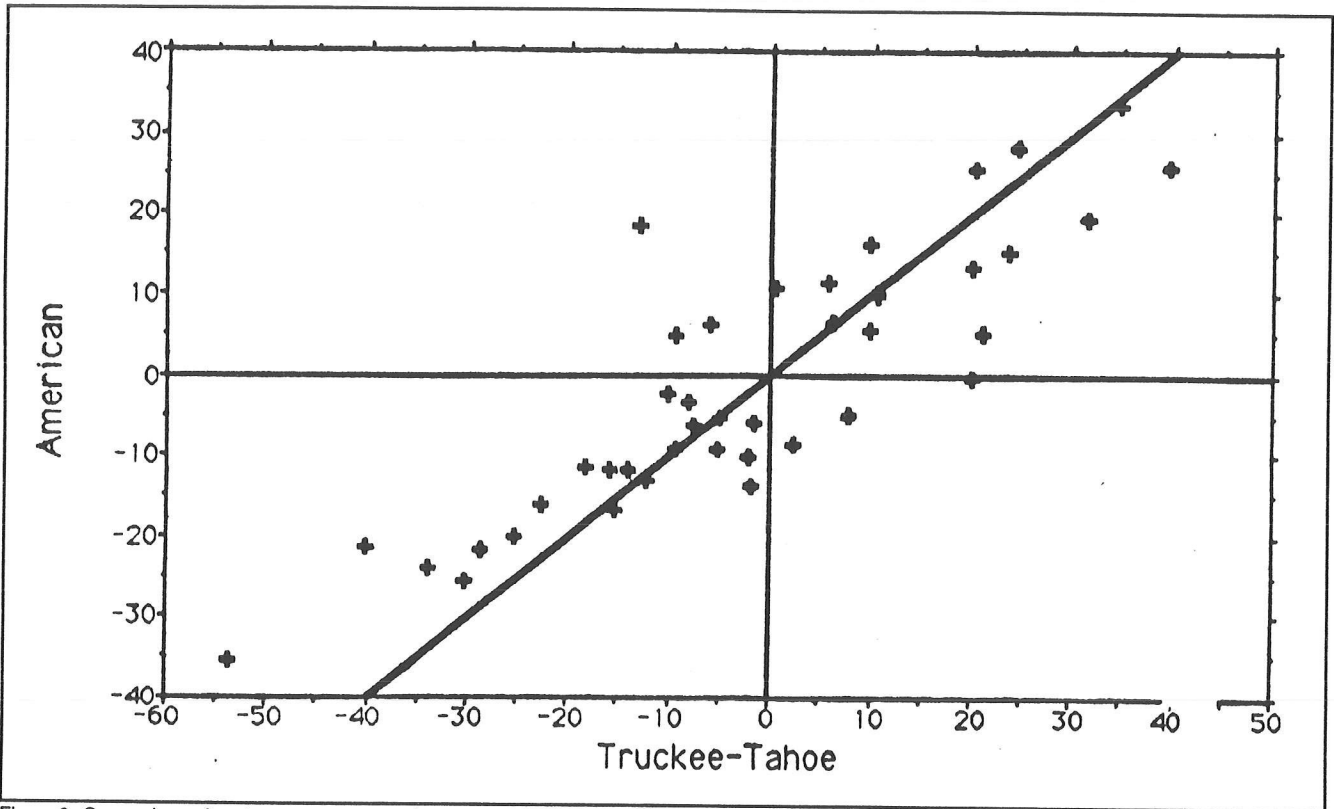


Figure 6. Comparison of east versus west annual mean orographic departures from normal (percentage change from normal ratios).

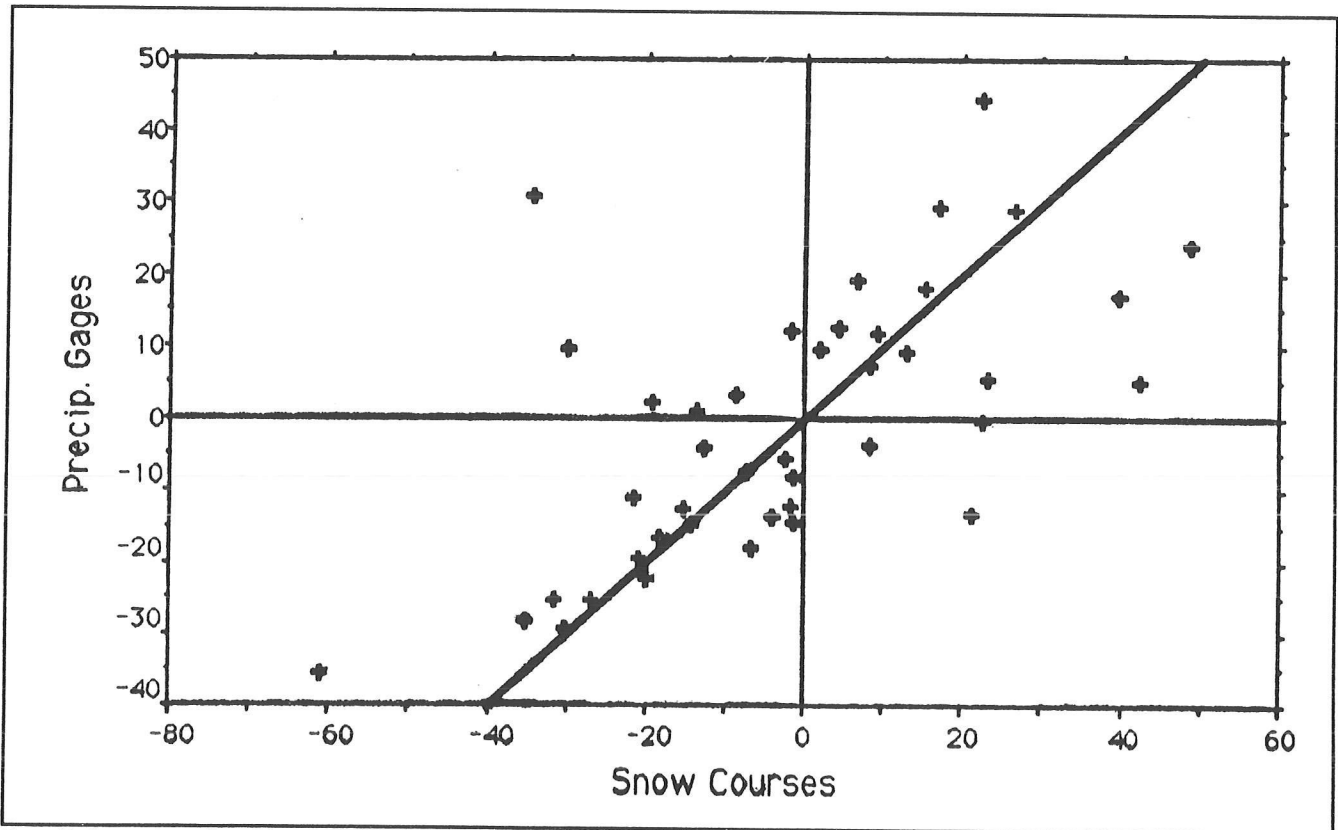


Figure 7. Comparison of precipitation versus snow course annual mean orographic departures from normal (percentage change from normal ratios).

We also examined the spatial coherency of high or low orographic effects at a seasonal level using precipitation gauge and snow-course data. It was found that basins on either side of the Sierra crest usually have greater or less than normal precipitation gains with elevation simultaneously on a seasonal basis. It was also found that the precipitation gauge data representing lower elevations and the snow-course data for higher elevations normally show similar seasonal patterns of enhanced or reduced orographic effects. We thus conclude there is considerable spatial coherency with regard to enhanced or reduced orographic effects across the Sierra.

## References

---

- Aguado, E. 1990. "Elevational and Latitudinal Patterns of Snow Accumulation Departures from Normal in the Sierra Nevada". *Theoretical and Applied Climatology*.42:153-157.
- Aguado, E, D Cayan, L Riddle, and M Roos. 1992. "Climatic Fluctuations in the Timing of West Coast Streamflow". *Journal of Climate*. In press.
- Cayan, DR, LG Riddle, and E Aguado. 1992. "The Influence of Precipitation and Temperature on Seasonal Streamflow in California". Accepted for publication pending revisions, *Water Resources Research*.
- Gleick, PH. 1987. "The Development and Testing of a Water-Balance Model for Climate Impact Assessment: Modeling the Sacramento Basin". *Water Resources Research* 23:1049-1061.
- \_\_\_\_\_. 1989. "Climate Change, Hydrology and Water Resources". *Rev. Geophys* 27:329-344.
- Lettenmaier, DP, and TY Gan. 1990. "Hydrologic Sensitivities of the Sacramento-San Joaquin River Basin, California, to Global Warming". *Water Resources Research* 26:69-86.
- Reece, B, and E Aguado. 1992. "Accumulation and Melt Characteristics of Northeastern Sierra Nevada Snowpacks". To appear in Proceedings of the Symposium: Managing Water Resources During Global Change.
- Williams, P Jr, and EL Peck. 1962. "Terrain Influences on Precipitation in the Intermountain West as Related to Synoptic Situations". *Journal of Applied Meteorology* 1:343-347.



# A Stochastic Model of Temporal Variations in Monthly Temperature, Precipitation, Snowfall, and Resulting Snowpack

Richard L. Orndorff, Richard G. Craig, and John F. Stamm

**Abstract:** We report a Monte Carlo representation of the long-term inter-annual variability of monthly snowfall on a detailed (1 km) grid of points throughout the southwest. An extension of the local climate model of the southwestern United States (Stamm and Craig 1992) provides spatially-based estimates of mean and variance of monthly temperature and precipitation. The mean is the expected value from a canonical regression using independent variables that represent controls on climate in this area, including orography. Variance is computed as the standard error of the prediction and provides site-specific measures of (1) natural sources of variation and (2) errors due to limitations of the data and poor distribution of climate stations. Simulation of monthly temperature and precipitation over a sequence of years is achieved by drawing from a bivariate normal distribution. The conditional expectation of precipitation, given temperature in each month, is the basis of a numerical integration of the normal probability distribution of log precipitation below a threshold temperature (3°C) to determine snowfall as a percent of total precipitation. Snowfall predictions are tested at stations for which long-term records are available. At Donner Memorial State Park (elevation 1811 meters) a 34-year simulation — matching the length of instrumental record — is within 15 percent of observed for mean annual snowfall. We also compute resulting snowpack using a variation of the model of Martinec *et al* (1983). This allows additional tests by examining spatial patterns of predicted snowfall and snowpack and their hydrologic implications.

Simulation of seasonal snowpack is an important part of a surface hydrologic model of the southwestern United States. Seasonal snowpack directly affects infiltration and recharge and produces a runoff lag due to water storage. Modeling snowpack during glacial cycles is important because it was the metamorphosis of perennial snowpacks that produced glaciers that occupied many of the higher mountain ranges in the southwest during Quaternary glacial stages. Two-dimensional models of regional surface hydrology are necessary to better understand the system and also to link climate models with proxy evidence of climate change.

Atmospheric General Circulation Models have been used in an attempt to understand Quaternary climate change on a worldwide scale (Kutzbach 1987; COHMAP Members 1988; Street-Perrott 1991), but their resolution is not fine enough for investigation of localized climate change (Kutzbach 1987). For this reason, a local climate model (taking some boundary conditions from global models) has been developed at Kent State University that gives temperature and precipitation based on independent variables available for both the present and last glacial maximum. The model is statistically based instead of physically based, and it can be solved at a resolution as fine as 1 kilometer. The local climate model is simpler and less time consuming computationally than

global models and may be used to represent uncertainty via a Monte Carlo simulation.

Snow simulation models fall into two categories: energy balance models and index models. Energy balance models rely on mathematical expressions that quantify the exchange of energy between the snowpack and its environment. Index models use one or more parameters as an index of energy exchange. Hoggan *et al* (1987) and Obled and Rosse (1977) model energy balances within snowpacks. Anderson (1973), Speers *et al* (1978), Motoyama (1990), and Martinec *et al* (1983) discuss models wherein surface temperature is the main index of energy exchange across the upper snow surface. We have chosen the methodology of Martinec *et al* (1983) because it seems most appropriate for this simulation based on the information available from the local climate model.

## Methodology

---

To evaluate spatial and seasonal variations of climate in the southwestern United States, we use a previously reported local climate model that computes monthly temperature and precipitation from a set of independent variables (Stamm and Craig 1992; Stamm 1991). Independent variables are computed from spatial variations of boundary conditions that include terrain elevation, insolation, CO<sub>2</sub> concentration, January and July winds, and January and July sea-surface temperatures. Solutions are the product of a canonical regression function, which is calibrated using climate data from 641 stations from six states (AZ, CA, CO, NM, NV, UT) west of 105° west longitude. These data are averaged from 1980-1984 "Summary of the Day" records (U.S. West 1988). Validation of the LCM, using data from 98 climate stations, indicates no significant departures of LCM solutions from climate data (Stamm 1991).

All independent variables can be solved at any point within the calibration domain. For convenience of display here, and as an illustration of the method, we choose to compute climate for a gridded domain that includes the entire drainage basin tributary to Pyramid Lake (Figure 1). The LCM computes five mean canonical variates for each grid point for each year; the LCM also computes standard deviations for each of the five canonical variates ( $s_v$ ).

Figure 2 shows spatial distribution of the standard deviation of the first canonical variate for the solution domain. The standard deviation is greatest in the mountainous areas of the Sierra Nevada and lowest in the northeastern portions of the solution domain, which lie within the Great Basin. This pattern probably reflects the greater natural variability of climate in the mountainous areas as well as the paucity of instrumental records available to parameterize the canonical equations. To represent the uncertainty inherent in the climate model estimates, we make draws from a normal distribution for the first of the five canonical variates for

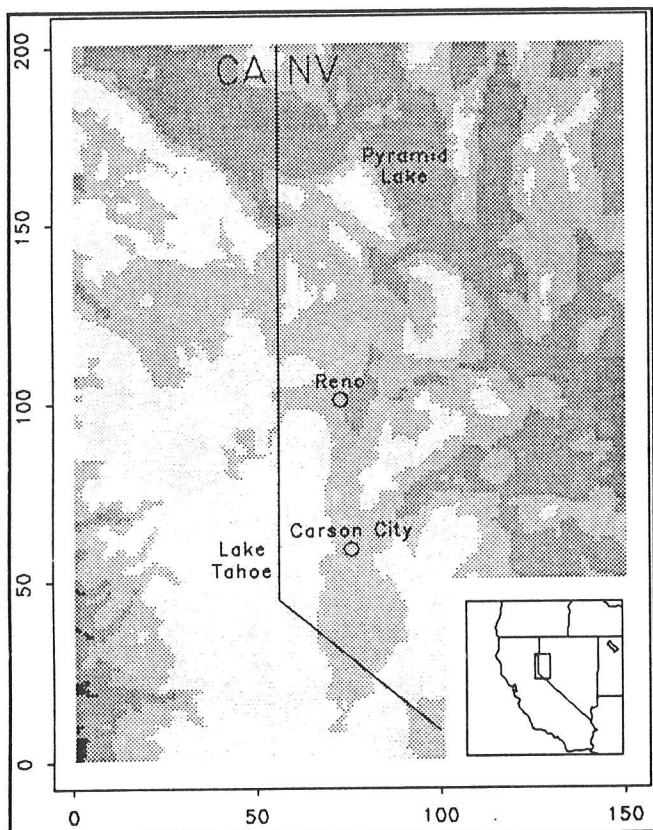


Figure 1. Solution domain consisting of the drainage basin tributary to Pyramid Lake, Nevada.

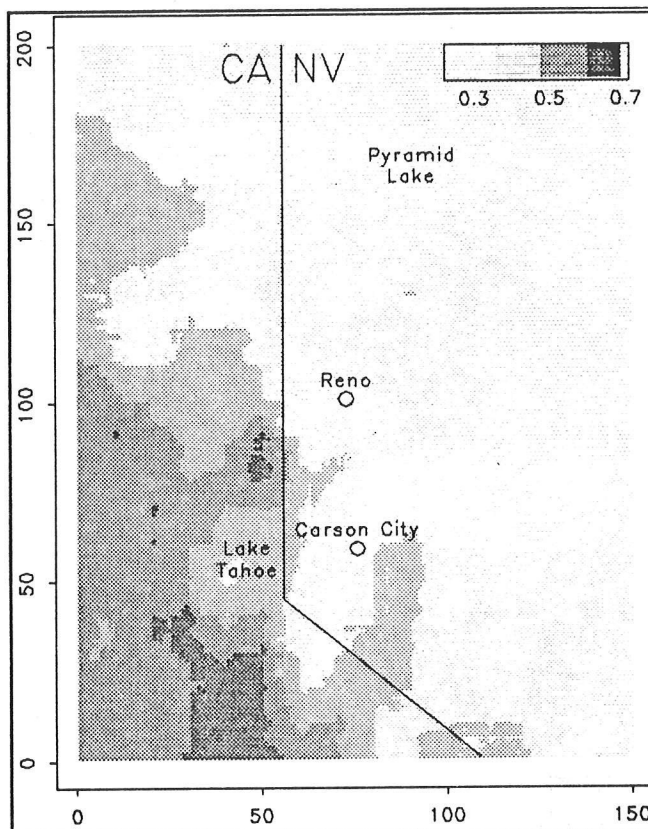


Figure 2. Spatial distribution of the standard deviation of the first canonical variate solved at a 1-km grid cell spacing.

each simulated year. This preserves the correlation structure within and between the months. The five variates are then transformed into monthly temperature and precipitation for use by the snow model.

Temperature predicted by the local climate model (at each grid cell) ( $T_m$ ) is accepted as the mean of a normal distribution, and the log of the predicted precipitation value ( $P_m$ ) is accepted as the mean of a log normal distribution. Variances of temperature ( $s_t^2$ ) and log precipitation ( $s_p^2$ ) are calculated from calibration station data for each month (for a total of 24 values). Snow accumulation is assumed to be the fraction of precipitation that occurs below a critical temperature,  $T_{crit}$  ( $3^\circ\text{C}$ ). We use monthly temperature and precipitation correlation coefficients, again calculated from calibration station data, to construct a bivariate normal distribution (Anderson 1958). We integrate that distribution from  $-\infty$  to  $+\infty$  in log precipitation and from  $-\infty$  to  $T_{crit}$  in temperature to calculate the fraction of precipitation that falls as snow in that grid cell. The integration area is hachured in Figure 3.

The snow ablation routine uses the degree-day factor method of Martinec *et al* (1983) to compute snowmelt within each of the grid cells. Meltwater depth is calculated from the number of degree-days and a degree-day factor:

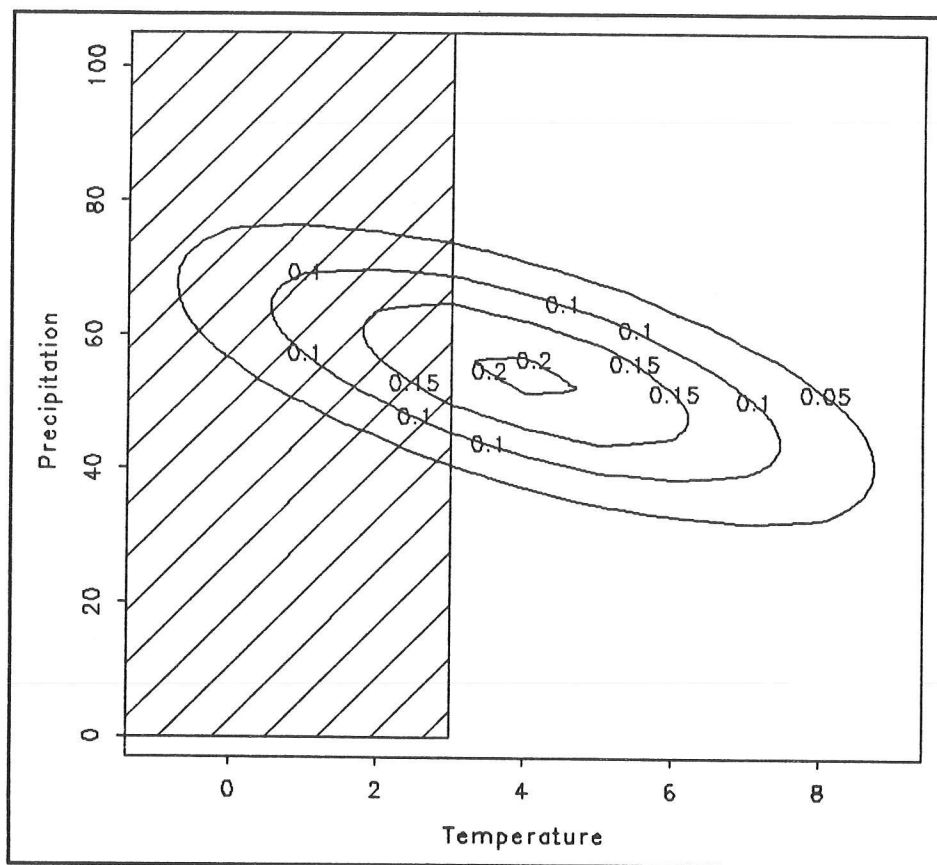


Figure 3. Integration of a bivariate normal distribution in temperature and precipitation space to determine the fraction of precipitation that falls as snow.

$$M = aT \tag{1}$$

where:

$M$  = daily snowmelt depth

$T$  = number of degree-days

$a$  = degree-day factor = 1.1  $R$

$R$  = ratio of snow density to water density

We assume a constant degree-day factor of 0.11 cm/°C/day for this study. The monthly snowmelt ( $Q$ ) is computed from the snowmelt depth and the ratio ( $S$ ) of snow-covered area to total area within each grid cell.

$$Q = MS \tag{2}$$

$S$  varies from zero to one. During the addition of new snow,  $S$  is very close to one, while ablation during the melt season causes increasing patchiness, thus decreasing  $S$ . Since the natural variation of  $S$  cannot be computed within our model, it is treated as a random variable drawn from a beta distribution over the range zero to one.

## Results

Canonical variates computed by the LCM are randomly perturbed to generate 34 years (matching the length of record) of temperature and precipitation estimates for Donner Memorial State Park (chosen for its illustrious snowfall history; see, for example, McGlashan 1966). The snow model then computes snowfall and snowpack for each month of those 34 years. As Figure 4 shows, the annual cycle dominates the temperature and precipitation signals. There is a factor of two variation in maximum precipitation. The precipitation signal is bimodal (over one year), and that is reflected in the snowfall curve. There is no perennial snowpack for any year within the 34-year solution period. This is not surprising, since these solutions are affected by the 1 km<sup>2</sup> cell size and, therefore, do not capture microtopographic effects that could result in sub-grid-cell size perennial snowpacks.

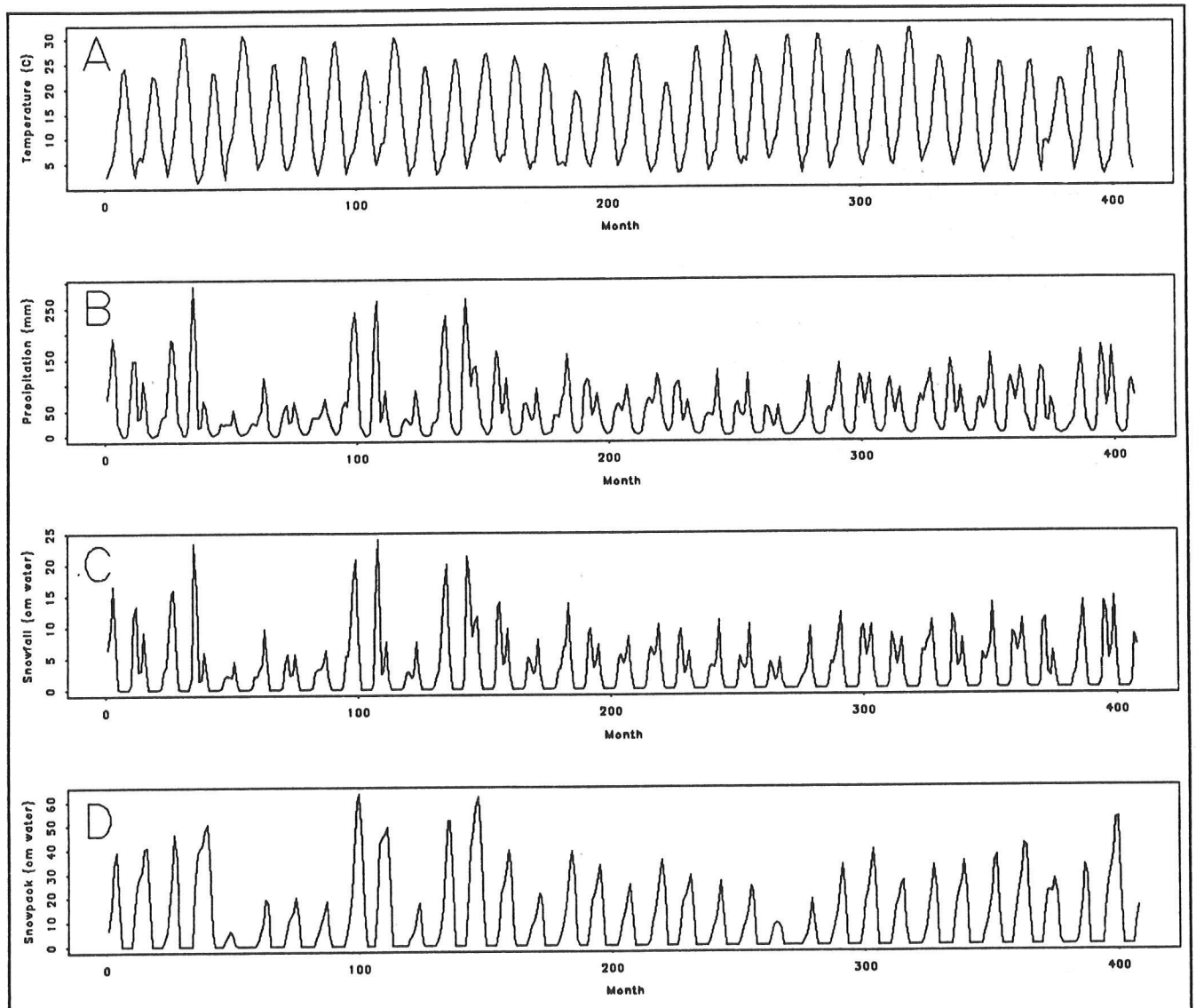


Figure 4. Temperature (A), precipitation (B), snowfall (c), and snowpack (d) from a 34-year simulation at Donner Memorial State Park, California.

Figures 5 and 6 show the monthly means of modeled snowfall and snowpack plotted versus monthly means of observed snowfall (U.S. West 1988) and snowpack (courtesy of K. Redmond, Western Regional Climate Center). For snowfall (Figure 5), the model over-predicted for November and March and under-predicted for January, February, April, and May. Modeled mean annual snowfall is under-predicted by 14.5 percent. For snowpack (Figure 6), the model under-predicted slightly for January and February and over-predicted for March, April, May, October, and November. March, April, and May snowpack are the most grossly overpredicted.

At present, the snow simulation model assumes a constant density (0.1 g/cm<sup>3</sup>) for the snowpack, and snowmelt depth is correlated with this density (equation 1). We expect snowpack density to increase during the spring months (Newark *et al* 1989). Were we to account for this increase, snowpack ablation would also increase, resulting in lower monthly means of modeled snowpack (equation 2) and better fit of modeled and observed snowpack.

The LCM can compute temperature and precipitation for a gridded domain (Stamm and Craig 1992). Solving the snow model at each point of a 1-kilometer grid that includes the entire drainage area of Pyramid Lake (Figure 1) based on the output of the local climate model provides 2-dimensional solutions that illustrate spatial as well as temporal variations in predicted snowpack. Figure 7 shows snowpack extent for April in the second year of a stochastic simulation. Two years are needed to reach a quasi-equilibrium, since the run is started with no extant snowpack. We illustrate solutions for this month because ablation late in the snow season has produced topographically correlated variations in

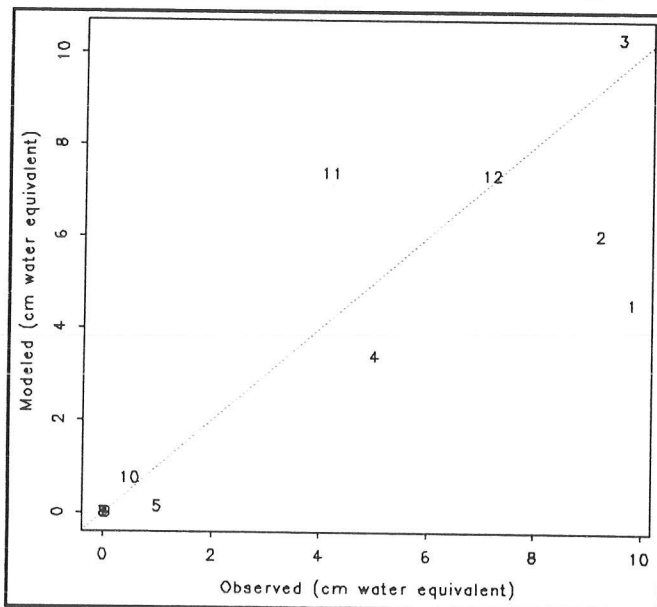


Figure 5. Monthly means of modeled versus observed snowfall for a 34-year simulation at Donner Memorial State Park, California. (Numbers relate to months.)

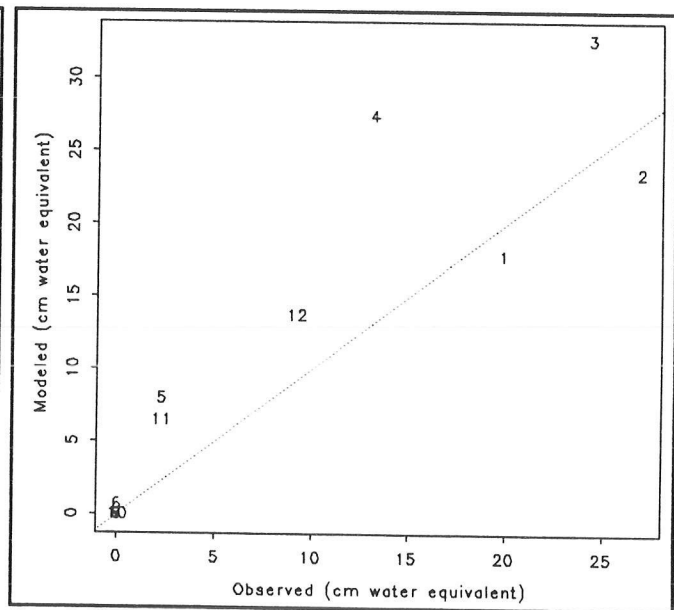


Figure 6. Monthly means of modeled versus observed snowpack for a 34-year simulation at Donner Memorial State Park, California. (Numbers relate to months.)

snowpack extent. The model predicts April snowpack for the Sierra Nevada but not in the lower-lying areas of the solution domain. We expect to extend this model to compute effects of such snowpack on seasonal runoff.

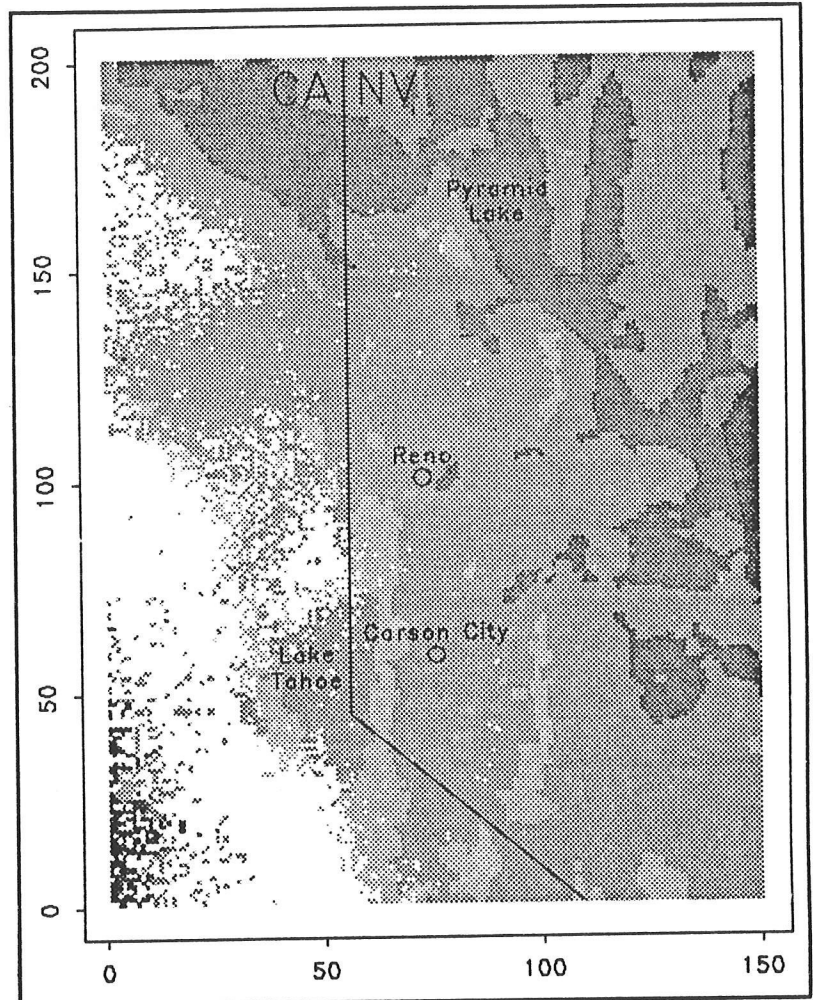


Figure 7. Snowpack extent (in white) for April in the second year of a stochastic simulation solved at a 1-km grid cell spacing.

## References

---

- Anderson, EA. 1973. *National Weather Service river forecast system - snow accumulation and ablation model*. NOAA Technical Memorandum NWS HYDRO-17.
- Anderson, TW. 1958. *An introduction to multivariate statistical analysis*. John Wiley and Sons, Inc., New York.
- COHMAP Members. 1988. Climatic changes in the last 18000 years: observations and model simulations. *Science* 241:1043-1052.
- Hoggan, DH, JC Peters, and W Loehlein. 1987. Real-time snow simulation model for the Monongahela River basin. *Water Resources Bulletin* 23(6):1141-1147.
- Kutzbach, JE. 1987. Model simulations of the climatic patterns during the deglaciation of North America, pp 425-446 in *North America and adjacent oceans during the last deglaciation*. WF Ruddiman and HE Wright Jr (eds). Geological Society of America. Boulder, CO. The Geology of North America Vol. K-3.
- Martinec, J, A Rango, and E Major. 1983. *The snowmelt-runoff model (SRM) user's manual*. NASA Reference Publication 1100.
- McGlashan, CF. 1966. *History of the Donner Party*. University of Michigan, Ann Arbor.
- Motoyama, H. 1990. Simulation of seasonal snowcover based on air temperature and precipitation. *Journal of Applied Meteorology* 29:1104-1110.
- Newark, MJ, LE Welsh, RJ Morris, and WV Dnes. 1989. Revised ground snow loads for the 1990 National Building Code of Canada. *Canadian Journal of Civil Engineering* 16:267- 278.
- Obled, C, and B Rosse. 1977. Mathematical models of a melting snowpack at an index plot. *Journal of Hydrology* 32:139- 163.
- Speers, D, D Kuehl, and V Schermerhorn. 1978. Development of the operational snow band SSAR model. pp 369-378 in *Modeling of Snow Cover Runoff*. SC Colbeck and M Ray (eds). US Army Cold Regions Research and Engineering Laboratory, Hanover, NH.
- Stamm, JF. 1991. *Modeling local paleoclimates and validation in the southwest United States*. PhD Dissertation, Kent State University, Kent, OH.
- Stamm, JF, and RG Craig. 1992. Validation of a semi-lagrangian, canonical regression model of climates in the southwestern United States. *Proceedings of the Eighth Annual Pacific Climate Workshop*. California Department of Water Resources, Interagency Ecological Studies Program Technical Report 31, pp. 163-171.
- Street-Perrott, FA. 1991. GCM modeling of paleoclimates. pp 167-178 in *Future Climate Change and Radioactive Waste Disposal*. Goodess and JP Palutikof (eds). Climate Research Unit, Norwich, England.
- US West. 1988. *Climate Data, Volume 1.1, Summary of the Day*. US West Optical Publishing, Denver.

# Appendix A

## **AGENDA**

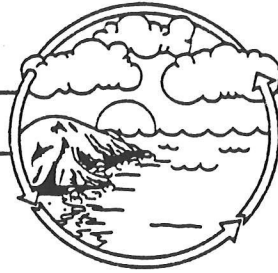
---

Ninth Annual Pacific Climate (PACLIM) Workshop,  
April 21-24 1992



---

PACLIM



Climate Variability  
of the Eastern  
North Pacific  
and Western  
North America

---

Ninth Annual Pacific Climate (PACLIM) Workshop  
April 21-24, 1992  
FIRELIGHT FORUM  
AGENDA

6:00-6:45 pm Dinner

Tuesday Eve., April 21, 1992:

*Current Climate Variations*

Moderator: Walt Dean

7:00-7:20 pm Welcome and Announcements at Firelight Forum

7:20-7:40 pm "A Status Report on the California Drought"  
*Maurice Roos, California Department of Water Resources*

7:40-8:00 pm "Development of a Distributed Database Network for Management of  
Climate and Ocean Data"  
*Douglas R. McLain, Gary D. Sharp, NOAA Center for Ocean  
Analysis and Prediction, Monterey, California*

8:00-8:20 pm "Recent Regional Climate Anomalies in the Western United States,  
and 1991-92 Relations to ENSO"  
*Kelly T. Redmond, Western Regional Climate Center, Reno,  
Nevada*

8:20-8:40 pm "Atmospheric/Oceanic Circulation Changes Related to Extremes in  
the Southern Oscillation"  
*Vernon E. Kousky, Climate Analysis Center, Washington, DC*

8:40-8:55 pm "Effects of the 1992 ENSO condition along the California Coast"  
*John McGowan, Scripps Institution of Oceanography*

8:55- Social (at Firelight Forum)

**Wednesday Morn., April 22, 1992:**

7:30-8:15 am Breakfast

***Invited Talks, Long Term Monitoring*** Moderator: **Dan Cayan**

8:30-8:45 am "Overview of NSF's Long-Term Ecological Research (LTER) Program"  
*Fred Swanson, Oregon State University*

8:45-9:15 am "Climate Studies in the LTER Program"  
*David Greenland, University of Oregon*

9:15-9:45 am "Arctic Tundra LTER Climate/Hydrology Issues"  
*Douglas Kane, University of Alaska*

9:45-10:15 am "Desertification: Responses of Arid Landscapes and Ecosystems to Resources Redistribution at the Jornada LTER"  
*Ross Virginia, San Diego State University*

10:15-10:35 am Coffee Break

10:35-11:05 am "The Role of Climate in Pelagic Ecology: The Importance of Monitoring"  
*John McGowan, Scripps Institution of Oceanography*

11:05-11:35 am "The U.S. Geological Survey NAWQA Program Plans for Assessing the Nation's Water Quality"  
*Robert Hirsch, U.S. Geological Survey, Reston, Virginia*

11:35-12:05 pm "An Investigation of the Water, Energy, and Biogeochemical Budgets of Loch Vale and Other Rocky Mountain Watersheds"  
*John Turk, U.S. Geological Survey, Denver, Colorado*

12:05-1:00 pm Lunch

**Wednesday Aft., April 22, 1992:**

***Invited Talks, Long Term Monitoring (cont'd)***

1:30-2:00 pm "Long-Term Ecological Research Along Biome Transitions"  
*Manuel Molles, University of New Mexico*

2:00-2:30 pm "The Sequoia-Kings Canyon National Park Ecosystem Observation Program"  
*David Graber, Sequoia-Kings Canyon National Park*

2:30-3:00 pm "Global Change Research in the Andrews Forest LTER Program"  
*Fred Swanson, Oregon State University*

3:00-3:30 pm Coffee Break

**Wednesday Aft., April 22, 1992:            *Posters***

3:30-4:00 pm    *Poster Introductions* (One minute each)

6:00-6:45 pm    *Dinner*

**Wednesday Eve., April 22, 1992:**

*Climate Smorgasbord*

*Moderator:    John Dracup*

- 7:00-7:20 pm    "An Objective Classification of Climatic Regions in the Pacific Ocean"  
*Henry F. Diaz, Timothy J. Brown, NOAA/ERL and CIRES, Boulder, Colorado*
- 7:20-7:40 pm    "Simulated Streamflow Responses to Climate Change in American and Carson Rivers of the Sierra Nevada, California and Nevada"  
*Michael D. Dettinger, Anne E. Jeton, U.S. Geological Survey, San Diego, California*
- 7:40-8:00 pm    "Growth Rate Changes and Skeletal  $\delta^{18}O$  in E. Pacific Corals Back Through the End of the Little Ice Age"  
*Braddock Linsley, R. Dunbar, G. Wellington, D. Mucciarone, Rice University*
- 8:00-8:20 pm    "Reflections on the California Pollen Record"  
*David P. Adam, U.S. Geological Survey, Menlo Park, California*
- 8:20-8:40 pm    "Climate Change and Salmonid Production in the North Pacific Ocean"  
*Robert C. Francis, School of Fisheries, Univ. of Washington*
- 8:40-            *Social*

**Thursday Morn., April 23, 1992:**

7:30-8:15 am    *Breakfast*

*Climate vs. Surface Hydrology*

*Moderator:    Mike Dettinger*

- 8:30-8:50 am    "A Mechanism Linking Solar-Irradiance Variations and Regional Precipitation"  
*Charles A. Perry, U.S. Geological Survey, Lawrence, Kansas*
- 8:50-9:10 am    "U.S. Streamflows in Relation to the High Index Phases of the Southern Oscillation"  
*Ercan Kahya, John A. Dracup, UCLA*

Thursday Morn., April 23, 1992:

*Climate vs. Surface Hydrology* (cont'd)

- 9:10-9:30 am "Potential Effects of Climate Change on Windward and Leeward Drainage Basins in the Sierra Nevada"  
*Alex Pupacko, U.S. Geological Survey, Carson City, Nevada*
- 9:30-9:50 am "Sierra Nevada Orographic Precipitation and Links to Atmospheric Circulation"  
*Brian Reece, Edward Aguado, Dan Cayan, Larry Riddle, San Diego State University*
- 9:50-10:20 am Coffee Break
- 10:20-10:40 am "A Study of 1000 Year Storms in California"  
*James D. Goodridge, Chico, California*
- 10:40-11:00 am "Regional-Scale Simulations of the Western U.S. Climate"  
*J. Roads, J. Bossert, S. Chen, Scripps Institution of Oceanography and Los Alamos National Laboratories*
- 11:00-11:20 am "An Analysis of Monthly and Seasonal Precipitation Patterns in Mexico"  
*Arthur V. Douglas, Phillip J. Englehart, Creighton University*
- 11:20-11:40 am "Precipitation Variability in the Southwestern U.S. and northern Mexico over the Last 90 Years"  
*George Kiladis and Henry Diaz, Univ. of Colorado and NOAA*
- 11:40-12:00 pm "Effect of a Modeled Snow Cover on the North American Hydrologic Cycle"  
*S. Marshall, J. Roads, G. Glatzmaier, Los Alamos National Laboratories and Scripps Institution of Oceanography*
- 12:00-1:00 pm Lunch

Thursday Aft., April 23, 1992:

*Global/Regional Climate Variability* Moderator: Kelly Redmond

- 1:30-1:50 pm "Regional Simulations of GCM Extreme Circulations in the Western United States"  
*C. Wang, C. Kao, J. Bossert, S. Chen, Los Alamos Natl. Lab*
- 1:50-2:10 pm "Comparison of 1992 and 1987 ENSO Conditions with the Climatological Mean Oceanographic Conditions in the Eastern Equatorial Pacific"  
*Dick Barber, Francisco Chavez, Duke University and Monterey Bay Aquarium Research Institute*

Thursday Aft., April 22, 1992:

*Global/Regional Climate Variability (cont'd)*

- 2:10-2:30 pm "Year-to-Year Changes of Vertical Temperature Distribution in the California Current: 1954-1986"  
*Jerrold G. Norton, Douglas R. McLain, NOAA, Monterey, Calif.*
- 2:30-2:50 pm "Upwelling and Productivity in the Eastern Tropical Pacific Ocean"  
*Paul Fiedler and Valerie Philbrick, SW Fisheries Science Center*
- 2:50-3:20 pm Coffee Break
- 3:20-3:40 pm "Mechanisms for Intraseasonal Variations of North American Climate"  
*Ron Gelaro and Tom Murphree, Monterey, California*
- 3:40-4:00 pm "A Case Study of Ship Track Evolution"  
*Arunas P. Kuciauskas, Naval Research Lab & Postgraduate School, Monterey, California*
- 4:00-4:20 pm "Upper Ocean Thermal Behavior Since 1942: The Pacific and Related Ecological Pattern"  
*Gary D. Sharp, CIRIOS, Monterey, California*
- 4:20-4:40 pm "Volcanic or Extra-Terrestrial Influences on Global Temperature and Carbon Dioxide"  
*Charles D. Keeling, Timothy P. Whorf, Scripps Institution of Oceanography*
- 4:40-5:00 pm "A Study of Elevational Patterns of Climate on the Leeward Slope of East Maui, Hawaii"  
*T. Giambelluca, W. Minyard, L. Loope, Haleakala N.P., Hawaii*
- 5:00-5:20 pm "Sea Surface Temperature and the Subsequent Freshwater Survival Rate of Some Salmon Stocks: A Surprising Link Between the Climate of Land and Sea"  
*D.J. Blackbourn, Canada Department of Fisheries and Oceans*
- 6:00-7:00 pm Dinner

Thursday Eve., April 23, 1992:

- 7:30-8:20 pm "Climatic Effects on Vegetation Dynamics in Grand Canyon": A Photographic Documentation, (Present vs. 1889-90)  
*Robert H. Webb and Janice E. Bowers, U.S. Geological Survey, Tucson, Arizona*
- 8:20- Social

Friday Morn., April 24, 1992:

7:30-8:45 am Breakfast

*Paleoclimate* Moderator: Caroline Isaacs

9:00-9:20 am "Preliminary Pollen Analysis of a Core from the Northern Gulf of California: No Support for the Depressed Jet Stream"  
*Owen Davis, Timothy Jull, Lloyd Keigwin, Univ. of Arizona*

9:20-9:40 am "Climate Change in Southern California During the Medieval Warm Period Inferred from Fish Scale and Charcoal Deposition in the Varied Sediments of the Santa Barbara Basin"  
*T. Baumgartner, R. Byrne, A. Soutar, V. Ferreira, Ensenada, Baja California*

9:40-10:00 am "Salinity and River Discharge Record in San Francisco Bay over the Past 4000 Years"  
*Lynn Ingram, Department of Geology, Stanford University, CA*

10:00-10:20 am "The Influence of Late Holocene Climatic Variations on the Frequency of Large Floods in the Southwestern U.S."  
*Lisa L. Ely, Dept. of Geosciences, Univ. of Arizona, Tucson, AZ*

10:20-10:50 am Coffee Break

10:50-11:10 am "Cd/Ca Ratios in Foraminifera from San Francisco Bay: Evidence for Decreasing Upwelling off California Over the Past 4,000 Years"  
*A. van Geen, S.N. Luoma, C.C. Fuller, R. Anima, H.E. Clifton, U.S. Geological Survey, Menlo Park, California*

11:10-11:30 am "The Holocene History of an Estuary on Santa Rosa Island, Coastal California"  
*K. Cole, G. Liu, W. Halvorson, J. Dugan, University of Minnesota*

11:30-12:00 pm Adjourn

12:00-1:00 pm Lunch

Appendix B  
**POSTERS**

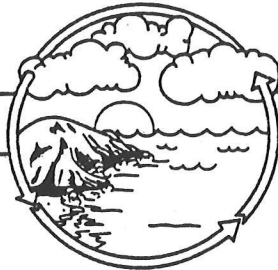
---

Ninth Annual Pacific Climate (PACLIM) Workshop,  
April 21-24 1992



---

PACLIM



Climate Variability  
of the Eastern  
North Pacific  
and Western  
North America

---

**Ninth Annual Pacific Climate (PACLIM) Workshop**  
**April 21-24, 1992**  
**FIRELIGHT FORUM**  
**POSTERS**

- "Climatic Variability in the Ancestral Pacific Ocean: Analog for Modern Climatic Change in Western North America"  
*Roger Y. Anderson, University of New Mexico, and Walter E. Dean, U.S. Geological Survey, Denver, Colorado*
- "Tree-Ring Time Series from South-Coastal Alaska and the Pacific Northwest: Associations with Anomalies of Northeastern Pacific Climate"  
*R.D. D'Arrigo, B.M. Buckley, G.C. Jacoby, Y. Shi, Lamont-Doherty Geological Observatory, Palisades, New York*
- "Climatic Response of Tree-Ring Time Series from South Coastal Alaska"  
*G.C. Jacoby, Y. Shi, R.D. D'Arrigo, B.M. Buckley, Lamont-Doherty Geological Observatory, Palisades, New York*
- "Preliminary Inventory of A.D. 1450 - 1900 El Niño Events as Recorded by  $\delta^{13}C$  in the Santa Barbara Basin"  
*Arndt Schimmelmann, Mia J. Tegner, Memorie K. Yasuda, Scripps Institution of Oceanography*
- "Ecophysiological Responses to CO<sub>2</sub> Enrichment during Deglaciation: Stomatal Densities and  $^{13}C/^{12}C$  from Leaves in Packrat Middens"  
*Pete Van de Water, University of Arizona*
- "Past Fluctuations in the Late Spring Secondary Precipitation Maximum in the Interior Pacific Northwest"  
*Kenneth Lee Petersen, Westinghouse Hanford Company, Richland, Washington*
- "Microscopic Charcoal Evidence from the Santa Barbara Basin: Fire History During the Last 400 Years"  
*Scott Mensing, University of California, Berkeley, California*
- "Marine-Continental Correlations in the Pacific Northwest: The Terrestrial Record (Preliminary Report)"  
*David P. Adam, U.S. Geological Survey, Menlo Park, California*

- "Flowering of Haleakala Silversword and the Pinatubo Volcano: What is the Connection?"  
*Lloyd L. Loope, Haleakala N.P., and Richard P. Pharis, University of Calgary*
- "Temporal Variation of the Physical and Chemical Environment of the Sacramento-San Joaquin Delta, California"  
*Peggy W. Lehman, California Department of Water Resources, Sacramento, Calif.*
- "Calibration of Two Sierra Nevada Watersheds and Application of a Geographic Information System to Model Parameterization"  
*Anne Jeton, U.S. Geological Survey, Carson City, Nevada*
- "Snow Measures as Predictors of Streamflow in the Sierra Nevada and Coast Ranges of California"  
*Larry Riddle, Dan Cayan, Scripps Institution of Oceanography, and Ed Aguado, San Diego State University California*
- "A Multi-basin Seasonal Streamflow Model for the Sierra Nevada"  
*Dan Cayan, and Larry Riddle, Scripps Institution of Oceanography*
- "A Stochastic Model of Temporal Variations in Monthly Temperature, Precipitation and Resulting Snow-Fall"  
*Richard Craig, Rik Orndorff, Kent State University, and John Stamm, Princeton University*
- "Statistical Analysis of the Current Five Year California Drought"  
*F. Wade Freeman, John A. Dracup, Civil Engineering Department, UCLA*
- "Use of Regression Models to Estimate Effects of Climate Change on Monthly Streamflow in the American and Carson River Basins, California-Nevada"  
*Lowell F.W. Duell, Jr., U.S. Geological Survey, San Diego, California*
- "Relationship of San Francisco Rainfall to El Niño"  
*Jan Null, National Weather Service Forecast Office, Redwood City, California*
- "Effects of Late Holocene Climate Change on Forest Fires and Related Alluvial Activity in Yellowstone National Park"  
*Grant A. Meyer, Stephen G. Wells, A.J. Timothy Jull, Robert C. Balling, Jr.*
- "Statistical Analysis of Global Warming Data"  
*Leonard J. Lane and Mary H. Nichols, USDA-ARS Southwest Watershed Research Center, Tucson, Arizona*
- "A Mechanism Linking Solar-Irradiance Variations and Regional Precipitation"  
*Charles A. Perry, U.S. Geological Survey*
- "Correlation of Marine and Terrestrial Records of Climate Change in the Western United States"  
*James V. Gardner, U.S. Geological Survey, Menlo Park, California, Walter E. Dean, U.S. Geological Survey, Denver, Colorado*

Appendix C  
**ATTENDEES**

---

Ninth Annual Pacific Climate (PACLIM) Workshop,  
April 21-24 1992



David Adam  
U.S. Geological Survey - MS 915  
345 Middlefield Road  
Menlo Park, CA 94025  
(415)329-4970, fax FTS 459-4975

R. Scott Anderson  
E.S.&Q. Studies Program  
Box 6013, North. Arizona Univ.  
Flagstaff, AZ 86011  
(602)523-5821, fax 602-523-7290

Gary E. Barbato  
NOAA/National Weather Service  
660 Price Avenue - Forecast Office  
Redwood City, CA 94063-1497  
(415) 364-4610, fax 415-364-2599

David J Blackburn  
Pacific Biological Station  
Dept of Fisheries/Oceans  
Hammond Bay Road  
Nanaimo, BC, CANADA V9R 5K6  
(604)756-7089, fax 604-756-7053

Daniel Cayan  
Scripps Inst. of Oceanography  
A-0224, Univ of CA-San Diego  
La Jolla, CA 92093-0224  
(619) 534-4507, 619-534-8561

Peter Comanor  
National Park Service, 490  
Wildlife & Vegetation Division  
P.O. Box 37127 (WASO 490)  
Washington, D.C. 20013-7127  
(202)343-8126

Edward Aguado  
San Diego State University  
Dept of Geography  
San Diego, CA 92182  
(619)594-5930, fax 619-594-4938

Lisa Ramirez Bader  
US Geological Survey  
Box 25046, ms 939  
DFC  
Denver, CO 80225  
(303)236-5547, fax 303-236-5448

Timothy Baumgartner  
Scripps Institution of Oceanography  
0227  
Univ. Calif. at San Diego  
La Jolla, CA 92093-0227  
619-534-2171, fax 619-534-0300

Roger Byrne  
Department of Geography  
University of California  
Berkeley, CA 94720  
510-643-8108

Kenneth Cole  
115 Green Hall, NPS/CPSU  
Dept. of Forest Resources  
University of Minnesota  
St. Paul, MN 55108  
612-624-4296, fax 612-625-5212

Rosanne D'Arrigo  
Lamont-Doherty Geological Observ.  
Tree-Ring Laboratory  
Palisades, NY 10964  
914-359-2900, ext. 517, fax 914-365-3046

Ernest P. Dagher  
National Weather Service  
660 Price Avenue  
Redwood City, CA 94063  
(415)364-2422, 415-364-2599

Walter E. Dean  
U.S. Geological Survey,  
Box 25046, MS 939, DFC  
Denver, CO 80225  
(303) 236-5760

Henry Diaz  
NOAA/ERL,  
325 Broadway  
Boulder, CO 80303  
(303) 497-6649, fax 303-497-6750

John Dracup  
University of California,  
4532 Boelter Hall  
Los Angeles, CA 90024-1593  
(310) 825-2176, fax 310-206-2222

Eric Edlund  
University of California at Berkeley  
Dept of Geography,  
501 Earth Sciences Bldg.  
Berkeley, CA 94720  
(510) 643-8108, fax 510-642-3370

Pamela G. Emch  
1917 Vanderbilt Ln., #3  
Redondo Beach, CA  
90278 213-379-3734

Paul Fiedler  
NOAA/NMFS/Southwest Fisheries  
Center  
P.O. Box 271  
La Jolla, CA 92038-0271  
619-546-7016, fax 619-546-7003

Owen Davis  
University of Arizona,  
Geosciences Department-Bldg #77  
Tucson, AZ 85721  
(602) 621-7953, fax 602-621-2672

Michael Dettinger  
U.S. Geological Survey,  
5735 Kearny Villa Rd, Suite O  
San Diego, CA 92123  
(619)557-6700, fax 619-557-5428

Arthur V. Douglas  
Creighton University  
Dept. of Atmos. Sciences, Chairman  
Omaha, NE 68178-0110  
402-280-2464, fax 402-280-2140

Lowell F.W. Duell, Jr.  
U.S. Geological Survey,  
5735 Kearny Villa Rd- Suite O  
San Diego, CA 92123  
(619)557-6700, fax 619-557-5428

Lisa Ely  
University of Arizona,  
Dept of Geosciences, Bldg. 77  
Tucson, AZ 85721  
(602)621-2022, fax 602-621-2672

Daniel B. Fagre  
Glacier National Park  
West Glacier, MT 59926  
406-888-5441, fax 406-888-5581

Dianne Fox  
USGS  
Box 25046  
ms 939  
DFC  
Denver, CO 80225FTS 776-1647, FAX  
303-236-5448

Robert C. Francis  
University of Washington  
FRI WH-10  
Seattle, WA 98195  
206-543-4650, fax 206-685-7471

James V. Gardner  
U.S. Geological Survey,  
345 Middlefield Rd., MS -999  
Menlo Park, CA 94025  
(415) 354-3087, fax 415-354-3191

David M. Graber  
National Park Service  
Sequoia and Kings Canyon National  
Parks  
Three Rivers, CA 93271  
209-565-3173,-3171, fax 209-565-3497

Robert M.  
U.S. Geological Survey  
436 National Center  
Reston, VA 22092  
703-648-5041, fax 703-648-5070

Bonnie Lynn Ingram  
Stanford University  
Dept. of Geology  
Stanford, CA 94305  
510-643-7686, fax 510-643-9980, hm  
525-7464

Gordon C. Jacoby  
Lamont-Doherty Geological  
Observatory  
Tree-Ring Laboratory  
Palisades, NY 10964  
(914) 359-2900, ext. 616, fax 914-365-  
3046

F. Wade Freeman  
609 Kelton Ave.  
Los Angeles, CA 90024  
310-206-8612, fax 310-206-2222

James Goodridge  
31 Rondo Court  
Chico, CA 95928  
(916) 345-3106

David Greenland  
University of Oregon  
Dept. of Geography  
Eugene, OR 97403-1251  
503-346-4541, fax 503-346-2067

Peter Kyle House  
University of Arizona  
Dept. of Geosciences, Bldg. 77  
Tucson, AZ 85721  
602-621-2022

Caroline Isaacs  
U.S. Geological Survey,  
345 Middlefield Road, MS-999  
Menlo Park, CA 94025  
(415)354-3014, 415-354-3191

Anne Jeton  
US Geological Survey  
705 N. Plaza Street, Rm 224  
Carson City, NV 89701  
(702)887-7628, fax 702-887-7629

Ercan Kahya  
UCLA  
405 Hilgard Ave., 4815 Boelter Hall  
Los Angeles, CA 90024  
~~213~~-206-8612, fax ~~213~~-206-2222  
310 310

Douglas L. Kane  
University of Alaska  
Institute of Northern Engineering  
Water Research Center  
Fairbanks, AK 99775  
907-474-7808, fax 907-474-6087

Charles David Keeling  
Scripps Inst. of Oceanography,  
0220, University of CA-San Diego  
La Jolla, CA 92093-0220  
(619)534-6001, 619-534-0784

George Kiladis  
University of Colorado  
CIRES Box 449  
Boulder, CO 80309  
303-492-1401, fax 303-492-2468

Vernon E. Kousky  
NOAA/NWS/NMC/Climate Anal. Ctr.  
Rm. 605 WWB, 5200 Auh Rd.  
Camp Springs, MD 20746  
301-763-8227, fax 301-763-8395

Arunas Kuciauskas  
Naval Research Laboratory  
Code 442  
Monterey, CA 93943-5005  
408-647-4784, fax 408-647-4769

John Laurmann  
University of CA-Marine Sci Inst.,  
c/o 3372 Martin Road  
Carmel, CA 93923-8230  
408-625-6696

Peggy Lehman  
CA Dept of Water Resources  
3251 "S" Street - Room B-9  
Sacramento, CA 95816  
(916) 445-3478

Chin-I Lin  
Pacific Gas & Electric  
R&D Department  
3400 Crow Canyon Road  
San Ramon, CA 94583  
(415)866-5396, fax 510-866-5318

Braddock Linsley  
Rice University  
Dept of Geology & Geophysics  
P.O. Box 1892  
Houston, TX 77251  
(713)527-4880, fax 713-285-5214

Lloyd L. Loope  
NPS-Haleakala Nat'l Park  
P.O. Box 369  
Makawao, Maui, HI 96768  
(808)572-1983, fax 808-572-1304

Susan Marshall  
Los Alamos Natl. Laboratories  
EES-5, ms K401  
Los Alamos, NM 87545  
505-665-4788, fax 505-665-3107

Ana Mackay  
U.S. Geological Survey  
1675 W. Anklam Road  
Tucson, AZ 85745  
FTS 762-6821

John A. McGowan  
Univ. of California @ San Diego  
Scripps Inst. Oceanography, m.s. 0228  
La Jolla, CA 92093-0228/619-534-2074,  
fax 619-534-0300

Douglas McLain  
NOAA National Ocean Service, COAP  
2560 Garden Grove Rd., #101  
Monterey, CA 93940  
(408) 647-2412, fax 408-647-4225

Christi McMichael  
6280 Acorn St.  
San Diego, CA 92115  
619-286-1592, fax 619-594-4938

Ted Melis  
4500 West Speedway Rd.  
Tucson, AZ 85745  
602-670-6815, fax 765-6806 or 670-6806

Scott Mensing  
U.C. Berkeley  
Dept. of Geography  
501 Earth Sciences  
Berkeley, CA 94720  
510-643-8108

Grant Meyer  
University of New Mexico  
Dept of Geology  
Albuquerque, NM 87108  
(505)277-5261, fax 505-277-8843

Manuel C. Molles, Jr.  
University of New Mexico  
Dept. of Biology  
167 Castetter Hall  
Albuquerque, NM 87131-1091  
505-277-3050, 3411, fax 505-277-0304

John P Monteverdi  
4425 View St.  
Oakland, CA 94611  
510-613-4320

Tom Murphree  
Dept of Meteorology, MR-ME,  
Naval Postgraduate School  
Monterey, CA 93943-5000  
(408)646-2723/2516, fax 408-646-3061

Mary Nichols  
USDA-ARS  
2000 E. Allen Rd.  
Tucson, AZ 85719  
602-670-6481, fax 602-670-6493

Jerry Norton  
Pac. Fisheries Environ. Group,  
SWFSC/NMFS  
P.O. Box 831  
Monterey, CA 93942  
(408) 375-6497, fax 408-646-3319

Jan Null  
National Weather Service  
660 Price Avenue  
Redwood City, CA 94063  
(415)364-4610, fax 415-364-2599

Richard Orndorff  
Kent State University  
Dept. of Geology  
Kent, OH 44242  
216-672-7987

Ralf D. Otto  
visiting German grad. student  
see: Steve Piper's address  
619-534-4230, fax 619-534-0784

Kathy Pagan  
48243 Turquoise St.  
Fremont, CA 94539  
510-656-7654

David Parsons  
National Park Service  
Three Rivers, CA 93271  
209-565-3170, fax 209-565-3497

Sue Pelmulder  
10825 Farallone Ave.  
Chatsworth, CA  
91311 310-206-8612, fax 310-206-2222

Elise Pendall  
University of Arizona  
Dept. of Geosciences  
Tucson, AZ 85721  
602-629-9604

Charles Perry  
US Geological Survey  
Water Resources Division  
4821 Quail Crest Place  
Lawrence, KS 66049  
(913)842-9909, fax 913-832-3500

Kenneth P. Petersen  
Westinghouse Hanford Co.,  
P.O. Box 1970, MS # H4-14  
Richland, WA 99352  
509-376-9765, (509) 376-4081

David H. Peterson  
U.S. Geological Survey,  
345 Middlefield Road, MS 496  
Menlo Park, CA 94025  
(415) 354-3366, fax 415-354-3363

Cynthia H. Pilska  
MBARI  
160 Central Ave.  
Pacific Grove, CA 93950  
(408) 647-3719, fax 408-649-8587

Stephen C. Piper  
Scripps Inst. of Oceanography, A-020  
La Jolla, CA 92093-0220619-534-4230,  
fax 619-534-0784

Douglas R. Powell  
P.O. Box 2654  
2418 Acton St.  
Berkeley, CA 94702  
510-843-6879, or 707-664-2194

Alex Pupacko  
USGS, WRD  
705 N. Plaza Street, rm. 224  
Carson City, NV 89701  
702-887-7600, fax 702-887-7629

John Quadros  
48243 Turquoise St.  
Fremont, CA 94539  
510-656-7654

Kelly Redmond  
Western Regional Climate Center  
Desert Research Institute  
P.O. Box 60220  
Reno, NV 89506-0220(702) 677-3139,  
fax 702-677-3157

Brian Reece  
USGS - WRD  
705 N. Plaza St., Rm. 224  
Carson City, NV 89701  
702-887-7671, fax 702-887-7629

John Roads  
Scripps Institution of Oceanography,  
0224  
La Jolla, CA 92093-0224  
(619)534-2099, 619-534-8561

Arndt Schimmelmann  
Scripps Institution of Oceanography,  
A-015, University of CA-San Diego  
La Jolla, CA 92093-0215  
(619) 534-4605, fax 619-534-0784

John F. Stamm  
Princeton University  
Department of Civil Engin. & Oper.  
Research  
Princeton, NJ 08544  
609-258-4411, fax 609-258-1270

Fred Swanson  
U.S. Forest Service  
3200 Jefferson Way  
Corvallis, OR 97331  
503-750-7355, fax 503-750-7329

Sus Tabata  
Inst. of Ocean Sciences  
P.O. Box 6000  
9860 West Saanich Road  
Sidney, BC, Canada V8L 4B2  
(604) 363-6573, fax 604-363-6746

Larry Riddle  
Scripps Institution of Oceanography,  
0224, University of CA-San Diego  
La Jolla, CA 92093-0224  
(619)534-1869, fax 619-534-8561

Maurice Roos  
CA Dept of Water Resources,  
1416 - 9th Street  
P.O. Box 942836  
Sacramento, CA 94236-0001  
(916)653-8366

Gary Sharp  
CIRIOS  
2560 Garden Road, Suite 101  
Monterey, CA 93940  
(408)647-4215, FAX 408-647-4225

Fred F.Y. Su  
Science Applications International  
Corp.  
10260 Campus Point Dr.  
San Diego, CA 92121  
619-546-6607, fax 619-546-6584

Robert N. Swanson  
Pacific Gas & Electric  
77 Beale Street, Rm 1694  
San Francisco, CA 94106  
(415)973-1331, FAX 415-973-1016

Mia Tegner  
Scripps Institution of Oceanography  
La Jolla, CA 92093-0201  
619-534-2059, fax 619-534-5306

John Turk  
USGS  
Box 25046, ms 415  
Denver Fed. Center  
Denver, CO 80225  
303-236-4882, fax 303-236-4912

Alexander van Geen  
USGS  
345 Middlefield Rd  
ms 465  
Menlo Park, CA 94025  
415-329-4184, fax 415-329-4463

Peter K Van de Water

1051 N. Warren  
Tucson, AZ 85719  
(602)881-7418

Ross A. Virginia  
Systems Ecology Research Group  
San Diego State University  
San Diego, CA 92182  
619-594-6519, fax 619-594-5676

Roy A. Walters  
U.S. Geological Survey  
1206 N. Lawrence  
Tacoma, WA 98416  
(206)593-6505, fax 206-383-7967

Ching-hua Tina Wang  
Los Alamos Natl. Laboratories  
IGPP, ms K305  
Los Alamos, NM 87545  
(505) 665-5967, fax 505-665-3107

Robert H. Webb  
U.S. Geological Survey  
1675 W. Anklam Road  
Tucson, AZ 85745  
(602)670-6821, fax 602-670-6806

Stephen G. Wells  
Dept. of Earth Sciences - 036  
Riverside, CA  
92521 714-787-4367, fax 714-787-4324

G. James West  
3429 Oyster Bay  
Davis, CA 95616  
(916)978-5132, Fax 916-978-5284

Andrea Woodward  
University of Washington  
College of Forestry/CPSU AR-10  
Seattle, WA 98195206-543-9138, fax  
206-543-3254

Memorie Yasuda  
Scripps Inst. of Oceanography  
Univ. of Calif. at San Diego  
9500 Gilman Drive  
La Jolla, CA 92093-0215  
(619)534-6510, fax 619-534-0784

James R. Young  
Southern California Edison  
G.O. 1, Room 405  
2244 Walnut Grove Avenue  
Rosemead, CA 91770  
(818)302-9191, 818-302-9730



